

**UNIVERSITÀ DEGLI STUDI
DI MODENA E REGGIO EMILIA**

Dottorato di ricerca in “Molecular and regenerative medicine”

Ciclo XXXIV

**Organic Bioelectronic Devices for Selective Biomarker
Sensing: Towards Integration with Living Systems**

in co-tutela con la Linköpings universitet

Candidato: DIACCI Chiara

Relatore italiano (Tutor): Prof. Carlo Augusto Bortolotti

Relatore svedese (Tutor): Prof. Daniel Simon

Coordinatore del Corso di Dottorato: Prof. Michele De Luca

ABSTRACT

Inorganic materials have been the main players of the semiconductor industry for the past forty years. However, there has been a continuous interest and growth in the research and in the application of organic semiconductors (OSCs) as active materials in electronic devices, due to the possibility to process these materials at low temperature on flexible substrates, fabricate them on large-area, and upscale their fabrication using cost-effective strategies such as printing. Because of these features, organic electronic devices are rapidly emerging as biosensors for biomarkers, with a high potential for becoming a high-throughput tool even deployable at the point-of-care.

One of the most used and studied platforms is the organic electrochemical transistor (OECT). OECTs have been largely used as biosensors in order to transduce and amplify electrical signals or detect biological analytes upon proper functionalization with specific biorecognition units. OECTs can operate at low voltages, are easy to fabricate on different substrates, and are compatible with the aqueous environment, and can therefore be interfaced with living systems, ranging from mammals to plants. The OECT device configuration includes a gate electrode that modulates the current in the channel through an electrolyte, which can be not only a buffered solution but even a complex biological fluid. When OECTs are operated as biosensors, the sensing mechanism relies on the current variation generated from specific reactions with the analyte of interest. These devices are paving the way to the development of point-of-care technologies and portable biosensors with fast and label-free detection. Moreover, OECTs can help to reveal new biological insight and allow a better understanding of physiological processes.

During my PhD, I focused on design, fabrication, and validation of different OECT-based biosensors for the detection of biomarkers that are relevant for healthcare applications, thus showing their high potential as a proper sensing platform. We developed sensors towards different analytes, ranging from small molecules to proteins, with ad hoc designed materials strategies to endow the device with selectivity towards the species of interest. Most notably, I also demonstrated the possibility of integrating OECTs in plants, as an example of interfacing these biosensors with living systems. In the first two papers, we developed screen printed OECTs, presenting PEDOT:PSS as the semiconducting material on the channel. In the first case, the device also featured a PEDOT:PSS gate electrode which was further functionalized with biocompatible gelatin and the enzyme urease to ensure selectivity toward the analyte of interest, namely urea. The biosensor was able to monitor increasing urea concentrations with a limit of detection of 1 μM . In the second paper the screen-printed carbon gate electrode was first modified with platinum and then we ensured selectivity towards the analyte uric acid, a relevant biomarker for wound infection, by entrapping urate oxidase in a dual-ionic-layer

hydrogel membrane to filter out charged interfering agents. The biosensor exhibited a 4.5 μM limit of detection and selectivity even in artificial wound exudate. In the third paper we designed an interleukin-6 (IL6) OECT based biosensor able to detect the cytokine down to the pM regime in PBS buffer. The mechanism of detection relied on the specific binding between an aptamer, used as sensing unit on the gate electrode, and the IL6 in solution, allowing for detection ranging from physiological to pathological levels.

In the last two papers we developed OECT based biosensors to be interfaced with the plant world. In the fourth paper we presented a glucose sensor, based on the enzyme glucose oxidase (GOx) to detect glucose export from chloroplasts. In particular, we demonstrated real-time glucose monitoring with temporal resolution of 1 minute in complex media. In the fifth paper, we developed implantable OECT-based sugar sensors for *in vivo* real-time monitoring of sugar transport in poplar trees. The biosensors presented a multienzyme-functionalized gate endowing the device with specificity towards glucose and sucrose. Most notably, the OECT sensors did not cause a significant wound response in the plant, allowing us to demonstrate that OECT-based sensors are attractive tools for studying transport kinetics in plants, *in vivo* and real-time.

POPULÄRVETENSKAPLIG SAMMANFATTNING

Oorganiska material har varit huvudaktörerna i halvledarindustrin under de senaste fyrtio åren. Det har emellertid funnits ett kontinuerligt intresse och tillväxt inom forskning för tillämpningar av organiska halvledare (OSC) som aktiva material i elektroniska apparater, på grund av möjligheten att bearbeta dessa material vid låga temperaturer, på flexibla substrat, tillverka dem på stora ytor och skala med kostnadseffektiva strategier såsom tryckning. På grund av dessa funktioner växer organiska elektroniska enheter snabbt fram som biosensorer för biomarkörer, med hög potential att bli ett genomgående verktyg som även kan användas vid vårdplatsen. En av de mest använda och studerade plattformarna är den organiska elektrokemiska transistorn (OECT). OECT har i stor utsträckning använts som biosensorer för att transducera och förstärka elektriska signaler eller upptäcka biologiska analyter vid korrekt funktionalisering med specifika bio-igenkännande enheter. OECT kan fungera vid låga spänningar, de är lätta att tillverka på olika substrat och kompatibla med den vattenhaltiga miljör, därför kan de kopplas till levande system, allt från däggdjur till växter. Dessa enheter banar väg för utvecklingen av point-of-care teknologier och portabla biosensorer med snabb och etikettfri detektering. Dessutom kan de hjälpa till att avslöja nya biologiska insikter och möjliggöra en bättre förståelse för fysiologiska processer.

OECT-enhetens konfiguration inkluderar en gate-elektrod som modulerar strömmen i kanalen genom en elektrolyt, som inte endast behöver vara en buffrad lösning utan till och med en komplex biologisk vätska. När OECT används som biosensorer är avkänningsmekanismen beroende av spänningsvariationen som genereras från specifika reaktioner med analyten av intresse. Under min doktorsexamen fokuserade jag på design, tillverkning och validering av olika OECT-baserade biosensorer för detektering av biomarkörer som är relevanta för tillämpningar inom vård och visar därmed deras höga potential som riktiga avkänningsplattformar. Vi utvecklade sensorer för olika analyter, allt från små molekyler till proteiner, med ad hoc-designad materialstrategi för att ge enheten selektivitet gentemot arten av intresse. Framför allt visade jag också möjligheten att integrera OECT i växter, som ett exempel på gränssnittet mellan dessa biosensorer och levande system. I de två första artiklarna utvecklade vi skärmtryckta OECT: er och presenterade PEDOT: PSS som halvledande material i kanalen.

I det första fallet innehöll anordningen också en PEDOT:PSS gate-elektrod som ytterligare funktionaliserades med biokompatibelt gelatin och enzymet ureas för att säkerställa selektivitet mot analyten av intresse, nämligen urea. Biosensorn kunde övervaka ökande ureakoncentrationer med en detektionsgräns på 1 μM . I den andra artikeln modifierades först den skärmtryckta kol baserade gate-elektroden med platina och sedan säkerställde vi selektivitet mot analyten urinsyra, en relevant

biomarkör för sårinfektion, genom att fånga upp uratoxidase i ett dubbelt jonskikt hydrogel-membran för att filtrera bort laddade störande medel. Biosensorn uppvisade en detektions- och selektivitetsgräns på 4.5 μM även i artificiell sårutsöndring. I den tredje artikeln designade vi en interleukin-6 (IL6) OECT-baserad biosensor som kunde detektera cytokinnivåer ner till pikomolar nivåer i PBS-buffert. Detektionsmekanismen är beroende av den specifika bindningen mellan en aptamer, som används som avkänningsenhet hos gate-elektroden, och IL6 i lösning, vilket möjliggör detektering som sträcker sig från fysiologiska till patologiska nivåer.

I de två sista artiklarna utvecklade vi OECT-baserade biosensorer för att koppla samman med växtvärlden. I den fjärde artikeln uppvisade vi en glukosensor, baserad på enzymet glukosoxidase (GOx) för att detektera glukosexport från kloroplast. I synnerhet visade vi glukosövervakning i realtid med tidsmässig upplösning på 1 minut i komplexa medier. I den andra artikeln utvecklade vi implanterbara OECT-baserade sockersensorer för in vivo, realtidsövervakning av sockertransport i poppelträd. Biosensorerna presenterade en multienzymfunktionaliserad gate som ger enheten specificitet mot glukos och sackaros. Framför allt orsakade inte OECT-sensorerna signifikant sårrespons i växterna, vilket gjorde att vi kunde visa att OECT-baserade sensorer är attraktiva verktyg för att studera transportkinetik i växter, in vivo och realtid.

SOMMARIO

I materiali inorganici sono stati i protagonisti dell'industria dei semiconduttori negli ultimi quarant'anni. Tuttavia, c'è un continuo interesse e crescita nella ricerca e nell'applicazione di semiconduttori organici (OSC) come materiali per dispositivi elettronici, grazie alla possibilità di processarli a bassa temperatura, su substrati flessibili e di fabbricarli utilizzando diverse strategie come lo stampaggio. Grazie a queste caratteristiche, i dispositivi elettronici organici stanno rapidamente emergendo come piattaforme per biosensori di biomarcatori, con un forte potenziale di diventare uno strumento utilizzabile come point-of-care.

Una delle piattaforme più utilizzate e studiate è il Transistor Elettrochimico Organico (OECT). Gli OECT sono stati ampiamente utilizzati come biosensori per trasdurre e amplificare segnali elettrici o rilevare analiti biologici previa funzionalizzazione con specifiche unità di bioriconoscimento. Gli OECT possono operare a basso voltaggio, sono facili da fabbricare su diversi substrati e compatibili con l'ambiente acquoso, quindi possono essere interfacciati con sistemi viventi, dai mammiferi al mondo vegetale. La configurazione degli OECT include un elettrodo di gate che modula la corrente del canale attraverso un elettrolita, che può essere non solo una soluzione tampone ma anche un fluido biologico complesso. Quando gli OECT vengono utilizzati come biosensori, il meccanismo di rilevamento si basa sulla variazione di corrente generata da reazioni specifiche con l'analita di interesse.

Durante il mio dottorato di ricerca, mi sono concentrata sulla progettazione, fabbricazione e validazione di biosensori basati su OECT per il rilevamento di biomarcatori per applicazioni cliniche e ambientali, mostrando il loro potenziale come piattaforma di rilevamento. Abbiamo sviluppato sensori verso diversi tipi di analiti, dalle piccole molecole alle proteine, usando materiali progettati ad hoc per dotare i dispositivi di selettività verso le specie di interesse. In particolare, abbiamo anche dimostrato la possibilità di integrare gli OECT nelle piante, per dimostrare la loro compatibilità con sistemi viventi. Nei primi due articoli, abbiamo sviluppato OECT stampati, che presentano PEDOT:PSS come materiale semiconduttore sul canale. Nel primo caso, il dispositivo presenta anche un elettrodo di gate di PEDOT:PSS che è stato ulteriormente funzionalizzato con gelatina biocompatibile e l'enzima ureasi per garantire la selettività verso l'analita di interesse, ovvero l'urea. Il biosensore è in grado di monitorare varie concentrazioni di urea con un limite di detection di $1\mu\text{M}$. Nel secondo articolo l'elettrodo di gate di carbonio stampato è stato prima modificato con platino e successivamente abbiamo assicurato la selettività del biosensore verso l'acido urico, un biomarcatore rilevante per l'infezione di ferite, intrappolando l'urato ossidasi in una membrana a doppio strato ionico per filtrare gli interferenti. Il biosensore ha un limite di rilevamento di $4,5\mu\text{M}$ anche in essudato artificiale ed è selettivo per l'analita di interesse. Nel terzo articolo abbiamo progettato un biosensore per la detection di

interleuchina-6 (IL6) in grado di rilevare livelli di citochina in concentrazioni pM in PBS. Il meccanismo di rilevamento si basa sul legame specifico tra un aptamero, utilizzato come unità di rilevamento sull'elettrodo di gate, e l'IL6 in soluzione, consentendo il rilevamento da livelli fisiologici a patologici.

Negli ultimi due articoli abbiamo sviluppato biosensori basati su OECT per interfacciare il mondo vegetale. Nel quarto articolo abbiamo presentato un sensore, basato sull'enzima glucosio ossidasi (GOx) per rilevare l'esportazione di glucosio da cloroplasti. In particolare, abbiamo dimostrato il monitoraggio di glucosio in tempo reale con una risoluzione temporale di 1 minuto. Nel secondo articolo, abbiamo sviluppato sensori impiantabili basati su OECT per il monitoraggio in vivo e in tempo reale del trasporto di zuccheri negli alberi di pioppo. I biosensori presentano un elettrodo di gate funzionalizzato con diversi enzimi in modo da conferire al dispositivo una specificità nei confronti di glucosio e saccarosio. In particolare, i dispositivi non hanno causato significativi danni al tessuto, consentendoci di dimostrare che i sensori basati su OECT possono rappresentare soluzioni alternative per studiare la cinetica di trasporto nelle piante, in vivo e in tempo reale.

ACKNOWLEDGMENTS

I want to start this acknowledgment by expressing how lucky and glad I feel in having had the possibility to join two laboratories for my PhD journey: The Laboratory of Organic Electronics in Linköping (LOE) and in Modena (LEO).

Then I want to express my infinite gratitude to all my supervisors, to **Magnus Berggren**, to **Daniel Simon** for coming to Modena and introducing me to the possibility to join his bioelectronic research team in Sweden. I also want to thank him for giving me the chance to participate in many interesting research areas and for helping me and advising me regarding my academic journey. I want to also thank **Eleni Stavrinidou**, for adopting me as PhD student in my first year of study, when I was feeling a little bit lost, and for guiding me, supporting me and showing me the electronic plant world and its many applications.

I want to express a deep and special gratitude to the supervisor that introduced me to the bioelectronic world and that accompanied me till the end of this journey, **Carlo Augusto Bortolotti**. If I have decided to join organic bioelectronic research in the first place it is because of the enthusiasm that he was showing for science during the university courses, when I was a master student. I also want to thank him for giving me the possibility to join his research team and for teaching me the basis of the experimental method. Plus, I also want to thank him because he has been an extremely valuable advisor when I had to decide about my PhD path and my future academic career.

A special thank also to **Fabio Biscarini**, and his group in Modena. In specific to **Marcello** and **Matteo** for being amazing mentors, both during my master and my PhD. To **Martina** and **Sophia** for being super friendly and for making the laboratory of Modena an amazing place. To **Pippy** for the long and helpful calls about science and future choices.

A sincere thanks to **Totte Niittylä** for the fruitful collaboration and to **Takao Someya** for the visit to his lab in Tokyo. A special thank also to **Simone Fabiano** and **Valerio Beni** for making me feel very welcome in the new laboratory.

I met so many amazing people during these 4 years in Sweden, many left before me, but they will always be close friends even when they will be in the opposite part of the world. A first and most special thanks to the best supportive friend I had, to **Nadia**, for pushing me over the limit, for supporting me, for making me a stronger person and for always being there. To **Maria** and **Mina** for the amazing time spent all together and for making Sweden to feel like home. To **Dennis**, my desk buddy and flatmate, for sharing together this experience from the very beginning to the very end. To **Xeno** for the help and the support he gave me in the laboratory, for being a super good teacher and

the best trampoline buddy. To **Sami** for being always cheerful and helpful and for organizing many amazing events and activities in Norrköping. To **Marie** for being supportive and a good conference company. To **Tobias, Michela, Eva, Jee, Donghyun, Bernhard, Johannes and Daniel** for being amazing friends and making this PhD lighter and easier. Another special thanks to the e-plant group: **Gwen, Iwona, Daniela, Adam, Mannan, Cyril, Ilaria and Vasilis** for the collaborations, for the fun and the experienced they shared with me in working with plants. I want to also thank **Erik Gabrielsson, Pelle and Astrid** for the collaboration and for helping me in the laboratory.

A thanks goes to all the people I have met in Sweden. **Ludovico, Eric G, Jennifer, Mery, Yannis, Hamid, Mehmet, Tero, Arghya, Benjamin, Dag, Giancarlo, Stefano, Jacky, Evelina, Sara, Laura, Jonathan Lonny, Nara, Theresia, Ulrika, Maciej, Oliya, Saumya, Cristian, Olga, Mario, Fareed, Luca, Simona, Katriann, Hanne, Josefin, Chiara M., David and Robert** and all the other LOE members for all the fun and the good time spent in Norrköping.

Then would like to thank **George** and all **my friend in Italy** for the emotional support and the encouragement they showed me in these 4 years.

Finally, a most grateful thanks to **my family (mam, dad, my brother Alessandro, Marina and little Arianna)** because since the beginning they have always supported me and pushed me to be the best version of myself. They always have encouraged me to take the right choice and they always have welcomed me back home with open arms.

LIST OF PAPERS AND CONTRIBUTION

Paper I

Label free urea biosensor based on organic electrochemical transistors.

Marcello Berto, **Chiara Diacci**, Lorenz Theuer, Michele Di Lauro, Daniel T Simon, Magnus Berggren, Fabio Biscarini, Valerio Beni, Carlo A Bortolotti.

Flexible and Printed Electronics, 2018.

Contribution: device printing, device characterization

Paper II

Flexible Printed Organic Electrochemical Transistors for the Detection of Uric Acid in Artificial Wound Exudate.

Marina Galliani, **Chiara Diacci**, Marcello Berto, Matteo Sensi, Valerio Beni, Magnus Berggren, Marco Borsari, Daniel T Simon, Fabio Biscarini, Carlo A Bortolotti.

Advanced Materials Interfaces, 2020.

Contribution: experimental and device design, master student experiment supervision, manuscript writing.

Paper III

Organic electrochemical transistor-based aptasensor for interleukin-6 label-free detection.

Chiara Diacci, Marcello Berto, Tero Petri Ruoko, Samuel Lienemann, Daniel T. Simon, Magnus Berggren, Marco Borsari, Fabio Biscarini, Carlo A. Bortolotti.

Manuscript in preparation

Contribution: major contribution in the experimental part including microfabrication, measurements, data analysis and manuscript writing.

Paper IV

Real-Time Monitoring of Glucose Export from Isolated Chloroplasts Using an Organic Electrochemical Transistor.

Chiara Diacci, Jee Woong Lee, Per Janson, Gwennaël Dufil, Gábor Méhes, Magnus Berggren, Daniel T Simon, Eleni Stavrinidou.

Advanced Materials Technologies, 2020.

Contribution: major contribution in the experimental part including microfabrication, measurements, data analysis and manuscript writing.

Paper V

Diurnal in vivo xylem sap glucose and sucrose monitoring using implantable organic electrochemical transistor sensors.

Chiara Diacci, Tayebah Abedi, Jee Woong Lee, Erik O Gabrielsson, Magnus Berggren, Daniel T Simon, Totte Niittylä, Eleni Stavrinidou.

iScience, 2021.

Contribution: major contribution in the experimental part including microfabrication, measurements, data analysis and manuscript writing.

Contents

| | |
|--|----|
| 1. INTRODUCTION | 14 |
| 1.2 Biosensor | 14 |
| 1.3 Biosensor in healthcare and agriculture | 16 |
| 1.4 Aim of the thesis | 17 |
| 2. ORGANIC ELECTRONICS | 18 |
| 2.2 Organic Bioelectronics | 19 |
| 2.3 Fabrication methods | 21 |
| 3. ORGANIC TRANSISTORS | 22 |
| 3.2 Transistor | 22 |
| 3.3 Organic based transistors | 23 |
| 3.4 OECT device physics | 25 |
| 3.5 OECT as biosensor | 26 |
| 3.6 OECT for in vitro/in vivo applications | 29 |
| 4. CLINICAL BIOMARKERS | 31 |
| 4.2 Urea | 31 |
| 4.3 Uric Acid | 31 |
| 4.4 Interleukin 6 | 32 |
| 4.5 Glucose | 33 |
| 4.6 Sucrose | 34 |
| 5. EXPERIMENTAL TECHNIQUES | 35 |
| 5.2 Physical vapour deposition | 35 |
| 5.3 Spin coating | 35 |
| 5.4 Photolithography | 35 |
| 5.5 Printing | 35 |
| 5.6 Functionalization | 37 |
| 5.7 Electrochemical deposition | 37 |
| 5.8 Cyclic Voltammetry | 37 |
| 5.9 Electrochemical Impedance Spectroscopy | 39 |
| 5.10 Scanning electron microscopy | 41 |
| 5.11 Fourier transform Infrared spectroscopy | 41 |
| 5.12 Electrical measurements | 42 |
| 5.13 Green house | 43 |
| 6. SUMMARY OF PAPERS | 44 |
| 6.2 Paper I | 44 |

| | | |
|-----|-----------------------------|----|
| 6.3 | Paper II..... | 44 |
| 6.4 | Paper III..... | 45 |
| 6.5 | Paper IV..... | 45 |
| 6.6 | Paper V..... | 46 |
| 7. | CONCLUSION AND OUTLOOK..... | 47 |
| 8. | REFERENCES..... | 48 |

1. INTRODUCTION

1.2 Biosensor

Biosensors are systems/devices able to translate a biological event into a readout, that is proportional to the concentration of a given analyte in a sample. Nowadays, biosensors are essential tools present in various fields and are employed for many applications, from clinical tests to environmental monitoring. Typically, a biosensor is described by the following elements (fig. 1): i) the input, which is the analyte to be detected (e.g., metabolites, proteins, DNAs); ii) the biorecognition element, which is the biomolecule able to recognise specifically the analyte of interest (e.g., antibody, DNA, enzyme, cell); iii) the transducer, which allows the conversion of the physical/chemical event between input and biorecognition element into a measurable signal (the main transducers being optical, electrochemical, magnetic and amperometric); iv) the output, which is the processed signal (the output can be displayed under the form of colour, current or voltage variation).

When designed, a biosensor should feature some characteristics and attributes: it should be selective, being able to detect a specific analyte in a complex sample which may contains interfering molecules. Its response should be reproducible, i.e. yielding same the signal (within a given, quantifiable tolerance) for the same analyte concentration, in different experiments, and it should be sensitive to the analyte, in a concentration range useful for the diagnosis¹. Depending on the transducing principle used to detect the biological event in the sensing platform, biosensors can be divided in:

- Optical biosensors: these transducers are exploiting the optical properties of the light, taking advantage of phase or intensity changes taking place when the analyte binds the biorecognition element². The most established biosensors that are based on optical transducer are Surface Plasmon Resonance³ (SPR), Localized Surface Plasmon Resonance⁴ (LSPR) and Surface-enhanced Raman Scattering⁵ (SERS), which represent label-free techniques (no incubation with external molecules). While other optical biosensor, such as fluorometric and colorimetric assay⁶ are based on the addition of molecules to reveal optically the biding between analyte and sensing unit.

- Electrochemical biosensors: these devices exploit electrochemical processes to detect an analyte in solution. They measure variations of electrical signals caused by the biding between analyte and biorecognition element. Commonly the event is displayed as variation of current, potential or impedance. The most used techniques include Cyclic voltammetry (CV) and Electrochemical Impedance Spectroscopy (EIS)⁷.

- Magnetic biosensors: these devices employ the unique properties of magnetic/paramagnetic particles to monitor the biological interaction between analyte and sensing unit. They detect changes in magnetic properties upon molecules interaction⁸.

- Piezoelectric biosensors: these devices exploit piezoelectric crystal to detect biological binding events. They measure changes in the oscillation of the piezo, that are caused by mass changes upon binding between biorecognition unit and analyte⁹.

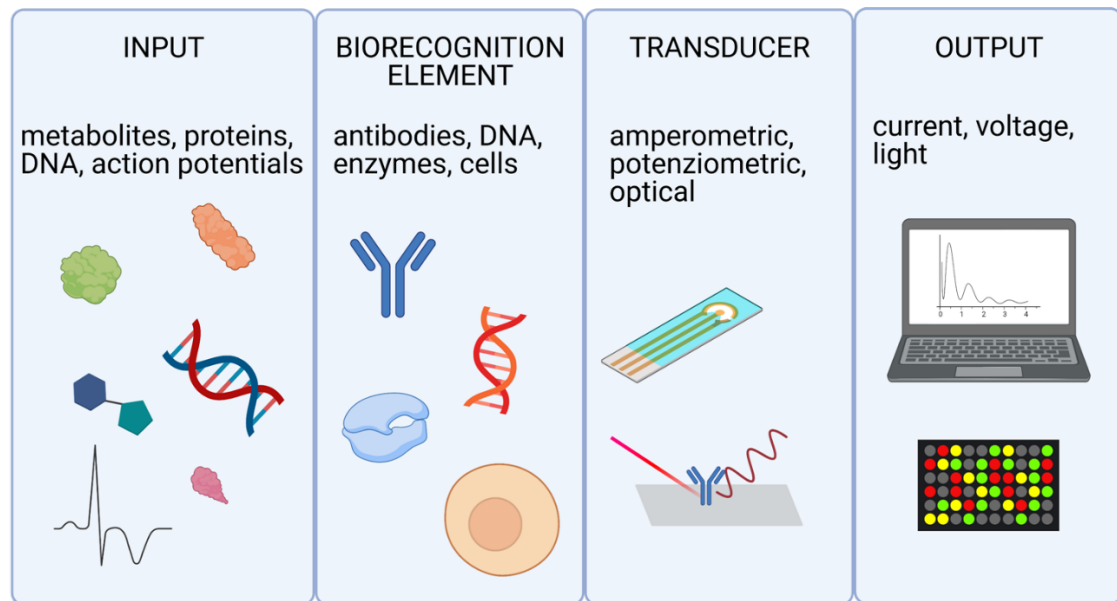


Figure 1: Building blocks of a biosensor. The input is the analyte to be detected and it can be represented by metabolites, proteins, DNAs, and action potentials. The biorecognition element is crucial to detect specifically the analyte of interest: it can be an antibody, a DNA/RNA oligo, an enzyme or even a whole cell. The transducer translates the biological signal into a measurable signal, which can be amperometric, potentiometric or optical. The output displays the signal, and can be under the form of current, voltage or light.

The first biosensor was introduced in 1956, by the efforts of Leland C. Clark Jr, who used a platinum electrode vs an Ag/AgCl reference electrode, to detect different oxygen concentrations in solution¹⁰ (fig. 2). This first demonstration led to the development of biosensors that were exploiting enzymatic units to detect glucose¹⁰ (by Leland Clark in 1962) and urea¹¹ (by Guilbault and Montalvo Jr in 1969). In 1980, the first immunosensor was proposed¹², followed by the first Surface Plasmon Resonance (SPR)-based immunosensor in 1983¹³ and its commercialization by Biacore in 1990¹⁴. Biosensor innovation moved forward with the creation of DNA based sensors¹⁵, able to recognize complementary oligonucleotide strands and thus opening the way to genetic tests, and with the introduction of nanomaterials to enhance the biosensor performance^{16,17}. Nowadays, biosensors are not necessarily confined to the laboratory bench and are ready to be interfaced directly with biological systems, under the form of wearable^{18,19} or implantable sensors²⁰⁻²².

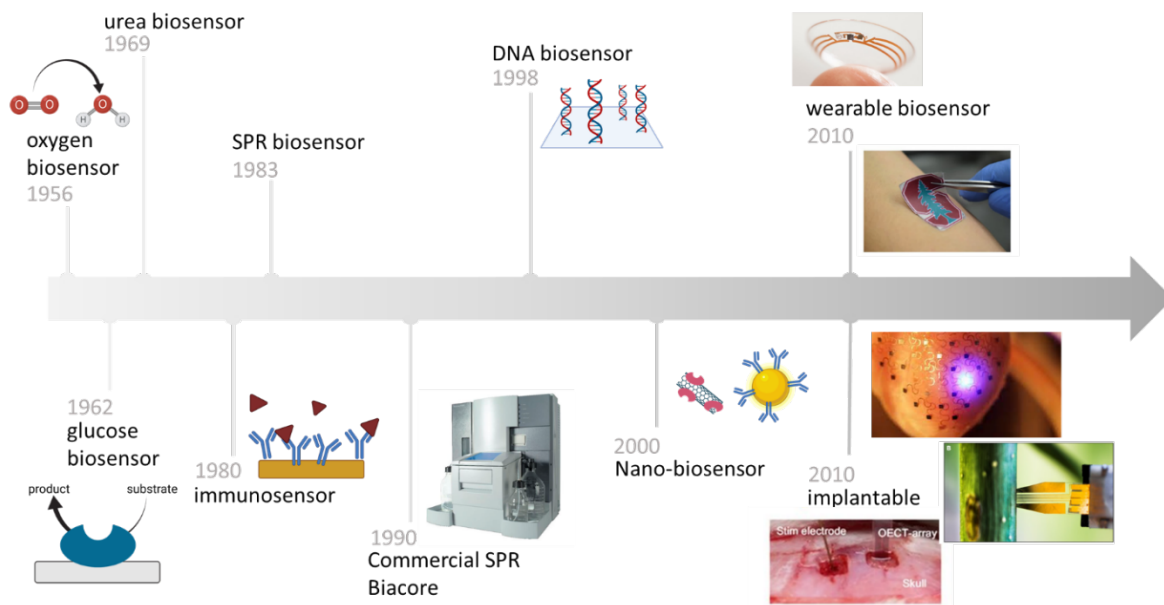


Figure 2: timeline for biosensor development

1.3 Biosensor in healthcare and agriculture

Biosensors are crucial tools in the healthcare system but also in many other fields such as food control, agriculture and environmental monitoring. In medical care, biosensors, together with other clinical tests, are used for diagnosis, screening and monitoring to evaluate pathological processes, thus representing an imperative necessity in the healthcare. Nowadays the healthcare system has an enormous impact on our economy, and just in the USA it is exceeding the 2.7\$ trillion per year²³. The cost of the diagnostic tests takes 10% of the budget and it is rapidly rising over time, with the introduction of molecular diagnostic for personalised medicine. The demands for screening and diagnosis are increasing and becoming virtually infinite, but the resources in terms of laboratory equipment and specialized handwork are finite, thus creating an urgent, critical situation. Equally important and challenging is the use of biosensors for environmental and agricultural applications²⁴. Climatic changes are becoming less predictable and more disruptive, causing huge economic problems in agriculture and ecological disasters. Thus, in view of establishing sustainable agriculture systems, biosensors would be highly necessary for smart monitoring, enabling control of plant physiology in real time and providing support to take environmentally affordable decisions²⁵.

For these reasons, there is a clear necessity to introduce disposable and cost-effective biosensors to advance healthcare and agriculture. Up to date, among the most used and standardized tests for analyte detection and quantification are Enzyme Linked Immunosorbent Assay²⁶ (ELISA), Mass Spectrometry²⁷ or High Performance Liquid Chromatography²⁸ (HPLC). Those techniques exhibit high sensitivity and selectivity towards a very large portfolio of analytes, even in complex fluids. In addition,

they are highly reliable and reproducible, an essential characteristic for clinical diagnosis. However, these methods require sample processing, thus increasing the amount of sample that needs to be collected, specialized personnel and equipment and are typically time consuming. In order to solve these limitations, research is focusing its efforts in automating biosensors, transforming them in a competitive technology that will abandon the laboratory bench in favour of portable devices embedded in an easy, user-centred set-up. To face the high demand and the new requirements biosensors should be compatible for large scale production, fabricated with cost-effective materials, reliable and robust. New biosensing platforms for advanced detection devices should be miniaturized systems, implantable or in field deployable for point-of-care applications in home testing. The introduction of new nanomaterials, such as carbon nanotubes²⁹ (CNTs) or nanoparticles³⁰ opened to many new possibilities for the biosensing field, together with new techniques for biosensor fabrication on conformable and ultra-thin substrates, such as parylene³¹⁻³³. Carbon-based, 2D materials are not the only novel players in the field of biosensing. Organic polymers are also among the new materials used for advancing the technology and are playing a major role in biosensor development, introducing innovative fabrication methods and new detection properties.

1.4 Aim of the thesis

The aim of this thesis is to develop organic based biosensors for the detection of various biomarkers. The fabrication of these devices includes cost-effective techniques for the creation of disposable and portable devices together with traditional microfabrication methods to create ad hoc biosensors for plant interfacing. In this thesis I have focused on understanding the working principle of Organic Electrochemical Transistors (OECT) and their properties for using them, after functionalization as effective biosensing platforms.

2. ORGANIC ELECTRONICS

Inorganic materials have been the main protagonists of the semiconductor industry for the past forty years. Traditional silicon-based electronics overcame many challenges in term of fabrication and exponentially increased demand, but they still present some limitations³⁴. For these reasons, there has been a growing interest in the application of organic semiconductors (OSCs) as active materials in electronic devices. OSCs include different types of materials, including small molecules, polymers and nanotubes, each of which can exist in the form of molecular crystals or amorphous films³⁵. OSCs are materials that present carbon atoms in their backbone and π -conjugated orbitals which contain delocalised electrons. These π orbitals are defined as the highest occupied molecular orbital (HOMO) and take the role of the valence band for inorganic semiconductors, while π^* orbitals are defined as lowest unoccupied molecular orbital (LUMO) and take the role of conduction band. Because of the π conjugated system the energy gap between LUMO and HOMO is small enough to permit charge transfer (fig. 3).

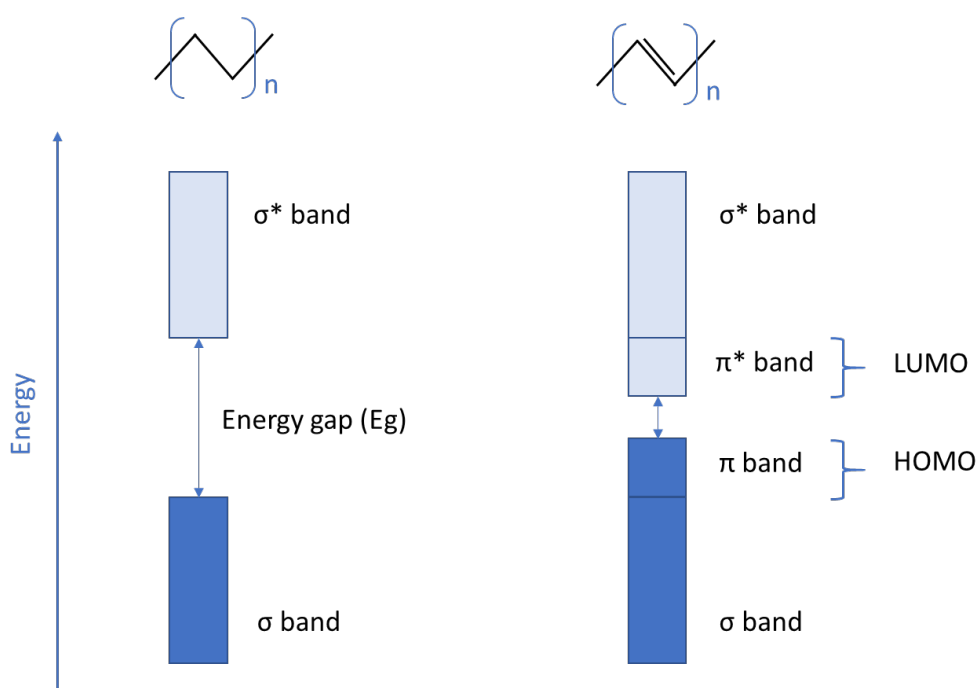


Figure 3: Structure and energetic levels of molecular orbitals for unconjugated and conjugated organic polymers. The presence of double bounds in organic conjugated polymers reduce the energy gap between HOMO and LUMO orbitals, allowing charge transfer from the π band to the π^* band.

When an electron jumps from HOMO to LUMO it causes a distortion of electron spatial distribution, causing a geometrical distortion and defining the region carrying the charge as a polaron. For some conductive polymers (e.g., polythiophene, polypyrrole) it is possible to identify a second structure with different energy, called bipolaron, which represent the bi-cation state of the polymer³⁶. Charge transport properties in OSCs depend on the molecular packing, the energy gap between HOMO and

LUMO, the temperature, and the degree of order in the solid state³⁷. Pure semiconducting polymers, without any addition/subtraction of external charges, show very poor electrical conductivity (insulator). Conductivity can be increased by adding dopant molecules that can donate/accept electrons and are define which primary charge carriers are transported in the semiconducting polymer. The delocalisation of π orbitals provides molecular stability giving low ionisation potential and high electron affinity, facilitating the doping process of the organic conjugated polymer. Organic semiconductors can be classified as: **p-type** (transporting holes) or **n-type** (transporting electrons). The difference lays in the primary charge carrier. In n-type semiconductors, an electron jumps from the HOMO level of the dopant to the LUMO of the semiconductor, allowing charges (electrons) to move through LUMO orbitals. In p-type semiconductors charge transport is described by hopping (jumping from one molecule to another), because an electron is taken from the HOMO orbital of the semiconductor and added to the LUMO orbital of the dopant molecule, leaving a hole in the conductive polymer backbone³⁸(fig. 4).

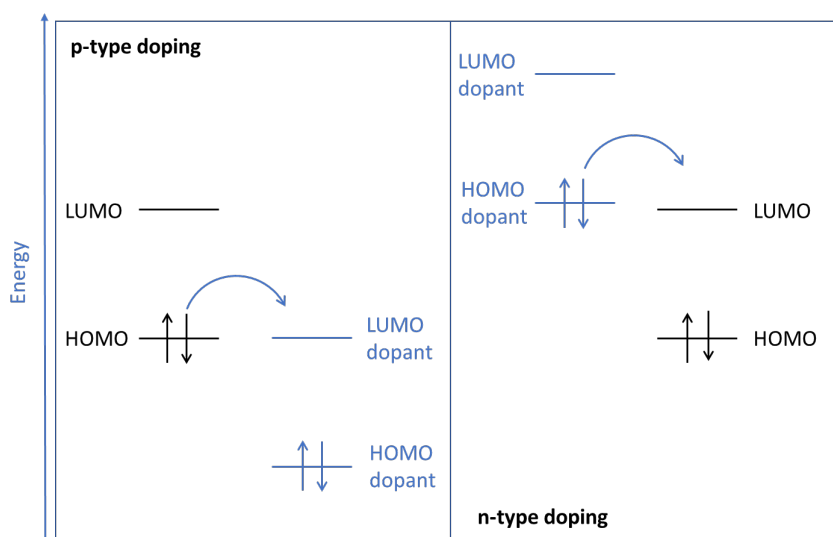


Figure 4: Schematic of energetic levels for dopant molecules. For p-type doping, an electron jumps from the HOMO orbital of the organic material to the LUMO orbital of the dopant molecule, leaving a hole as charge carrier in the conductive polymer. For the n-type doping an electron jumps from the HOMO orbital of the dopant molecule to the LUMO orbital of the organic material, adding an electron as charge carrier in the conduction band.

2.2 Organic Bioelectronics

Bioelectronics was first introduced by Luigi Galvani in the 18th century, when during the study of biological electrical signals, he connected a frog leg to its spinal cord, making it twitch³⁹. Since then, the applications of electronic devices for interfacing the biological world have grown exponentially, resulting in the creation of biosensors, electronic implants (e.g., pacemaker, cochlear implant) and drug delivery devices^{40–42}. The main limitation of traditional bioelectronic devices is represented by the material used to communicate with living systems. Organic conductive polymers and molecules represent ideal materials for interfacing biology and overcoming the limitation of inorganic

semiconductors. The main advantage lays in the property of OSCs to conduct both electronic and ionic charges^{43,44}; ions in fact, are one of the main signalling molecules that drive biological processes. Moreover, organic conductive materials, in contrast with silicon-based electronics, can interface directly with the biological milieu, because of their oxide-free surfaces, allowing a deeper interaction with events happening in biological fluids. The use of OSCs enables the fabrication of more biocompatible devices; organic materials are solution processable and allow easy chemical modifications, permitting the creation of soft or flexible devices that decrease the rheological mismatch between the biological tissue and the electronic component. Some organic polymers present a porous configuration, which can unlock specific properties and enhancing neural interfacing devices. This 3D structure permits the storage of high amount of charges at the electrode interface, decreasing the impedance and improving the signal to noise ratio. One of the most used and studied conductive polymers for bioelectronic devices is poly(3,4-ethylenedioxythiophene) doped with poly(styrene sulfonate) (PEDOT:PSS) (fig. 5a). This material is a polymeric mixed ion-electron conductor characterised by high hole conductivity ($>1000 \text{ S cm}^{-1}$), chemical stability, and versatility in manufacturing processes. PEDOT:PSS comprises rich polyanion (PSS-) regions interfacing a few PEDOT domains (fig. 5b), resulting in a hygroscopic material often presenting a porous gel structure⁴⁵. The hole density in PEDOT:PSS is modulated by ions in the electrolyte, entering the polymeric structure by application of a potential vs a reference electrode, creating a volumetric ion storage capacitance dependent on film thickness⁴⁶. PEDOT:PSS is commercially available and because of its solution processability is compatible with a wide range of fabrication techniques, including electropolymerization, spin-coating, printing, and physical vapour deposition (PVD). PEDOT based devices have been successfully employed in bioelectronics applications as electrode arrays to record brain signals⁴⁷, as cell scaffolds to stimulate and measure cell growth⁴⁸⁻⁵¹, as biosensors to record biomarkers^{22,52-54}, and as active materials for drug delivery devices⁵⁵.

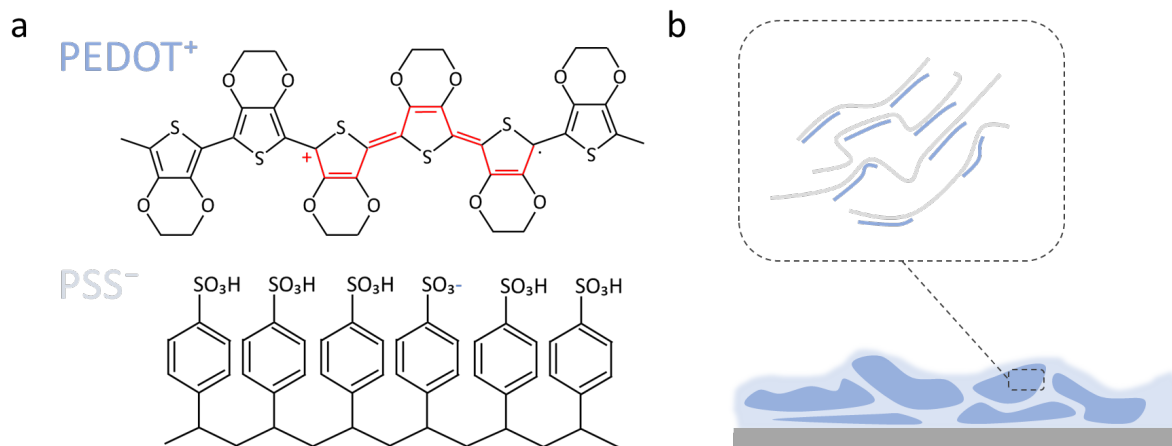


Figure 5: a) Chemical structure of the PEDOT:PSS conductive polymer. b) Representation of PEDOT:PSS film on a substrate. The magnification shows the peculiar porous polymeric structure, which contains rich PSS clusters (grey), interfaced by fewer PEDOT regions (blue).

2.3 Fabrication methods

The application of organic molecules and polymers in electronics has experienced a tremendous growth. This is because OSCs exhibit several practical advantages compared to traditional inorganic semiconductors. Organic polymers have low melting point and high solubility; characteristics which unlock the possibility to use these materials at low temperature and with solution processable techniques on flexible substrates (e.g., plastic or paper). OSCs are compatible with innovative and versatile fabrication techniques, such as solution casting, spin coating, ink-jet printing, and screen-printing, enabling fabrication on large-area and with cost-effectiveness^{56,57}. Nevertheless, organic polymers are compatible with traditional photolithographic techniques, such as vacuum evaporation, to achieve miniaturised systems for more challenging targets.

Printing techniques, commonly used in the graphic arts, can be applied to soluble organic conductive materials. The screen-printing process involves pushing the ink (organic polymer in solution) through a mesh that has openings on top, representing the pattern. In more details, the screen is covered by the ink, and a squeegee presses it through the mesh, transferring the pattern to the substrate. A well-defined pattern in screen-printing is often obtained using high viscosity ink solution, in order to produce thick film (>1 μm), while the resolution is determined from the mesh size and is generally in the range of 100 μm .⁵⁶ One of the most peculiar advantages of using organic semiconducting molecules to fabricate electronic circuit and devices is represented by the fact that some of these molecules can actively interact with biological units, polymerising inside the living system itself⁵⁸⁻⁶⁰. Recently it has been proved that 3-4,ethylenedioxythiophene (EDOT) based trimer can be absorbed by biological system and be polymerised by enzymatic units, physiologically present in the tissue, to create conductive pathways within the biological system⁶¹.

3. ORGANIC TRANSISTORS

3.2 Transistor

Transistors are three terminal devices able to amplify and/or switch electronic signals. All transistors share the same basic structure composed of input/output electrodes in contact with the semiconducting material in the channel and a control electrode contacting the semiconductor through a dielectric medium, that modulates the current flow. Nowadays transistors are essential components and building blocks for electrical circuits and are present in every ICU (integrated circuit unit). The first transistor was developed in 1947 at Bells Lab by the physicists John Bardeen, Walter Brattain, and William Shockley, whose resulted in a Nobel prize in 1956⁶². In their first prototype (fig. 6a) they developed a point-contact transistor (bipolar junction transistor) using germanium as semiconducting material on a metal base and two gold contacts on a triangular support to contact the channel. A more recent alternative to the bipolar junction device is the field effect transistor (FET). FET geometry includes the familiar three electrodes: source and drain electrodes in contact with the semiconductor, and a gate electrode separated by an insulator to modulate the current in the channel (fig. 6b).

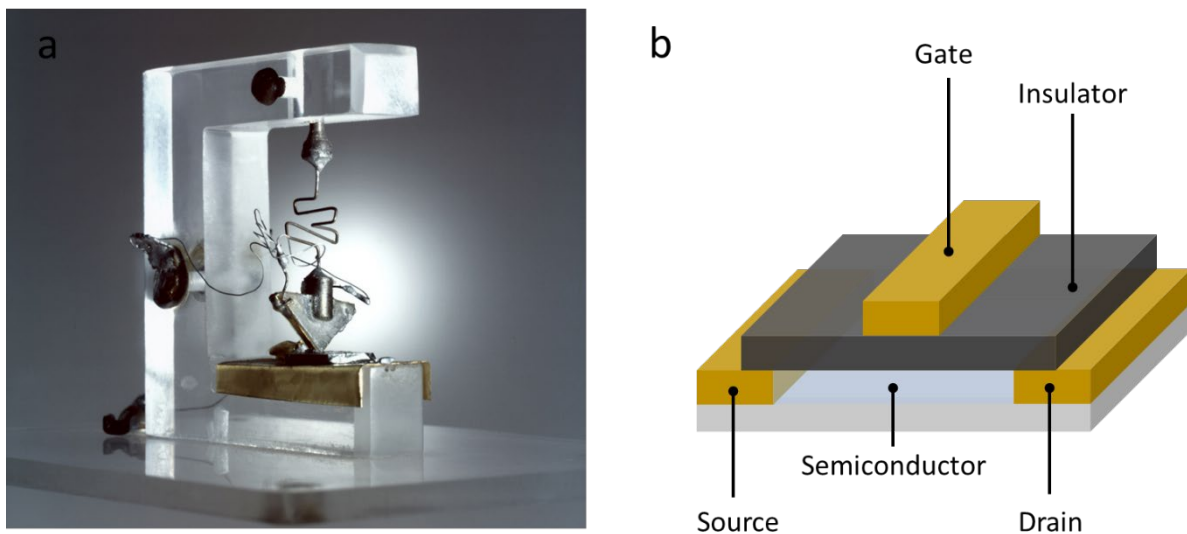


Figure 6: a) Reproduction of the first transistor, based on germanium as semiconducting material, made in 1947 by Jhon Bardeen, Walter Brattain and William Shockley. b) Schematic of a Field Effect Transistor (FET), presenting Source and Drain electrode in contact with the semiconductor and the Gate electrode on top of the insulating material.

FET devices didn't successfully perform until 1957, when the engineer Mohamed Atalla, studying the semiconducting properties of silicon, had the brilliant idea to passivate the surface with a layer of silicon oxide⁶³. This step overcame the problem related to the surface barrier that was preventing the electric field to influence the active material and thus introduced the metal-oxide-semiconductor field-effect transistor (MOSFET). MOSFETs were also the first miniaturised transistors compatible with a production process that was suitable for large scale, opening the way to high density integrated

circuits. Transistors can be used for various purposes including logic gates in digital circuits or as amplifiers. Since the aim of the thesis is to take advantage of the transistors' amplification property, we will not go deeper into their logic switching mechanisms.

3.3 Organic based transistors

Organic transistors share the same working principle as their inorganic counterparts. They are three electrode devices, in which the semiconducting material is represented by an organic polymer or molecule. The source and drain electrodes are connected to each other through a layer of OSC, while the gate electrode couples to the OSC through a dielectric which can be solid or liquid. In the case of an organic field effect transistor (OFET), the gate is separated from the channel by a thin layer of dielectric material (fig. 7a). The charge accumulation and current modulation in the channel is driven by the field effect, generated in the insulating material by the applied voltage at the gate electrode⁶⁴.

In some cases organic transistors operate with an electrolyte as the dielectric between gate and OSC, exploiting the mobile ions as charges to induce a field effect. In this configuration the gate can modulate the current in the channel through an electrolyte, which not only can be represented by a buffer solution, but also by complex biological fluids. The ion interaction with the OSC defines two different kinds of organic transistors: the electrolyte-gated field effect transistor (EGOFET)⁶⁵ and the organic electrochemical transistor (OECT)⁶⁶.

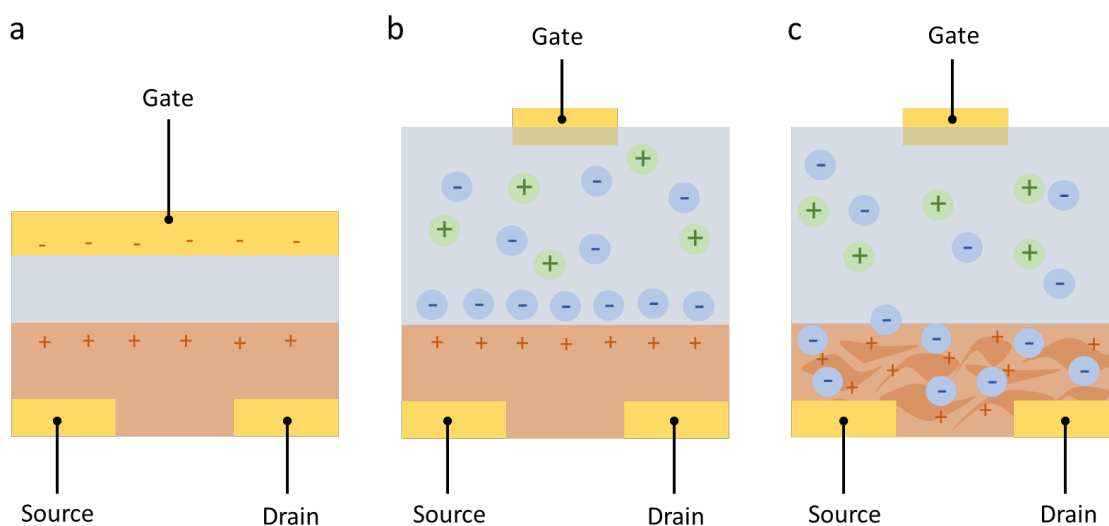


Figure 7: Schematic representations of organic transistors. a) OFET geometry presenting a solid dielectric material (blue) separating the organic polymer in the channel and the top gate electrode. b) EGOFET geometry presenting a solution as dielectric to separate the gate electrode and the conducting polymer. Upon bias application, ions migrate at the interface semiconductor/electrolyte, creating an electrical double layer. c) OECT geometry presenting a solution as dielectric to separate the gate electrode and the conducting polymer. In contrast to EGOFET, upon bias application, ions migrate inside the bulk of the conducting polymer.

The first demonstration of an EGOFET (water-gated) was reported by Kergoat *et al.* in 2010 using rubrene and poly(3-hexylthiophene) (P3HT) as organic materials⁶⁷. More generally, EGOFETs present

an organic semiconductor in the channel which is impermeable to ions (fig 7b). Therefore a voltage applied between gate and source (V_{GS}) induces the formation of electrical double layers (EDLs) at the gate/electrolyte and semiconductor/electrolyte interfaces. This process will dope/dedope the semiconducting polymer in the channel, modulating charges in proximity of the EDL, and thus modulating the current between source and drain (I_{DS}). The EDL is composed by the compact Helmholtz layer, made by a single row of solvated ions and a diffuse layer, and it can be compared to a capacitor⁶⁵. Because the capacitance is inversely proportional to the thickness and the double layer is extremely small, EGOFETs display very high capacitance, therefore they have the possibility to be operated at potentials below 1 V, showing significant advantages such as biological compatibility⁶⁸ and low-power consumption⁶⁵.

The OECT, in contrast with the EGOFET, presents a permeable polymer as semiconducting material in the channel. A voltage applied between source and gate drives the ions from the electrolyte inside the polymer matrix, consequently modulating the current in the channel (fig. 7c). The first OECT was described in 1980 by Wrighton *et al.*⁶⁹ using polypyrrole as OSC, but its popularity increased after some years when Andersson and Nilsson *et al.*⁷⁰ fabricated a device using PEDOT:PSS as active material. Up till now researchers have mainly exploited PEDOT:PSS as semiconducting polymer for many applications, but also focused their efforts in creating new geometries and finding new materials to optimise OECTs. As the name “electrochemical” suggests, the device operation is supposed to rely on Faradaic processes, involving reduction and oxidation of the conductive polymer. However, “electrochemical” may not be the best name, since some models describe the function as bulk capacitance rather than electrochemical changes of the channel material⁷¹. As recently proposed for a PEDOT:PSS based electrode, conductive polymers present a volumetric capacitance^{46,72}. PEDOT:PSS’s unique structure can be described by rich PSS regions carrying the fixed anions, and fewer PEDOT chains carrying the holes (fig. 5b). Upon bias application cations from the electrolyte are injected into the bulk of the polymer, and holes are extracted through the metal in contact with the polymer, decreasing their density. A capacitor is formed at the interface between the fixed sulfate moieties on the PSS chain and the injected cations, which present the same capacitance thickness described by the Helmholtz model in EGOFETs. Since the whole polymer contains many of these “sites” which are giving rise to capacitors, we can consider for some conductive polymer a capacitance which depends on the volume of the film⁷³. OECT can be based on p-type conducting polymers, such as PEDOT:PSS, or more challenging n-type conducting polymers, e.g., poly(benzimidazobenzophenanthroline) (BBL)⁷⁴ or NDI-T2⁷⁵. PEDOT:PSS is a p-type doped conductive polymer which presents mobile holes on the PEDOT backbone. The holes, compensated by the PSS fixed ionic charges, create a current flow in the channel upon bias application between source and drain. OECTs based on p-type polymers work in depletion

mode, meaning that without gate bias the current flows in the channel, creating an ON state. Upon positive gate bias application, cations in the electrolyte are injected into the polymeric matrix, compensating the fixed anions (PSS) and de-doping the channel. The decrease of compensating charges leads to a decrease of the number of holes and lower current values⁷⁶. On the contrary, n-type polymer based OECTs work in accumulation mode. Without gate bias there is no/limited current flow, creating an OFF state. Upon bias application ions are injected in the channel, accumulating opposite charges, which are responsible for the current when a voltage is applied between source and drain⁷⁶.

3.4 OECT device physics

The Bernards and Malliaras model⁷⁷ describes the OECT working mechanism dividing it into two circuits (fig. 8): (i) an electronic circuit, composed of a channel resistance, dependent on the voltages applied at the gate, and (ii) an ionic circuit, which describes electrical components in the solution. The channel resistance (R_{ch}) in the electronic circuit describes the charge flow between source and drain in accordance with Ohm's law and it varies with the charge amount accumulated into the porous channel. The ionic circuit is composed of the resistance of the electrolyte (R_e), representing ion movement, connected in series with two capacitances describing the ion storage at the gate (C_g) and in the channel (C_{ch}).

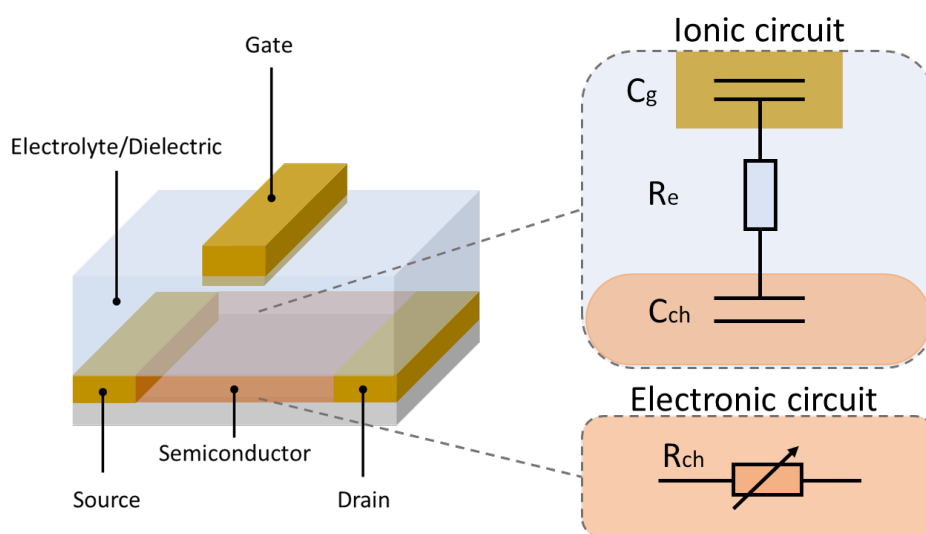


Figure 8: Schematic of an Organic Electrochemical Transistor (OECT) presenting a solution as dielectric material and a top gate electrode immersed into the electrolyte. The magnifications show the ionic circuit, composed by the gate and the channel capacitance in series with the electrolyte resistance and the electronic circuit of the channel, composed by a variable resistance.

OECTs can be mathematically described, relying on their similarity with MOSFETs. The current in the channel in the steady behaviour (not time dependent) can be described for two regimes: the linear regime (when V_{DS} is higher than $V_{GS}-V_T$) and the saturation regime (when V_{DS} is lower than $V_{GS}-V_T$).

$$I_{DS} = \mu C^* \frac{Wd}{L} \left(1 - \frac{V_{GS} - \frac{1}{2V_{DS}}}{V_T} \right) V_{DS}; \text{ linear regime} \quad (1)$$

$$I_{DS} = -\mu C^* \frac{Wd}{L} \frac{(V_{GS} - V_T)^2}{2V_T}; \text{ saturation regime} \quad (2)$$

Where I_{DS} is the current in the channel, μ is the charge mobility in the semiconductor, and C^* the volumetric capacitance. W , d , and L are the geometrical dimensions width, thickness, and length of the channel, respectively. V_{GS} is the gate voltage, V_{DS} the drain voltage, and V_T the threshold voltage, which is the voltage at which the device is in off-state and depends on capacitance and the intrinsic doping level of the polymer. The transconductance (g_m) is an important parameter to address in order to optimise an OECT and it is described by the equation:

$$g_m = \mu C^* \frac{Wd}{L} (V_T - V_{GS}) \quad (3)$$

The transconductance can be calculated from Eqns. 1 and 2 and is the derivative of the current in the channel with respect to the gate voltage. In OECTs, g_m scales with the channel dimension, and specifically with the thickness, in contrast with OFETs. This behaviour arises from the ionic charges penetrating the bulk of the polymer and not accumulating at the interface. Rivany *et al.* also demonstrated that g_m can be modulated (for fixed thickness) by increasing W/L ⁷⁸. Other parameters studied to optimise OECT devices are charge mobility μ and capacitance C^* , which are intrinsic to the semiconducting material⁷⁹.

OECTs have been fabricated using different geometries. In the bottom-contact configuration (BC), the conducting polymer is deposited on top of the substrate and S and D electrodes while the gate is separated from the channel by the electrolyte. In the top-contact (TC) configuration, the S and D electrodes are located on top of the channel, formed by the semiconducting polymer, while the gate electrode is in the same position as for the BC configuration. A vertical geometry for OECTs, similar to the OFET configuration, has been recently developed⁸⁰. The vertical position of the electrodes allows deposition of a thin layer of semiconducting polymer, reducing the length between source and drain and thus increasing transconductance. This type of OECT is mostly used for in vivo interfaces because of their smaller size and high signal amplification.

3.5 OECT as biosensor

OECTs offers a unique platform and an attractive tool for biosensing applications. The volumetric capacitance, arising from the ion penetration into the bulk of the polymeric channel, allows high signal amplification, and thus operation in low voltages regimes, preventing electrolysis and permitting low

power consumption⁸¹. Moreover, OECTs exhibit stability in aqueous environments, including body fluids, and allow easy functionalization strategies to interface living system, making them an appealing candidate for in vitro and in vivo applications⁸². OECT fabrication methods offer the possibility to fabricate them with low-cost printing techniques^{83,84} or with photolithography for more challenging applications^{22,32,33,85}. Moreover, they can be integrated with microfluidics⁸⁶, paving the way for lab-on-chip technologies. OECTs have been used for a broad range of biological applications, to record electrophysiological signals (e.g. electrocardiogram^{87,88} and electroencephalogram³²), as ion sensors^{89,90}, as enzymatic sensors^{54,86,91–93}, and immunosensors^{94–96}. OECTs as biosensors can be operated exploiting non-faradic or faradic reactions. The former is based on capacitive changes of the EDL at the gate electrode or at the channel that results in a minor/major ion electrostatic compensation and consequently a measurable current variation^{48,72}. On the contrary, in faradic processes, there is the presence of electrochemical reactions between the analyte in solution and the system. These reactions are called reduction (losing an electron) or oxidation (gaining an electron) and are involving electroactive molecules that can transfer electrons with the gate⁵³ or the channel material⁹¹ (a detailed description of electrochemical reactions is given in the experimental techniques).

Ions are the main contribution to the current modulation by the gate electrode through the electrolyte, thus their variation can affect the device properties, making OECT an ideal candidate for ion sensing. For the far more common p-type depletion mode OECT, increasing concentrations of ions induce higher ionic charge at the interface with the channel, de-doping more effectively the semiconducting polymer. Ions sensing with OECT based devices has been proved for various cations⁹⁷ and in combination with ion-selective membrane^{98,99}.

OECTs can interface with biology as enzymatic sensors, and for the past 15 years they have been integrated with various enzymatic units for the detection of various analytes, spanning from healthcare to agricultural applications. The working principle of an OECT-based enzymatic sensor relies on current variation caused by local pH changes¹⁰⁰, or electron transfer to gate electrode^{83,93,101,102} or channel⁹¹. OECT enzymatic sensing has been explained in detail for a (p-type) glucose sensor by Bernardis *et al.*¹⁰³ Enzymes can catabolise substrates into electrochemically active products and enable redox reactions at the gate electrode (fig. 9a). When the product of the reaction is oxidised at the electrode there is a current decrease in the channel, due to the semiconductor de-doping. In order to understand the physical process happening in the device we need to compare it with conventional electrochemistry, where the analyte detection is manifested in potential changes at the working electrode. In the OECT the electrolyte potential is determined by the capacitance at the electrode/electrolyte and channel/electrolyte interfaces (region 1). The addition of the analyte in the solution leads to electrons exchange with the gate electrode producing a potential drop at the interface (fig. 9b). Since the

potential at the gate electrode is fixed, the change happens in the electrolyte potential (region 2), causing consequently a current variation in the channel.

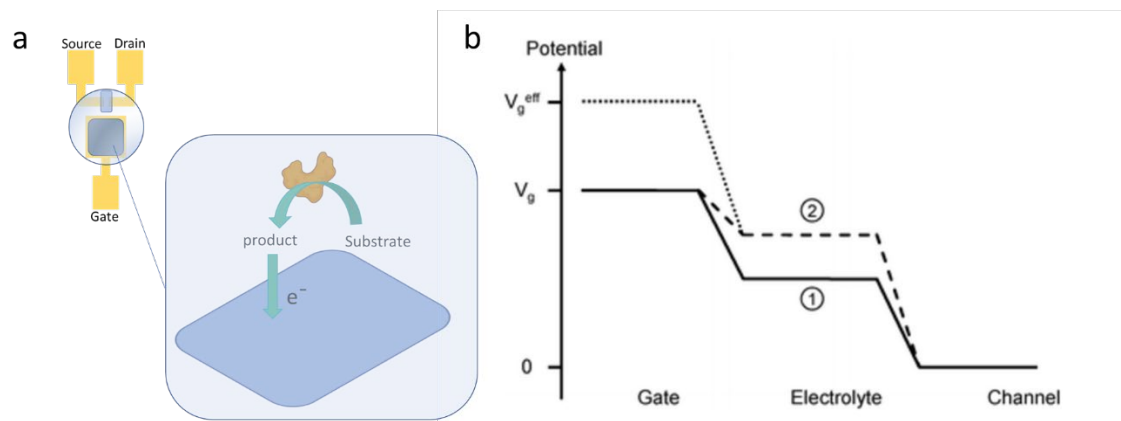


Figure 9: a) Representation of an enzymatic based OEET, presenting an enzymatic unit at the gate electrode, that in the presence of the specific substrate undergoes redox reaction. b) Potential representations for the OEET gate/electrolyte and channel/electrolyte interfaces in the absence (1) and in the presence (2) of the enzymatic substrate.

The proper enzymatic biosensor design includes geometry and functionalization optimisation. Enzymatic sensing is affected by geometrical factors and Cicoira *et al.*¹⁰⁴ demonstrated that the sensitivity for an OEET peroxide sensor increased as the gate electrode dimensions decreased. The explanation comes from the potential drop at the two interfaces (fig. 9b). For large gate, the potential drop at the gate/electrolyte interface is minimum, thus its variations are affecting less the electrolyte potential, when compared to small gate area. On the contrary, a small gate electrode induces larger current variations and should be preferable for developing enzymatic sensors. Modifications of the OEET electrode can also enhance the sensitivity. For example, deposition of nanoparticles^{92,105} or carbon nanotubes¹⁰⁶ can offer catalytic properties or easy functionalization surfaces to detect the analyte of interest. The enzymic units can be immobilised at the electrode surface, with chemical modification^{82,107} or entrapped in biocompatible membranes^{53,108,109}, which can also offer additional filtering and enhance the biosensor specificity^{84,110}.

OEETs have also been shown as effective platforms for immunosensors and nucleotide detection. Potential shifts happening at the gate electrode or in the channel can affect the semiconductor doping process and therefore be detected. When no redox reaction is involved with the addition of the analyte, the detection method relies purely on capacitive changes, and is considered non-faradic. OEET based immunosensors have been designed using various sensing units such as antibodies^{51,94–96}, oligonucleotide strands^{111,112}, or membranes¹¹³.

Biosensors, including OEETs, require biorecognition elements to selectively detect an analyte in solution. In biological processes, the interaction between proteins and molecules forms the basis of such selectivity. Enzymes have evolved in nature to selectively catabolise specific substrates and are

thus used to design biosensors for the detection of specific metabolites. Likewise, antibodies (Abs) are proteins from the immune system able to recognise and bind external factors with high selectivity and specificity. For these characteristics they are the most used and studied proteins for molecular recognition in bioelectronic devices. Abs are the gold standard for diagnostic assays (such as enzyme-linked immunosorbent assay, ELISA); however, they present some disadvantages, such as batch-to-batch variability, low long-term stability, and difficult chemical modifications¹¹⁴. Engineered recognition elements are rapidly emerging as a solution to overcome Abs' limitations and are based on protein or oligonucleotide scaffolds. Aptamers, in particular, are oligonucleotide-based recognition elements which present high selectivity, facility of synthesis, and low-cost development¹¹⁵. These probes are designed from scratch through a technique called systematic evolution of ligand by exponential enrichment (SELEX)¹¹⁶. The SELEX method first selects an oligonucleotide sequence able to bind the target molecule, then amplifies it to enrich the nucleotide pool. Aptamers have already been successfully employed in many biosensing platforms, including electrochemical biosensors¹¹⁷, immunoassays¹¹⁸, and OECT-based biosensors^{119,120}.

3.6 OECT for *in vitro/in vivo* applications

OECTs have been coupled with living cells, from mammal to plant, as powerful tools to study electrical properties or for monitoring physiological processes. Since the current in the channel is strongly dependent on ion movement, OECTs have been used to monitor tissue integrity of living cells *in vitro*^{48,68}. OECT devices have also proven to be a versatile tool for drug screening^{121,122}, to record action potentials from cardiomyocytes with high spatiotemporal resolution^{123,124}, to monitor cellular health¹²⁵ and after functionalization to record metabolite export in real-time⁹².

Implantable devices are gaining a lot of attention as powerful tools to record physiological processes in living organisms, revealing biological insight and allowing an overall investigation of the biological systems. Traditionally, *in vivo* recordings are performed with non-conformable apparatus, using rigid metal electrodes and probes or disruptive methods that create tissue damage and potentially alter local physiological processes^{126,127}. On the other hand, OECTs are proving their versatility for *in vivo* recording because of their unique characteristics. OECT based devices can be fabricated on ultra-thin or flexible substrates³², they can be miniaturised with high signal amplification, and they ensure high signal-to-noise ratio (SNR)⁷⁶. OECTs fabricated on flexible substrates have been used to record electrocardiography (ECG)^{87,128}, electrooculography (EOG)¹²⁹, and electroencephalography (EEG)^{32,88,130,131}. In parallel, ultra-thin OECTs with a more rigid encapsulation have been used to interface with the brain³³ or record neurotransmitters²¹. The integration of electronics, specifically OECTs, with the plant world is revealing a broad range of applications, from energy harvesting to plant physiology recording. In the first example, Stavrinidou *et al.* design an electronic circuit in a living rose,

featuring OECTs as one of the main components¹³². In other cases, OECTs were interfaced with plants to record ion variations^{133–135} or metabolites¹⁰⁸.

4. CLINICAL BIOMARKERS

The OECT-based biosensors presented in this thesis were validated for the detection of biomarkers that are relevant for healthcare and agricultural applications, thus showing their high potential as a proper sensing platform. We developed sensors towards different analytes, ranging from small molecules to proteins.

4.2 Urea

Urea is the end product of protein catabolism; it is a small molecule (fig. 10a) that derives from amino acid deamination and ammonia conversion. Physiologically, it is dissolved in the blood and expelled by the kidney in the urine. Commonly, urea is measured in the blood as Blood Urea Nitrogen (BUN), or in the urine as a test for glomerular filtration. Urea, together with creatinine, is associated with various pathologies including chronic kidney disease (CKD), acute kidney injury (AKI), and kidney stones¹³⁶. In comparison with physiological concentration of urea in blood (5-10 mM), in CKD patients urea levels can increase up to 50-70 mM, making it a useful biomarker for diagnosis. Urea, as clinical analyte, is generally measured with a multistep enzymatic method that involves urea hydrolysis (fig. 10b) and ammonium quantification with dye indicator¹³⁶. Urea can also serve as an environmental biomarker to monitor water pollution¹³⁷, and its levels are also controlled for prevention of food (e.g. milk) adulteration¹³⁸.

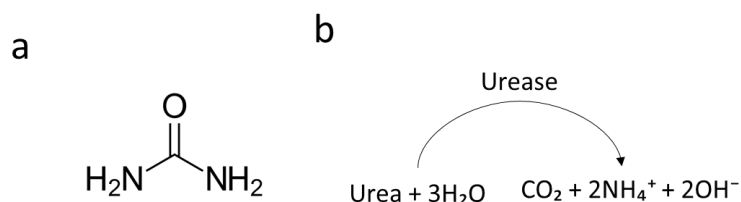


Figure 10: a) Urea molecular structure, b) Urea hydrolysis reaction by the enzyme urease.

4.3 Uric Acid

Uric acid (UA) is the end product of purine catabolism (fig. 11a). The human body lacks the enzyme Urate Oxidase, necessary to metabolise UA, hence the metabolite is dissolved in the blood and expelled in the urine. Uric acid levels can be monitored to check for wound infections, because it can reveal the presence of bacteria in the exudate, therefore a possible bacterial contamination. UA is physiologically present in the wound exudate, under the form of Urate in concentrations that vary between 220-750 μM ¹⁰¹. Some bacteria normally present on the skin can colonise the open tissue and give rise to infection. These bacteria, such as *P. aeruginosa*, can metabolise UA, decreasing its concentration in the wound exudate below 100 μM and making it an effective biomarker for wound infection. Abnormal UA levels in blood (higher than 400 μM) are also associated with bad nutrition

(excessive purine intake) and metabolic disorders¹³⁹. These conditions are leading to gout and urate crystals precipitation in joints or other tissues, inducing inflammation. The gold standard techniques for UA detection are a colorimetric assay based on the reduction of the chromogen sodium tungstate and an enzymatic assay (fig. 11b) coupled to Uv-vis absorption spectroscopy¹⁴⁰.

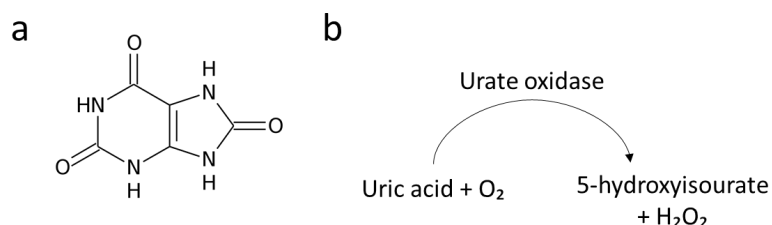


Figure 11: a) Uric acid molecular structure. b) Uric acid catabolism by the enzyme urate oxidase

4.4 Interleukin 6

Interleukin 6 (IL6) is a multifunctional cytokine synthesised by a diverse class of cells, including mononuclear phagocytes, fibroblasts, and vascular endothelial cells. IL6 is a low molecular weight protein of 21kDa with an isoelectric point is 6.17, thus presenting an overall negative charge at physiological pH (fig. 12). IL6 has a pleiotropic effect, and it is involved in different pathways, from the immune reaction activation to the haematopoiesis¹⁴¹. IL6 is a pro-inflammatory agent, responsible for the acute phase response and an anti-inflammatory agent, inhibiting other cytokine releases¹⁴². Physiologically, IL6 is present in serum in femtomolar concentrations spanning from 100 to 200fM¹⁴³. Increased levels of IL6 are associated with infection, tissue damage, and many chronic pathological states, such as cancer¹⁴⁴, chronic inflammation, and inflammaging¹⁴⁵. Recently, IL6 received a lot of attention because high levels (>3.5 pM) of this cytokine have been correlated with severe Covid-19 infection and respiratory failure¹⁴⁶. Cytokine detection and quantification are essential for precise monitoring of various diseases and because of their extremely low concentrations in bodily fluids, they require highly sensitive and selective detection methods. Typically, in clinical tests, cytokines are quantified using enzyme-linked immunosorbent assays (ELISA) and antibody arrays, both methods requiring specialised equipment and trained personnel¹⁴⁷.



Figure 12: Molecular structure of interleukin 6 (PBD:1IL6)

4.5 Glucose

Glucose is one of the most widely quantified and studied clinical biomarkers. Glucose is part of the class of carbohydrates as a monosaccharide¹⁴⁸ (fig. 13a). It is the main source of energy for cells, and it plays an important role in metabolism regulation. It is stored in the form of glycogen in mammals as an energy reserve¹⁴⁸. Glucose is used as the main biomarker to diagnose and monitor diabetes, a metabolic disease that affects 9,8% of the world population¹⁴⁹. Diabetes is a long-term pathology derived from abnormal levels of insulin in the body¹⁵⁰. Insulin is a hormone produced by the pancreatic cells that daily regulates the glucose levels in the blood, allowing its absorption for energetic demands. Because of these daily insulin variations, glucose is a biomarker that needs to be detected and quantified regularly, for this reason, many methods have been developed to assist diabetic patients with portable glucose sensors¹⁵⁰. Commonly, glucose detection devices require a drop of blood (invasive methods) for the electrochemical detection of molecular oxygen, released as a result of the glucose catabolism by the enzyme Glucose oxidase (GOx)¹⁵⁰ (fig. 13b). Glucose detection can also help to anticipate epileptic seizures, due to sudden glucose concentration decrease for dysregulated metabolism in some parts of the brain¹⁵¹. Glucose is the main energy source not only of the animal kingdom but also in the plant world¹⁵². In contrast to mammals, which need to get glucose from external sources, plants can convert solar energy into chemical energy via photosynthetic process. During daytime, the plant stores the excess of sugars in starch granules in chloroplasts, while during night-time it is used as metabolic support^{152,153}. Glucose also is an important signalling molecule in plants and is related to metabolism, stress responses, and growth¹⁵⁴, thus providing useful insight in plant physiology for agricultural applications.

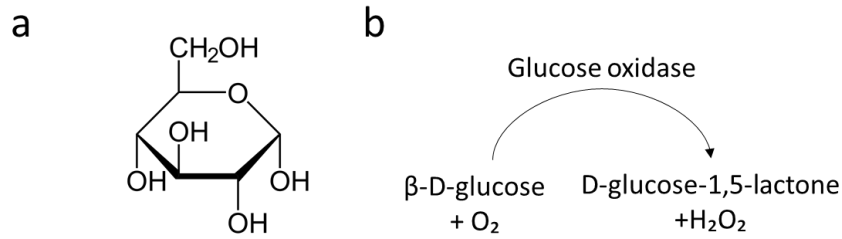


Figure 13: a) Glucose molecular structure. b) Glucose catabolism by the enzyme glucose oxidase

4.6 Sucrose

Sugars, especially glucose and sucrose, are responsible for plant metabolism, cell signalling, and carbon allocation¹⁵⁵. In several tree species, sucrose is the main form of transported carbon because it is an efficient energy storage molecule, it is soluble in water, and it is not as highly reactive as glucose¹⁵⁶. In plants, sucrose (fig. 14a) is transported mostly in the phloem and in minor quantity within the xylem transpiration stream¹⁵⁷. Understanding metabolic pathways of sugars and their regulation can provide new biological insights into plant physiology. In order to address these questions, researchers need methods with high spatial and temporal resolution and real-time quantification. Sugar analysis in plants is commonly performed by invasive methods that imply the disposal of the organism or tissue after sample collection¹⁵⁸. Once collected, the sample is typically analysed using enzymatic assays (fig. 14b), mass spectrometry, or high-performance liquid chromatography to quantify sugars levels.

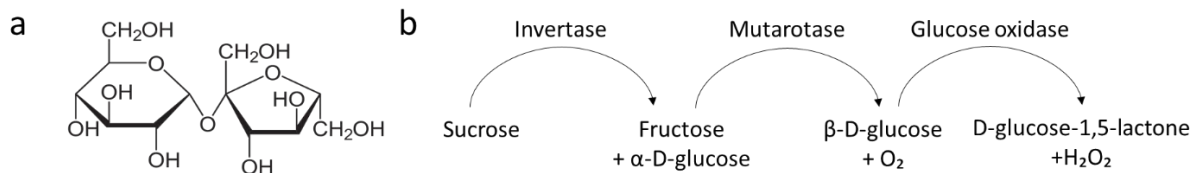


Figure 14: a) Sucrose molecular structure, composed by a molecule of glucose and fructose. b) Sucrose conversion till peroxide by three enzymatic units: Invertase, Mutarotase and Glucose Oxidase.

5. EXPERIMENTAL TECHNIQUES

5.2 Physical vapour deposition

Surfaces of non-conductive materials such as glass or plastic can be made electrically conductive depositing on their surface a thin layer of metal, using a technique called Physical Vapour Deposition (PVD). PVD exploits the metal phase transition from solid to vapour and its deposition on a substrate, due to condensation. The PVD requires high vacuum to ensure a uniform film growth and to facilitate the vapour phase. The vapour phase can be achieved by thermally treating the metal in the chamber or through electron sputtering¹⁴². In thermal evaporation, materials to be evaporated are placed on specific holding boats or around resistive wires that are exposed to high direct current to increase the temperature and allow the material evaporation¹⁴³. The material deposition rate is controlled by adjusting the current passing through the holding boat and it is measured thanks to a quartz crystal microbalance. During the process, the material condenses both on the substrate and the crystal surface, allowing one to control the thickness and the growing rate of the film. In this thesis, PDV has been used to evaporate thin layers of chromium and gold on PEN substrates in order to fabricate OECT.

5.3 Spin coating

Spin coating is a technique used to deposit a thin and uniform layer of soluble material on a solid substrate. A small amount of solution is drop casted in the center of the wafer, which undergoes fast rotation to uniformly spread the material all over the surface. Different thicknesses can be achieved using different spinning velocities and solution viscosities; the higher is the angular speed of the rotation the thinner the film. The solvents used are usually volatile and they partially evaporate during the spinning, leaving a solid material on the surface which can be further baked. In this thesis, spin coating technique has been used during the microfabrication process to deposit semiconducting polymer, photoresist and resist.

5.4 Photolithography

Photolithography is a process used to transfer a geometrical pattern to a substrate exploiting UV light. The process is commonly used in microfabrication because it allows to pattern geometries with nm resolution. It requires specific photomask and photoresist which are sensitive to light. Photoresists can be positive or negative; in the first case the resist that is exposed to light becomes soluble to a developer, creating on the substrate the same geometry present on the mask. In the case of negative photoresist, the portion exposed to the light undergoes cross-linking becoming insoluble to the developer and producing the negative image of the mask on the substrate. Subsequently, the developed substrate is subject to an etching process, which can be chemical or physical, depending on the material to be patterned. Chemical or wet etching uses solvents that can solubilise the uncovered

material and remove it from the surface. Physical etching, typically used to remove polymer, is a process that uses reactive ions to bombard the uncovered surface of the wafer. As a last step, the remaining resist is stripped away using the appropriate solvent and the substrate can be further processed with new layers. The photolithographic process as shown in figure 15 can be summarised by these steps:

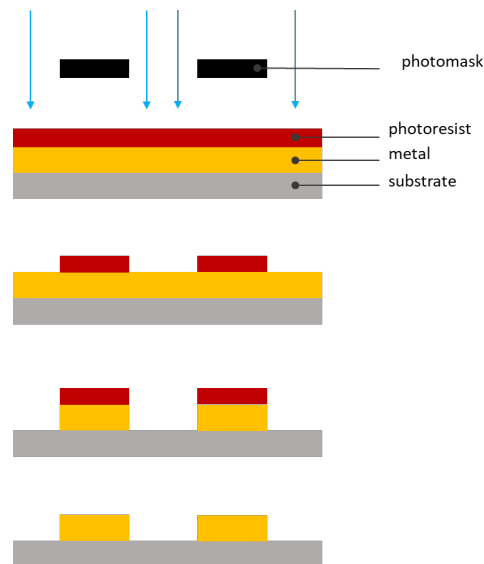


Figure 15: Schematic of photolithographic gold patterning using a positive photoresist.

- 1) The wafer surface is carefully cleaned and dried to remove any particles which could lead to uneven photoresist deposition.
- 2) The resist material is spin-coated on the metal surface with a specific thickness and is baked to remove the remaining solvent.
- 3) The substrate is exposed to UV light through a photomask.
- 4) The photoresist exposed to UV light is removed using a developer reagent.
- 5) The underlying material is chemically or physically etched.
- 6) The remaining photoresist is stripped away chemically.

In this thesis, photolithography has been used for the fabrication of OECTs on PEN substrates. In particular, the gold and chromium layers were chemically etched, while the PEDOT:PSS was physically etched using O_2 and CF_4 reactive plasma. The substrate was subsequently encapsulated using SU-8 2010.

5.5 Printing

Organic semiconductors are soluble in water or organic solvents, enabling their use in printing processes. Screen printing is a low-cost technique to pattern layers of organic or inorganic material in the form of inks on different substrates, including plastic and paper. This technique enables high

volume and large-scale production, and the possibility to print on flexible substrate. The screen-printing process necessitates a frame that presents a screen mesh with the pattern to be printed, and a squeegee that presses the ink through the mesh till the substrate (fig. 16). Using-screen printing technique it is possible to achieve a resolution of 75 μm and a minimum thickness of $1\mu\text{m}$ ¹⁴⁴. After the printing process the substrate is usually thermally cured, before proceeding with new layers. In this thesis, screen-printing technique had been used to fabricate OECT device with PEDOT:PSS as semiconducting material.

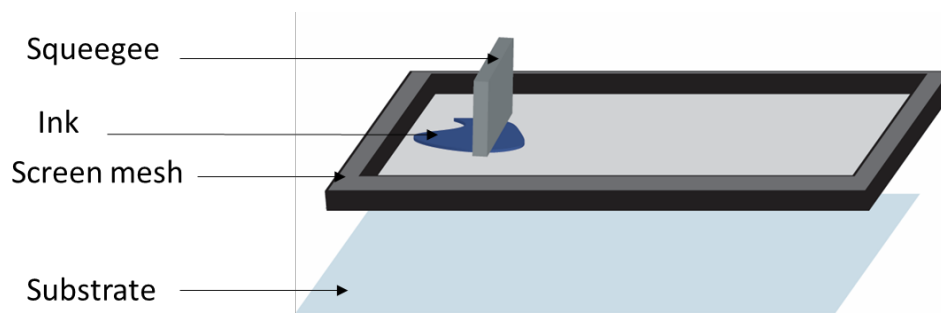


Figure 16: Schematic representation of screen-printing process. The ink is deposited on the screen and pushed through the mesh, transferring a specific pattern on the substrate.

5.6 Functionalization

Functionalization is a surface modification to enable interaction between the electronic interface with the biological surrounding. It includes processes to entrap or bind biological molecules that can respond to the analyte in solution. Biocompatible materials such as chitosan, gelatin or nafion are mostly used to entrap enzymatic units because they provide a stable and porous environment. Moreover, biological units such as antibody or oligonucleotide strands can be attached to a substrate through chemical reactions on bare surfaces or on substrates previously modified using a self-assembly monolayer (SAM). The functionalization strategies used in this thesis include enzyme entrapment in chitosan and porcine derived gelatines and thiol bonding between oligonucleotide strands and AuNPs.

5.7 Electrochemical deposition

Electrochemical deposition is a process used to cover a conducting surface with a layer of a different material, present in solution. Electrochemical deposition requires an electrochemical cell and involves electron transfer from/to electrodes to create layers or nanostructures. In the electrochemical cell two electrodes, an anode and a cathode are immersed in a solution containing the ionic compound of the material to deposit. When a potential is applied, positive ions migrate to the cathode and get reduced, accepting electrons, while negative ions travel to the anode getting oxidized. The potential applied determines the rate at which electrons are exchanged and can affect the morphology of the materials. Electrochemical deposition can be used to polymerize monomers, present in solution, and create

conductive material. For example, EDOT in poly(styrene sulfonate) solution can be oxidised to produce radical cations that will react with each other creating a film of PEDOT:PSS on the electrode¹⁴⁵. In a similar way, metals can be deposited and shaped in nanostructures applying a potential to create a nucleation process that allows the formation of nanoparticles¹⁴⁶. In this thesis, electrochemical deposition has been used to deposit a platinum layer on a printed OECT carbon gate electrode and to deposit AuNPs and PtNPs on a PEDOT:PSS gate electrode.

5.8 Cyclic Voltammetry

Cyclic voltammetry is a technique used to study the electrochemical properties of a system. It allows to characterize oxidation and reduction processes of species in solution and property of different electrode materials. The typical electrochemical set-up is composed of a Working Electrode (WE), a Reference Electrode (RE) and a Counter Electrode (CE) (fig. 17a). The WE is used to study electrochemical events happening in the cell. It requires well defined geometry and a clean surface. The RE is used as a reference point against which the potential is applied at the WE and presents a stable equilibrium potential. The CE closes the circuit and allows a current flow between WE and CE. During cyclic voltammetry, a potential is applied from a potentiostat at the working electrode, changing its energy level and allowing electron transfer between electrode and electroactive species in solution or immobilized on a surface. The plot in figure 17b is called voltammogram and represents the typical “duck shape” of a redox reaction. The applied potential is represented on the X-axis, while the current passing at the WE is represented on the Y-axis. The electrode is scanned forward from negative to positive potentials, giving an anodic current, then reversely from positive to negative, recording a cathodic current. The peaks present in the voltammogram represent the oxidation peak in the anodic current region and the reduction peak in the cathodic one. These peaks are the result of electron transfer between species in solution and the WE¹⁴⁷.

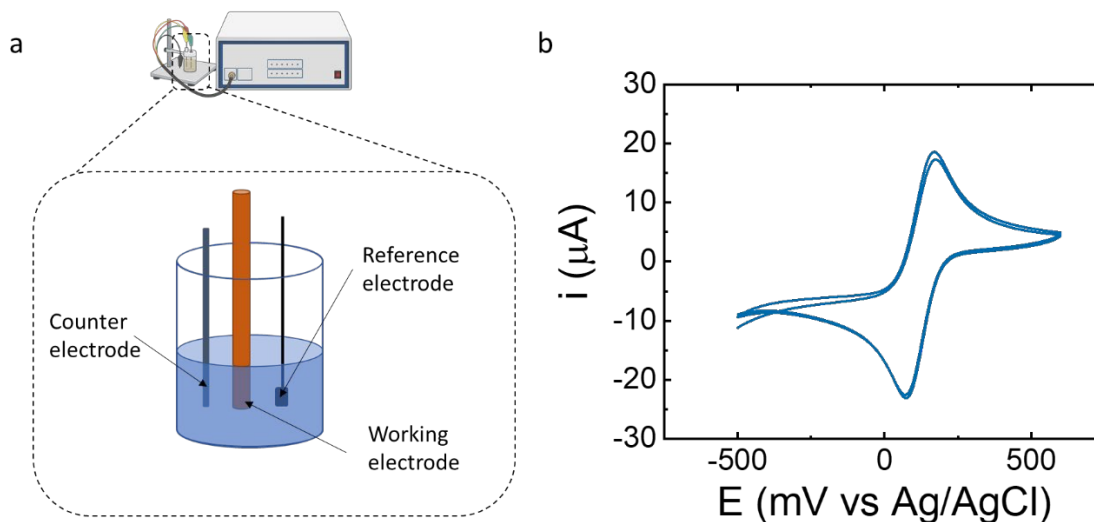


Figure 17: a) Potentiostat connected to an electrochemical cell. The magnification shows the set up to perform a cyclic voltammetry, composed by a working electrode (orange) a reference electrode (black) and a counter electrode (grey). b) Cyclic voltammety curve for a reversible redox reaction.

An electroactive specie in solution presents an equilibrium state between reduced and oxidated states, described by the Nerst equation:

$$E = E^0 + \frac{RT}{nF} \ln \frac{(Ox)}{(Red)}$$

Where E is the potential of the electrochemical cell, E^0 is the standard potential of the species in solution, R and F are the universal gas and Faraday constant, respectively, n is the number of electrons exchanged, T is the Temperature and (Ox) and (Red) are the concentrations of the oxidized and reduced species, respectively. The typical “duck shape” of a cyclic voltammetry derives from the diffusion of the species from the bulk to the electrode. When the electrode is scanned forward the anodic current starts to increase, as a consequence of the oxidation of the electroactive species near the electrode surface. The current reaches the maximum point (peak anodic current) when the species reaches the electrode also from the bulk via diffusion. The potential increase produces high quantity of oxidised species next to the electrode, creating a layer that slows down the diffusion of reduced specie from the bulk, thus producing the current decrease. When the final potential is reached, the electrode is scanned reversely, and the cathodic current shows the reduction peak. From the voltammogram, it is possible to study the reversibility of the process, the number of oxidation states and electrode surface properties (such as capacitance). In this thesis, Cyclic Voltammetry has been used to control the AuNPs deposition on the PEDOT:PSS gate electrode.

5.9 Electrochemical Impedance Spectroscopy

Electrochemical Impedance Spectroscopy (EIS) is a widely employed technique that allows to study electrical component of a system, including surface and bulk properties. Compared to other electrochemical techniques, which study steady-state of electrodes, the EIS allows separation of events on a time scale, because of the application of alternate current or voltage¹⁴⁸. Because of these features, EIS represents a valuable method to study surface modifications, such as biomolecule immobilisation and binding events. Electrical Impedance describes the resistance of electron flow, recorded applying alternate potentials of small amplitude and recording a current with a phase shift (fig. 18). Impedance Z is the ratio between the voltage $V(t)$ and a phase shifted current $I(t)$ as a function of time:

$$Z = \frac{V(t)}{I(t)} = \frac{V_0 \sin(\omega t)}{I_0 \sin(\omega t + \varphi)}$$

$$\omega = 2\pi f$$

where V_0 and I_0 are the voltage and current amplitude respectively, ω is the angular directly proportional to the frequency f , t is the time and φ is the phase shift. As showed in figure 18, Impedance Z can be represented as function of the real impedance Z' and the imaginary impedance Z'' by the modulus $|Z|$ and the phase shift ϕ .

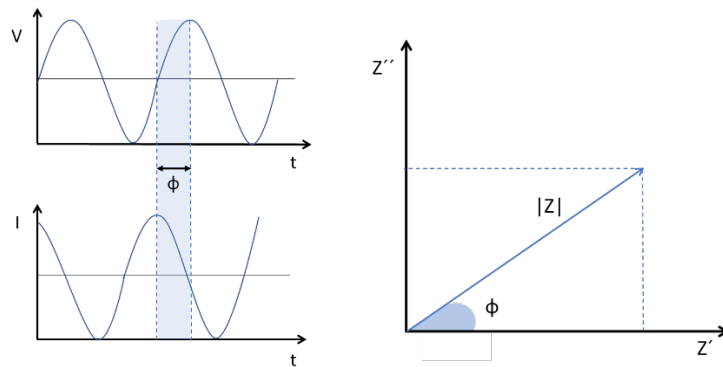


Figure 18: Diagram showing the phase shift between the voltage and the current in function of time. Impedance as complex value in a Z'' and Z' plot, given by the modulus $|Z|$ and the phase angle ϕ .

The term spectroscopy derives from the application of different frequencies to measure an impedance spectrum that allows to study many system parameters. Impedance can be displayed using two different plots: Bode plot, where $|Z|$ and ϕ are plotted as a function of $\log f$ and the Nyquist plot which depicts Z'' and Z' on y and x-axis respectively. In order to extract parameters that describe the system, the Impedance spectra is often interpreted in terms of an equivalent circuit. The most common and simplistic circuit that describes the system is called Randles circuit (fig. 19) which consists in a solution resistance (R_s), in series with other elements, such as a Capacitance (C_{dl}) which describe the Electrical

Double layer at the electrode interface, a charge transfer resistance (R_{ct}) and the Warburg element (W) to describe the diffusion.

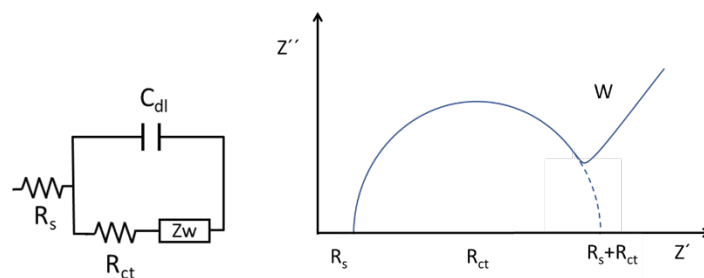


Figure 19: Randles equivalent circuit of a simple electrode in contact with an electrolyte. The C_{dl} describes the charge at the electrode/electrolyte interface, R_s is the resistance of the solution, R_{ct} is the resistance to transfer of charge from the solution to the electrode (redox reaction) and the Warburg impedance to describe the diffusion from the bulk to the electrode surface. The Nyquist plot displays Z'' vs Z' and allows the extraction of the system parameters.

EIS can be used for analytical applications to detect molecules in the bulk. Biomolecules can be immobilised at the surface of the electrode to detect biological events, such as antibody-antigen binding. Commonly a small redox molecule, like ferrocyanide $[Fe(CN)_6]^{4-}$, is added in the solution together with the analyte. When the electrode surface is modified with molecules or sensing units the charge transfer resistance term, that is related to ET processes involving the small redox probe in solution, increases because the redox molecules are impeded from reacting with the electrode. When an analyte in solution binds a sensing element immobilised on the surface, it is possible to observe a further increase in R_{ct} , therefore binding events can be detected following the behaviour of the charge transfer resistance. Alternately they can be detected following C_{dl} variations. Molecules present at the surface can induce changes in the thickness and in the charge of the electrical double layer.¹⁴⁹ In this thesis, EIS has been used to study the functionalization and the analyte binding of the AuNPs/PEDOT:PSS gate electrode.

5.10 Scanning electron microscopy

The optical microscope is a powerful tool to study surface modifications. However, light diffraction limits the resolution of this technique. Higher resolution can be obtained using Scanning Electron Microscopy (SEM). SEM takes advantage of accelerated electrons to achieve a shorter wavelength, compared to visible photons, and a better resolution. SEM represents an advanced tool to study surfaces and sample features. The sample is scanned by an electron beam in a high vacuum environment. The sample surface sends signals back to a detector which can describe the morphology, the topography and the composition of the analyzed area with a spatial resolution of 1 nm. The sample needs to be electrically conductive and grounded to avoid surface charge accumulation, which may lead to artefacts and poor resolution. The SEM working principle relies on the interaction between the electrons from the beam

and the sample. This interaction can be elastic and non-elastic. The non-elastic interaction occurs when an incoming electron (from the beam) collides with the electric field of the sample atom, resulting in an electron expulsion from the valence band and X-ray radiation emission. This electron, called Secondary Electron (SE), presents low energy and comes from the sample regions closer to the surface, generating the topographical image. Elastic interactions instead represent collisions where the incoming electron deflect back from deeper region of the sample. This electron is called Back Scattered Electron (BSE) and presents a different direction, but a similar energy. SE, BSE and X-ray are detected from specific detectors to form an image and provide useful insight about sample composition and morphology. In this thesis SEM has been used to study the morphology of the PEDOT:PSS gate electrode modified with AuNPs.

5.11 Fourier transform Infrared spectroscopy

Matter interacts with the whole electromagnetic spectrum, from the gamma ray to X-ray and specific wavelengths can be used to study its composition. The Fourier Transform Infrared Spectroscopy (FTIR) uses the infrared region IR ($4000 - 600 \text{ cm}^{-1}$) to gain useful information. The sample is irradiated with an IR beam recording the molecular absorption by functional groups. Molecular bonds which present a dipole are responding to infrared radiations, because of their natural vibrational frequencies. When these bonds interact with IR, they increase vibration and oscillation intensity absorbing specific wavelength radiations. The radiations are collected by a detector to create an interferogram and subsequently translated to a spectrum using the Fast Fourier Transform function. An IR spectrum plots the light intensity versus the wavenumber (cm^{-1}), measuring the amount of light absorbed by each different functional group at specific wavelength. The absorbance spectrum is calculated as:

$$A = \log \left(\frac{I_0}{I} \right)$$

Where A is the absorbance, I_0 is spectrum background intensity, and I is the sample intensity spectrum. The sample preparation for this technique is essential. Since plastic and glass can absorb the IR radiations in high quantity, the cell for the measurement is made of ionic material such as potassium bromide (KBr). To overcome some limitations of the traditional FTIR, the Attenuated Total Reflection ATR can be used. In this set up, sample does not require any preparation and measurements are achieved fast without interruption. The ATR uses a crystal, most commonly made of zinc selenide (ZnSe), on which the IR ray hits with a 45° angle, and it is reflected to the interface between the crystal surface and the sample. This generates evanescent waves which undergo numerous internal reflections and get attenuated where the sample absorb energy. The IR beam then exit the crystal and is collected by the detector. In this thesis the FTIR has been used to ensure the presence of oligonucleotide strands on the AuNPs/PEDOT:PSS gate electrode.

5.12 Electrical measurements

Source Measure Units (SMUs) are instrument used to record the OECT electrical characteristics and measure the biosensor detection range. SMUs are able to supply a potential to the system in analysis, while measuring a current. Characterization of a transistor can be achieved by collecting transfer and the output curves. The transfer curve (fig. 20a) is measured by keeping the voltage between source and drain fixed and sweeping the voltage at the gate electrode. The output characteristics is obtained by sweeping the voltage between source and drain at a fixed gate voltage (fig. 20b).

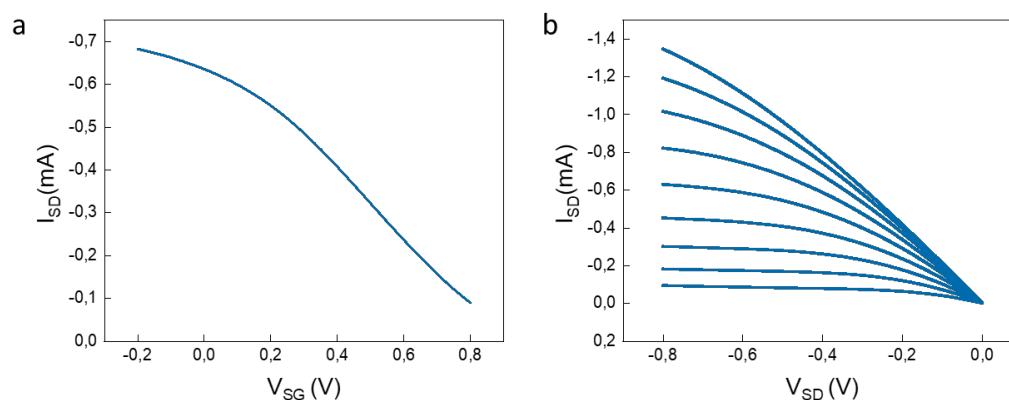


Figure 20: a) PEDOT:PSS transfer characteristic obtain keeping fixed the voltage between source and drain at -0.3V and sweeping the gate voltage from -0.2V to 0.8V. (b) OECT output characteristic obtain sweeping the source drain voltage from 0V to -0.8V for different gate voltages.

To prove the sensitivity and the range of detection of an OECT biosensor transfer characteristics are often used. The transfer characteristics are firstly performed in a control buffer until stabilisation, then the gate electrode is incubated with increasing analyte concentrations and recorded until further current stabilisation. Alternatively, both the voltage between source and drain and the gate voltage can be kept constant, and the drain current can be measured as a function of time. The current is continuously recorded and increasing or decreasing concentration of the analyte are consecutively added to the sensing area. In this thesis electrical measurements have been used to assess the analyte sensing of the OECT, *in vivo* and *in vitro*.

5.13 Green house

Plants are grown inside a greenhouse to monitor and keep constant the growing conditions. The greenhouse provides a well define photoperiodic condition and a controlled humidity. In this thesis the greenhouse has been used to growth the Tobacco plants and the Poplar trees for the *in vitro* and *in vivo* experiment.

6. SUMMARY OF PAPERS

6.2 Paper I

Label free urea biosensor based on organic electrochemical transistors.

In this paper we developed a biosensor for the detection of urea. Urea is an important biomarker not only in medical diagnosis, where it is an indicator of kidney and liver dysfunction, but also in food safety and environmental control. We demonstrated a urea biosensor using the enzymatic unit urease entrapped in a gelatin hydrogel, onto a fully printed PEDOT:PSS-based organic electrochemical transistor (OECT). We showed a response against increasing urea concentration in phosphate saline buffer (PBS), with a limit of detection as low $1 \mu\text{M}$ and a time of response of 2-3 minutes. The sensing mechanism relies on the modulation of the channel conductivity induced by the ionic species that are produced from the urea hydrolysis. We fabricated the OECTs using screen-printing technique on flexible substrates to ensure a significant reduction in manufacturing time and costs making these enzymatic OECT-based biosensors as appealing candidates for monitoring of urea levels at the point-of-care or in the field.

Contribution: device printing, device characterization

6.3 Paper II

Flexible Printed Organic Electrochemical Transistors for the Detection of Uric Acid in Artificial Wound Exudate.

In this paper we developed a low-cost sensor, that can provide real-time monitoring of wound infection. The sensing platform can be used as a tool to improve chronic wounds management, at the hospital and at home. In particular we used a printed organic electrochemical transistors (OECT) biosensor for monitoring the analyte uric acid (UA), which is correlated to bacterial infection in wounds, and we demonstrated its detection properties using artificial wound exudate. We developed the biosensor exploiting the enzymatic catalysis of UA to 5-hydroxyisourate, by Uricase. We entrapped the enzyme in a dual-ionic-layer hydrogel membrane onto the gate to ensure selectivity. This dual membrane can filter and hinder possible interference analytes that will lead to nonspecific faradic reactions, for example, the direct oxidation of UA. The biosensor showed a reproducible response in phosphate buffer saline and in complex solutions mimicking the wound exudate with a high sensitivity for the pathological levels of UA in wounds ($<200 \mu\text{M}$) and exhibited a limit of detection of $4.5 \mu\text{M}$ in artificial wound exudate.

Contribution: experimental and device design, master student experiment supervision, manuscript writing.

6.4 Paper III

Organic electrochemical transistor-based aptasensor for interleukin-6 label-free detection.

In this paper we developed an OECT based biosensor for the detection of interleukin 6 (IL6), an important biomarker associated to various pathological processes, including chronic inflammation, inflammaging, cancer and severe COVID-19 infection. We ensured the selectivity of the biosensor against IL6 using aptamers as sensing units, engineered oligonucleotide strands, able to bind specifically the cytokine of interest. We developed an easy functionalization method based on gold nanoparticles deposition onto the PEDOT:PSS gate electrode for the subsequential electrodeposition of the thiolate aptamers. We proved a detection range from picomolar to nanomolar concentrations for IL6 and the selectivity of the device when compared to the detection of Tumor Necrosis Factor (TNF), an analogous cytokine whose levels are also high in inflammatory processes.

Contribution: major contribution in the experimental part including microfabrication, measurements, data analysis and manuscript writing.

6.5 Paper IV

Real-Time Monitoring of Glucose Export from Isolated Chloroplasts Using an Organic Electrochemical Transistor.

In this paper we reported a biosensor based on organic electrochemical transistors (OECT) as an useful devices for real-time monitoring of plant biological processes. OECTs can interface directly with the electrolyte enabling the detection of biological events and at the same time, providing a fast and amplified signal. So far, these devices have mainly been applied to cells or body fluids for the development of clinical tools to use in diagnostic. We showed a first and direct detection of biomolecules from organelles using an OECT glucose sensor applied to chloroplasts, which are the plant organelles responsible for the light-to-chemical energy conversion of the photosynthesis. We proved real-time monitoring of the exportation of glucose for two distinct metabolic phases (day-time and night-time) and we quantified the dynamic exportation with a time resolution of 1 min, demonstrating a dynamics an order of magnitude better than conventional methods.

Contribution: major contribution in the experimental part including microfabrication, measurements, data analysis and manuscript writing.

6.6 Paper V

Diurnal in vivo xylem sap glucose and sucrose monitoring using implantable organic electrochemical transistor sensors.

In this paper we described the first-ever demonstration of a molecule detection through an enzyme reaction chain and the first-ever direct sensing inside biological tissue via implantable organic electrochemical transistor. We showed for the first time an OECT-based sucrose and glucose sensor directly implanted into the xylem tissue of poplar trees (*Populus tremula x tremuloides*), a tissue responsible for transpiration. We report a real-time, *in-vivo* monitoring of sucrose and glucose variations over 48 hours. We demonstrate that the OECT sensor can operate in in-vivo environment, and that it can detect important biological metabolites directly from the tissue of interest, monitoring relevant biological event over time. As a demonstration of the proof-of-concept and the kind of biological insights this new technology enables, we observed previously uncharacterized diurnal changes in sucrose levels in the xylem sap. Our technology outperforms conventional methods, making it an attractive tool for studying biological processes in general, without interfering with the system physiology.

Contribution: major contribution in the experimental part including microfabrication, measurements, data analysis and manuscript writing.

7. CONCLUSION AND OUTLOOK

This thesis provides a description of organic based biosensors, developed using organic electrochemical transistors as the sensing platform, for the detection of five different analytes relevant for both medical and environmental applications. We focused on developing functionalization strategies to transform OECTs in selective sensors for specific analytes and we prove their detection in complex media and in *in vivo* system. We used two fabrication methods to develop the OECT based biosensors: a cost-effective method, using screen-printing techniques in order to have disposable and portable devices for home care or in-field applications, and an ad hoc design, using microfabrication techniques for more selective targets. We studied various factors and functionalities of the OECT to optimize the functionalization method and the sensing range, achieving highly effective biosensors for all the applications.

Looking forward, we continue working on developing innovative enzymatic detection methods exploiting the properties of specific enzymes to enable direct electron transfer (DET) together with novel conductive materials that can be polymerized through biological reactions. DET can open major advantages in biosensor development, such as the absence of toxic mediators or toxic byproducts, and the operation at voltages close to zero, which avoids undesirable parasitic redox reactions and enables an even lower power consumption¹⁶⁷. DET based biosensors have the potential to become a candidate for *in vivo* applications. However they present many challenges regarding functionalization and enzyme optimization¹⁶⁸. I believe OECTs and organic based devices, because of their fabrication techniques, materials, and operating conditions are promising platforms for personalized systems for molecular diagnostic. However, the OECT sensors require standardization and enhanced reliability before they can become point-of-care system or wearable devices. Moreover, they will require integration with e.g., microfluidic systems, integrated circuit, and portable power supplies for their use as wearable/implantable devices.

8. REFERENCES

1. Bhalla, N., Jolly, P., Formisano, N. & Estrela, P. Introduction to biosensors. *Essays Biochem.* **60**, 1–8 (2016).
2. Damborský, P., Švitel, J. & Katrlík, J. Optical biosensors. *Essays Biochem.* **60**, 91–100 (2016).
3. Estevez, M.-C., Otte, M. A., Sepulveda, B. & Lechuga, L. M. Trends and challenges of refractometric nanoplasmonic biosensors: A review. *Anal. Chim. Acta* **806**, 55–73 (2014).
4. Anker, J. N. *et al.* Biosensing with plasmonic nanosensors. *Nature Materials* vol. 7 442–453 (2008).
5. Mosier-Boss, P. A. Review of SERS substrates for chemical sensing. *Nanomaterials* **7**, 142 (2017).
6. CHRISTOPOULOS, T. K. & DIAMANDIS, E. P. 14 - FLUORESCENCE IMMUNOASSAYS. in (eds. Diamandis, E. P. & Christopoulos, T. K. B. T.-I.) 309–335 (Academic Press, 1996). doi:<https://doi.org/10.1016/B978-012214730-2/50015-7>.
7. Ronkainen, N. J., Halsall, H. B. & Heineman, W. R. Electrochemical biosensors. *Chem. Soc. Rev.* **39**, 1747–1763 (2010).
8. Nabaei, V., Chandrawati, R. & Heidari, H. Magnetic biosensors: Modelling and simulation. *Biosens. Bioelectron.* **103**, 69–86 (2018).
9. Pohanka, M. Overview of Piezoelectric Biosensors, Immunosensors and DNA Sensors and Their Applications. *Mater. (Basel, Switzerland)* **11**, 448 (2018).
10. Heineman, W. R. & Jensen, W. B. Leland c. clark jr.(1918–2005). *Biosens. Bioelectron.* **8**, 1403–1404 (2006).
11. Guilbault, G. G. & Montalvo, J. G. Urea-specific enzyme electrode. *J. Am. Chem. Soc.* **91**, 2164–2165 (1969).
12. Aizawa, M., Morioka, A. & Suzuki, S. An enzyme immunosensor for the electrochemical determination of the tumor antigen α -fetoprotein. *Anal. Chim. Acta* **115**, 61–67 (1980).
13. Liedberg, B., Nylander, C. & Lunström, I. Surface plasmon resonance for gas detection and biosensing. *Sensors and actuators* **4**, 299–304 (1983).
14. Jason-Moller, L., Murphy, M. & Bruno, J. Overview of Biacore systems and their applications. *Curr. Protoc. protein Sci.* **45**, 13–19 (2006).
15. Thorp, H. H. Cutting out the middleman: DNA biosensors based on electrochemical oxidation. *Trends Biotechnol.* **16**, 117–121 (1998).
16. Lee, S. H., Sung, J. H. & Park, T. H. Nanomaterial-based biosensor as an emerging tool for biomedical applications. *Ann. Biomed. Eng.* **40**, 1384–1397 (2012).
17. Zheng, G., Patolsky, F., Cui, Y., Wang, W. U. & Lieber, C. M. Multiplexed electrical detection of cancer markers with nanowire sensor arrays. *Nat. Biotechnol.* **23**, 1294–1301 (2005).
18. Parlak, O., Keene, S. T., Marais, A., Curto, V. F. & Salleo, A. Molecularly selective nanoporous membrane-based wearable organic electrochemical device for noninvasive cortisol sensing. *Sci. Adv.* **4**, (2018).
19. Keum, D. H. *et al.* Wireless smart contact lens for diabetic diagnosis and therapy. *Sci. Adv.* **6**,

- eaba3252 (2020).
20. Xu, L. *et al.* 3D multifunctional integumentary membranes for spatiotemporal cardiac measurements and stimulation across the entire epicardium. *Nat. Commun.* **5**, 3329 (2014).
 21. Xie, K. *et al.* Organic electrochemical transistor arrays for real-time mapping of evoked neurotransmitter release in vivo. *Elife* **9**, e50345 (2020).
 22. Diacci, C. *et al.* Diurnal in vivo xylem sap glucose and sucrose monitoring using implantable organic electrochemical transistor sensors. *iScience* **24**, (2021).
 23. Newman-Toker, D. E., McDonald, K. M. & Meltzer, D. O. How much diagnostic safety can we afford, and how should we decide? A health economics perspective. *BMJ Qual. & Saf.* **22**, ii11 LP-ii20 (2013).
 24. Ukhurebor, K. The Role of Biosensor in Climate Smart Organic Agriculture toward Agricultural and Environmental Sustainability. in 1–16 (2020). doi:10.5772/intechopen.93150.
 25. Arora, N. K. Impact of climate change on agriculture production and its sustainable solutions. (2019).
 26. Lequin, R. M. Enzyme Immunoassay (EIA)/Enzyme-Linked Immunosorbent Assay (ELISA). *Clin. Chem.* **51**, 2415–2418 (2005).
 27. Glish, G. L. & Vachet, R. W. The basics of mass spectrometry in the twenty-first century. *Nat. Rev. Drug Discov.* **2**, 140–150 (2003).
 28. Malviya, R., Bansal, V., Pal, O. & Sharma, P. High performance liquid chromatography: A short review. *J. Glob. Pharma Technol.* **2**, 22–26 (2010).
 29. Balasubramanian, K. & Burghard, M. Biosensors based on carbon nanotubes. *Anal. Bioanal. Chem.* **385**, 452–468 (2006).
 30. Pingarrón, J. M., Yanez-Sedeno, P. & González-Cortés, A. Gold nanoparticle-based electrochemical biosensors. *Electrochim. Acta* **53**, 5848–5866 (2008).
 31. Lee, W. *et al.* Transparent, conformable, active multielectrode array using organic electrochemical transistors. *Proc. Natl. Acad. Sci.* **114**, 10554–10559 (2017).
 32. Spyropoulos, G. D., Gelinas, J. N. & Khodagholy, D. Internal ion-gated organic electrochemical transistor: A building block for integrated bioelectronics. *Sci. Adv.* **5**, eaau7378 (2019).
 33. Williamson, A. *et al.* Localized Neuron Stimulation with Organic Electrochemical Transistors on Delaminating Depth Probes. *Adv. Mater.* **27**, 4405–4410 (2015).
 34. Mitzi, D. B., Chondroudis, K. & Kagan, C. R. Organic-inorganic electronics. *IBM J. Res. Dev.* **45**, 29–45 (2001).
 35. Fahlman, M. *et al.* Interfaces in organic electronics. *Nat. Rev. Mater.* **4**, 627–650 (2019).
 36. Plieth, W. 11 - Intrinsically Conducting Polymers. in (ed. Plieth, W. B. T.-E. for M. S.) 323–363 (Elsevier, 2008). doi:https://doi.org/10.1016/B978-044452792-9.50013-0.
 37. Bässler, H. & Köhler, A. Charge transport in organic semiconductors. *Unimolecular Supramol. Electron.* **1** 1–65 (2011).
 38. 1 The Electronic Structure of Organic Semiconductors 1.1. (2015).
 39. Bresadola, M. Medicine and science in the life of Luigi Galvani (1737–1798). *Brain Res. Bull.* **46**, 367–380 (1998).

40. Cohen-Karni, T., Langer, R. & Kohane, D. S. The smartest materials: the future of nanoelectronics in medicine. *ACS Nano* **6**, 6541–6545 (2012).
41. Birmingham, K. *et al.* Bioelectronic medicines: a research roadmap. *Nat. Rev. Drug Discov.* **13**, 399–400 (2014).
42. Song, Y., Min, J. & Gao, W. Wearable and implantable electronics: moving toward precision therapy. *ACS Nano* **13**, 12280–12286 (2019).
43. Simon, D. T., Gabrielsson, E. O., Tybrandt, K. & Berggren, M. Organic Bioelectronics: Bridging the Signaling Gap between Biology and Technology. *Chemical Reviews* vol. 116 13009–13041 (2016).
44. Rivnay, J., Owens, R. M. & Malliaras, G. G. The rise of organic bioelectronics. *Chem. Mater.* **26**, 679–685 (2014).
45. Rivnay, J. *et al.* Structural control of mixed ionic and electronic transport in conducting polymers. *Nat. Commun.* **7**, 11287 (2016).
46. Volkov, A. V. *et al.* Understanding the Capacitance of PEDOT:PSS. *Adv. Funct. Mater.* **27**, 1–10 (2017).
47. Khodagholy, D. *et al.* NeuroGrid: Recording action potentials from the surface of the brain. *Nat. Neurosci.* **18**, 310–315 (2015).
48. Jimison, L. H. *et al.* Measurement of Barrier Tissue Integrity with an Organic Electrochemical Transistor. *Adv. Mater.* **24**, 5919–5923 (2012).
49. Herland, A. *et al.* Electrochemical control of growth factor presentation to steer neural stem cell differentiation. *Angew. Chemie - Int. Ed.* **50**, 12529–12533 (2011).
50. Lin, P., Yan, F., Yu, J., Chan, H. L. W. & Yang, M. The Application of Organic Electrochemical Transistors in Cell-Based Biosensors. *Adv. Mater.* **22**, 3655–3660 (2010).
51. Decataldo, F. *et al.* BMP-2 functionalized PEDOT:PSS-based OECTs for stem cell osteogenic differentiation monitoring. *Flex. Print. Electron.* **4**, (2019).
52. Curto, V. F. *et al.* Organic transistor platform with integrated microfluidics for in-line multi-parametric in vitro cell monitoring. *Microsystems Nanoeng.* **3**, 1–12 (2017).
53. Diacci, C. *et al.* Real-Time Monitoring of Glucose Export from Isolated Chloroplasts Using an Organic Electrochemical Transistor. *Adv. Mater. Technol.* **5**, (2020).
54. Strakosas, X. *et al.* Catalytically enhanced organic transistors for in vitro toxicology monitoring through hydrogel entrapment of enzymes. *J. Appl. Polym. Sci.* **134**, 1–7 (2017).
55. Arbring Sjöström, T. *et al.* A Decade of Iontronic Delivery Devices. *Adv. Mater. Technol.* **3**, (2018).
56. Klauk, H. *Organic electronics: materials, manufacturing, and applications.* (John Wiley & Sons, 2006).
57. Zschieschang, U. & Klauk, H. Organic transistors on paper: a brief review. *J. Mater. Chem. C* **7**, 5522–5533 (2019).
58. Dufil, G. *et al.* Enzyme-assisted in vivo polymerisation of conjugated oligomer based conductors. *J. Mater. Chem. B* **8**, 4221–4227 (2020).
59. Stavrinidou, E. *et al.* In vivo polymerization and manufacturing of wires and supercapacitors in

- plants. *Proc. Natl. Acad. Sci. U. S. A.* **114**, 2807–2812 (2017).
60. Liu, J. *et al.* Genetically targeted chemical assembly of functional materials in living cells, tissues, and animals. *Science (80-.)*. **367**, 1372–1376 (2020).
 61. Mantione, D. *et al.* Thiophene-Based Trimers for In Vivo Electronic Functionalization of Tissues. *ACS Appl. Electron. Mater.* **2**, 4065–4071 (2020).
 62. Ross, I. M. The invention of the transistor. *Proc. IEEE* **86**, 7–28 (1998).
 63. Arns, R. G. The other transistor: early history of the metal-oxide semiconductor field-effect transistor. *Eng. Sci. Educ. J.* **7**, 233–240 (1998).
 64. Lamport, Z. A., Haneef, H. F., Anand, S., Waldrip, M. & Jurchescu, O. D. Tutorial: Organic field-effect transistors: Materials, structure and operation. *J. Appl. Phys.* **124**, 71101 (2018).
 65. Kergoat, L., Piro, B., Berggren, M., Horowitz, G. & Pham, M. C. Advances in organic transistor-based biosensors: From organic electrochemical transistors to electrolyte-gated organic field-effect transistors. *Anal. Bioanal. Chem.* **402**, 1813–1826 (2012).
 66. Rivnay, J. *et al.* Organic electrochemical transistors. *Nat. Rev. Mater.* **3**, (2018).
 67. Kergoat, L. *et al.* A Water-Gate Organic Field-Effect Transistor. *Adv. Mater.* **22**, 2565–2569 (2010).
 68. Spanu, A., Martines, L. & Bonfiglio, A. Interfacing cells with organic transistors: a review of in vitro and in vivo applications. *Lab Chip* **21**, 795–820 (2021).
 69. White, H. S., Kittlesen, G. P. & Wrighton, M. S. Chemical derivatization of an array of three gold microelectrodes with polypyrrole: fabrication of a molecule-based transistor. *J. Am. Chem. Soc.* **106**, 5375–5377 (1984).
 70. Andersson, P. *et al.* Active Matrix Displays Based on All-Organic Electrochemical Smart Pixels Printed on Paper. *Adv. Mater.* **14**, 1460–1464 (2002).
 71. Berggren, M. & Malliaras, G. G. How conducting polymer electrodes operate. *Science (80-.)*. **364**, 233 LP – 234 (2019).
 72. Proctor, C. M., Rivnay, J. & Malliaras, G. G. Understanding volumetric capacitance in conducting polymers. *J. Polym. Sci. Part B Polym. Phys.* **54**, 1433–1436 (2016).
 73. Bernard, C., Ghestem, A., Ismailova, E., Herve, T. & Malliaras, G. G. organic transistors. (2013) doi:10.1038/ncomms2573.
 74. Sun, H. *et al.* Complementary Logic Circuits Based on High-Performance n-Type Organic Electrochemical Transistors. *Adv. Mater.* **30**, 1704916 (2018).
 75. Kawan, M. *et al.* Monitoring supported lipid bilayers with n-type organic electrochemical transistors. *Mater. Horizons* **7**, 2348–2358 (2020).
 76. Malliaras, G. G. *et al.* Organic electrochemical transistors. *Nat. Rev. Mater.* **3**, 17086 (2018).
 77. Bernards, D. A. & Malliaras, G. G. Steady-State and Transient Behavior of Organic Electrochemical Transistors. *Adv. Funct. Mater.* **17**, 3538–3544 (2007).
 78. Rivnay, J. *et al.* Organic Electrochemical Transistors with Maximum Transconductance at Zero Gate Bias. *Adv. Mater.* **25**, 7010–7014 (2013).
 79. Inal, S., Malliaras, G. G. & Rivnay, J. Benchmarking organic mixed conductors for transistors. *Nat. Commun.* **8**, 1767 (2017).

80. Donahue, M. J. *et al.* High-Performance Vertical Organic Electrochemical Transistors. *Adv. Mater.* **30**, 1705031 (2018).
81. Strakosas, X., Bongo, M. & Owens, R. M. The organic electrochemical transistor for biological applications. *J. Appl. Polym. Sci.* **132**, 1–14 (2015).
82. Strakosas, X., Wei, B., Martin, D. C. & Owens, R. M. Biofunctionalization of polydioxothiophene derivatives for biomedical applications. *J. Mater. Chem. B* **4**, 4952–4968 (2016).
83. Di Lauro, M. *et al.* Label free urea biosensor based on organic electrochemical transistors. *Flex. Print. Electron.* **3**, 024001 (2018).
84. Galliani, M. *et al.* Flexible Printed Organic Electrochemical Transistors for the Detection of Uric Acid in Artificial Wound Exudate. *Adv. Mater. Interfaces* (2020) doi:10.1002/admi.202001218.
85. Khodagholy, D. *et al.* High transconductance organic electrochemical transistors. *Nat. Commun.* **4**, 1–6 (2013).
86. Pappa, A. M. *et al.* Organic Transistor Arrays Integrated with Finger-Powered Microfluidics for Multianalyte Saliva Testing. *Adv. Healthc. Mater.* **5**, 2295–2302 (2016).
87. Campana, A., Cramer, T., Simon, D. T., Berggren, M. & Biscarini, F. Electrocardiographic recording with conformable organic electrochemical transistor fabricated on resorbable bioscaffold. *Adv. Mater.* **26**, 3874–3878 (2014).
88. Cea, C. *et al.* Enhancement-mode ion-based transistor as a comprehensive interface and real-time processing unit for in vivo electrophysiology. *Nat. Mater.* 1–8 (2020) doi:10.1038/s41563-020-0638-3.
89. Ghittorelli, M. *et al.* High-sensitivity ion detection at low voltages with current-driven organic electrochemical transistors. *Nat. Commun.* **9**, 1441 (2018).
90. Romele, P. *et al.* Multiscale real time and high sensitivity ion detection with complementary organic electrochemical transistors amplifier. *Nat. Commun.* **11**, 3743 (2020).
91. Pappa, A. M. *et al.* Direct metabolite detection with an n-type accumulation mode organic electrochemical transistor. *Sci. Adv.* **4**, 1–8 (2018).
92. Diacci, C. *et al.* Real-Time Monitoring of Glucose Export from Isolated Chloroplasts Using an Organic Electrochemical Transistor. *Adv. Mater. Technol.* **5**, (2020).
93. Khodagholy, D. *et al.* Organic electrochemical transistor incorporating an ionogel as a solid state electrolyte for lactate sensing. *J. Mater. Chem.* **22**, 4440–4443 (2012).
94. Macchia, E., Ghittorelli, M., Torricelli, F. & Torsi, L. Organic electrochemical transistor immuno-sensor operating at the femto-molar limit of detection. *Proc. - 2017 7th Int. Work. Adv. Sensors Interfaces, IWASI 2017* 68–72 (2017) doi:10.1109/IWASI.2017.7974217.
95. Gentili, D. *et al.* Integration of organic electrochemical transistors and immuno-affinity membranes for label-free detection of interleukin-6 in the physiological concentration range through antibody-antigen recognition. *J. Mater. Chem. B* **6**, 5400–5406 (2018).
96. Kim, D. J. *et al.* Organic electrochemical transistor based immunosensor for prostate specific antigen (PSA) detection using gold nanoparticles for signal amplification. *Biosens. Bioelectron.* **25**, 2477–2482 (2010).
97. Lin, P., Yan, F. & Chan, H. L. W. Ion-Sensitive Properties of Organic Electrochemical Transistors. *ACS Appl. Mater. Interfaces* **2**, 1637–1641 (2010).

98. Sessolo, M., Rivnay, J., Bandiello, E., Malliaras, G. G. & Bolink, H. J. Ion-Selective Organic Electrochemical Transistors. 4803–4807 (2014) doi:10.1002/adma.201400731.
99. Han, S., Yamamoto, S., Polyravas, A. G. & Malliaras, G. G. Microfabricated Ion-Selective Transistors with Fast and Super-Nernstian Response. *Adv. Mater.* **32**, 2004790 (2020).
100. Nishizawa, M., Matsue, T. & Uchida, I. Penicillin sensor based on a microarray electrode coated with pH-responsive polypyrrole. *Anal. Chem.* **64**, 2642–2644 (1992).
101. Galliani, M. *et al.* Flexible Printed Organic Electrochemical Transistors for the Detection of Uric Acid in Artificial Wound Exudate. *Adv. Mater. Interfaces* **7**, 2001218 (2020).
102. Pappa, A. M. *et al.* Organic Transistor Arrays Integrated with Finger-Powered Microfluidics for Multianalyte Saliva Testing. *Adv. Healthc. Mater.* **5**, 2295–2302 (2016).
103. Bernards, D. A. *et al.* Enzymatic sensing with organic electrochemical transistors. *J. Mater. Chem.* **18**, 116–120 (2008).
104. Cicoira, F. *et al.* Influence of Device Geometry on Sensor Characteristics of Planar Organic Electrochemical Transistors. *Adv. Mater.* **22**, 1012–1016 (2010).
105. Kergoat, L. *et al.* Detection of glutamate and acetylcholine with organic electrochemical transistors based on conducting polymer/platinum nanoparticle composites. *Adv. Mater.* **26**, 5658–5664 (2014).
106. Mak, C. H. *et al.* Highly-sensitive epinephrine sensors based on organic electrochemical transistors with carbon nanomaterial modified gate electrodes. *J. Mater. Chem. C* **3**, 6532–6538 (2015).
107. Strakosas, X. *et al.* A facile biofunctionalisation route for solution processable conducting polymer devices. *J. Mater. Chem. B* **2**, 2537 (2014).
108. Diacci, C. *et al.* Diurnal in vivo xylem sap glucose and sucrose monitoring using implantable organic electrochemical transistor sensors. *iScience* **24**, 101966 (2021).
109. Berto, M. *et al.* Label free urea biosensor based on organic electrochemical transistors. *Flex. Print. Electron.* **3**, (2018).
110. Liao, C., Zhang, M., Niu, L., Zheng, Z. & Yan, F. Organic electrochemical transistors with graphene-modified gate electrodes for highly sensitive and selective dopamine sensors. *J. Mater. Chem. B* **2**, 191–200 (2014).
111. Tao, W. *et al.* A sensitive DNA sensor based on an organic electrochemical transistor using a peptide nucleic acid-modified nanoporous gold gate electrode. *RSC Adv.* **7**, 52118–52124 (2017).
112. Liao, C. & Yan, F. Organic Semiconductors in Organic Thin-Film Transistor-Based Chemical and Biological Sensors. *Polym. Rev.* **53**, 352–406 (2013).
113. Wustoni, S. *et al.* An organic electrochemical transistor integrated with a molecularly selective isoporous membrane for amyloid- β detection. *Biosens. Bioelectron.* **143**, 111561 (2019).
114. Škrlec, K., Štrukelj, B. & Berlec, A. Non-immunoglobulin scaffolds: a focus on their targets. *Trends Biotechnol.* **33**, 408–418 (2015).
115. Toh, S. Y., Citartan, M., Gopinath, S. C. B. & Tang, T.-H. Aptamers as a replacement for antibodies in enzyme-linked immunosorbent assay. *Biosens. Bioelectron.* **64**, 392–403 (2015).
116. Zhuo, Z. *et al.* Recent Advances in SELEX Technology and Aptamer Applications in

- Biomedicine. *International Journal of Molecular Sciences* vol. 18 (2017).
117. Feng, L., Chen, Y., Ren, J. & Qu, X. A graphene functionalized electrochemical aptasensor for selective label-free detection of cancer cells. *Biomaterials* **32**, 2930–2937 (2011).
 118. Nezlin, R. Use of aptamers in immunoassays. *Mol. Immunol.* **70**, 149–154 (2016).
 119. Saraf, N., Woods, E. R., Peppler, M. & Seal, S. Highly selective aptamer based organic electrochemical biosensor with pico-level detection. *Biosens. Bioelectron.* **117**, 40–46 (2018).
 120. Picomolar Detection of Epinephrine Using Aptamer Based Organic Electrochemical Transistor. *ECS Meet. Abstr.* (2018) doi:10.1149/ma2018-02/58/2129.
 121. Huerta, M., Rivnay, J., Ramuz, M., Hama, A. & Owens, R. M. Early Detection of Nephrotoxicity In Vitro Using a Transparent Conducting Polymer Device. *Appl. Vitro. Toxicol.* **2**, 17–25 (2016).
 122. Romeo, A. *et al.* Drug-induced cellular death dynamics monitored by a highly sensitive organic electrochemical system. *Biosens. & Bioelectron.* **68**, 791–797 (2015).
 123. Gu, X., Yao, C., Liu, Y. & Hsing, I.-M. 16-Channel Organic Electrochemical Transistor Array for In Vitro Conduction Mapping of Cardiac Action Potential. *Adv. Healthc. Mater.* **5**, 2345–2351 (2016).
 124. Yao, C., Li, Q., Guo, J., Yan, F. & Hsing, I. M. Rigid and flexible organic electrochemical transistor arrays for monitoring action potentials from electrogenic cells. *Adv. Healthc. Mater.* **4**, 528–533 (2015).
 125. Lin, B. P., Yan, F., Yu, J., Chan, H. L. W. & Yang, M. The Application of Organic Electrochemical Transistors in Cell-Based Biosensors. 3655–3660 (2010) doi:10.1002/adma.201000971.
 126. O’Connor, T. F., Rajan, K. M., Printz, A. D. & Lipomi, D. J. Toward organic electronics with properties inspired by biological tissue. *J. Mater. Chem. B* **3**, 4947–4952 (2015).
 127. Leccardi, M. J. I. A. & Ghezzi, D. Organic electronics for neuroprosthetics. *Healthc. Technol. Lett.* **7**, 52–57 (2020).
 128. Braendlein, M., Lonjaret, T., Leleux, P., Badier, J.-M. & Malliaras, G. G. Voltage Amplifier Based on Organic Electrochemical Transistor. *Adv. Sci.* **4**, 1600247 (2017).
 129. Leleux, P. *et al.* Organic Electrochemical Transistors for Clinical Applications. *Adv. Healthc. Mater.* **4**, 142–147 (2015).
 130. Rivnay, J. *et al.* High-performance transistors for bioelectronics through tuning of channel thickness. *Sci. Adv.* **1**, e1400251–e1400251 (2015).
 131. Dionne, K., Redfern, R. L., Nichols, J. J. & Nichols, K. K. Analysis of tear inflammatory mediators: A comparison between the microarray and Luminex methods. *Mol. Vis.* **22**, 177–88 (2016).
 132. Stavrinidou, E. *et al.* Electronic plants. *Sci. Adv.* **1**, (2015).
 133. Vurro, F. *et al.* Development of an in vivo sensor to monitor the effects of vapour pressure deficit (VPD) changes to improve water productivity in agriculture. *Sensors (Switzerland)* **19**, (2019).
 134. Coppedè, N. *et al.* An in vivo biosensing, biomimetic electrochemical transistor with applications in plant science and precision farming. *Sci. Rep.* **7**, 1–9 (2017).
 135. Janni, M. *et al.* In Vivo Phenotyping for the Early Detection of Drought Stress in Tomato .

- Plant Phenomics* **2019**, 1–10 (2019).
136. Salazar, J. H. Overview of urea and creatinine. *Lab. Med.* **45**, e19–e20 (2014).
 137. Tran, T. Q. N., Das, G. & Yoon, H. H. Nickel-metal organic framework/MWCNT composite electrode for non-enzymatic urea detection. *Sensors Actuators B Chem.* **243**, 78–83 (2017).
 138. Dhawan, G., Sumana, G. & Malhotra, B. D. Recent developments in urea biosensors. *Biochem. Eng. J.* **44**, 42–52 (2009).
 139. Cirillo, P. *et al.* Uric Acid, the Metabolic Syndrome, and Renal Disease. *J. Am. Soc. Nephrol.* **17**, S165 LP-S168 (2006).
 140. Barr, W. G. Barr WG. Uric Acid. In: Walker HK, Hall WD, Hurst JW, editors. *Clin. Methods Hist. Phys. Lab. Exam. 3rd Ed. Bost. Butterworths* Chapter 165 (1990).
 141. Damas, P. *et al.* Sepsis and serum cytokine concentrations. *Crit. Care Med.* **25**, (1997).
 142. Tanaka, T., Narazaki, M. & Kishimoto, T. IL-6 in inflammation, immunity, and disease. *Cold Spring Harb. Perspect. Biol.* **6**, a016295–a016295 (2014).
 143. Arican, O., Aral, M., Sasmaz, S. & Ciragil, P. Serum levels of TNF- α , IFN- γ , IL-6, IL-8, IL-12, IL-17, and IL-18 in patients with active psoriasis and correlation with disease severity. *Mediators Inflamm.* **2005**, 273–279 (2005).
 144. Kumari, N., Dwarakanath, B. S., Das, A. & Bhatt, A. N. Role of interleukin-6 in cancer progression and therapeutic resistance. *Tumor Biol.* **37**, 11553–11572 (2016).
 145. Pinti, M. *et al.* Aging of the immune system: Focus on inflammation and vaccination. *Eur. J. Immunol.* **46**, 2286–2301 (2016).
 146. Coomes, E. A. & Haghbayan, H. Interleukin-6 in Covid-19: A systematic review and meta-analysis. *Rev. Med. Virol.* **30**, e2141 (2020).
 147. Stenken, J. A. & Poschenrieder, A. J. Bioanalytical chemistry of cytokines - A review. *Analytica Chimica Acta* vol. 853 95–115 (2015).
 148. Kohlmeier, M. Glucose. in *Food Science and Technology* (ed. Kohlmeier, M. B. T.-N. M.) 193–210 (Academic Press, 2003). doi:<https://doi.org/10.1016/B978-012417762-8.50036-3>.
 149. Saeedi, P. *et al.* Global and regional diabetes prevalence estimates for 2019 and projections for 2030 and 2045: Results from the International Diabetes Federation Diabetes Atlas, 9th edition. *Diabetes Res. Clin. Pract.* **157**, 107843 (2019).
 150. Villena Gonzales, W., Mobashsher, A. T. & Abbosh, A. The Progress of Glucose Monitoring-A Review of Invasive to Minimally and Non-Invasive Techniques, Devices and Sensors. *Sensors (Basel)*. **19**, 800 (2019).
 151. Fei, Y., Shi, R., Song, Z. & Wu, J. Metabolic Control of Epilepsy: A Promising Therapeutic Target for Epilepsy. *Front. Neurol.* **11**, 1–16 (2020).
 152. Zeeman, S. C., Smith, S. M. & Smith, A. M. The diurnal metabolism of leaf starch. *Biochem. J.* **401**, 13–28 (2006).
 153. Neuhaus, H. E. & Schulte, N. Starch degradation in chloroplasts isolated from C3 or CAM (crassulacean acid metabolism)-induced *Mesembryanthemum crystallinum* L. *Biochem. J.* **318** (Pt 3, 945–953 (1996).
 154. Smeekens, S., Ma, J., Hanson, J. & Rolland, F. Sugar signals and molecular networks controlling

- plant growth. *Current Opinion in Plant Biology* vol. 13 273–278 (2010).
155. Ward, J. M., Kuhn, C., Tegeder, M. & Frommer, W. B. Sucrose Transport in Higher Plants. **178**, (1998).
 156. Farrar, J., Pollock, C. & Gallagher, J. Sucrose and the integration of metabolism in vascular plants. *Plant Sci.* **154**, 1–11 (2000).
 157. Mahboubi, A. & Niittylä, T. Sucrose transport and carbon fluxes during wood formation. *Physiol. Plant.* **164**, 67–81 (2018).
 158. Filip, M., Vlassa, M., Coman, V. & Halmagyi, A. Simultaneous determination of glucose, fructose, sucrose and sorbitol in the leaf and fruit peel of different apple cultivars by the HPLC-RI optimized method. *Food Chem.* **199**, 653–659 (2016).
 159. Pahade, V. S., Chavan, P. S. & Baisane, V. P. A review paper on Vapour deposition coating. *Int. J. Eng. Appl. Sci.* **3**, (2016).
 160. Bashir, A., Awan, T. I., Tehseen, A., Tahir, M. B. & Ijaz, M. Chapter 3 - Interfaces and surfaces. in (eds. Awan, T. I., Bashir, A. & Tehseen, A. B. T.-C. of N.) 51–87 (Elsevier, 2020). doi:<https://doi.org/10.1016/B978-0-12-818908-5.00003-2>.
 161. Parashkov, R., Becker, E., Riedl, T., Johannes, H.-H. & Kowalsky, W. Large area electronics using printing methods. *Proc. IEEE* **93**, 1321–1329 (2005).
 162. Benoudjit, A., Bader, M. M. & Wan Salim, W. W. A. Study of electropolymerized PEDOT:PSS transducers for application as electrochemical sensors in aqueous media. *Sens. Bio-Sensing Res.* **17**, 18–24 (2018).
 163. Tonelli, D., Scavetta, E. & Gualandi, I. Electrochemical Deposition of Nanomaterials for Electrochemical Sensing. *Sensors (Basel)*. **19**, 1186 (2019).
 164. Elgrishi, N. *et al.* A Practical Beginner’s Guide to Cyclic Voltammetry. *J. Chem. Educ.* **95**, 197–206 (2018).
 165. Lisdat, F. & Schäfer, D. The use of electrochemical impedance spectroscopy for biosensing. *Anal. Bioanal. Chem.* **391**, 1555–1567 (2008).
 166. Bertok, T. *et al.* Electrochemical Impedance Spectroscopy Based Biosensors: Mechanistic Principles, Analytical Examples and Challenges towards Commercialization for Assays of Protein Cancer Biomarkers. *ChemElectroChem* **6**, 989–1003 (2019).
 167. Bollella, P. & Katz, E. Enzyme-Based Biosensors: Tackling Electron Transfer Issues. *Sensors (Basel)*. **20**, 3517 (2020).
 168. Milton, R. D. & Minteer, S. D. Direct enzymatic bioelectrocatalysis: differentiating between myth and reality. *J. R. Soc. Interface* **14**, 20170253 (2017).

Paper I

Label free urea biosensor based on organic electrochemical transistors.

Flexible and Printed Electronics



PAPER

Label free urea biosensor based on organic electrochemical transistors

RECEIVED
9 April 2018

REVISED
24 May 2018

ACCEPTED FOR PUBLICATION
30 May 2018

PUBLISHED
14 June 2018

Marcello Berto¹ , Chiara Diacci², Lorenz Theuer^{2,3}, Michele Di Lauro¹, Daniel T Simon², Magnus Berggren², Fabio Biscarini^{1,4}, Valerio Beni^{3,5} and Carlo A Bortolotti^{1,5}

¹ Dipartimento di Scienze della Vita, Università di Modena e Reggio Emilia, Via Campi 103, I-41125 Modena, Italy

² Laboratory of Organic Electronics, Department of Science and Technology, Linköping University, SE-601 74 Norrköping, Sweden

³ Department of Printed Electronics, RISE Acreo, Research Institute of Sweden, Norrköping, Sweden

⁴ Istituto Italiano di Tecnologia—Center for Translational Neurophysiology, Via Fossato di Mortara 17-19, I-44121 Ferrara, Italy

⁵ Authors to whom any correspondence should be addressed.

E-mail: carloaugusto.bortolotti@unimore.it and valerio.beni@ri.se

Keywords: organic bioelectronics, urease, gelatin, OECT, screen-printing

Supplementary material for this article is available [online](#)

Abstract

The quantification of urea is of the utmost importance not only in medical diagnosis, where it serves as a potential indicator of kidney and liver dysfunction, but also in food safety and environmental control. Here, we describe a urea biosensor based on urease entrapped in a crosslinked gelatin hydrogel, deposited onto a fully printed PEDOT:PSS-based organic electrochemical transistor (OECT). The device response is based on the modulation of the channel conductivity by the ionic species produced upon urea hydrolysis catalyzed by the entrapped urease. The biosensor shows excellent reproducibility, a limit of detection as low as 1 μM and a response time of a few minutes. The fabrication of the OECTs by screen-printing on flexible substrates ensures a significant reduction in manufacturing time and costs. The low dimensionality and operational voltages (0.5 V or below) of these devices contribute to make these enzymatic OECT-based biosensors as appealing candidates for high-throughput monitoring of urea levels at the point-of-care or in the field.

Introduction

Organic electronics is rapidly becoming a major player in the field of biosensing [1–3], since it provides technological routes to cost-effective, miniaturizable, low-power consuming devices that can also be fabricated on flexible substrates. Biosensors based on organic field effect transistor architectures, and in particular on electrolyte-gated organic transistors (EGOTs) featuring the electrolyte as an integral part of the device, have been shown to challenge state-of-the-art biosensing approaches [1, 4–14]. Such devices have the advantage of combining the high selectivity offered by the use of biological molecules (antibodies, enzymes), whose specific interaction with the analyte of interest is transduced as an electronic signal, with the intrinsic amplification capability of the field effect making it possible to reach sensitivity comparable or even better than those of commercial platforms (e.g. ELISA). Most notably, they can be fabricated on soft

and flexible substrate [6, 15–20] and their response is label free and, in most cases, very rapid when not in real-time. EGOTs encompass the so-called electrolyte-gated organic field effect transistors (EGOFETs) [21–23] and organic electrochemical transistors (OECTs) [6, 12, 24]: both are three-electrode devices, with the source and drain electrodes connected by an organic semiconductor film (the channel), and the latter directly coupled to the third electrode, the gate, through an electrolyte solution. For both EGOFETs and OECTs, the potential applied to the gate controls the source drain current I_{DS} by driving the movement of ions in the electrolyte solution: at the current level of understanding, the main difference between these two device families is ascribed to the fact that ions penetrate in the bulk of the channel (usually composed by conductive polymers) of OECTs, while in the case of EGOFETs they are believed to sit at the electrolyte/OSC interface without penetrating the channel [6]. All the technological advances ensured by EGOTs make

them ideal candidates for in-field operation, not only for point-of-care diagnosis but also for environmental or food safety issues, allowing for frequent monitoring all along a given value chain [21, 25].

Urea is a perfect example of an analyte that needs to be monitored with disposable, portable biosensors that find applications in several fields. In clinical analysis, urea is usually used as a key indicator, together with creatinine, of chronic kidney disease (CKD). In CKD patients urea levels can reach values of ~50–70 mM that are about ten times those recorded in healthy patients [26, 27]. In the food industry, urea detection finds growing application in quality control of milk and associated products, because of urea being a chemical increasingly used as an adulterant [27, 28]. A high concentration of urea in fresh water, originating from field fertilization and in minor levels from manure spills, has been related to toxic effects due to ammonia formation which also leads to algae blooming [29].

Due to the importance of monitoring urea levels across different fields, many different urea biosensors have been demonstrated, exploiting diverse transduction mechanisms. These include amperometric [30, 31], potentiometric [32, 33], thermometric [34] and optical transducers [35, 36]; in addition, a few examples of electronic urea biosensors were reported [37]. The vast majority of the described urea biosensors display detection limits down to 1 μM and linear ranges typically covering two to three orders of magnitude and spanning the micromolar and low millimolar ranges. The response time is typically within a few minutes, with only a few examples reaching the sub-minute timescale [28].

Here, we present an organic electronic urea biosensor featuring an OECT screen printed on a flexible substrate (polyethylene terephthalate, PET) as a transducer. The biosensing was achieved by confinement of the enzyme urease (EC 3.5.1.5) in a gelatin hydrogel bridging the PEDOT:PSS gate electrode and channel; urease catalyzes the hydrolysis of urea to ammonium and bicarbonate ions [38], and the former de-dopes the PEDOT:PSS channel causing a decrease of the drain current. The biosensor features a limit of detection (LOD) of 1 μM and responds across three orders of magnitude in about 2–3 min. To the best of our knowledge, this is the first example of a urea biosensor based on OECT.

Materials and methods

Device fabrication

The OECTs used in this work were manufactured on A4 size 125 μm thick PET substrates (Polyfoil Bias) by screen-printing. Prior to use the PET foils were thermally treated (140 $^{\circ}\text{C}$, 45 min) to minimize their deformation during the subsequent curing steps.

As a first step in the manufacturing process the conductive tracks were printed using a commercial Ag ink (Ag5000, DuPont, UK). Following this, carbon contact pads were printed using a commercial carbon ink (C2130307D1, Gwent, UK). These carbon contact pads have the functions (i) to allow electrical connection between the Ag conductive tracks and the PEDOT:PSS layers (channel and gate) and (ii) to avoid direct contact between the Ag and the PEDOT:PSS. The use of Ag and carbon for the conductive tracks allowed us to avoid PEDOT:PSS/Ag cross-reactivity, without compromising their overall resistance.

Gate and channel of the OECTs were printed using a commercially available PEDOT:PSS ink (Clevious™ SV3, Heraeus Group, Germany). Finally, the manufactured OECTs were coated with a dielectric layer (5018, DuPont, UK) leaving exposed only the sensing area (gate and channel) and the connecting pads at the far end of the Ag conductive tracks. All inks were printed and cured following the indications provided by the manufacturers. A semi-automatic screen printer (DEK Horizon 03i printer, ASM Assembly Systems GmbH, Germany) was used to fabricate the electrodes and other components.

The final device is 45 \times 8 mm in size with a yield of ~50 devices for a sheet. The exposed surface of the gate electrode measures 2 mm², while the exposed surface of the square-shaped channel is 4 mm². This results in a channel/gate ratio of 2 (figure 1(c)). The stretched design allows for the placement of the OECT in bulk solutions and use of a ZIF plug for connectivity.

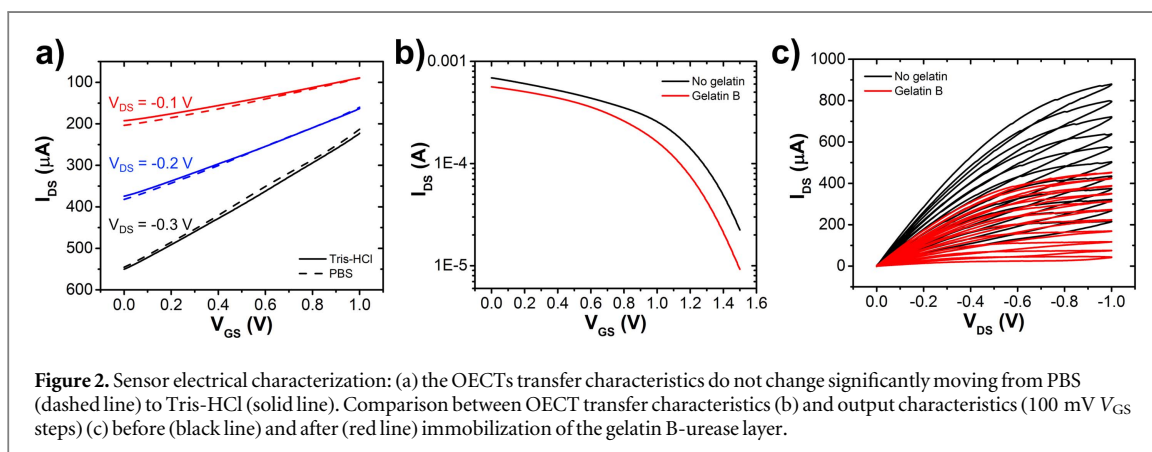
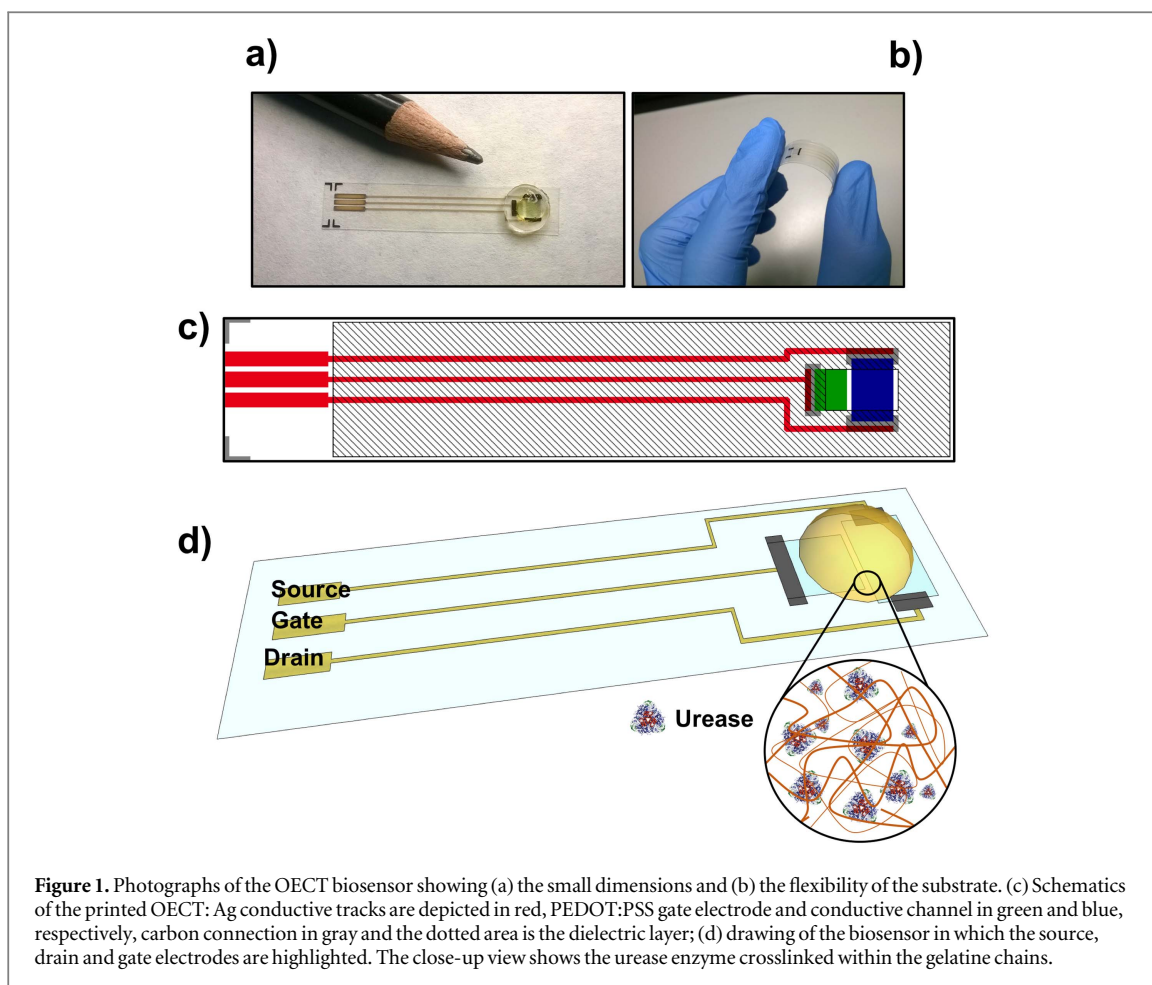
Urease enzyme (0.4 mg ml⁻¹) was immobilized in 3% bovine gelatin in Tris/HCl and crosslinked with 1% v/v glutaraldehyde [39]. 30 μl of gelatin solution was drop-casted onto the OECT and kept at 4 $^{\circ}\text{C}$ for 2 h.

Electrical characterization

Electrical measurements were acquired in buffer solutions (phosphate buffer saline (PBS) 50 mM, pH 7.4 and Tris/HCl 50 mM, pH 7.3) confined in a polydimethylsiloxane pool, as shown in figure 1(a) by means of an Agilent B2902A Source Meter Unit. All measurements were carried out at room temperature. The I - V transfer characteristics were performed by sweeping the gate-source voltage (V_{GS}) from 0.0 to +1.0 V while leaving the drain-source voltage (V_{DS}) constant at -0.4 V.

Reagents

Gelatin B and gelatin A, glutaraldehyde, Tris, HCl, phosphate salts, urease and urea were purchased from Sigma-Aldrich.



Results and discussion

The OECTs were printed on PET (figure 1), with source and drain electrodes made of carbon, PEDOT:PSS gate electrode and PEDOT:PSS also as channel material. In the particular configuration used here, the gate electrode area is half of the channel area (figure 1(c)).

We first characterized the devices without any immobilized biomolecule, by collecting output and transfer characteristics both in (i) PBS 50 mM pH 7.3 and Tris-HCl 50 mM pH 7.4 (figure 2(a)): the transfer characteristics recorded at V_{DS} ranging from -0.1 V

to -0.3 V are almost superimposable, indicating that the OECT response is basically the same in the two widely used buffers. We therefore chose to use Tris-HCl, because it ensures long-term storage with retention of enzymatic activity: in fact, urease immobilized in Tris/gelatin hydrogel showed a notable half-life of 240 d [28, 39]. As anticipated in the introduction, our biosensor exploits Jack bean urease, which was immobilized in a gelatin hydrogel, crosslinked with glutaraldehyde and deposited on the OECT (figure 1(c)) [40] with the electrolyte solution embedded in the gelatin ensuring the OECT operation via the gate-controlled (de-)doping of the channel [41].

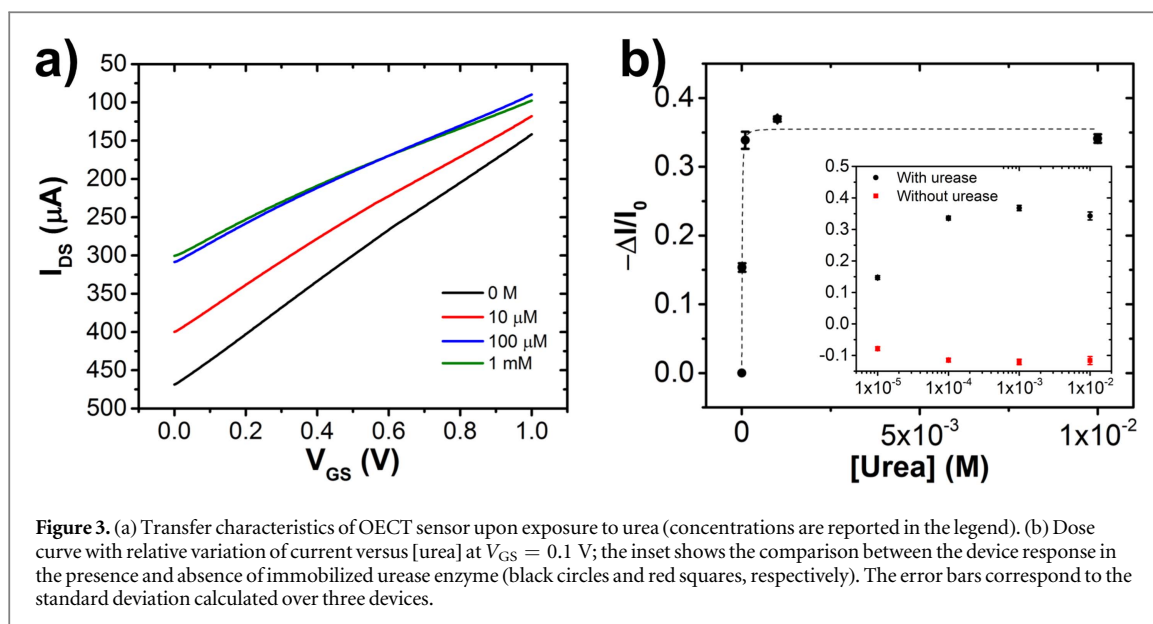


Figure 3. (a) Transfer characteristics of OECT sensor upon exposure to urea (concentrations are reported in the legend). (b) Dose curve with relative variation of current versus [urea] at $V_{GS} = 0.1$ V; the inset shows the comparison between the device response in the presence and absence of immobilized urease enzyme (black circles and red squares, respectively). The error bars correspond to the standard deviation calculated over three devices.

Gelatin is a collagen-derived, water-soluble protein, especially rich in (hydroxyl)proline and glycine [42]. Depending on the processing and origin, different types of gelatin can be obtained: the most common are type A and B gelatin, resulting from alkaline or acidic treatment of collagen, respectively [41, 42].

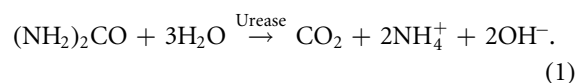
We checked whether the switch from a liquid electrolyte to the gelatin/enzyme hydrogel would affect the OECT response: to this end, we recorded transfer and output characteristics of the OECT after deposition of $30 \mu\text{l}$ of glutaraldehyde/urease crosslinked gelatin B hydrogel in Tris-HCl 50 mM, pH 7.4, and compared them to those obtained for the same devices in Tris-HCl 50 mM, pH 7.4. The results are displayed in figures 2(b) and (c): minor qualitative differences in both the transfer and output curves indicate that the gelatin does not hinder efficient gate modulation of the drain current; yet, I_{DS} is markedly lower when the OECT is operated in gelatin.

Both the transfer and output characteristics invariably show a current decrease upon shifting the gate voltage towards more positive values: such behavior is an indirect evidence of cations penetrating the channel and de-doping of it resulting in a depletion-mode operation [6, 43–45]. Ions migrations into and out of the conductive channel have different kinetics, as shown by the hysteresis recorded in I_{DS} but this effect is mitigated by the presence of the gelatin layer onto the OECT (figure 2(c)).

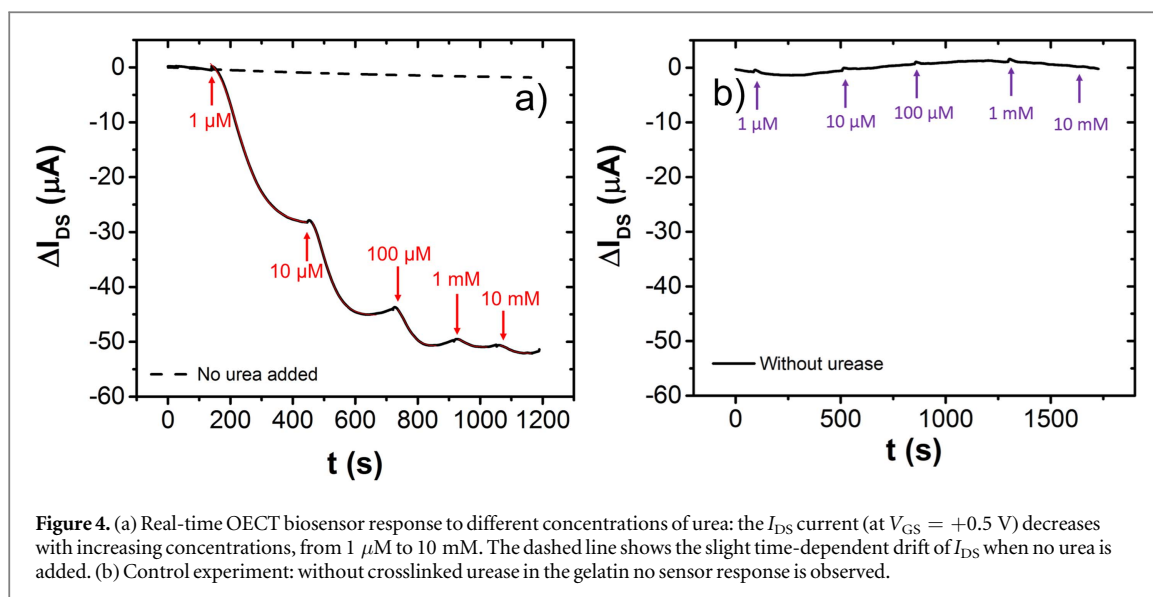
We then exposed the OECT with immobilized urease in a gelatin B-based gel to solutions containing increasing levels of urea, ranging from $1 \mu\text{M}$ to 10 mM, and recorded transfer characteristics monitoring the corresponding changes in I_{DS} . An overlay of the transfer curves obtained at different [urea] is given in figure 3(a). The drain current decreases upon exposure to urea, and higher urea concentrations induce a larger drop in I_{DS} . The current decreases

steeply at low [urea], and the changes are less marked when reaching the mM range, with the transfer characteristics recorded at 1–10 mM being almost superimposable. We built a calibration curve for the urea OECT biosensor by plotting the normalized change in the drain current $-\Delta I/I_0$ as a function of [urea], at a fixed V_{GS} (here, at $V_{GS} = +0.1$ V). ΔI is the difference between the drain current I_{DS} at a given urea concentration and the current recorded in Tris-HCl only, I_0 . The calibration curve is depicted in figure 3(b): it is apparent that the OECT can detect the presence of urea in test Tris-HCl solutions down to $1 \mu\text{M}$, and that the response sets into a plateau for [urea] > 1 mM.

We ascribe the observed decrease in I_{DS} to a decrease in conductivity of the OECT channel, as a consequence of the ammonium ions, which are generated as a product of the hydrolysis of urea by the Ni-dependent enzyme. In fact, urease catalyzes the hydrolysis of urea as described by equation (1) [38].



We hypothesize that the NH_4^+ cations diffuse through the gelatin B hydrogel and penetrate the channel, de-doping it, and causing a drop in I_{DS} . The ammonium cations interact tightly with the PSS^- in the channel and the binding is irreversible, at least in the minute timescale: in fact, even exposing the device, after reaction with urea, to Tris-HCl only, the current could not be restored to its initial I_0 value (data not shown). The enzymatic hydrolysis of urea also leads to an increase in $[\text{OH}^-]$, therefore impacting on the pH. This might also affect the device response [46], but we believe that in the present configuration the ammonium/channel interaction is the dominating factor. In fact, the measurements were performed in a buffered environment, so the solution pH should be unaffected by the urea hydrolysis, at least at the lowest



concentrations. Moreover, we believe that gelatin B, besides serving for the enzyme immobilization, also acts as a ‘selectivity filter’. Gelatin B is negatively charged at nearly neutral pH, with an isoelectric point (IEP) of about 5: it is reasonable to infer that positively charged NH_4^+ ions pass through the gelatin hydrogel and penetrate the PEDOT:PSS channel, while OH^- should be repelled due to electrostatic repulsion. This is conceptually similar to the observed selectivity of PEDOT:PSS electrodes for positively charged dopamine with respect to negatively charged interfering agents uric and ascorbic acids (UA and AA, respectively) [47] or to the effect of Nafion (negatively charged) used to prevent UA and AA diffusion to gate electrode of an OECT biosensors [48] while attracting positively charged epinephrine. A somehow opposite trend can therefore be expected by reversing the hydrogel charge. This hypothesis is backed up by the following control experiment: we prepared OECT biosensors with immobilized urease but substituting gelatin B with gelatin A, whose IEP is about 7 or higher [42]. In this case, addition of urea still impacts on the drain current, but this time it leads to higher drain current as the urea concentration is increased (figure S1, available online at stacks.iop.org/FPE/3/024001/mmedia).

To gain more insights into the response time of the biosensor, we recorded the I_{DS} current as a function of time at a fixed $V_{GS} = +0.5$ V, monitoring its changes upon addition of increasing concentrations of urea. It can be seen from figure 4(a) that the I_{DS} drop occurs in a few seconds and that the steady state is typically reached in less than two minutes.

To prove that the current decrease is due to enzymatic hydrolysis of urea and not to operational instability of the transistor nor to unspecific interaction of urea with the device materials, we functionalized the OECT with gelatin B, crosslinked with glutaraldehyde but in the absence of urease, and

exposed it to urea-containing solutions. This control experiments show that, in the absence of the enzyme, the I_{DS} is basically unaffected by the addition of urea (figure 4(b)), allowing us to ascribe the OECT response to the enzymatic biocatalysis. All these experiments provide proof of the retention of catalytic activity of urease upon confinement in the gel, as could be expected based on previous literature [28, 39].

The vast majority of the enzyme-based OECT biosensors described in the literature make use of redox proteins (such as glucose oxidase, lactate oxidase, alcohol dehydrogenase) [12, 20, 49, 50], in some cases displaying remarkably low LODs [18, 51]. The working principle is typically based on electrochemical reduction/oxidation processes involving some of the products generated by the biocatalysis taking place at the gate electrode; such faradic processes contribute to the drain current. Here, instead, we use an enzyme belonging to a different class (urease is a hydrolase, at variance with all the above-mentioned proteins, which are oxidoreductases) and, as a result, the response of our device is not based on electron transfer processes at the device interfaces, but rather on the different conductivity of the conductive polymer constituting the channel, as a consequence of the enzymatic reactions taking place in the electrolyte. The lack of Faradaic processes at the gate is witnessed by the purely capacitive nature of the measured leakage current (supplementary figure S2).

Conclusions

In this work we report the use of screen-printing for the large-scale manufacturing of PEDOT:PSS-based OECTs and their use in the development of urea biosensors.

The demonstrated sensor was based on the enzymatic conversion of urea from the urease enzyme immobilized onto the OECTs.

The retention of catalytic activity of the protein was ensured by the use of a gelatin/Tris hydrogel, which also contributes to the response specificity by allowing only positive charged ammonium ions penetrating the bulk of the PEDOT:PSS channel. A number of control experiments were performed to ascribe the device response to the products of urea catalysis by the confined enzyme that leads to a urea-dependent variation in the drain current. The response time (2–3 min), LOD (1 μ M) and dynamic range (three orders of magnitude) of the biosensor are in line with state-of-the-art detection strategies for urea in biological samples. We demonstrate our device in model aqueous solutions, and we plan to test it with real world samples such as milk or human fluids. Due to the proposed working mechanism, we expect that variability in pH and ionic strength might affect the sensor response; these aspects will be addressed in further works.

Moreover, we demonstrated screen-printing onto flexible substrate as a suitable manufacturing technique for the large-scale and cost-effective production of Organic Electrochemical Transistor paving, in this way, their way towards the area of biosensors for point-of-care.

Acknowledgments

Funding for CD, VB, DTS and MB was provided by the Swedish Foundation for Strategic Research (Smart Intra-body network; grant RIT15-0119) for the financial support. Funding for LT was provided by the BIORAPID project (EU H2020 Marie Skłodowska-Curie grant agreement No. 643056) for financial support. CAB acknowledges the 'Fondazione di Vigonola' for support. The authors would also like to acknowledge Ms Marie Nilsson for mask design and OECT fabrication.

ORCID iDs

Marcello Berto  <https://orcid.org/0000-0002-3356-8829>

References

- [1] Manoli K, Magliulo M, Mulla M Y, Singh M, Sabbatini L, Palazzo G and Torsi L 2015 *Angew. Chem., Int. Ed.* **54** 12562–76
- [2] Pappa A M, Parlak O, Scheiblin G, Mailley P, Salleo A and Owens R M 2017 *Trends Biotechnol.* **36** 45–59
- [3] Simon D T, Gabriellsson E O, Tybrandt K and Berggren M 2016 *Chem. Rev.* **116** 13009–41
- [4] Casalini S, Dumitru A C, Leonardi F, Bortolotti C A, Herruzo E T, Campana A, de Oliveira R F, Cramer T, Garcia R and Biscarini F 2015 *ACS Nano* **9** 5051–62
- [5] Macchia E, Ghittorelli M, Torricelli F and Torsi L 2017 *2017 7th IEEE Int. Workshop on Advances in Sensors and Interfaces (IWASI)* (Piscataway, NJ: IEEE) pp 68–72
- [6] Rivnay J, Inal S, Salleo A, Owens R M, Berggren M and Malliaras G G 2018 *Nat. Rev. Mater.* **3** 17086
- [7] Berto M et al 2016 *Anal. Chem.* **88** 12330–8
- [8] Berto M et al 2018 *Adv. Biosyst.* **2** 1700072
- [9] Diacci C, Berto M, Di Lauro M, Bianchini E, Pinti M, Simon D T, Biscarini F and Bortolotti C A 2017 *Biointerphases* **12** 05F401
- [10] Mulla M Y, Tuccori E, Magliulo M, Lattanzi G, Palazzo G, Persaud K and Torsi L 2015 *Nat. Commun.* **6** 6010
- [11] Magliulo M, De Tullio D, Vikholm-Lundin I, Albers W M, Munter T, Manoli K, Palazzo G and Torsi L 2016 *Anal. Bioanal. Chem.* **408** 3943–52
- [12] Strakosas X, Bongo M and Owens R M 2015 *J. Appl. Polym. Sci.* **132** 1–14
- [13] Scheiblin G, Aliane A, Strakosas X, Curto V F, Coppard R, Marchand G, Owens R M, Mailley P and Malliaras G G 2015 *MRS Commun.* **5** 507–11
- [14] Hai W, Goda T, Takeuchi H, Yamaoka S, Horiguchi Y, Matsumoto A and Miyahara Y 2018 *Sensors Actuators B* **260** 635–41
- [15] Guozhen S and Zhiyong F 2016 *Flexible Electronics: From Materials to Devices* (Singapore: World Scientific)
- [16] Lipomi D J and Bao Z 2017 *MRS Bull.* **42** 93–7
- [17] Lin P, Luo X, Hsing I M and Yan F 2011 *Adv. Mater.* **23** 4035–40
- [18] Liao C, Mak C, Zhang M, Chan H L W and Yan F 2015 *Adv. Mater.* **676**–81
- [19] Campana A, Cramer T, Simon D T, Berggren M and Biscarini F 2014 *Adv. Mater.* **26** 3874–8
- [20] Bihar E, Deng Y, Miyake T, Saadaoui M, Malliaras G G and Rolandi M 2016 *Sci. Rep.* **6** 27582
- [21] Cramer T, Campana A, Leonardi F, Casalini S, Kyndiah A, Murgia M and Biscarini F 2013 *J. Mater. Chem. B* **1** 3728
- [22] Huang W, Diallo A K, Dailey J L, Besar K and Katz H E 2015 *J. Mater. Chem. C* **3** 6445–70
- [23] Wang D, Noël V and Piro B 2016 *Electronics* **5** 9
- [24] Kergoat L, Piro B, Simon D T, Pham M C, Noël V and Berggren M 2014 *Adv. Mater.* **5658**–64
- [25] White S P, Dorfman K D and Frisbie C D 2016 *J. Phys. Chem. C* **120** 108–17
- [26] Levey A S, Bosch J P, Breyer L J, Greene T, Rogers N and Roth D 2001 *J. Am. Med. Assoc.* **286** 3065
- [27] Dhawan G, Sumana G and Malhotra B D 2009 *Biochem. Eng. J.* **44** 42–52
- [28] Singh M, Verma N, Garg A and Redhu N 2008 *Sensors Actuators B* **134** 345–51
- [29] Tran T Q N, Das G and Yoon H H 2017 *Sensors Actuators B* **243** 78–83
- [30] Pizzariello A, Stredanský M, Stredanská S and Miertuš S 2001 *Talanta* **54** 763–72
- [31] Luo Y C and Do J S 2004 *Biosens. Bioelectron.* **20** 15–23
- [32] Osaka T, Komaba S, Seyama M and Tanabe K 1996 *Sensors Actuators B* **36** 463–9
- [33] Eggenstein C, Borchardt M, Diekmann C, Gründig B, Dumschat C, Cammann K, Knoll M and Spener F 1999 *Biosens. Bioelectron.* **14** 33–41
- [34] Gündüz T, Kihç E and Çakirer O 1995 *Talanta* **42** 1757–9
- [35] Kovács B, Nagy G, Dombi R and Tóth K 2002 *Biosens. Bioelectron.* **18** 111–8
- [36] Tsai H C and Doong R A 2005 *Biosens. Bioelectron.* **20** 1796–804
- [37] Piccinini E, Bliem C, Reiner-Rozman C, Battaglini F, Azzaroni O and Knoll W 2017 *Biosens. Bioelectron.* **92** 661–7
- [38] Krajewska B 2009 *J. Mol. Catal. B* **59** 9–21
- [39] Srivastava P K, Kayastha A M and Srinivasan R 2001 *Biotechnol. Appl. Biochem.* **34** 55
- [40] Kuijpers A J, Engbers G H M, Krijgsveld J, Zaat S A J, Dankert J and Feijen J 2000 *J. Biomater. Sci. Polym. Ed.* **11** 225–43
- [41] de Wael K, Verstraete A, Van Vlierberghe S, Dejonghe W, Dubruel P and Adriaens A 2011 *Int. J. Electrochem. Sci.* **6** 1810–9
- [42] Hafidz R and Yaakob C 2011 *Int. Food Res. J.* **18** 813–7
- [43] Bernards D A and Malliaras G G 2007 *Adv. Funct. Mater.* **17** 3538–44

- [44] Tarabella G, Mahvash Mohammadi F, Coppedè N, Barbero F, Iannotta S, Santato C and Cicoira F 2013 *Chem. Sci.* **4** 1395
- [45] Giridharagopal R, Flagg L Q, Harrison J S, Ziffer M E, Onorato J, Luscombe C K and Ginger D S 2017 *Nat. Mater.* **16** 737–42
- [46] Kirchan A E, Kim K T, Steward M K and Choi S 2017 *TRANSDUCERS 2017—19th Int. Conf. Solid-State Sensors, Actuators Microsystems* pp 214–7
- [47] Giordani M, Berto M, Di Lauro M, Bortolotti C A, Zoli M and Biscarini F 2017 *ACS Sensors* **2** 1756–60
- [48] Mak C H, Liao C, Fu Y, Zhang M, Tang C Y, Tsang Y H, Chan H L W and Yan F 2015 *J. Mater. Chem. C* **3** 6532–8
- [49] Yang S Y, Cicoira F, Byrne R, Benito-Lopez F, Diamond D, Owens R M and Malliaras G G 2010 *Chem. Commun.* **46** 7972–4
- [50] Braendlein M, Pappa A-M, Ferro M, Lopresti A, Acquaviva C, Mamessier E, Malliaras G G and Owens R M 2017 *Adv. Mater.* **29** 1605744
- [51] Fu Y, Wang N, Yang A, Law H K, Li L and Yan F 2017 *Adv. Mater.* **29** 1703787

Supporting Information

Label free urea biosensor based on Organic ElectroChemical Transistors

Marcello Berto^a, Chiara Diacci^b, Lorenz Theuer^{b,c}, Michele Di Lauro^a, Daniel T. Simon^b, Magnus Berggren^b, Fabio Biscarini^{a,d}, Valerio Beni^{c*} and Carlo A. Bortolotti^{a*}

a. Dipartimento di Scienze della Vita, Università di Modena e Reggio Emilia, Via Campi 103, 41125 Modena, Italy

b. Laboratory of Organic Electronics, Department of Science and Technology, Linköping University, S-601 74 Norrköping, Sweden

c. Department of Printed Electronics, RISE Acreo, Research Institute of Sweden, Norrköping, Sweden

d. Istituto Italiano di Tecnologia – Center for Translational Neurophysiology, Via Fossato di Mortara 17-19, 44121 Ferrara, Italy

E-mails: carloaugusto.bortolotti@unimore.it

valerio.beni@ri.se

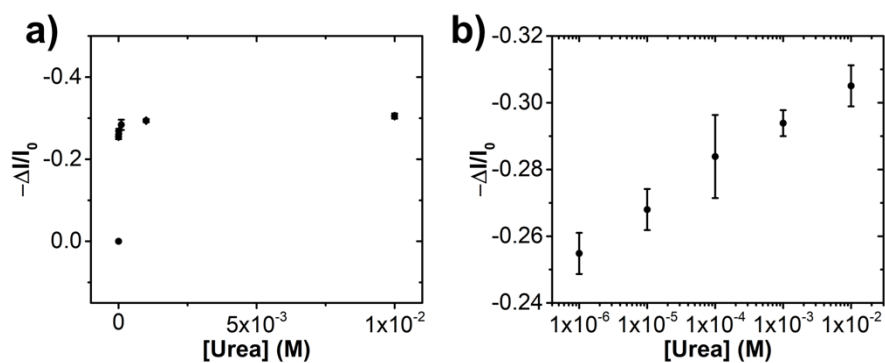


Figure S1. OECT-gelatin A sensor dose curve with relative variation of current versus [urea] at $V_{GS} = +0.1$ V in linear a) and logarithmic scale b). The I_{DS} current increases with increasing concentrations, from 1 μ M to 10 mM.

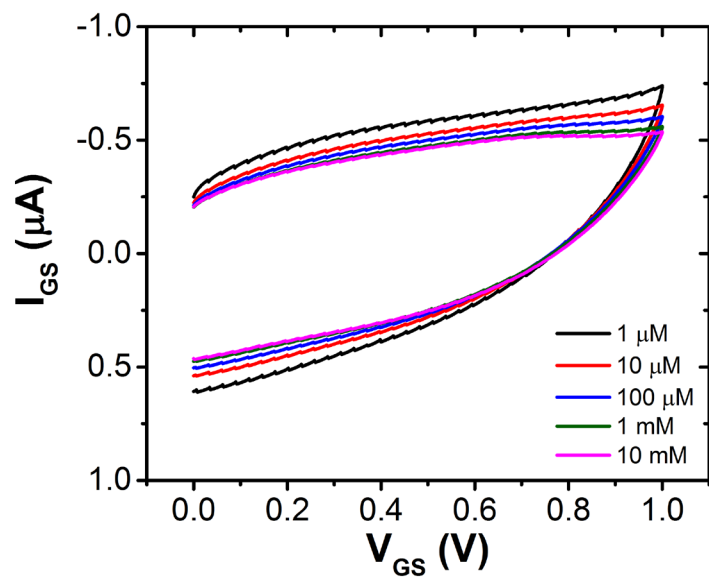


Figure S2. Gate-Source current response to increasing concentrations of urea: the I_{GS} does not change significantly over four orders of magnitude [urea] and does not show any faradaic event.

Paper II

Flexible Printed Organic Electrochemical Transistors for the Detection of Uric Acid in Artificial Wound Exudate.

Flexible Printed Organic Electrochemical Transistors for the Detection of Uric Acid in Artificial Wound Exudate

Marina Galliani, Chiara Diacci, Marcello Berto, Matteo Sensi, Valerio Beni, Magnus Berggren, Marco Borsari, Daniel T. Simon, Fabio Biscarini, and Carlo A. Bortolotti*

Low-cost, minimally invasive sensors able to provide real-time monitoring of wound infection can enable the optimization of healthcare resources in chronic wounds management. Here, a novel printed organic electrochemical transistors (OECT) biosensor for monitoring uric acid (UA), a bacterial infection biomarker in wounds, is demonstrated in artificial wound exudate. The sensor exploits the enzymatic conversion of UA to 5-hydroxyisourate, catalyzed by Uricase entrapped in a dual-ionic-layer hydrogel membrane casted onto the gate. The sensor response is based on the catalytic oxidation of the hydrogen peroxide, generated as part of the Uricase regeneration process, at the Pt modified gate. The proposed dual membrane avoids the occurrence of nonspecific faradic reactions as, for example, the direct oxidation of UA or other electroactive molecules that would introduce a potentially false negative response. The biosensor is robust and its response is reproducible both in phosphate buffer saline and in complex solutions mimicking the wound exudate. The sensor has a high sensitivity in the range encompassing the pathological levels of UA in wounds (<200 μm) exhibiting a limit of detection of 4.5 μm in artificial wound exudate. All these characteristics make this OECT-based biosensor attractive for wound monitoring interfaced to the patient.

1. Introduction

Wound care is an important medical treatment: if neglected, it may slow down or hamper the healing process^[1,2] and possibly lead to serious complications.^[3] Advanced wound care technologies envision the acquisition and communication of data about the wound status directly from the patient home through smart bandages. A slower wound healing process can arise from a variety of endogenous or exogenous factors, including bacterial infections. During the healing process of a wound, exogenous bacteria and/or the ones who normally belong to the skin microbiota (e.g., *Staphylococcus aureus*, *Escherichia coli*, *Pseudomonas aeruginosa*) can reach the underlying tissues and proliferate, causing a prolonged inflammation which, in the worst case, leads to a chronic status of the wound.^[4] Smart bandages have been developed to monitor generic physiological indicators such as pH,^[5,6] temperature,^[7,8]

oxygen,^[9] or moisture level.^[10] Other indicators of wound infections and healing processes are variations of the level of metalloproteinases,^[11] cytokines,^[12] and uric acid (UA).^[13] The latter, in the form of urate, is present in wound exudate in concentrations varying between 220 and 750 $\times 10^{-6}$ M.^[14] The human body cannot catabolize UA since it lacks a specific enzyme and UA is physiologically eliminated through urine. As a consequence of bad nutrition and metabolic disorders^[15,16] or diseases like cancer^[17] or diabetes,^[18] UA levels in bodily fluids can increase leading to gout^[19,20] and urate crystals precipitation in joints, kidney, and other tissues.^[19] On the contrary, some bacteria, such as *P. aeruginosa*, can specifically metabolize UA^[13,21,22] with subsequent decrease of its concentration in the wound exudate below 200 $\times 10^{-6}$ M. As a result, the UA level in skin wound can be monitored as an effective marker of bacterial infection.

Label-free biosensors based on organic (semi-) conductive polymers may represent ideal devices to be interfaced with wound environment: they detect complex biological signals in aqueous media and translate them into an electronic output; they are operated at low voltages and require low power sources and they can be fabricated into flexible materials^[23–25] with large-area techniques such as screen printing^[26–29] and inkjet printing^[30] on low-cost substrates (paper, plastic foils, textiles). Moreover, they can be manufactured as impalpable patches adhering on the skin to record physiological signals.^[31–33]

M. Galliani, C. Diacci, Dr. M. Berto, Dr. M. Sensi, Prof. F. Biscarini, Dr. C. A. Bortolotti
Dipartimento di Scienze della Vita
Università di Modena e Reggio Emilia
Via Campi 103, Modena 41125, Italy
E-mail: carloaugusto.bortolotti@unimore.it

C. Diacci, Prof. M. Berggren, Prof. D. T. Simon
Laboratory of Organic Electronics
Department of Science and Technology
Linköping University
Bredgatan 33, Norrköping 60221, Sweden

Dr. V. Beni
Department of Smart Hardware
RISE AB
Research Institutes of Sweden
Bredgatan 33, Norrköping 60221, Sweden

Prof. M. Borsari
Dipartimento di Scienze Chimiche e Geologiche
Università di Modena e Reggio Emilia
Via Campi 103, Modena 41125, Italy

Prof. F. Biscarini
Istituto Italiano di Tecnologia—Center for Translational Neurophysiology
Via Fossato di Mortara 17-19, Ferrara 44121, Italy

 The ORCID identification number(s) for the author(s) of this article can be found under <https://doi.org/10.1002/admi.202001218>.

DOI: 10.1002/admi.202001218

Biosensors based on organic electrochemical transistors (OECTs) biosensors are particularly appealing for those applications that, while not requiring ultra-low limits of detection, benefit from other features offered by this architecture, such as easy integration with readout circuits, stability, and the possibility of controlling the dynamic range through device design. OECTs were already demonstrated for detection of metabolites^[34–36] in complex media, cytokines,^[37] and neurotransmitters.^[38,39] When operated in the so-called faradic mode, OECTs exploit a redox reaction taking place at the gate, similarly to what happens in electrochemical amperometric sensors. Nevertheless, the OECT architecture provides amplification of the faradic current, thus enabling higher sensitivity.^[40] Moreover, the readout electronics for OECTs are simpler and less expensive than the potentiostats necessary to drive amperometric sensors.^[41]

The present work demonstrates a low-cost and disposable printed OECT sensor for UA detection in complex solutions mimicking wound exudate. The OECT-based sensors are screen printed on flexible PET (polyethylene terephthalate) foil,^[42] featuring poly(3,4-ethyl-enedioxythiophene):poly(styrenesulfonate) PEDOT:PSS as the conducting polymer for the channel and amorphous carbon as the gate electrode. Amorphous carbon is a suitable material for the gate electrode since it is cost effective, its printing process is well established, and it can be employed as a substrate for further modification via electrochemical deposition of metals, such as platinum,^[43] or gold.^[44] Previous works have demonstrated the possibility of coupling transistors operating in liquid (in particular graphene-FET) to enzymes, to obtain biosensors selective for neurotransmitters,^[45–47] drugs,^[46] or biomarkers.^[48,49]

Our approach for UA detection is based on the catalytic activity of the enzyme Urate oxidase (UOx, also known as Uricase) that ultimately produces hydrogen peroxide. One of

the innovative features of our device architecture with respect to previously reported detection of UA with OECT^[23] is the architecture of the sensing element, composed by two layers of hydrogels integrated on top of the gate electrode surface. The two hydrogel layers consist of a polycation and a polyanion network, one on top of the other. Their function is to create a charge-selective barrier that prevents the flow of charged molecules to the gate electrode, suppressing in this way parasitic Faradic reactions due to the oxidation of electroactive molecules present in the measuring medium. Such functionalization is aimed to allow only hydrogen peroxide to diffuse to the gate, where it can be oxidized to oxygen, thus ensuring the specificity of the sensor response. The dynamic range observed spans both the pathological and physiological UA levels in wounds and exhibits robust response also in complex media of medical relevance. This device architecture, which is simple to manufacture and to scale up into high throughput production, may represent a disposable and easy to use solution to be integrated in adhesive strips or bandages for advanced wound care systems.

2. Results and Discussion

The device layout exhibits a planar geometry with all-printed amorphous carbon gate, source and drain electrodes, the latter bridged by a printed channel made of PEDOT:PSS conducting polymer (Figure 1A). In order to enhance gate modulation capability and catalyze the oxidation of hydrogen peroxide within the 0–1 V potential range, a Pt layer was electrodeposited on the gate^[50] (Figure S1A, Supporting Information). In 50×10^{-3} M phosphate buffer saline (PBS), the carbon gate exhibits no oxidation processes below 1 V,^[44] also in the presence of the Pt layer (Figure S1B, Supporting Information). Both the transfer

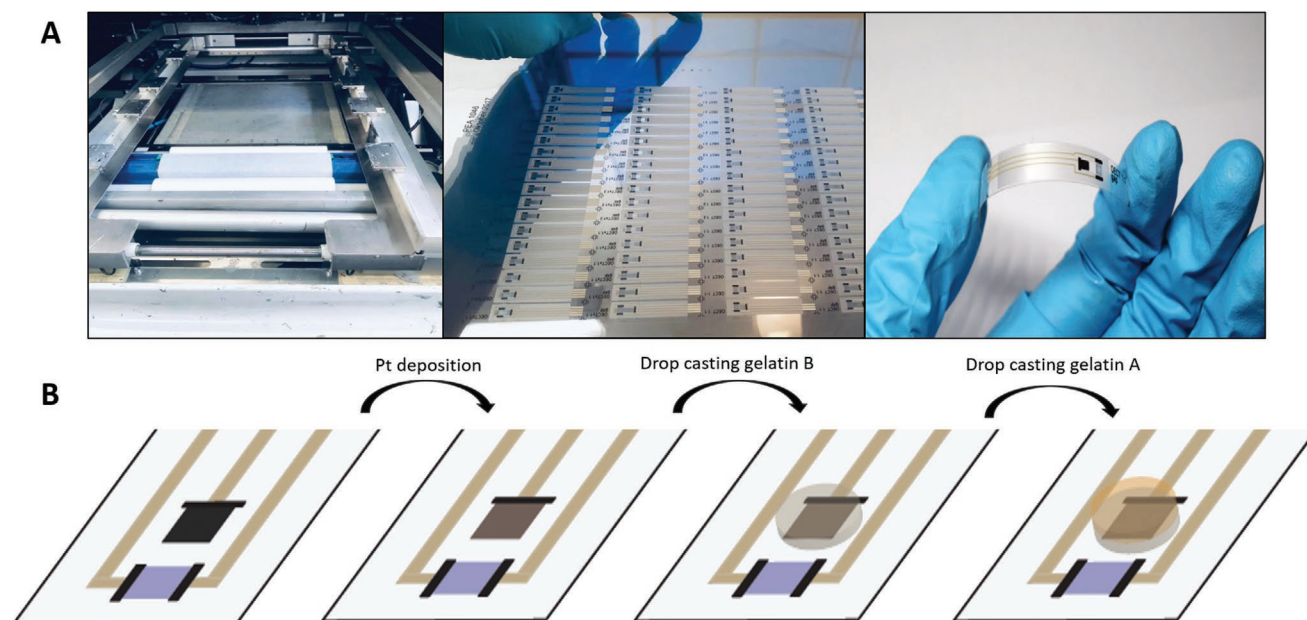


Figure 1. OECT fabrication and functionalization. A) Screen printing apparatus and printed OECT on PET foil. B) Steps for the gate functionalization (from left to right): i→ii Platinum electrochemical deposition, ii→iii drop casting of gelatin B (grey), and iii→iv drop casting of gelatin A (orange) cross-linked with Uricase enzymes.

characteristics (I_{DS} versus V_{GS} at constant V_{DS}) and the output curves (I_{DS} versus V_{DS} at constant V_{GS}) show that, at variance with what can be achieved with the C gate, the C/Pt gate can lead to drain current modulation as expected from a depletion-mode OECT. The gate electrode was further modified to enable enzyme immobilization and enhance sensor selectivity: a negatively charged gelatin B layer is deposited onto the platinized gate electrode and subsequently a positively charged gelatin A layer, with cross-linked Uricase, is deposited on the gelatin B membrane (Figure 1B). Gelatin A and B are natural hydrogels derived from porcine skin; they are biocompatible and provide a robust environment for enzymes.^[29,51–54] The use of gelatin represents a valuable functionalization strategy for wound-monitoring biosensors, as they were already used for wound patches and scaffolds.^[55–57] The gelatin A layer is permeable to UA and therefore allows it to reach Uricase, which catalyzes its oxidation to 5-hydroxyisourate that finally spontaneously converts into allantoin (Figure 2A).^[58] The gelatin A layer, formed by a positively charged polymeric network with mobile anions to balance its charge, also enhances selectivity by hindering diffusion of cations to the gate.

The enzyme returns to its resting state through the reduction of molecular oxygen to H_2O_2 , which is then oxidized at the platinum layer (Figure 2A).

The gelatin B layer, sandwiched between the electrodeposited Pt and gelatin A, is instead formed by a negatively charged

network with mobile counteranions; as a consequence, its role is to hinder diffusion of anionic electroactive species to the gate, which could provide potential Faradic response. The gate functionalization strategy does not affect the electrical behavior of the OECT; as reported in Figure S2, Supporting Information, the leakage current I_{GS} is almost three orders of magnitude lower than the current in the channel I_{DS} .

Our sensing strategy therefore relies on the indirect quantification of UA through oxidation of hydrogen peroxide. Before constructing a dose curve of our device to UA, we first performed a series of control experiments, in the absence of Uricase, to assess the effectiveness of the dual-ionic-layer hydrogel in allowing H_2O_2 diffusion while preventing UA from reaching the gate.

We quantify the sensor response as the signal S , corresponding to the current variation normalized to the current in the absence of analyte, that is, $S = \Delta I/I = -(I_{UA} - I_0)/I_0$, where I_{UA} and I_0 are the drain current values at a finite molar concentration [UA] and at [UA] = 0 M, respectively. Normalization to the initial current is an effective strategy to minimize device-to-device variations, widely used in organic electronic biosensing.^[34]

Figure 2B shows the normalized current variation as a function of [UA] for OECT gated by a C gate with an electrodeposited Pt layer only (C/Pt) or further modified by gelatin B and A hydrogels (C/Pt/GelB/GelA) with black and blue dots,

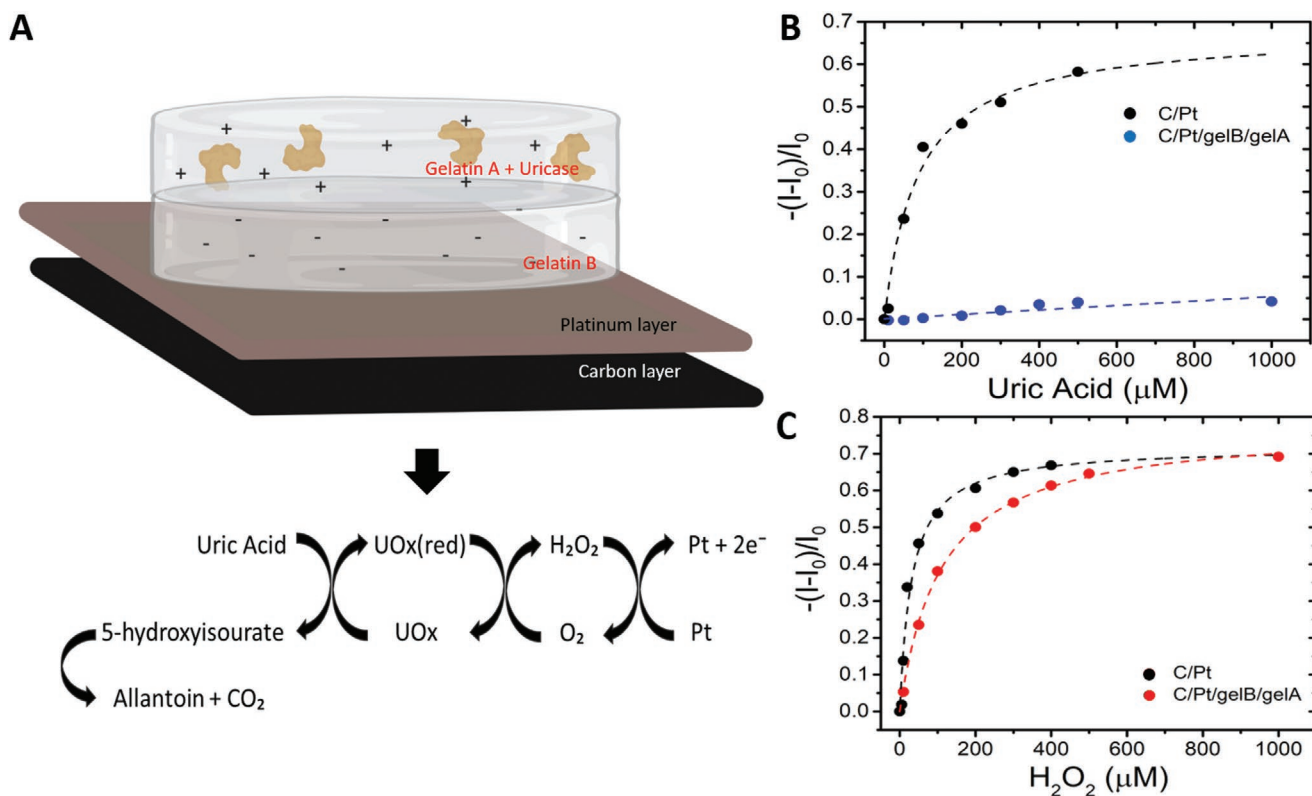


Figure 2. Functionalization strategy. A) Top: Functionalized gate presenting a platinum layer on top of the carbon printed gate enzyme (the cartoon representation is not on scale). Bottom: the reactions involved in the enzymatic detection of UA. B) Normalized current variation at fixed $V_{GS} = 0.5$ V, as a function of [UA] for OECT gated by a bare platinum gate (C/Pt, black dots) and at a Platinum gate further functionalized gate with Gelatin A and B (C/Pt/GelB/GelA, blue dots). C) Normalized current variation as a function of $[H_2O_2]$ for OECT gated by C/Pt (black dots) and by C/Pt/GelB/GelA (red dots) electrodes.

respectively. It is apparent that UA can be electrochemically oxidized at the C/Pt gate, leading to a drain current decrease, while the drain current variation is negligible for C/Pt/GelB/GelA gated OEET, indicating that direct oxidation of UA at the latter gate is impaired by the two-layer-hydrogel. It is therefore likely that diffusion of other negatively charged species, which could be oxidized in the same potential range at the gate, will be prevented by gelatin B. Figure 2C depicts the normalized current changes of OEETs gated by C/Pt and C/Pt/GelB/GelA electrodes as a function of $[H_2O_2]$: a similar response is obtained in the absence (black circles) and presence (red circles) of the two gelatin layers, suggesting that the dual-ionic-layer hydrogel does not hinder diffusion of hydrogen peroxide to the gate, a necessary requisite for our sensing scheme.

We then turned to the detection of UA through quantification of H_2O_2 produced in relation to the enzymatic conversion of UA to 5-hydroxyisourate. Since chitosan has been widely reported as a biocompatible matrix to entrap the enzymes,^[34,59–61] its application, in replacement of gelatin A, in the dual biopolymer hydrogel was tested. Devices featuring the Uricase, entrapped either in gelatin A (C/Pt/GelB/GelA+UOx) either in chitosan (C/Pt/GelB/Chit+UOx) were manufactured and their performances compared. For both OEETs, we measured the real-time response to increasing concentration of UA in PBS (Figure 3A and Figure S3, Supporting Information), operating the transistor at constant biases applied at the gate ($V_{GS} = +0.5$ V) and at the channel ($V_{SD} = -0.4$ V), since these potential values guarantee high transconductance and therefore the maximum signal amplification^[62] (Figure S3, Supporting Information). We noticed that, for each investigated [UA], measurements performed with the Gelatin layers (i.e., for devices gated by C/Pt/GelB/GelA+UOx) reached the steady state response faster when compared to the chitosan functionalization method (Figure S3, Supporting Information).

We hypothesized that the slower response from the C/Pt/GelB/Chit+UOx-based OEET might be due to the extended hydrogen bond network within crosslinked chitosan that might slow down diffusion of H_2O_2 toward the gate. While gelatin is a mixture of proteins, chitosan is a polysaccharide, and more precisely a random copolymer of beta(1-4)-linked D-glucosamine

and N-acetyl-D-glucosamine, thus comprising a high number hydroxyl and amine residues. Moreover, gelatin layers are charged around neutral pH (negatively or positively charged, depending on the curing process), while chitosan is uncharged, and this may favor its collapse to an insoluble layer.^[63] Last, the expected average molecular mass (MM) of the gelatin used in this study ranged from 50 to 100 kDa, while for range for the low molecular weight chitosan ranged from 50 to 190 kDa. This difference might impact the layer viscosity and therefore the diffusion properties of molecules within the hydrogel.

Therefore, we relied on the functionalization strategy based on the gelatin A/gelatin B hydrogels to perform multiple experiments to increase the data statistics. For each I_{DS} versus time measurement (Figure 3A), we extracted the sensor response S , expressed as the normalized drain current change, as previously described, for UA concentrations ranging from 10×10^{-6} M to 1×10^{-3} M, and we averaged the results obtained with four independent measurements to construct the dose curve in Figure 3B.

The response increases monotonically in the investigated concentration range and tends to saturate for [UA] approaching the millimolar range; the estimated limit of detection (LOD) is 10.5×10^{-6} M. Most notably, the sensor can quantify UA levels both in the physiological (green box) and in pathological range (red box), the latter associated with lower [UA] values typically found in wounds infected by bacteria.^[13]

The working principle of electrolyte gated organic transistors, and in particular of OEET based biosensor, is yet to be fully elucidated. Our interpretation of the device response to H_2O_2 (either produced by Uricase or directly added to the electrolyte solution as in the aforementioned control experiments) can be depicted as follows. During non-Faradic OEET operational regime, a positive bias is applied to the gate electrode, forcing cations, present in the electrolyte, to drift into the porous PEDOT:PSS channel, thus lowering the channel conductivity (dedoping). Conversely, here, in the presence of UA and Uricase, the OEET works in the Faradic regime: H_2O_2 oxidation takes place at the gate and might lead to concomitant reduction of PEDOT, with accompanying penetration of cations in the semiconductor channel, resulting in a decrease of the drain current.^[38,44] Alternatively, the working principle underlying the operation of OEETs as enzyme-based

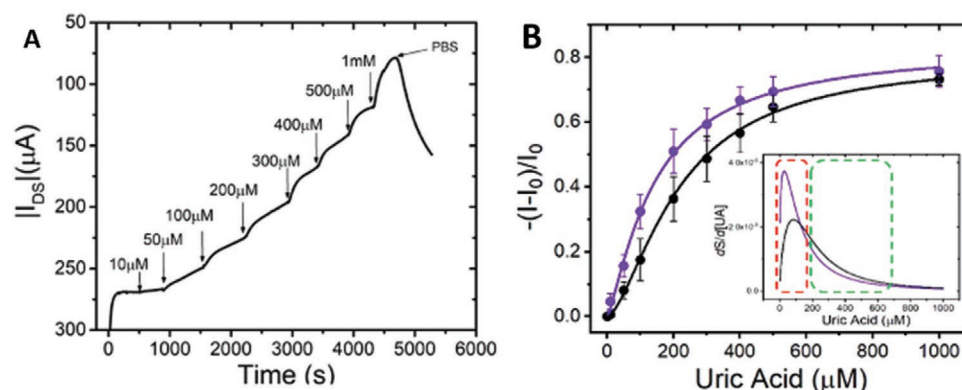


Figure 3. Uric acid detection in complex media. A) Real-time drain current changes at increasing uric acid concentrations in PBS buffer. B) Normalized current change (signal $S = -(I_{UA} - I_0)/I_0$) in PBS (black dots) and in artificial wound exudate (violet dots) as a function of [UA]. Error bars represent the standard error from four measurements. The inset shows the derivative of the signal S in PBS and in artificial wound exudate as black and violet curves, respectively. Pathological and physiological levels are marked as red and green boxes, respectively.

biosensors has been previously described^[64] in terms of increased electrolyte potential caused by an increase in H₂O₂ concentration through the Nernst equation, resulting in a more positive effective gate potential, which impacts on the cation drift in the porous PEDOT:PSS channel and thus decreases the drain current.^[65–67]

To mimic the complex environment of an infected wound, we performed measurements in an aqueous solution serving as artificial wound exudate,^[14] the composition of which can be found in the Experimental Section. We first assessed whether the C/Pt/GelB/GelA+UOx-gated OECTs could be operated even in such a more complex medium: as witnessed by the transfer and output characteristics in Figure S4, Supporting Information, current modulation in the same voltage range can still be achieved, and this result indicates that our OECTs are robust enough to withstand operation also in complex media, such as an artificial biological fluid. Nevertheless, differences in the electrical performances of the device when switching from operation in PBS to artificial exudate can be observed this finding might indicate that the device is somehow sensitive to the nature of the matrix, likely due to changes in the double layer capacitance as the ionic composition of the medium is altered.

We then performed multiple real-time measurements in artificial wound exudate solutions spiked with UA in the same [UA] range that was previously explored in PBS. A typical I_{DS} versus time response to increasing [UA] values in artificial wound exudate, provided in Figure S5, Supporting Information, indicates that the biosensor can be used to detect increasing UA concentration, even in an environment mimicking a biological milieu. The dose curve in the artificial wound exudate is provided in Figure 3B: the biosensor response closely parallels the one obtained in PBS and the calculated LOD is as low as 4.5×10^{-6} M in the artificial wound exudate. The derivative of the dose-curve response shows that our sensor exhibits the highest sensitivity below 200×10^{-6} M, namely, in the pathological region (red box), and lower sensitivity in the physiological range ($200\text{--}700 \times 10^{-6}$ M, green box). The device response plotted against the logarithm of [UA] is reported in Figure S6, Supporting Information, for both PBS and artificial wound exudate, and in both cases shows a linear trend in the 50×10^{-6} M to 1×10^{-3} M range.

3. Conclusion

We reported a printed UA biosensor based on OECT architecture, which exploits a biocompatible dual layer functionalization strategy to both immobilize the selective biorecognition element and to hinder parasitic reactions from charged interfering compounds. We demonstrated that our OECT-based biosensor can operate in artificial biological fluids, still maintaining similar sensitivity as for model solutions like PBS buffer. In addition, the OECT biosensor based on porcine-skin derived gelatin shows a faster response when compared to other substrates often used for enzyme entrapping. The device architecture and performance make the demonstrated device particularly attractive for wound infection monitoring. In view of future system integrations, these biosensors can be further engineered and coupled with devices for the local delivery of antibiotics, thus realizing a closed loop system loco-regional approach for wound care.

Moreover, the different electrical response upon switching from PBS to the artificial wound exudate might open to the possibility to monitor changes in the levels of polyelectrolytes in complex samples besides monitoring the specific response enabled by the presence of the biorecognition unit, possibly disentangling the response of redox active species (Faradic) from that of other compounds (non-Faradic) through the use of multivariate analysis, although this falls beyond the scope of the present paper. Eventually, the gate modification by a bipolar membrane (a cation- and an anion-selective membrane in contact with one another, as described in the present work) could be further exploited by getting inspiration from the ion bipolar membrane diodes architecture,^[68] which is also based on a stack of a cation- and anion-exchange membranes and that was successfully demonstrated as logic element and integrated with electrochromic display.^[69]

4. Experimental Section

Device Fabrication: OECTs were manufactured by screen-printing technique. As substrate was used a 125 μm thick PET foil, thermally treated (45 min at 140 °C) to confer more resistance to deformation by subsequent curing steps. Conductive tracks were printed using an Ag ink (Ag5000, DuPont, UK), whereas carbon contact pads and the gate were printed using a commercial carbon ink (C2130307DI, Gwent, UK). The organic semiconductor was printed in the channel using a commercial PEDOT: PSS ink (Clevios™ SV3, Heraeus Group, Germany). As the final step, the printed OECTs were coated with a dielectric layer (5018, DuPont, UK) leaving uncovered the gate and channel areas and the connecting pads. Devices were printed using a semi-automatic screen printer (DEK Horizon 03i printer, ASM Assembly Systems GmbH, Germany). Both the channel and the gate exposed areas measure 4 mm².

Device Functionalization: A potassium hexachloroplatinate (K₂PtCl₆, Sigma Aldrich) 10×10^{-3} M solution in H₂SO₄ 0.5 M was used, as platinum source, to modify the OECT carbon electrode. The electrodeposition was performed at a fixed voltage of -0.5 V with a potentiostat (CH Instrument Potentiostat 760c model), using a micro Ag/AgCl reference electrode (Elbatech, Livorno Italy) and a platinum wire as the counter electrode. The negatively charged layer was made of Gelatin from porcine skin (gel strength 300, type-B, Sigma Aldrich). Gelatin type B aqueous solution was prepared from dissolving dried gelatin in 50×10^{-3} M PBS at 60 °C for 1 h. The final gelatin layer on the gate electrode was obtained from a 3 μL drop of gelatin solution (3.5%) crosslinked with 1% v/v glutaraldehyde. The device was then stored at 4 °C for 24 h. A second layer of gelatin was then drop cast on the device. Uricase enzyme from *Bacillus fastidiosus* is immobilized in a gelatin type-A (Sigma Aldrich), positively charged at physiologic pH, with glutaraldehyde as the crosslinking agent. A 6 μL drop of 1% gelatin type A PBS solution, 1.7 mg mL⁻¹ enzyme TRIS buffer solution, and 1% v/v glutaraldehyde aqueous solution were cast on the gate area. The devices were left 4 h at 4 °C before use. Due to the important role played by the layer thickness in the device response, we controlled for variations in thickness by always using the same amount of gelatin on gate electrodes of constant area. The data reproducibility indirectly confirms that this procedure was successful in keeping the thickness constant.

The chitosan layer was obtained from a 6 μL drop of chitosan solution (final concentration 0.3 mg mL⁻¹), 1.7 mg mL⁻¹ enzyme, crosslinked with 1% v/v glutaraldehyde. Chitosan was first dissolved in 0.05 M acetic acid solution, while Uricase was dissolved in TRIS buffer solution. The devices were left 4 h at 4 °C before use. In all the sensors, the final content of the enzyme was 0.09 U.

Electrical Characterization and Data Analysis: Electric measurements were performed using an Agilent B2912A Source Measure Unit in PBS 50×10^{-3} M, pH 7.4, at room temperature. Transfer characteristics were

recorded sweeping the gate voltage (V_{GS}) from 0 to 1 V and fixed drain-source voltage (V_{DS}) of -0.4 V. Output characteristics were measured scanning the V_{DS} from 0 to -0.8 V, while sweeping the V_{GS} from 0 to 1 V with 10 steps of 0.1 V each. The response of each sensor to the addition of the analyte was measured in real-time at constant bias mode: V_{GS} and V_{DS} were fixed at $+0.5$ and -0.4 V, respectively, and the I_{DS} was registered as a function of time.

To obtain the normalized response S to increasing UA concentrations as $S = \Delta I/I = -(I_{UA} - I_0)/I_0$, I_{UA} was taken as the drain current recorded 300 s after each UA injection, while I_0 is the current recorded in the absence of analyte. 1×10^{-3} M concentration in PBS normalized response was obtained with the average of only two devices.

The LOD is the lowest concentration detectable from the device and has been calculated as $LOD = S_{buffer} + 3\sigma$, where S_{buffer} is the signal for PBS and artificial wound exudate in absence of analyte and σ is their standard deviation. σ has been obtained from the PBS and artificial wound exudate I_{DS} current values during the stabilization time.

Artificial Wound Exudate: The artificial wound exudate medium was prepared by dissolving in water sodium chloride 124×10^{-3} M, magnesium chloride 831×10^{-6} M, calcium chloride 2.48×10^{-3} M, sodium bicarbonate 36.8×10^{-3} M, glucose 5×10^{-3} M, albumin 150×10^{-6} M, lactic acid 90% 10×10^{-6} M. Measured pH: 6.72 (ref. [14]).

Supporting Information

Supporting Information is available from the Wiley Online Library or from the author.

Acknowledgements

V.B. would like to acknowledge the Swedish Foundation for Strategic Research (BioCom Lab, grant RIT15-0119) for financial support. C.D., M.B., and D.T.S. acknowledge the support provided by the Swedish Foundation for Strategic Research and the Knut and Alice Wallenberg Foundation for this research. This work was conducted within the framework of the BioCom Lab projects. Additional assistance with mask design and printing was provided by Ulrika Linderhed and Marie Nilsson at RISE AB, Norrköping, Sweden.

Conflict of Interest

The authors declare no conflict of interest.

Keywords

enzymatic detection, flexible biosensors, organic electrochemical transistors, uric acid, wound care

Received: July 8, 2020

Revised: September 18, 2020

Published online: October 7, 2020

- [1] C. E. Fife, M. J. Carter, D. Walker, *Wound Repair Regener.* **2010**, *18*, 154.
- [2] C. K. Sen, G. M. Gordillo, S. Roy, R. Kirsner, L. Lambert, T. K. Hunt, F. Gottrup, G. C. Gurtner, M. T. Longaker, *Wound Repair Regener.* **2009**, *17*, 763.
- [3] H. Derakhshandeh, S. S. Kashaf, F. Aghabaglou, I. O. Ghanavati, A. Tamayol, *Trends Biotechnol.* **2018**, *36*, 1259.
- [4] I. Negut, V. Grumezescu, A. M. Grumezescu, *Molecules* **2018**, *23*, 2392.

- [5] T. Guinovart, G. Valdés-Ramírez, J. R. Windmiller, F. J. Andrade, J. Wang, *Electroanalysis* **2014**, *26*, 1345.
- [6] P. Salvo, V. Dini, A. Kirichain, A. Janowska, T. Oranges, A. Chiricozzi, T. Lomonaco, F. Di Francesco, M. Romanelli, *Sensors* **2017**, *17*, 2952.
- [7] P. Salvo, N. Calisi, B. Melai, B. Cortigiani, M. Mannini, A. Caneschi, G. Lorenzetti, C. Paoletti, T. Lomonaco, A. Paolicchi, *Biosens. Bioelectron.* **2017**, *91*, 870.
- [8] R. Jarosova, S. E. McClure, M. Gajda, M. Jovic, H. H. Girault, A. Lesch, M. Maiden, C. Waters, G. M. Swain, *Anal. Chem.* **2019**, *91*, 8835.
- [9] S. Schreml, R. J. Meier, M. Kirschbaum, S. C. Kong, S. Gehmert, O. Felthaus, S. Küchler, J. R. Sharpe, K. Wöltje, K. T. Weiß, *Theranostics* **2014**, *4*, 721.
- [10] D. McColl, B. Cartlidge, P. Connolly, *Int. J. Surg.* **2007**, *5*, 316.
- [11] M. P. Caley, V. L. C. Martins, E. A. O'Toole, *Adv. Wound Care* **2015**, *4*, 225.
- [12] S. Barrientos, O. Stojadinovic, M. S. Golinko, H. Brem, M. Tomic-Canic, *Wound Repair Regener.* **2008**, *16*, 585.
- [13] P. Kassal, J. Kim, R. Kumar, W. R. de Araujo, I. M. Steinberg, M. D. Steinberg, J. Wang, *Electrochem. Commun.* **2015**, *56*, 6.
- [14] N. J. Trengove, S. R. Langton, M. C. Stacey, *Wound Repair Regener.* **1996**, *4*, 234.
- [15] P. Cirillo, W. Sato, S. Reungjui, M. Heinig, M. Gersch, Y. Sautin, T. Nakagawa, R. J. Johnson, *J. Am. Soc. Nephrol.* **2006**, *17*, S165.
- [16] H. K. Choi, K. Atkinson, E. W. Karlson, W. Willett, G. Curhan, *N. Engl. J. Med.* **2004**, *350*, 1093.
- [17] S. C. Howard, D. P. Jones, C.-H. Pui, *N. Engl. J. Med.* **2011**, *364*, 1844.
- [18] F. P. Cappuccio, P. Strazzullo, E. Farinaro, M. Trevisan, *JAMA, J. Am. Med. Assoc.* **1993**, *270*, 354.
- [19] P. Richette, T. Bardin, *Lancet* **2010**, *375*, 318.
- [20] M. Heinig, R. J. Johnson, *Cleveland Clin. J. Med.* **2006**, *73*, 1059.
- [21] T. R. Dargaville, B. L. Farrugia, J. A. Broadbent, S. Pace, Z. Upton, N. H. Voelcker, *Biosens. Bioelectron.* **2013**, *41*, 30.
- [22] M. A. Rouf, R. F. Lomphey, *J. Bacteriol.* **1968**, *96*, 617.
- [23] C. Liao, M. Zhang, M. Y. Yao, T. Hua, L. Li, F. Yan, C. Mak, M. Zhang, H. L. W. Chan, F. Yan, *Adv. Mater.* **2015**, *27*, 676.
- [24] L. J. Currano, F. C. Sage, M. Hagedon, L. Hamilton, J. Patrone, K. Gerasopoulos, *Sci. Rep.* **2018**, *8*, 15890.
- [25] D. Khodagholy, V. F. Curto, K. J. Fraser, M. Gurfinkel, R. Byrne, D. Diamond, G. G. Malliaras, F. Benito-Lopez, R. M. Owens, *J. Mater. Chem.* **2012**, *22*, 4440.
- [26] L. Contat-Rodrigo, C. Pérez-Fuster, J. V. Lidón-Roger, A. Bonfiglio, E. García-Breijo, *Org. Electron.* **2017**, *45*, 89.
- [27] G. Scheiblin, A. Aliane, X. Strakosas, V. F. Curto, R. Coppard, G. Marchand, R. M. Owens, P. Mailley, G. G. Malliaras, *MRS Commun.* **2015**, *5*, 507.
- [28] G. Scheiblin, A. Aliane, R. Coppard, R. M. Owens, P. Mailley, G. G. Malliaras, in *Org. Field-Effect Transistors XIV; Org. Sensors Bioelectron. VIII*, SPIE, Bellingham **2015**, p. 95681E.
- [29] M. Berto, C. Diacci, L. Theuer, M. Di Lauro, D. T. Simon, M. Berggen, F. Biscarini, V. Beni, C. A. Bortolotti, *Flexible Printed Electron.* **2018**, *3*, 024001.
- [30] G. Mattana, A. Loi, M. Woytasik, M. Barbaro, V. Noël, B. Piro, *Adv. Mater. Technol.* **2017**, *2*, 1700063.
- [31] O. J. Rauhala, S. Dominguez, G. D. Spyropoulos, J. J. Ferrero, T. R. Boyers, P. Jastrzebska-Perfect, C. Cea, D. Khodagholy, J. N. Gelinas, *Adv. Mater. Technol.* **2020**, *5*, 1900663.
- [32] C. Cea, G. D. Spyropoulos, P. Jastrzebska-Perfect, J. J. Ferrero, J. N. Gelinas, D. Khodagholy, *Nat. Mater.* **2020**, *19*, 679.
- [33] A. Campana, T. Cramer, D. T. Simon, M. Berggren, F. Biscarini, *Adv. Mater.* **2014**, *26*, 3874.
- [34] C. Diacci, J. W. Lee, P. Janson, G. Dufil, G. Méhes, M. Berggren, D. T. Simon, E. Stavrinidou, *Adv. Mater. Technol.* **2020**, *5*, 1900262.
- [35] A. Pappa, V. F. Curto, M. Braendlein, X. Strakosas, M. J. Donahue, M. Fiochi, G. G. Malliaras, R. M. Owens, *Adv. Healthcare Mater.* **2016**, *5*, 2295.

- [36] X. Strakosas, M. Huerta, M. J. Donahue, A. Hama, A. Pappa, M. Ferro, M. Ramuz, J. Rivnay, R. M. Owens, *J. Appl. Polym. Sci.* **2017**, *134*, 44483.
- [37] D. Gentili, P. D'Angelo, F. Militano, R. Mazzei, T. Poerio, M. Brucale, G. Tarabella, S. Bonetti, S. L. Marasso, M. Cocuzza, L. Giorno, S. Iannotta, M. Cavallini, *J. Mater. Chem. B* **2018**, *6*, 5400.
- [38] L. Kergoat, B. Piro, D. T. Simon, M. C. Pham, V. Noël, M. Berggren, *Adv. Mater.* **2014**, *26*, 5658.
- [39] H. Tang, P. Lin, H. L. W. Chan, F. Yan, *Biosens. Bioelectron.* **2011**, *26*, 4559.
- [40] I. Gualandi, E. Scavetta, F. Mariani, D. Tonelli, M. Tessarolo, B. Fraboni, *Electrochim. Acta* **2018**, *268*, 476.
- [41] I. Gualandi, M. Marzocchi, E. Scavetta, M. Calienni, a. Bonfiglio, B. Fraboni, *J. Mater. Chem. B* **2015**, *3*, 6753.
- [42] Z. Bao, Y. Feng, A. Dodabalapur, V. R. Raju, A. J. Lovinger, *Chem. Mater.* **1997**, *9*, 1299.
- [43] L. Theuer, J. Randek, S. Junne, P. Neubauer, C.-F. Mandenius, V. Beni, *Processes* **2020**, *8*, 321.
- [44] M. Sensi, M. Berto, A. Candini, A. Liscio, A. Cossarizza, V. Beni, F. Biscarini, C. A. Bortolotti, *ACS Omega* **2019**, *4*, 5374.
- [45] M. S. Chae, Y. K. Yoo, J. Kim, T. G. Kim, K. S. Hwang, *Sens. Actuators, B* **2018**, *272*, 448.
- [46] H. H. Bay, R. Vo, X. Dai, H. H. Hsu, Z. Mo, S. Cao, W. Li, F. G. Omenetto, X. Jiang, *Nano Lett.* **2019**, *19*, 2620.
- [47] G. E. Fenoy, W. A. Marmisollé, O. Azzaroni, W. Knoll, *Biosens. Bioelectron.* **2020**, *148*, 111796.
- [48] E. Piccinini, C. Bliem, C. Reiner-Rozman, F. Battaglini, O. Azzaroni, W. Knoll, *Biosens. Bioelectron.* **2017**, *92*, 661.
- [49] T. Berninger, C. Bliem, E. Piccinini, O. Azzaroni, W. Knoll, *Biosens. Bioelectron.* **2018**, *115*, 104.
- [50] I. Katsounaros, W. B. Schneider, J. C. Meier, U. Benedikt, P. U. Biedermann, A. A. Auer, K. J. J. Mayrhofer, *Phys. Chem. Chem. Phys.* **2012**, *14*, 7384.
- [51] A. P. Periasamy, Y.-J. Chang, S.-M. Chen, *Bioelectrochemistry* **2011**, *80*, 114.
- [52] S. Karacaoğlu, S. Timur, A. Telefoncu, *Artif. Cells, Blood Substitutes, Biotechnol.* **2003**, *31*, 357.
- [53] P. Jolly, A. Miodek, D.-K. Yang, L.-C. Chen, M. D. Lloyd, P. Estrela, *ACS Sens.* **2016**, *1*, 1308.
- [54] D. Bagal-Kestwal, R. M. Kestwal, B. H. Chiang, M. S. Karve, *Sens. Actuators, B* **2011**, *160*, 1026.
- [55] E. Vatankhah, M. P. Prabhakaran, G. Jin, L. G. Mobarakeh, S. Ramakrishna, *J. Biomater. Appl.* **2014**, *28*, 909.
- [56] K. Ulubayram, A. N. Cakar, P. Korkusuz, C. Ertan, N. Hasirci, *Biomaterials* **2001**, *22*, 1345.
- [57] Y. S. Choi, S. B. Lee, S. R. Hong, Y. M. Lee, K. W. Song, M. H. Park, *J. Mater. Sci.: Mater. Med.* **2001**, *12*, 67.
- [58] P. E. Erden, E. Kiliç, *Talanta* **2013**, *107*, 312.
- [59] C. Liao, M. Zhang, L. Niu, Z. Zheng, F. Yan, *J. Mater. Chem. B* **2014**, *2*, 191.
- [60] S. Islam, M. A. R. Bhuiyan, M. N. Islam, *J. Polym. Environ.* **2017**, *25*, 854.
- [61] J. R. Anusha, C. J. Raj, B.-B. Cho, A. T. Fleming, K.-H. Yu, B. C. Kim, *Sens. Actuators, B* **2015**, *215*, 536.
- [62] D. A. Bernards, G. G. Malliaras, *Adv. Funct. Mater.* **2007**, *17*, 3538.
- [63] H.-S. Lee, M. Q. Yee, Y. Y. Eckmann, N. J. Hickok, D. M. Eckmann, R. J. Composto, *J. Mater. Chem.* **2012**, *22*, 19605.
- [64] D. A. Bernards, D. J. Macaya, M. Nikolou, J. A. DeFranco, S. Takamatsu, G. G. Malliaras, *J. Mater. Chem.* **2008**, *18*, 116.
- [65] O. Yaghmazadeh, F. Cicoira, D. a. Bernards, S. Y. Yang, Y. Bonnassieux, G. G. Malliaras, *J. Polym. Sci., Part B: Polym. Phys.* **2011**, *49*, 34.
- [66] H. Tang, F. Yan, P. Lin, J. Xu, H. L. W. Chan, *Adv. Funct. Mater.* **2011**, *21*, 2264.
- [67] M. E. Welch, T. Doublet, C. Bernard, G. G. Malliaras, C. K. Ober, *J. Polym. Sci., Part A: Polym. Chem.* **2015**, *53*, 372.
- [68] E. O. Gabrielsson, K. Tybrandt, M. Berggren, *Lab Chip* **2012**, *12*, 2507.
- [69] A. Malti, E. O. Gabrielsson, X. Crispin, M. Berggren, *Adv. Mater.* **2015**, *27*, 3909.

**ADVANCED
MATERIALS**
INTERFACES

Supporting Information

for *Adv. Mater. Interfaces*, DOI: 10.1002/admi.202001218

Flexible Printed Organic Electrochemical Transistors for the
Detection of Uric Acid in Artificial Wound Exudate

*Marina Galliani, Chiara Diacci, Marcello Berto, Matteo
Sensi, Valerio Beni, Magnus Berggren, Marco Borsari, Daniel
T. Simon, Fabio Biscarini, and Carlo A. Bortolotti**

Supporting Information

Flexible Printed Organic Electrochemical Transistors for the Detection of Uric Acid in Artificial Wound Exudate

*Marina Galliani, Chiara Diacci, Marcello Berto, Matteo Sensi, Valerio Beni, Magnus Berggren, Marco Borsari, Daniel T. Simon, Fabio Biscarini, Carlo A. Bortolotti**

Marina Galliani, Chiara Diacci, Dr. Marcello Berto, Dr. Matteo Sensi, Prof. Fabio Biscarini and Dr. Carlo A. Bortolotti.

Dipartimento di Scienze della Vita, Università di Modena e Reggio Emilia, Via Campi 103, 41125 Modena, Italy.

E-mail: carloaugusto.bortolotti@unimore.it

Chiara Diacci, Prof. Magnus Berggren and Prof. Daniel T. Simon.

Laboratory of Organic Electronics, Department of Science and Technology, Linköping University, SE-601 74 Norrköping, Sweden.

Prof. Fabio Biscarini.

Istituto Italiano di Tecnologia — Center for Translational Neurophysiology, Via Fossato di Mortara 17-19, 44121 Ferrara, Italy.

Prof. Marco Borsari.

Dipartimento di Scienze Chimiche e Geologiche, Università di Modena e Reggio Emilia, Via Campi 103, 41125 Modena, Italy.

Dr. Valerio Beni.

Department of Smart Hardware, RISE AB, Research Institutes of Sweden, Norrköping, Sweden.

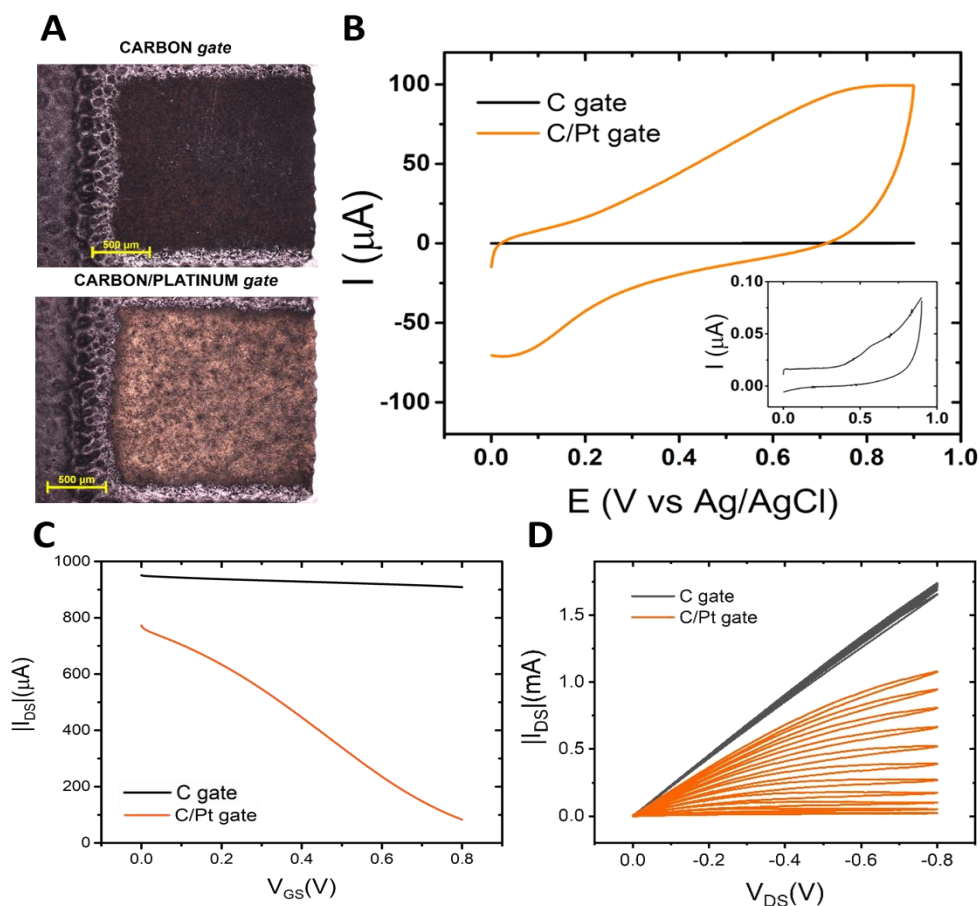


Figure S1: Platinum functionalization step. (A) Optical microscopy image of the gate presenting a platinum layer on top of the carbon printed gate. (B) Cyclic voltammetry showing the capacitive behaviour of Carbon gate (C gate, black curve) and Carbon gate covered with Platinum (C/Pt gate, orange) recorded in 50mM PBS, voltage range 0 V-0.9 V and scan rate 50mV/s. The inset shows a magnification of the C gate, black curve. (C, D) Overlay of transfer measured at fixed $V_{SD} = -0.4V$ (C) and output characteristics measured in 50mM PBS buffer, V_{GS} scanning from 0.0V to +1.0V with steps of +0.1V(D) for C and C/Pt gated OECT in black and orange, respectively.

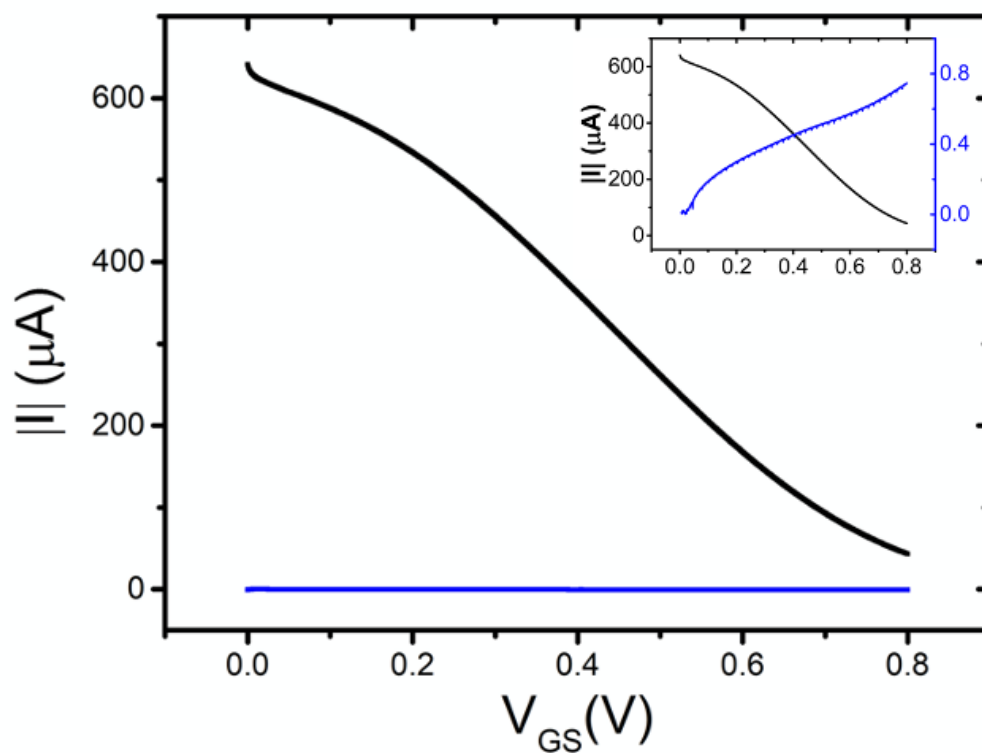


Figure S2: typical electrical response for C/Pt/GelB/GelA+UOx gated OECTs operated in PBS. In black, the transfer curve I_{DS} vs I_{GS} for constant $I_{DS} = -0.4V$; in blue, the leakage current I_{GS} .

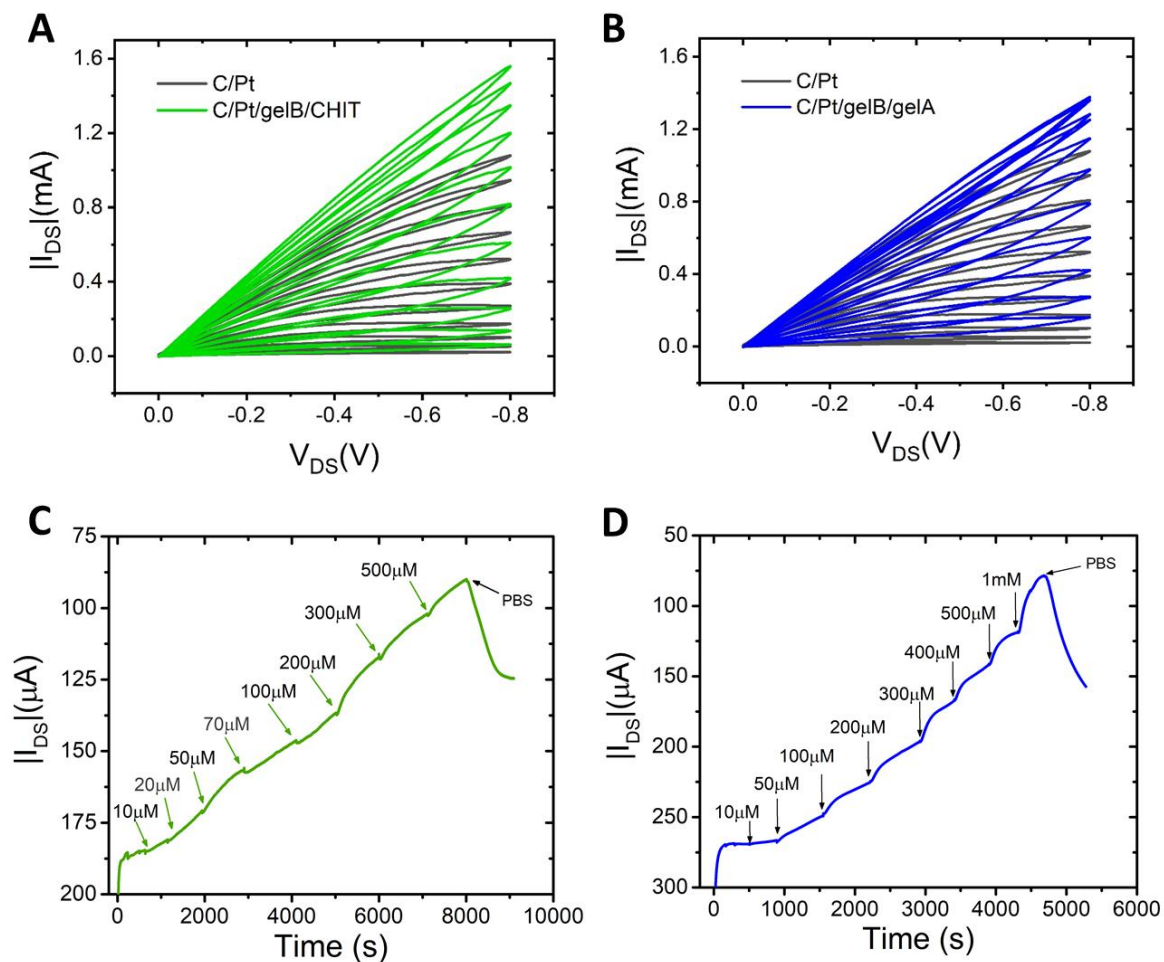


Figure S3: Chitosan and Gelatin-A performance. (A) Output characteristics of C/Pt/GelB/Chit+UOx and C/Pt/GelB/GelA+UOx OECTs (A) and (B), respectively. Measured in 50mM PBS buffer, V_{GS} scanning from 0.0V to +1.0V with steps of +0.1V. (C) Drain current vs. time response of a C/Pt/GelB/Chit+UOx OECT for increasing concentration of uric acid. (D) Drain current vs. time response of a C/Pt/GelB/GelA+UOx OECT for increasing concentration of uric acid.

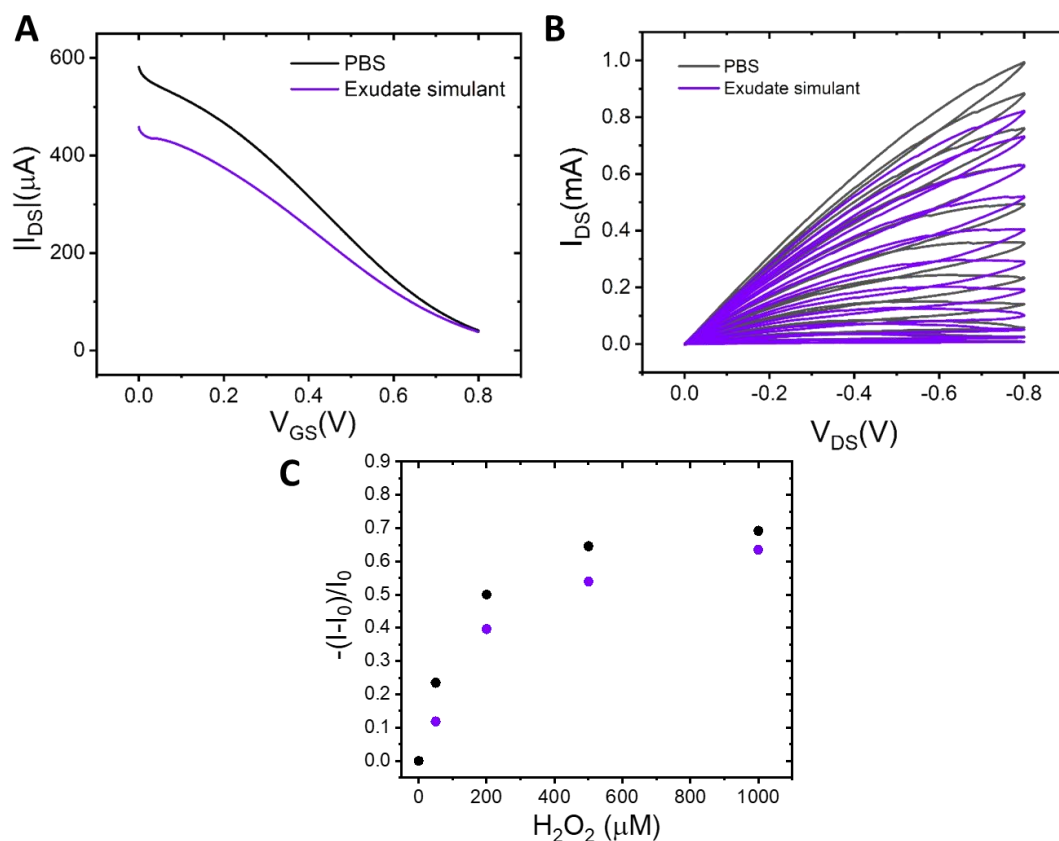


Figure S4: electrical characteristics in PBS and exudate simulant. (A) Transfer characteristics of C/Pt/GelB/GelA+UO_x gated OECT in PBS buffer (black line) and exudate simulant (violet line) measured at fixed $V_{SD} = -0.4\text{V}$. (B) Output characteristics of the functionalized OECT in PBS buffer (black line) and exudate simulant (violet line), V_{GS} scanning from 0.0V to +1.0V with steps of +0.1V. (C) Normalized response of the biosensor to increasing concentrations of H_2O_2 in PBS (black dots) and exudate simulant (violet dots).

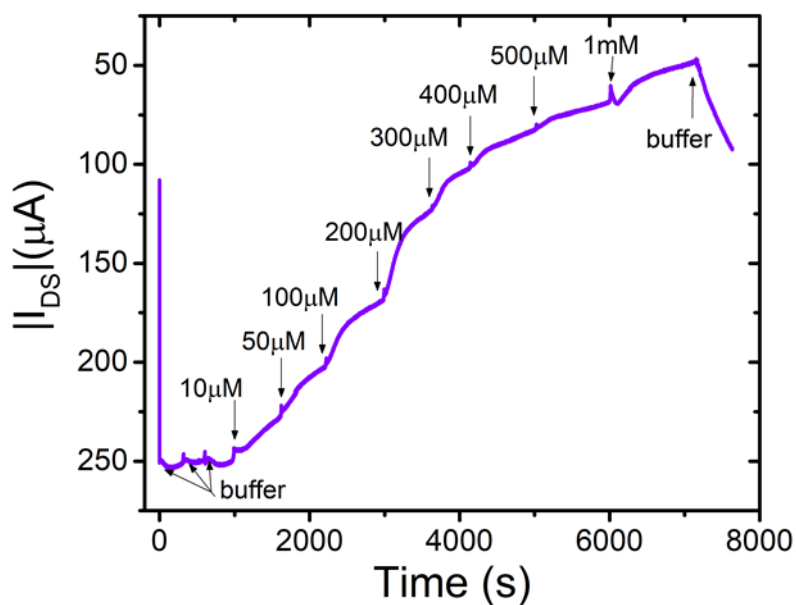


Figure S5: Uric acid detection in complex media. Drain current versus time response of a C/Pt/GelB/GelA+UOx gated OECT operated in exudate simulant, at different UA concentrations.

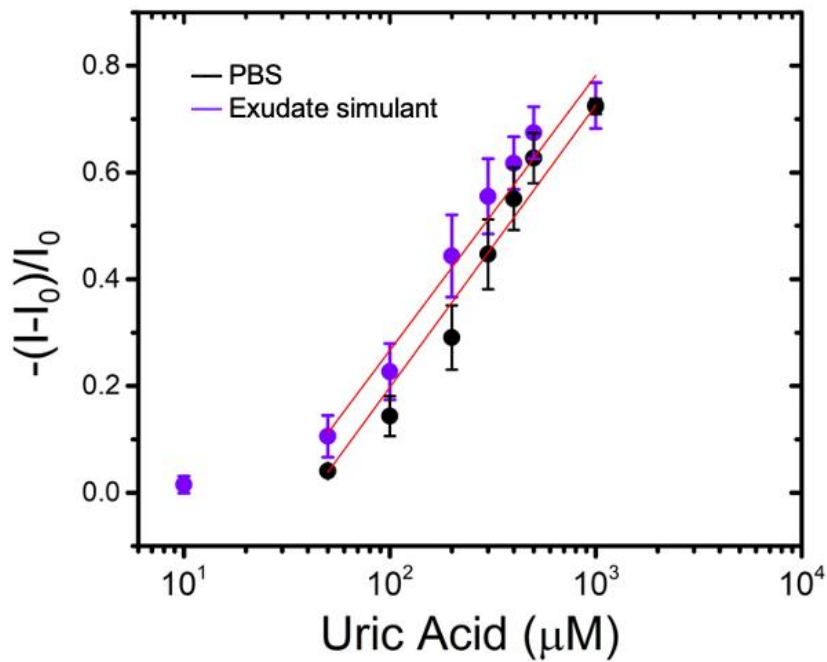


Figure S6: calibration curve for C/Pt/GelB/GelA+UOx gated OECT operated in PBS and exudate simulant, at different UA concentrations.

Paper III

Organic electrochemical transistor-based aptasensor for interleukin-6 label-free detection.

Organic electrochemical transistor-based aptasensor for interleukin-6 label-free detection

Chiara Diacci^{1,2}, Marcello Berto², Tero Petri Ruoko¹, Samuel Lienemann¹, Daniel T. Simon¹, Magnus Berggren¹, Marco Borsari³, Fabio Biscarini², Carlo A. Bortolotti²

1. Laboratory of Organic Electronics, Department of Science and Technology, ITN, Linköping University, 601 74, Norrköping, Sweden.
2. Dipartimento di Scienze della Vita, Università di Modena e Reggio Emilia, via Campi 103, 41125 Modena, Italy.
3. Dipartimento di Scienze Chimiche e Geologiche, Università di Modena e Reggio Emilia, via Campi 103, 41125 Modena, Italy.

Abstract

Here we show an OECT based biosensor for the detection of interleukin 6 (IL6), an important biomarker associated to various pathological processes, including chronic inflammation, inflammaging, cancer and severe COVID-19 infection. We functionalized the biosensor using aptamers as sensing units, engineered oligonucleotide strands, able to bind specifically the cytokine of interest. Moreover, we developed an easy functionalization strategy based on gold nanoparticles deposition onto the PEDOT:PSS gate electrode for the subsequential electrodeposition of the thiolate aptamers. We proved a detection range from picomolar to nanomolar concentrations for IL6 and the selectivity of the device when compared to the detection of Tumor Necrosis Factor (TNF), an analogous cytokine whose levels are also high in inflammatory processes.

Introduction

Cytokines are bioactive proteins involved in pro- and anti-inflammatory processes ¹. Environmental stimuli, stress or diseases may trigger the release of these proteins in a ripple effect for the activation of the immune system and/or various metabolic pathways ^{2,3}. Cytokine monitoring can thus be used to track progression of, *e.g.*, infection ⁴, cancer ⁵, or chronic inflammatory processes ⁶. Interleukin-6 (IL-6) is a low molecular weight glycoprotein, which

belongs to the family of cytokines. IL-6 has multiple functions, since it can act both as an anti-inflammatory protein, inhibiting other cytokines release, or in pro-inflammatory processes, triggering the acute phase response of the innate immune system^{7,8}. In physiological conditions and due to the local mode of action, IL-6 is present in low concentrations (200 fM) in human serum. In contrast, IL-6 concentrations can be much higher in acute (>40 pM)^{9,10} or chronic pathologies (>240 fM)^{11,12}. Recently, IL-6 has been associated with severe COVID-19 (SARS-CoV-2) infection¹³. From preliminary studies, high levels (>3.5 pM)¹⁴ of IL-6 have been correlated with respiratory failure and death, making this cytokine an important marker for the disease and pandemic progression^{15,16}. Cytokine – and in particular IL-6 – detection and quantification are thus an essential tool for precise monitoring of various diseases. Cytokines are present in fM-pM concentrations in bodily fluids; therefore, their detection requires both high sensitivity and selectivity. State of the art quantification methods include enzyme-linked immunosorbent assays (ELISA) and antibody arrays. Although these methods are robust and standardised, they require bulky equipment and laborious protocols, characteristics that hinder their usage at the point of care or even in at-home settings¹⁷. For this reason, research has been focused in developing novel biosensor technologies for the detection of these inflammatory biomarkers, with miniaturized platform, such as electrochemical sensors^{18–21} or Field Effect Transistors (FETs)^{22–26}. Organic electrochemical transistors (OECTs) are now considered one of the most promising organic electronics technologies due to their signal amplification capability, low operation voltages, ease of fabrication, and ability to operate in aqueous environments^{27–30}. OECTs are three terminal devices, where the gate electrode can modulate the current in the channel (source-drain current, I_{SD}), employing the electrolyte as the dielectric layer; small changes in gate voltage establish electrochemical modulation of the organic electronic channel, increasing or decreasing its conductivity^{31,32}. Via proper functionalization, OECTs can selectively detect the metabolite of interest through changes in I_{SD} ^{29,33}. OECTs have been used as the sensing platform for a number of analytes, exploiting the possibility of modulating I_{SD} either through faradaic reactions at the gate, or via non-faradaic mechanisms that relies purely on the permeability of the semiconducting channel to ions from the electrolyte. The detection mechanism is usually

achieved through specific enzymatic reactions^{34–42}, molecularly imprinted polymers^{43,44}, or using non-faradaic antibody-antigen recognition^{45–50}.

Although antibodies remain the gold standard sensing units (*e.g.*, in ELISA), there is a growing interest in finding innovative, more reproducible and robust solutions, based on protein or oligonucleotide scaffolds⁵¹. Aptamers are oligonucleotide-based recognition elements which have been gaining interest due to their high selectivity, facility of synthesis, and low-cost development⁵². These probes are generated through a technique called Systematic Evolution of Ligand by Exponential Enrichment (SELEX), based on selection and amplification of oligonucleotide sequences which are able to bind target molecules⁵³. Aptamer have already been employed successfully in electrochemical biosensors^{54–57}, immunoassays^{58–60}, and OECT-based biosensors^{26,61–63}.

In this work, we present a planar OECT-based biosensor for label-free detection of IL-6 via aptamer recognition. In addition, we describe an easy functionalization method using Au nanoparticles (AuNPs) deposition and electrochemical aptamer functionalization on the organic electronic gate electrode surface.

Discussion

OECTs were fabricated on a polyethylene naphthalate (PEN) foil with standard photolithographic techniques and presented the gate electrode and the channel in a planar configuration (Fig. 1A). Gold source, drain, and gate electrodes delineated the transistor geometry and a thin layer of poly(3,4-ethylenedioxythiophene) doped with polystyrene sulfonate (PEDOT:PSS) constituted the channel. An additional layer of PEDOT:PSS was deposited on the active area of the gate electrode to increase its capacitance and to better modulate the channel at low applied voltages (Fig. 1A).

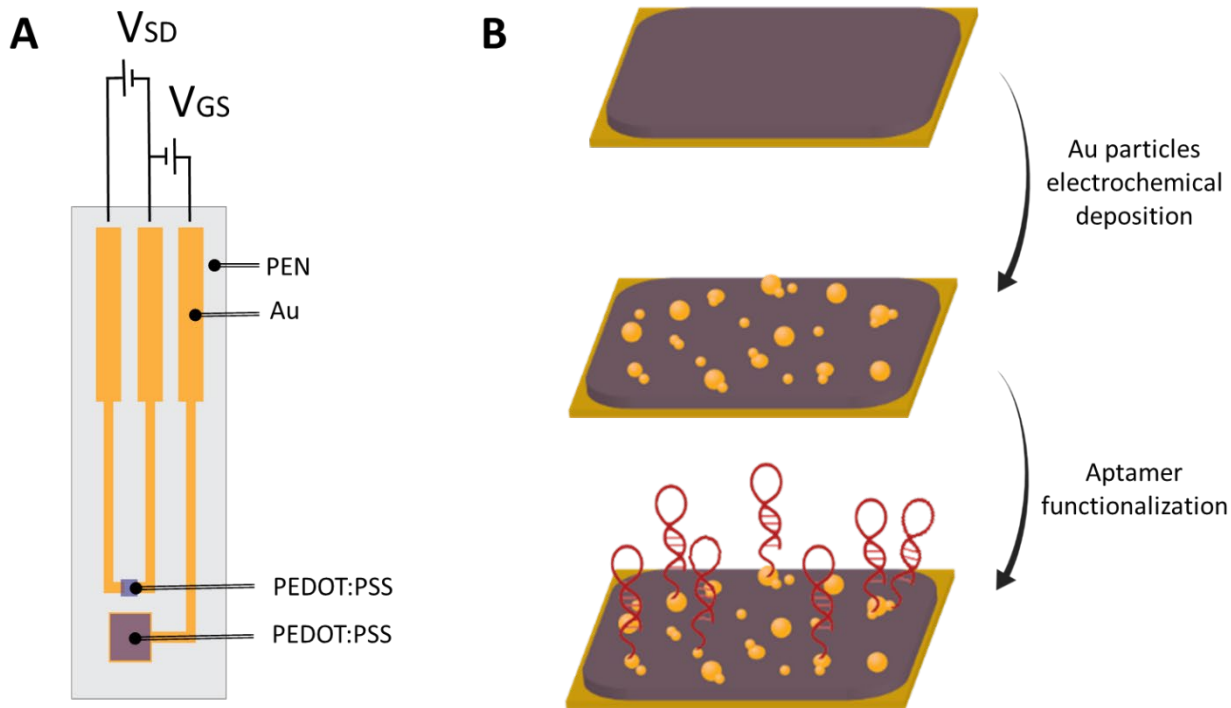


Figure 1. OECT-based aptasensor. (A) Schematic representation of the PEDOT:PSS based transistor planar configuration. (B) Gate functionalization steps: AuNP electrochemical deposition on PEDOT:PSS followed by aptamer functionalization of the resulting composite.

Conducting polymers and their composites have been widely used for analyte detection, even in cases where they lack intrinsic specificity. Deposition of nanoparticles of different materials on polymer surfaces can provide additional physical-chemical properties, such as electro-catalytic activity using platinum nanoparticles (PtNPs) for peroxide detection^{34,41} or an easier surface for functionalization, such as AuNPs for thiolate sensing units^{64–67}. Here, the gate electrode was modified with AuNPs in order to provide a platform for aptamer binding. AuNP modification was performed via electrochemical deposition of HAuCl_4 on the PEDOT:PSS film (Fig. 1B). The microscope optical images in Figure 2 show the presence of the AuNPs/aggregates (Fig. 2B) when compared to a bare PEDOT:PSS gate electrode (Fig. 2A). Through scanning electron microscopy (SEM), it was possible to study the disposition and dimension of the Au particles, visible as disperse aggregates with sub-micron dimensions. Fig. 2D and 2E clearly demonstrate the presence of AuNPs on the surface, when compared to the bare PEDOT:PSS device in Fig. 2C and 2E. The presence of gold on top of PEDOT:PSS layer was further demonstrated through cyclic

voltammetry with ferricyanide $[\text{Fe}(\text{CN})_6]^{3-/4-}$. The bare PEDOT:PSS electrode did not show electrochemical redox peaks from ferricyanide, while the composite PEDOT:PSS/AuNP did show characteristic peaks (Fig. S1A). In contrast with a planar bare gold gate electrode with the same geometry, the PEDOT:PSS coated gate and PEDOT:PSS/AuNP showed better channel modulation, higher transconductance (Fig. S1B), and faster transfer characteristic stabilization over time (Fig. S1C).

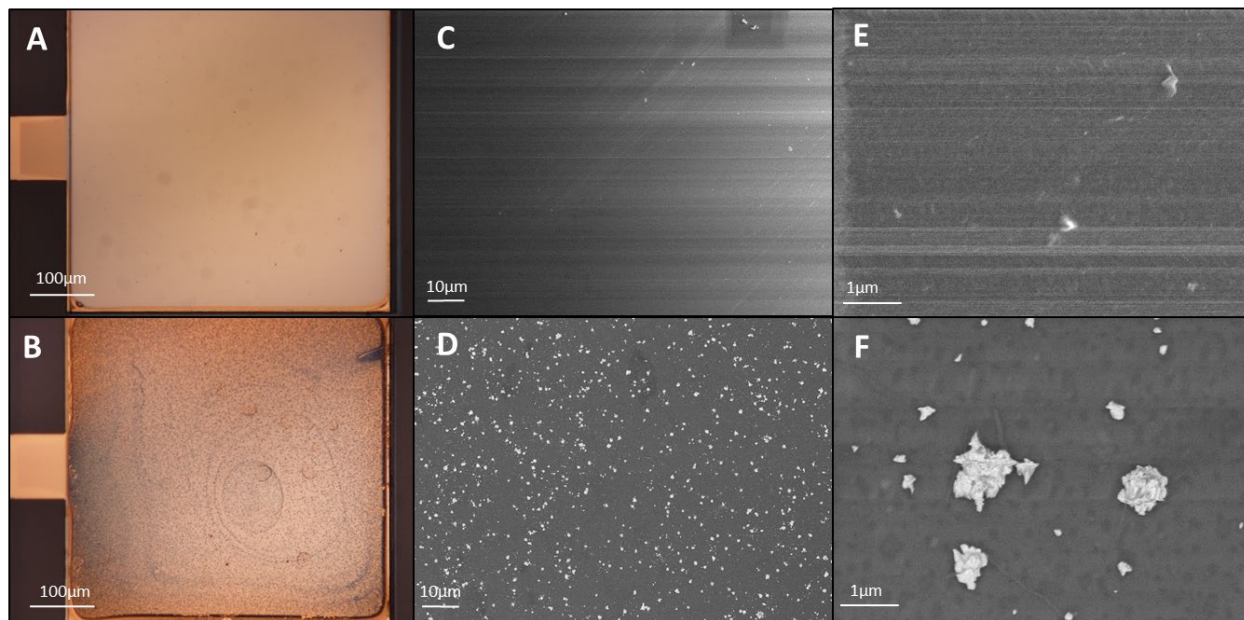


Figure 2. Modified gate electrode. Optical microscope images of (A) PEDOT:PSS gate electrode and (B) PEDOT:PSS/AuNP. SEM images of (C, E) PEDOT:PSS and (D, F) the AuNP modified gate.

The specific aptamer sequence selective for IL-6 was developed by Kristen L. Rhinehardt et al, through SELEX, and evaluated with molecular dynamics analysis and Surface Plasmon Raman imaging (SPRi) ⁶⁸. Furthermore, the sequence has already been proved applicable for IL-6 biosensing technology based on Surface-Enhanced Raman Spectroscopy (SERS) ⁶⁹. Aptamer functionalization was performed via electrochemical disulphide reduction at the gate electrode. In solution, aptamers are present in their stabilized form, with the thiolate ending protected through a 6-mercapto-1-hexanol (MCH) residue (Fig. 3A). MCH is a molecule often used in combination with aptamers to create an antifouling layer on the sensing surface ^{70,71}. We took advantage from the aptamer-MCH configuration, performing an electrochemical reduction at the gate electrode, binding both aptamer and linker to the gold particles. Figure 3B shows cyclic voltammetry of a PEDOT:PSS/AuNP gate electrode in aptamer solution. We observed a decrease

of cathodic current over time and the decrease of the reduction peak around -600 mV vs Ag/AgCl, indicating the binding of aptamer and MCH to the electrode. In order to prove the presence of the aptamer on the PEDOT:PSS/AuNP surface, we performed faradaic electrochemical impedance spectroscopy (EIS) analysis on the gate electrode before and after aptamer deposition (Fig. 3C). The binding of the aptamer and MCH to the AuNPs on the gate electrode created a barrier to the negatively charged redox molecule and consequently an increase in the electron transfer resistance (R_{ct}), visible as a widening of the semicircular component of the trace toward larger Z' .

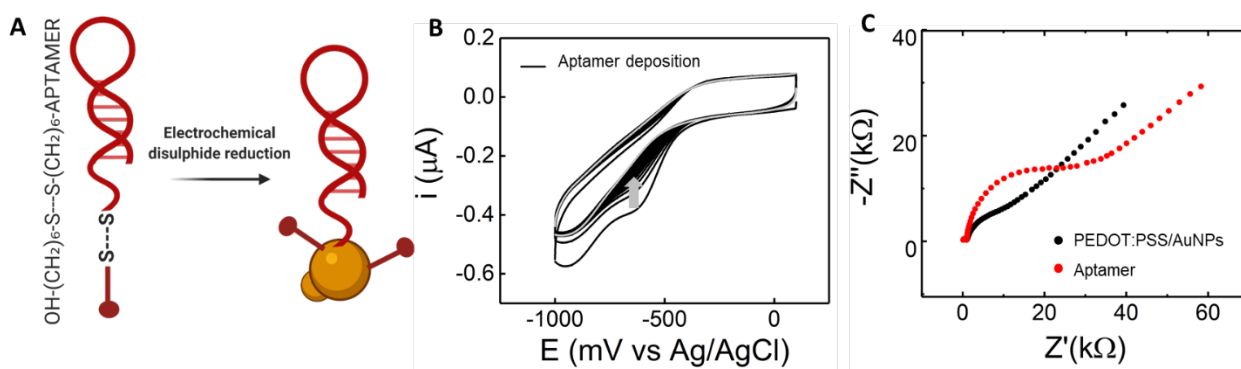


Figure 3. Aptamer functionalization. (A) Schematic representation of aptamer in solution and electrochemical disulphide reduction for AuNPs functionalization. (B) Cyclic voltammetry of PEDOT:PSS/AuNP gate electrode in 1 μ M aptamer solution from 0V to 1V, 50mV/s for 30 cycles. The grey curve shows the last cycle. (C) Impedance spectroscopy in ferricyanide 5mM for PEDOT:PSS gold particles electrode (black) and aptamer functionalized gate (red).

The functionalized gate surface was further studied using Fourier-transform infrared spectroscopy (FTIR) in attenuated total reflection (ATR) mode (Fig. 4). FTIR-ATR confirms the presence of oligonucleotides (aptamers) bound to the PEDOT:PSS/AuNP composite. The PEDOT:PSS peaks are stronger than the aptamer ones, due to the greater abundance of the polymer compared to the DNA monolayer on the gold particles. In Fig. 4 it is possible to notice visible changes from the PEDOT:PSS/AuNP composite (orange spectra) to the PEDOT:PSS/AuNP/Aptamer functionalized electrode (purple spectra). Specifically, there is an increase in absorption at 1100 cm^{-1} (phosphate groups), along with weaker increases at 1230 cm^{-1} (amine and phosphate groups) and 1600–1700 cm^{-1} (amine and carbonyl groups). These changes in the spectra are overlapping in absorption region with a reference electrode, which exhibit just bare gold and aptamer on the surface (violet spectra).

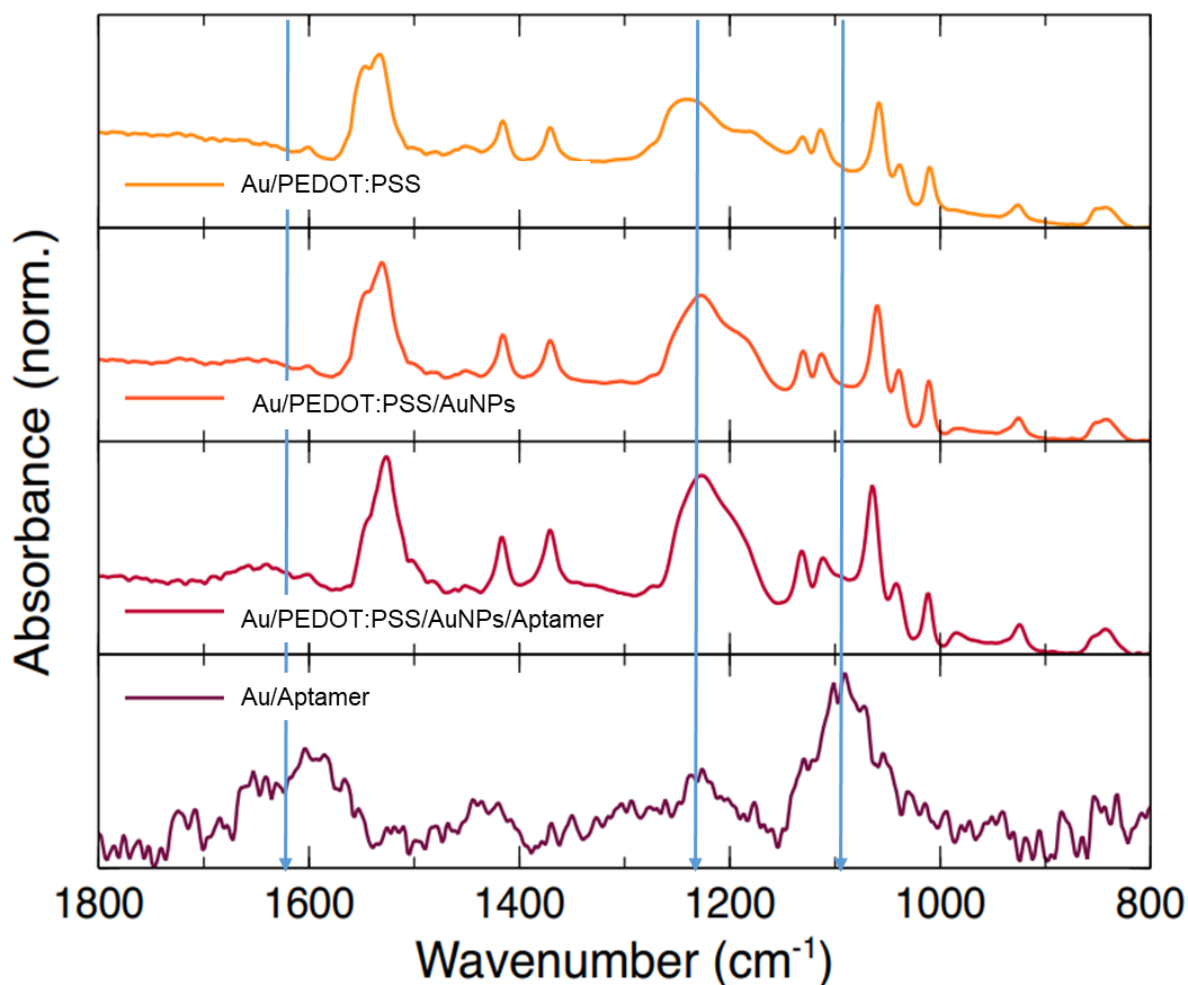


Figure 4. FTIR-ATR measurements. FTIR-ATR spectra for PEDOT:PSS electrode (yellow), PEDOT:PSS/AuNP electrode (orange), PEDOT:PSS/AuNP/aptamer electrode (purple), and Au/aptamer electrode (violet).

We monitored the OECT response for different concentrations of IL-6, sweeping the voltage between source and gate (V_{GS}) from 0.0 V to 0.6 V and keeping the voltage between source and drain (V_{DS}) fixed at -0.3 V (Fig. 1A). The measurements were performed in phosphate buffer plus 0.05 % Tween-20 (polysorbate 20), containing increasing IL-6 concentrations from 10 pM to 500 nM. Tween-20 is a detergent commonly used in standard techniques like ELISA to reduce unspecific binding⁷². Here, we diluted the analyte of interest in solutions containing Tween-20 to prevent possible protein absorption on PEDOT:PSS or uncovered gold surfaces. Figure 5A shows an overlay of the transfer characteristics for increasing concentrations of IL-6. The curves are characterized by a monotonic decrease of I_{SD} proportional to [IL-6] when the gate is functionalized with aptamer. In order to quantitatively define the response of the biosensor, we

constructed the dose curve calculating the normalized response (NR), for IL-6 analyte (Fig. 5B) and for a control molecule TNF (Tumor Necrosis Factor), an analogous cytokine with different structure but similar function. Increasing concentrations of TNF did not induce a marked and precise effect on the device behaviour, with $NR_{I_{DS}}$ consistently around -0.1 V (Fig. 5C, also observed with EIS in Fig. S2). The detection mechanism of OECT biosensors relies on the channel de-doping, induced by the ion migration from the electrolyte, upon application of increasing V_{GS} . The drain current I_{SD} depends on applied voltages and intrinsic material properties, and can be described by the following equation⁷³ :

$$I_{SD} = \frac{q\mu p_0 W}{LV_p} \left(V_p - V_{GS}^{eff} + \frac{V_{DS}}{2} \right) V_{DS} \quad (1)$$

Where q is the electronic charge, μ is the hole mobility in the channel, p_0 is the initial hole density in the semiconductor, W and L represent the channel width and length, V_p is the pinchoff voltage and V_{GS}^{eff} is the effective gate voltage, which depends on a voltage offset V_{offset} directly proportional to the concentration if IL-6 (fig 5D):

$$V_{GS}^{eff} = V_{GS} + V_{offset} \quad (2)$$

The offset voltage represents a potential variation happening at gate/electrolyte interface⁷³, induced by the binding between IL-6 and aptamer, which consequently determine a current variation in the channel. As showed in figure 5D, increasing concentration of IL-6 are producing an offset voltage variation (black dots), not present with the control cytokine TNF (red dots). We further investigated the electrical characteristics, studying the changes in transconductance g_m (slope of the transfer curve) for increasing concentration of analytes (Fig. S4A and S4B). We calculated the normalized response for g_m (NR_{g_m}) and for V_{GS} at which devices show the maximum transconductance ($NR_{V_{GS}}$), comparing the relative changes between 0 and increasing analyte concentrations. While the normalised response of g_m varied following both [IL-6] and [TNF], implying that Δg_m may have a contribution from the device stress itself (Fig. S4C), the normalised response for (V_{GS}) at maximum transconductance is more selective to IL-6 concentrations (Fig. S4, in particular S4D). The V_{GS} shows a decreasing behaviour, upon increasing IL-6 concentration, in contrast with the static TNF behaviour. We hypothesised that this potential

change (V_{GS}) may be attributed to conformational aptamer adjustments upon IL-6 binding, which could affect the charge density closer to the electrode surface, modifying the interface potential.

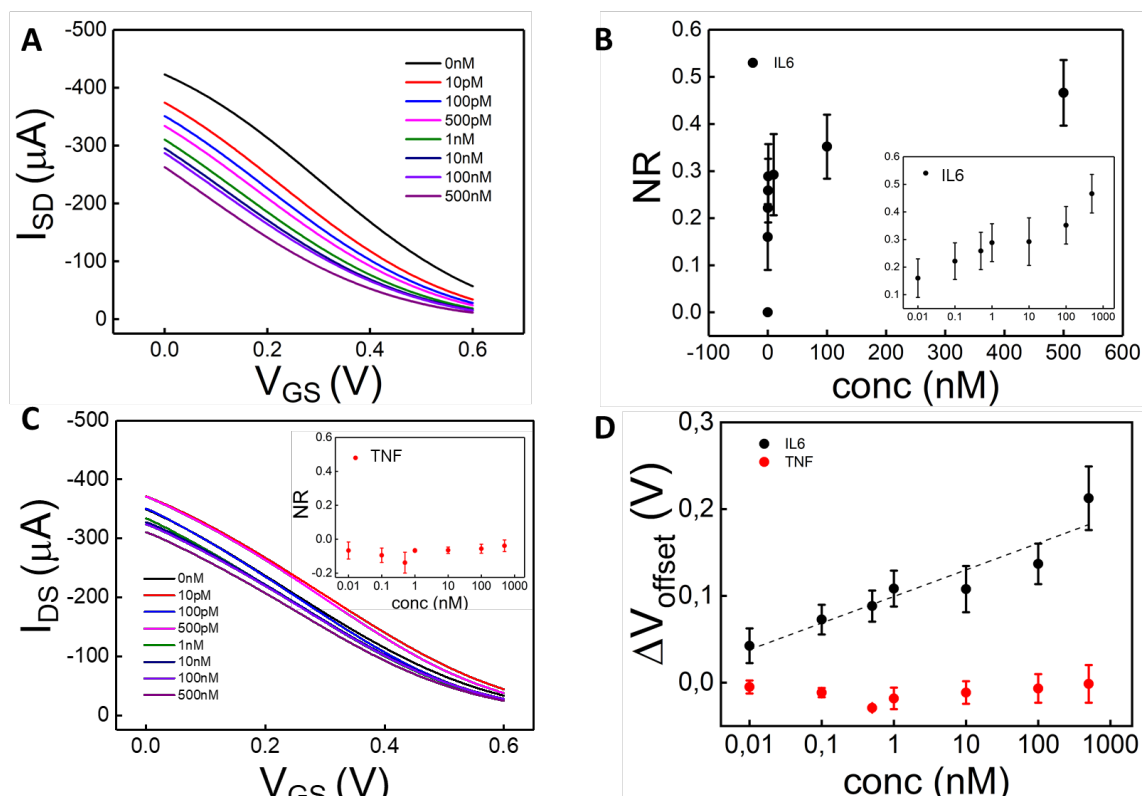


Figure 5. Interleukin-6 sensing. (A) Transfer characteristics of OECT based aptasensor for increasing concentration of IL-6 in Tween buffer, recorded at fixed V_{SD} -0.3V and sweeping V_{GS} from 0V to 0.6V. (B) Normalized response obtained for V_{GS} 0.3V upon increasing concentration of IL-6 (black dots). The inset shows the lin/log graph (C) Transfer characteristics of OECT based aptasensor for increasing concentration of TNF in Tween 20 buffer, recorded at fixed V_{SD} -0.3V and sweeping V_{GS} from 0V to 0.6V. The inset shows the Normalized response obtained for V_{GS} 0.3V upon increasing concentration of TNF (red dots). Error bars represent the standard error for four TNF measurements on different devices. (D) Gate voltage variations obtain for increasing concentration of IL-6 (black dots) and TNF (red dots).

Conclusion

In this work, we showed an aptamer based OECT biosensor for protein recognition. The sensor can discriminate concentration of the analyte of interest in physiological and pathological concentration ranges against another analogous protein. The OECT shows changes in electrical characteristics such as I_{SD} current and V_{SG} for the maximum g_m , providing information on the binding between aptamer and protein. Moreover, we show an easy functionalization strategy based on electrochemical Au nanoparticle deposition and electrochemical reduction of the sensing unit at the gate electrode.

Materials and Methods

Device fabrication

A circular 4-inch substrate was obtained by cutting polyethylene naphthalate (PEN) foil (Teonex Q65HA, 125 μm , Peutz Folien GMBH). After cleaning the PEN foil with water and acetone, 2 nm chromium (Cr) and 50 nm gold (Au) were thermally evaporated onto the surface. Gold contacts, wirings and gates were patterned using a Shipley 1805 positive resist and photolithography (Karl Suss MA/BM 6 mask aligner), then wet etched in I_2/KI solution for Au, and $\text{H}_2\text{O}_2/\text{NH}_4\text{Cl}/\text{H}_2\text{O}$ for Cr. The substrate was then stripped with acetone. Channels and gates were fabricated with a PEDOT:PSS (Clevios PH1000) solution with 5% v/v ethylene glycol and 1% v/v GOPS (3-glycidyloxypropyl)trimethoxysilane) and dodecylbenzenesulfonic acid (1 drop per 5 ml) using a Shipley 1813 positive resist. The substrate was then dry reactive ion etched with CF_4/O_2 and stripped with acetone. As a final step, the substrate was encapsulated with SU-8 2010 (MicroChem) and openings were defined using wet etching with developer mr-Dev 600 (Microresist Technology). Chemicals were used as received from Sigma-Aldrich unless stated otherwise.

Gate functionalization

Gold nanoparticles were formed by applying -0.273 V vs Ag/AgCl in 3 mM HAuCl_4 in 0.1 M KCl for 60 seconds through electrochemical deposition (CH Instruments potentiostat 760c model with a three-electrode setup) at the gate electrode. Devices were then rinsed thoroughly with DI water. The aptamer sequence (5'-CTTCCAACGCTCGTATTGTCAGTCTTTAGT-3') was found in literature and purchased with a thiol group at the 5' end from Sigma Aldrich. A solution of 1 μM aptamer in 10 mM phosphate buffered saline (PBS) was used for electrochemical deposition of the oligomer on the gold particles, using cyclic voltammetry for 30 cycles from 0.1 V to -1 V at 50 mV/s on the gate electrode. After DI water rinsing, the surface electrode was re-arranged in a solution of KCl 50mM for 20 cycles from -0.1 V to 0.1 V at 50 mV/s. The active area of the device was then incubated in 0.05 % Tween 20 buffer in 10 mM PBS for 1h. Gold nanoparticle deposition was observed performing cyclic voltammetry in 5 mM ferricyanide solution at the gate electrode from -0.5 V to 0.5 V at 50mV/s for 2 cycles. AuNP deposition was also studied with optical

microscopy and scanning electron microscopy (SEM). Aptamer deposition was observed through impedance measurements in 5 mM ferricyanide and with Fourier-transform infrared spectroscopy in attenuated total reflectance mode (FTIR-ATR) using a Bruker Equinox 55 spectrometer equipped with a Bruker Platinum ATR single reflection accessory. The spectra were accumulated over 50 scans in the range 4000 to 500 cm^{-1} with a resolution of 4 cm^{-1} using a zero-filling factor of 2. The background measurement was PEN with a thermally evaporated Au layer, like the substrate used for device preparation. (Additional corrections, such as baseline adjustments, have not been applied on the measured data.)

Electrical characterization

Electrical measurements were performed in 10 mM PBS buffer with or without 0.05 % Tween 20. Source, gate, and drain electrodes were connected to a Keithley 2600 source meter and all measurements were carried out at room temperature. The transfer characteristics were performed by keeping the voltage between source and drain fixed at $V_{SD} = -0.3$ V and sweeping the voltage between source and gate V_{SG} from 0 V to 0.6 V. The gate electrode was incubated with increasing concentration of IL-6 or TNF in Tween 20 buffer for 15 minutes and then recorded until current stabilization. Au, PEDOT:PSS, and PEDOT:PSS/AuNP electrodes were stabilized by sweeping gate voltage from 0 V to 0.6 V and keeping the source drain voltage fixed at -0.3 V for 15 minutes.

Data analysis

To quantify and compare different sensing devices, a normalized I_{DS} response ($NR_{I_{DS}}$) was defined as:

$$NR_{I_{DS}} = -\frac{(I_n - I_0)}{I_0} \quad (1)$$

where I_n is the current taken at $V_{SG} = 0.3$ V for each n^{th} concentration of IL-6 and TNF and I_0 is the baseline current at $V_{SG} = 0.3$ V for the solution at 0 M analyte concentration. The normalized g_m response was similarly calculated as:

$$NR_{g_m} = \frac{(g_{m,n} - g_{m,0})}{g_{m,0}} \quad (2)$$

where $g_{m,n}$ is the transconductance taken for each n^{th} concentration of IL-6 and TNF and $g_{m,0}$ is the transconductance for the solution at 0 M analyte concentration. The devices' sensing capability was also investigated by comparing relative changes at the V_{GS} for the maximum g_m using:

$$NR_{V_{GS}} = \frac{(V_{GS,n} - V_{GS,0})}{V_{GS,0}} \quad (3)$$

where $V_{GS,n}$ is the voltage between source and gate for maximum g_m taken for each n^{th} concentration of IL-6 and TNF and $V_{GS,0}$ is the voltage between source and gate for maximum g_m for the solution at 0 M analyte concentration.

References

1. Bienvenu, J., Monneret, G., Fabien, N. & Revillard, J. P. The Clinical Usefulness of the Measurement of Cytokines. *Clin. Chem. Lab. Med.* **38**, 267–285 (2000).
2. Holloway, A. F., Rao, S. & Shannon, M. F. Regulation of cytokine gene transcription in the immune system. *Mol. Immunol.* **38**, 567–580 (2002).
3. Spurlock, M. E. Regulation of metabolism and growth during immune challenge: an overview of cytokine function1. *J. Anim. Sci.* **75**, 1773–1783 (1997).
4. Velazquez-Salinas, L., Verdugo-Rodriguez, A., Rodriguez, L. L. & Borca, M. V. The Role of Interleukin 6 During Viral Infections . *Frontiers in Microbiology* vol. 10 1057 (2019).
5. Kumari, N., Dwarakanath, B. S., Das, A. & Bhatt, A. N. Role of interleukin-6 in cancer progression and therapeutic resistance. *Tumor Biol.* **37**, 11553–11572 (2016).
6. Gabay, C. Interleukin-6 and chronic inflammation. *Arthritis Res. Ther.* **8**, S3 (2006).
7. Nishimoto, N. & Kishimoto, T. Interleukin 6: from bench to bedside. *Nat. Clin. Pract. Rheumatol.* **2**, 619–626 (2006).
8. Tanaka, T., Narazaki, M. & Kishimoto, T. IL-6 in inflammation, immunity, and disease.

- Cold Spring Harb. Perspect. Biol.* **6**, a016295–a016295 (2014).
9. Molano Franco, D., Arevalo-Rodriguez, I., Roqué i Figuls, M. & Zamora, J. Interleukin-6 for diagnosis of sepsis in critically ill adult patients. *Cochrane Database Syst. Rev.* **2015**, CD011811 (2015).
 10. Damas, P. *et al.* Sepsis and serum cytokine concentrations. *Crit. Care Med.* **25**, (1997).
 11. Vainer, N., Dehlendorff, C. & Johansen, J. S. Systematic literature review of IL-6 as a biomarker or treatment target in patients with gastric, bile duct, pancreatic and colorectal cancer. *Oncotarget* **9**, 29820–29841 (2018).
 12. Lacroix, M. *et al.* Novel Insights into Interleukin 6 (IL-6) Cis- and Trans-signaling Pathways by Differentially Manipulating the Assembly of the IL-6 Signaling Complex*. *J. Biol. Chem.* **290**, 26943–26953 (2015).
 13. Liu, T. *et al.* The role of interleukin-6 in monitoring severe case of coronavirus disease 2019. *EMBO Mol. Med.* **12**, e12421 (2020).
 14. Herold, T. *et al.* Level of IL-6 predicts respiratory failure in hospitalized symptomatic COVID-19 patients. *medRxiv* 2020.04.01.20047381 (2020)
doi:10.1101/2020.04.01.20047381.
 15. Ulhaq, Z. S. & Soraya, G. V. Interleukin-6 as a potential biomarker of COVID-19 progression. *Med. Mal. Infect.* **50**, 382–383 (2020).
 16. Coomes, E. A. & Haghbayan, H. Interleukin-6 in Covid-19: A systematic review and meta-analysis. *Rev. Med. Virol.* **30**, e2141 (2020).
 17. Liu, G., Qi, M., Hutchinson, M. R., Yang, G. & Goldys, E. M. Recent advances in cytokine detection by immunosensing. *Biosens. Bioelectron.* **79**, 810–821 (2016).
 18. Loo, S. W. & Pui, T.-S. Cytokine and Cancer Biomarkers Detection: The Dawn of Electrochemical Paper-Based Biosensor. *Sensors* vol. 20 (2020).
 19. Russell, C. *et al.* Development of a needle shaped microelectrode for electrochemical

- detection of the sepsis biomarker interleukin-6 (IL-6) in real time. *Biosens. Bioelectron.* **126**, (2019).
20. Aydın, E. B. & Sezgintürk, M. K. An impedimetric immunosensor for highly sensitive detection of IL-8 in human serum and saliva samples: A new surface modification method by 6-phosphonohexanoic acid for biosensing applications. *Anal. Biochem.* **554**, (2018).
 21. Filik, H. & Avan, A. A. Electrochemical immunosensors for the detection of cytokine tumor necrosis factor alpha: A review. *Talanta* **211**, 120758 (2020).
 22. Diacci, C. *et al.* Label-free detection of interleukin-6 using electrolyte gated organic field effect transistors. *Biointerphases* **12**, 05F401 (2017).
 23. Berto, M. *et al.* EGOFET Peptide Aptasensor for Label-Free Detection of Inflammatory Cytokines in Complex Fluids. *Adv. Biosyst.* **2**, 1–8 (2018).
 24. Berto, M. *et al.* Biorecognition in organic field effect transistors biosensors: The role of the density of states of the organic semiconductor. *Anal. Chem.* **88**, 12330–12338 (2016).
 25. Parkula, V. *et al.* Harnessing Selectivity and Sensitivity in Electronic Biosensing: A Novel Lab-on-Chip Multigate Organic Transistor. *Anal. Chem.* **92**, 9330–9337 (2020).
 26. Khan, N. I. & Song, E. Detection of an IL-6 Biomarker Using a GFET Platform Developed with a Facile Organic Solvent-Free Aptamer Immobilization Approach. *Sensors* **21**, 1335 (2021).
 27. Nilsson, B. D. *et al.* Electrochemical Organic Transistors **. *Adv. Mater.* **14**, 51–54 (2002).
 28. Bernards, D. A. *et al.* Enzymatic sensing with organic electrochemical transistors. *J. Mater. Chem.* **18**, 116–120 (2008).
 29. Strakosas, X., Bongo, M. & Owens, R. M. The organic electrochemical transistor for biological applications. *J. Appl. Polym. Sci.* **132**, 1–14 (2015).
 30. Malliaras, G. G. *et al.* Organic electrochemical transistors. *Nat. Rev. Mater.* **3**, 17086 (2018).

31. Bernardis, D. A. & Malliaras, G. G. Steady-State and Transient Behavior of Organic Electrochemical Transistors. *Adv. Funct. Mater.* **17**, 3538–3544 (2007).
32. Nissa, J., Janson, P., Simon, D. T. & Berggren, M. Expanding the understanding of organic electrochemical transistor function. *Appl. Phys. Lett.* **118**, 053301 (2021).
33. Bernardis, D. A. *et al.* Enzymatic sensing with organic electrochemical transistors. *J. Mater. Chem.* **18**, 116–120 (2008).
34. Diacci, C. *et al.* Diurnal in vivo xylem sap glucose and sucrose monitoring using implantable organic electrochemical transistor sensors. *iScience* **24**, (2021).
35. Diacci, C. *et al.* Real-Time Monitoring of Glucose Export from Isolated Chloroplasts Using an Organic Electrochemical Transistor. *Adv. Mater. Technol.* **5**, (2020).
36. Galliani, M. *et al.* Flexible Printed Organic Electrochemical Transistors for the Detection of Uric Acid in Artificial Wound Exudate. *Adv. Mater. Interfaces* **7**, 2001218 (2020).
37. Pappa, A. M. *et al.* Organic Transistor Arrays Integrated with Finger-Powered Microfluidics for Multianalyte Saliva Testing. *Adv. Healthc. Mater.* **5**, 2295–2302 (2016).
38. Khodagholy, D. *et al.* Organic electrochemical transistor incorporating an ionogel as a solid state electrolyte for lactate sensing. *J. Mater. Chem.* **22**, 4440–4443 (2012).
39. Kergoat, L. *et al.* Detection of glutamate and acetylcholine with organic electrochemical transistors based on conducting polymer/platinum nanoparticle composites. *Adv. Mater.* **26**, 5658–5664 (2014).
40. Aliane, A. *et al.* Screen-printed organic electrochemical transistors for metabolite sensing. *MRS Commun.* **5**, 507–511 (2015).
41. Strakosas, X. *et al.* Catalytically enhanced organic transistors for in vitro toxicology monitoring through hydrogel entrapment of enzymes. *J. Appl. Polym. Sci.* **134**, 519 (2017).
42. Pappa, A. M. *et al.* Direct metabolite detection with an n-type accumulation mode

- organic electrochemical transistor. *Sci. Adv.* **4**, 1–8 (2018).
43. Zhang, L. *et al.* Selective recognition of Histidine enantiomers using novel molecularly imprinted organic transistor sensor. *Org. Electron.* **61**, 254–260 (2018).
 44. Parlak, O., Keene, S. T., Marais, A., Curto, V. F. & Salleo, A. Molecularly selective nanoporous membrane-based wearable organic electrochemical device for noninvasive cortisol sensing. *Sci. Adv.* **4**, (2018).
 45. Kim, D. J. *et al.* Organic electrochemical transistor based immunosensor for prostate specific antigen (PSA) detection using gold nanoparticles for signal amplification. *Biosens. Bioelectron.* **25**, 2477–2482 (2010).
 46. Gentili, D. *et al.* Integration of organic electrochemical transistors and immuno-affinity membranes for label-free detection of interleukin-6 in the physiological concentration range through antibody-antigen recognition. *J. Mater. Chem. B* **6**, 5400–5406 (2018).
 47. Macchia, E., Ghittorelli, M., Torricelli, F. & Torsi, L. Organic electrochemical transistor immuno-sensor operating at the femto-molar limit of detection. *Proc. - 2017 7th Int. Work. Adv. Sensors Interfaces, IWASI 2017* 68–72 (2017)
doi:10.1109/IWASI.2017.7974217.
 48. Decataldo, F. *et al.* BMP-2 functionalized PEDOT:PSS-based OECTs for stem cell osteogenic differentiation monitoring. *Flex. Print. Electron.* **4**, (2019).
 49. Guo, K. *et al.* A nanobody-functionalized organic electrochemical transistor for the rapid detection of SARS-CoV-2 and MERS antigens at the physical limit. 1–34 (2020).
 50. Yu, J. *et al.* Highly sensitive detection of caspase-3 activity based on peptide-modified organic electrochemical transistor biosensors. *Nanoscale* **13**, 2868–2874 (2021).
 51. Löfblom, J., Frejd, F. Y. & Ståhl, S. Non-immunoglobulin based protein scaffolds. *Curr. Opin. Biotechnol.* **22**, 843–848 (2011).
 52. Adachi, T. & Nakamura, Y. Aptamers: A Review of Their Chemical Properties and Modifications for Therapeutic Application. *Molecules* **24**, 4229 (2019).

53. Zhuo, Z. *et al.* Recent Advances in SELEX Technology and Aptamer Applications in Biomedicine. *International Journal of Molecular Sciences* vol. 18 (2017).
54. Feng, L., Chen, Y., Ren, J. & Qu, X. A graphene functionalized electrochemical aptasensor for selective label-free detection of cancer cells. *Biomaterials* **32**, 2930–2937 (2011).
55. Zhang, Y.-L., Huang, Y., Jiang, J.-H., Shen, G.-L. & Yu, R.-Q. Electrochemical Aptasensor Based on Proximity-Dependent Surface Hybridization Assay for Single-Step, Reusable, Sensitive Protein Detection. *J. Am. Chem. Soc.* **129**, 15448–15449 (2007).
56. Jolly, P. *et al.* Electro-Engineered Polymeric Films for the Development of Sensitive Aptasensors for Prostate Cancer Marker Detection. *ACS Sensors* acssensors.6b00443 (2016) doi:10.1021/acssensors.6b00443.
57. Kumar, L. S. S. *et al.* Label free nano-aptasensor for interleukin-6 in protein-dilute bio fluids such as sweat. *Anal. Methods* **8**, 3440–3444 (2016).
58. Toh, S. Y., Citartan, M., Gopinath, S. C. B. & Tang, T.-H. Aptamers as a replacement for antibodies in enzyme-linked immunosorbent assay. *Biosens. Bioelectron.* **64**, 392–403 (2015).
59. Ferreira, C. S. M. *et al.* DNA aptamers against the MUC1 tumour marker: design of aptamer–antibody sandwich ELISA for the early diagnosis of epithelial tumours. *Anal. Bioanal. Chem.* **390**, 1039–1050 (2008).
60. Wang, J., Lv, R., Xu, J., Xu, D. & Chen, H. Characterizing the interaction between aptamers and human IgE by use of surface plasmon resonance. *Anal. Bioanal. Chem.* **390**, 1059–1065 (2008).
61. Liang, Y., Guo, T., Zhou, L., Offenhäusser, A. & Mayer, D. Label-Free Split Aptamer Sensor for Femtomolar Detection of Dopamine by Means of Flexible Organic Electrochemical Transistors. *Mater. (Basel, Switzerland)* **13**, 2577 (2020).
62. Liang, Y., Wu, C., Figueroa-Miranda, G., Offenhäusser, A. & Mayer, D. Amplification of aptamer sensor signals by four orders of magnitude via interdigitated organic

- electrochemical transistors. *Biosens. Bioelectron.* **144**, 111668 (2019).
63. Picomolar Detection of Epinephrine Using Aptamer Based Organic Electrochemical Transistor. *ECS Meet. Abstr.* (2018) doi:10.1149/ma2018-02/58/2129.
 64. Spain, E., Keyes, T. E. & Forster, R. J. DNA sensor based on vapour polymerised pedot films functionalised with gold nanoparticles. *Biosens. Bioelectron.* **41**, 65–70 (2013).
 65. Gu, Y., Tseng, P.-Y., Bi, X. & Yang, J. H. C. Quantification of DNA by a Thermal-Durable Biosensor Modified with Conductive Poly(3,4-ethylenedioxythiophene). *Sensors (Basel)*. **18**, 3684 (2018).
 66. Su, W., Cho, M., Nam, J.-D., Choe, W.-S. & Lee, Y. Aptamer-Assisted Gold Nanoparticles/PEDOT Platform for Ultrasensitive Detection of LPS. *Electroanalysis* **25**, 380–386 (2013).
 67. Kim, M., Iezzi, R., Shim, B. S. & Martin, D. C. Impedimetric biosensors for detecting vascular endothelial growth factor (VEGF) based on poly(3,4-ethylene dioxythiophene) (PEDOT)/gold nanoparticle (Au NP) composites. *Front. Chem.* **7**, 1–11 (2019).
 68. Rhinehardt, K. L., Vance, S. A., Mohan, R. V, Sandros, M. & Srinivas, G. Molecular modeling and SPRi investigations of interleukin 6 (IL6) protein and DNA aptamers. *J. Biomol. Struct. Dyn.* **36**, 1934–1947 (2018).
 69. Muhammad, M., Shao, C. & Huang, Q. Aptamer-functionalized Au nanoparticles array as the effective SERS biosensor for label-free detection of interleukin-6 in serum. *Sensors Actuators B Chem.* **334**, 129607 (2021).
 70. Miodek, A. *et al.* Optimisation and characterisation of anti-fouling ternary SAM layers for impedance-based aptasensors. *Sensors (Switzerland)* **15**, 25015–25032 (2015).
 71. Aliakbarinodehi, N. *et al.* Aptamer-based Field-Effect Biosensor for Tenofovir Detection. *Sci. Rep.* **7**, 44409 (2017).
 72. Steinitz, M. Quantitation of the Blocking Effect of Tween 20 and Bovine Serum Albumin in ELISA Microwells. *Anal. Biochem.* **282**, 232–238 (2000).

73. Bernards, D. A. *et al.* Enzymatic sensing with organic electrochemical transistors. *J. Mater. Chem.* **18**, 116–120 (2008).

Supporting information

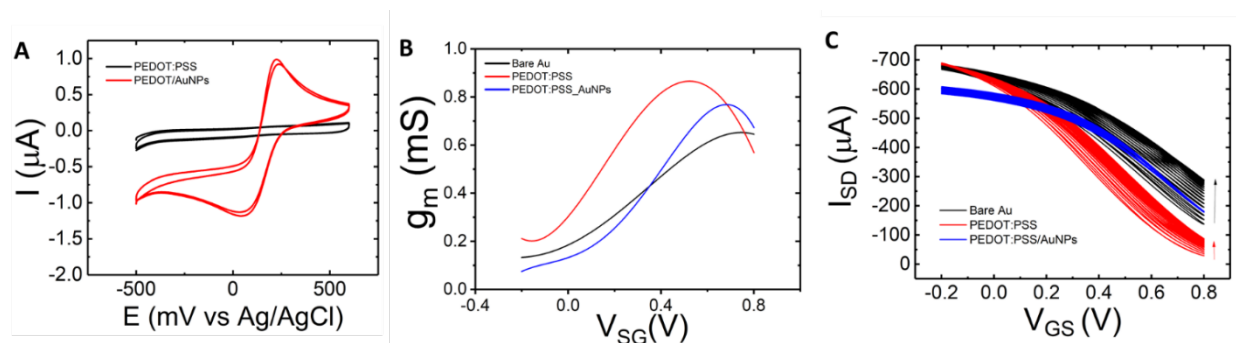


Figure S1. PEDOT:PSS/AuNP electrical characteristics. (A) Cyclic voltammetry in 5 mM ferricyanide from -0.5 V to 0.5 V at 50mV/s for PEDOT:PSS (black) and PEDOT:PSS/AuNP (red) gate electrode. (B) Transconductance g_m for bare Au (black), PEDOT:PSS (red), and PEDOT:PSS/AuNP (blue). (C) Transfer characteristics for bare Au (black), PEDOT:PSS (red), and PEDOT:PSS/AuNP (blue) gate electrodes modulating the same channel for 15 minutes. Transfer curves were obtained sweeping VSG back and forward from 0 V to 0.6 V and keeping VSD fixed at -0.3 V.

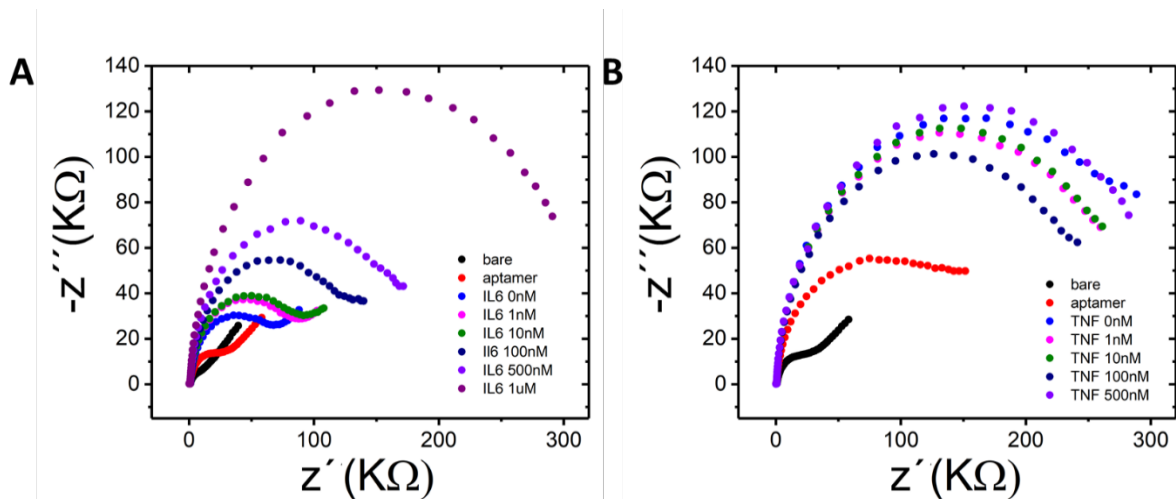


Figure S2. EIS measurements. Electrochemical impedance spectroscopy recorded in 5 mM ferricyanide for aptamer functionalized PEDOT:PSS/AuNP gate electrode as function of increasing concentrations of (A) IL-6 and (B) TNF in Tween 20 buffer.

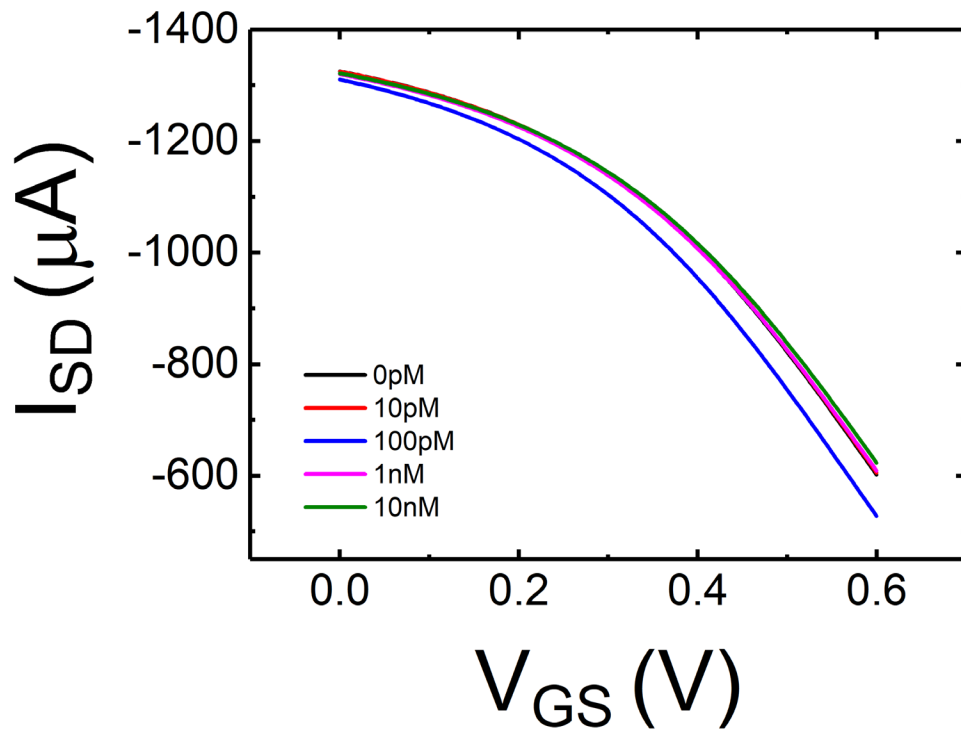


Figure S3. IL-6 detection on PEDOT:PSS/AuNP gate. Transfer characteristics of the PEDOT:PSS/AuNP-only (i.e., no aptamer) OECT for increasing concentration of IL-6 in PBS buffer, recorded at fixed $V_{SD} = -0.3V$ and sweeping V_{GS} from 0 V to 0.6 V.

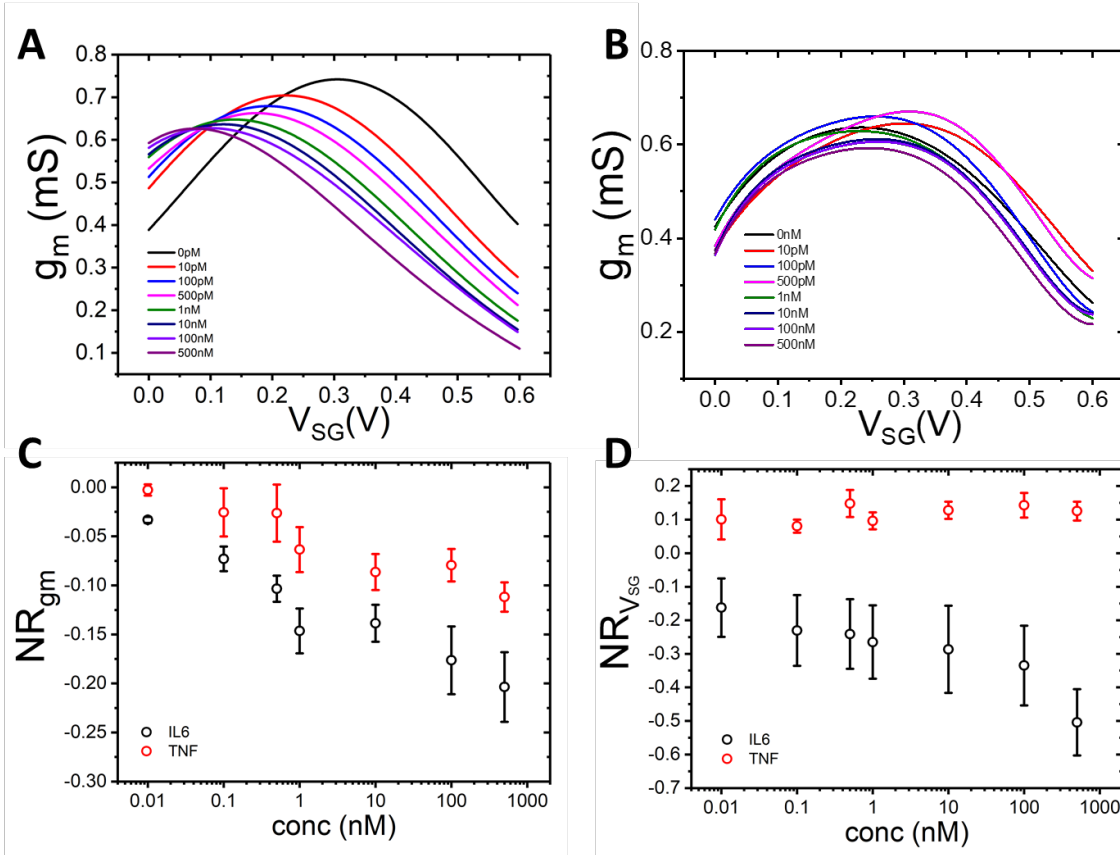


Figure S4. Transconductance of OECT based aptasensor. Change of g_m for increasing concentration of (A) IL-6 and (B) TNF in Tween 20 buffer, obtained from transfer curves recorded at fixed $V_{SD} = -0.3V$ and sweeping V_{SG} from 0 V to 0.6 V. (C) Normalized transconductance response as a function of [IL-6] (black circles) and [TNF] (red circles). (D) V_{SG} normalized response obtain from the VSG at the maximum of transconductance for IL-6 (red circles) and TNF (black circles). Error bars represent the standard error for five IL-6 measurements (red) and four TNF measurements (black) on different devices.

Paper IV

Real-Time Monitoring of Glucose Export from Isolated Chloroplasts Using an Organic Electrochemical Transistor.

Real-Time Monitoring of Glucose Export from Isolated Chloroplasts Using an Organic Electrochemical Transistor

Chiara Diacci, Jee Woong Lee, Per Janson, Gwennaël Dufil, Gábor Méhes, Magnus Berggren,* Daniel T. Simon, and Eleni Stavrinidou*

Biosensors based on organic electrochemical transistors (OECT) are attractive devices for real-time monitoring of biological processes. The direct coupling between the channel of the OECT and the electrolyte enables intimate interfacing with biological environments at the same time bringing signal amplification and fast sensor response times. So far, these devices are mainly applied to mammalian systems; cells or body fluids for the development of diagnostics and various health status monitoring technology. Yet, no direct detection of biomolecules from cells or organelles is reported. Here, an OECT glucose sensor applied to chloroplasts, which are the plant organelles responsible for the light-to-chemical energy conversion of the photosynthesis, is reported. Real-time monitoring of glucose export from chloroplasts in two distinct metabolic phases is demonstrated and the transfer dynamics with a time resolution of 1 min is quantified, thus reaching monitoring dynamics being an order of magnitude better than conventional methods.

Plants are able to convert energy from sunlight into sugars via the photosynthetic process.^[1] Chloroplasts are the organelles where the photosynthetic reactions take place, thus representing one of the most abundant natural energy conversion machineries. During the day, plants store excessive photosynthetic products in the form of starch granules in the chloroplasts. During the night, the stored starch is converted

into simpler sugars such as glucose and maltose that are then exported from the chloroplasts to be used for sucrose synthesis in order to supply the plant's energetic demands.^[2]


The rate of starch degradation and subsequent amount and rate of sugars export from chloroplasts will determine the plant's metabolism, growth, and development during night.^[3] In addition, it has been shown that the coordination between starch biosynthesis and starch degradation is important for the overall development and productivity of the plant.^[3] Sugars, apart from being energy sources, are also important signaling molecules related to metabolism, growth, stress responses, and development.^[4] Conventional methods for monitoring the export of sugars from chloroplasts are complex, labor intensive,

and lack the possibility of real-time monitoring. Most approaches are based on enzymatic assays,^[5–7] chromatography,^[7] mass spectrometry,^[8] or isotopic ¹⁴C labeling.^[9] These methods hinder real-time kinetic and dynamic *in vitro* studies as it is not possible to directly integrate the biological system to the detector therefore requiring sample collection and preparation. The observation of important physiological events and functions relevant to basic science and agriculture is therefore prevented.

Organic bioelectronic sensors, on the other hand, are ideal for interfacing with biology as they can translate complex biological input to an electronic readout signal. The organic electrochemical transistor (OECT)^[10] has been extensively used as a biochemical sensor due to its inherent signal transduction and amplification capability, specificity through biofunctionalization, operation at low voltages, robust device design, and easy fabrication, and most importantly its ability to operate in an aqueous environment at high threshold stability. The latter is a fundamental prerequisite for direct coupling with the biological world.^[11–14] The OECT includes an electrolyte as an integral part of the device configuration that couples the transistor channel with the gate. The sensing mechanism relies on the modulation of the channel current (I_{SD}) in the presence of analyte through a reaction that resides either on the gate of the transistor, within the electrolyte or directly on the channel.

So far, most of the OECT-based sensor studies have been focused on developing sensors and diagnostic tools that can be applied in mammalian-related systems, for example, the

C. Diacci, Dr. J. W. Lee, P. Janson, G. Dufil, Dr. G. Méhes, Prof. M. Berggren, Dr. D. T. Simon, Dr. E. Stavrinidou
Laboratory of Organic Electronics
Department of Science and Technology
Linköping University
601 74 Norrköping, Sweden
E-mail: magnus.berggren@liu.se; eleni.stavrinidou@liu.se
Dr. J. W. Lee, Prof. M. Berggren, Dr. E. Stavrinidou
Wallenberg Wood Science Center
Department of Science and Technology
Linköping University
601 74 Norrköping, Sweden

 The ORCID identification number(s) for the author(s) of this article can be found under <https://doi.org/10.1002/admt.201900262>.

© 2019 The Authors. Published by WILEY-VCH Verlag GmbH & Co. KGaA, Weinheim. This is an open access article under the terms of the Creative Commons Attribution-NonCommercial License, which permits use, distribution and reproduction in any medium, provided the original work is properly cited and is not used for commercial purposes.

The copyright line was changed on 2 August 2019 after initial publication.

DOI: 10.1002/admt.201900262

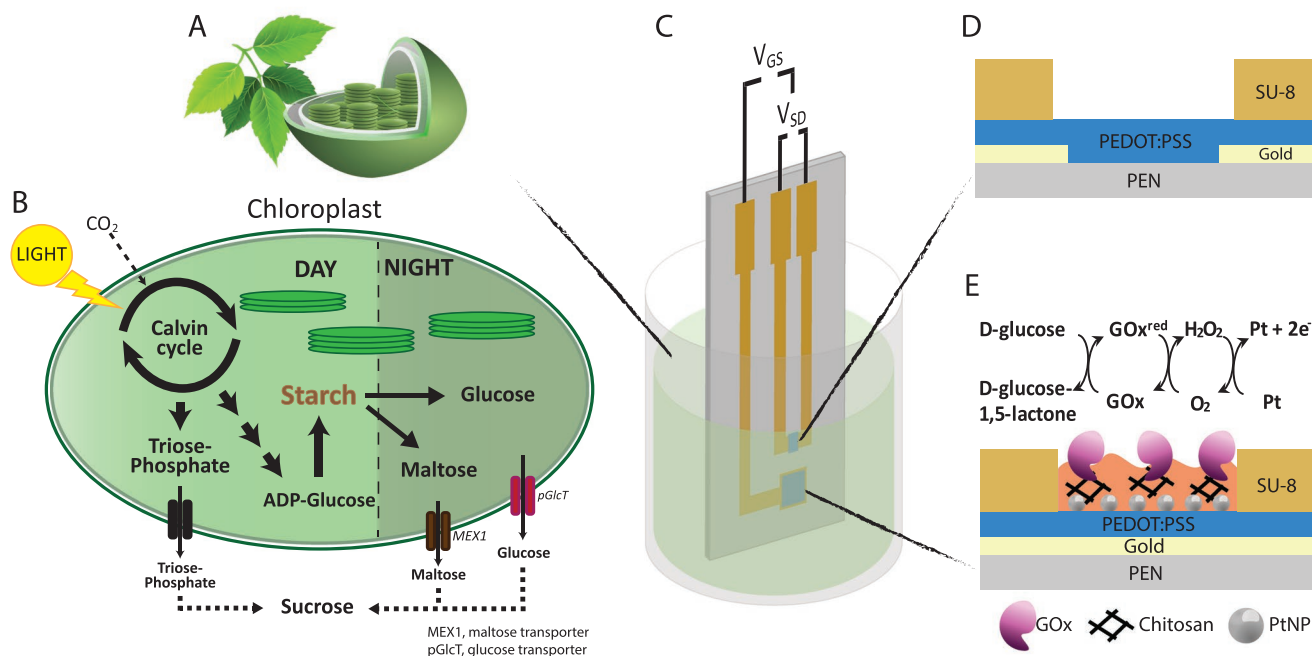


Figure 1. Overview of the experimental design for monitoring the export of glucose from isolated chloroplasts using an OECT-based glucose sensor. A) Schematic of chloroplast. B) Chloroplast in starch biosynthesis mode during daytime and starch degradation mode during nighttime. C) OECT setup for detecting glucose in isolated chloroplasts solution. D,E) Structure of OECT channel and gate, functionalized with glucose oxidase.

measurement of pH, detection of ions, metabolites, and neurotransmitters.^[15–22] Major efforts have been focused on the development of glucose sensors as glucose is one of the most important metabolites and is a crucial parameter and indicator for several diseases. A few demonstrations have been reported where glucose is monitored from natural samples such as sweat,^[21] saliva,^[20] or cell media.^[23] Until now no direct detection of biomolecules from cells or organelles has been reported. In *in vitro* cell studies, for example, the sensor is decoupled from the cell culture and is used as a stand-alone system.^[23,24]

In this work, for the first time, an OECT-based glucose sensor is directly coupled to isolated chloroplasts, the plant organelles responsible for photosynthesis, for real-time monitoring of glucose export (Figure 1). The OECT is manufactured using standard microfabrication techniques in a planar configuration shaped as a probe-like structure where the gate is biofunctionalized with glucose oxidase (GOx) cross-linked in a chitosan matrix. The chloroplasts are isolated from wild-type tobacco plants, a widely used model system in plant biology, in two distinct metabolic phases, in the starch biosynthesis mode and in the starch degradation mode (Figure 1a,b). We show that glucose is detected only in chloroplasts extracted during nighttime, in agreement with our understanding of the starch degradation process.^[25] In addition, we demonstrate the kinetics of the glucose export and compare it quantitatively with values previously reported. Our OECT sensor setup and methodology provides a new manner to specifically study metabolic process in chloroplasts, but can be used as a versatile tool by plant biologists to study various kinetic and dynamic processes in plants.

The OECT-based glucose sensor was fabricated with standard thin film and photolithography process protocols. Figure 1 shows the all-planar geometry of the device with channel and gate being

defined on the same substrate. Source, drain, and gate electrodes are based on Au, while the channel consists of a poly(3,4-ethylenedioxythiophene):poly(styrenesulfonate) (PEDOT:PSS) film. The gate is coated with a PEDOT:PSS layer in order to increase its capacitance and ability to fully modulate the channel, and it is further functionalized with platinum nanoparticles (PtNPs) along with the glucose oxidase enzyme. PtNPs are electrodeposited on a chitosan membrane that is previously drop-casted on the gate and has been activated with glutaraldehyde.^[26] The chitosan provides a desired environment for the enzyme since it is biocompatible, hydrophilic, and it has a high affinity to proteins due to electrostatic interactions. In addition, this immobilization strategy prevents the enzyme from unfolding and also gives the enzyme improved stability against environmental changes.^[27] When we apply positive gate bias, the channel current decreases as cations from the electrolyte enter the channel and compensate the PSS dopant, thus reducing the overall conductivity of the channel.^[28] When glucose is present in the solution it will couple to the glucose oxidase enzyme that is immobilized on the gate, and cause a set of redox reactions. D-glucose will be converted to D-glucose-1,5-lactone while the enzyme will be reduced. A product of this reaction, in the presence of oxygen, is hydrogen peroxide, H₂O₂, that can be oxidized on the PtNPs on the gate. As electrons are transferred at the gate, the effective gate potential shifts to cause a further decrease of the channel current. This rapid cascade of electrochemical reactions, which was triggered by adding glucose to the electrolyte, is directly coupled to current changes in the OECT, here representing the core principle of glucose sensing of the presented device platform.

To evaluate the basic operation and performance of the developed sensor system, first, we characterized the sensitivity of

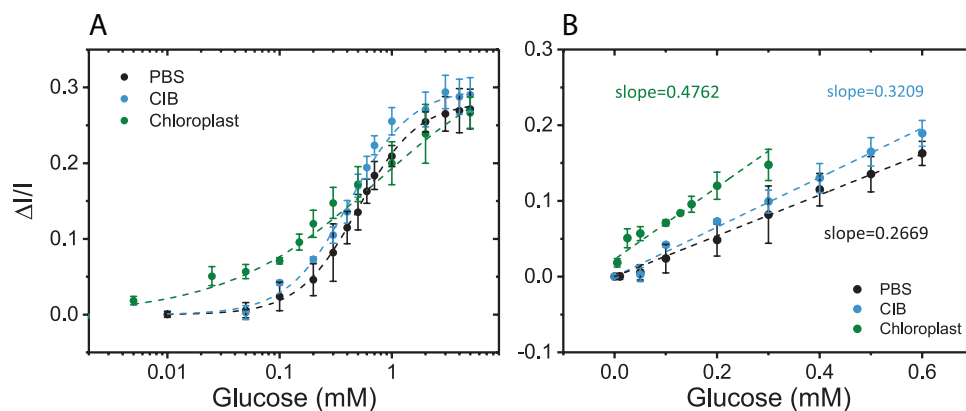


Figure 2. Glucose calibration curves of the OECT glucose sensor in different media. A) Normalized response of the OECT functionalized with GOx, to increasing glucose concentrations in PBS buffer (black), CIB buffer (blue), and in inactive chloroplasts solution (green). Dashed lines are fits to sigmoid function. Error bars represent the standard error from three measurements on three different devices. B) Comparison of linear region of glucose calibration curves in different media highlighting the change in sensitivity. Error bars represent the standard error from three measurements on three different devices.

the sensor and performed calibration curves for three different media. The measurements were performed in a phosphate buffer saline (PBS) solution, chloroplast isolation buffer (CIB) solution, and in an inactive isolated chloroplasts solution (CS) to mimic the complex media of the isolated chloroplasts (see **Figure 2**). The sensor was operated using a constant voltage difference applied to the channel, $V_{SD} = -0.4$ V and gate $V_{GS} = +0.5$ V. This is an operational regime where the transistor exhibits high transconductance and where H_2O_2 can be oxidized effectively. When no glucose is present in the solution the channel current stabilizes at a certain value. As soon as glucose is added to the solution the current decreases from I_0 to I_{gluc} . **Figure 2** displays the normalized response ($NR = -(I_{gluc} - I_0)/I_0$) of the sensor versus various glucose concentrations, from 10×10^{-6} to 5×10^{-3} M, in PBS and CIB, respectively. The sensor exhibits a linear response from 10 to 700×10^{-6} and turns saturated at higher concentration of glucose, in the range from 700×10^{-6} to 5×10^{-3} M. Further, since the sensing experiment will be performed in a complex media containing the chloroplasts, we tested the ability of the sensors to operate in such conditions as the physical dimensions of the chloroplast can influence the response and characteristics of the device, in part governed by an increase of the viscosity of the solution or by precipitation effects. Therefore, we calibrated the sensor in a CIB solution, with a known concentration of glucose and nonactive chloroplasts (CS). In this complex media, the device can sense glucose with a corresponding linear regime ranging from 10 to 300×10^{-6} . To ensure that no other interferences arise from the presence of chloroplasts, we used a control device where the enzyme was omitted. Here, no response was observed thus signifying that any recorded change in the output current of the sensors truly originates from changes in glucose concentrations (**Figure S1**, Supporting Information). The full range of the calibration curve was fitted with a sigmoid function that is used to describe processes where dose dependence is observed. **Figure 2B** includes a comparison of the different linear regions of the sensor while operated in different media with corresponding slopes defining the sensitivity of the device. The sensor exhibits higher sensitivity in the chloroplast solution

while compared with operation in buffer solutions, thus manifesting that our sensor device is appropriate to apply in complex media settings.

Having benchmarked the ability of the sensor to operate in complex media, we proceeded to monitor the glucose export from freshly isolated chloroplasts. The chloroplasts were extracted from tobacco plants using a modified isolation protocol^[29,30] in two distinct metabolic phases, during daytime and during nighttime. The chloroplasts in starch biosynthesis mode are extracted from leaves that are harvested in daytime (typically 6–8 h after the onset of the day cycle) while the chloroplasts that are in the starch degradation mode are harvested during nighttime, at least 2 h after the onset of dark cycle, to ensure that the chloroplasts enter the starch degradation mode but to avoid depletion of the accumulated starch.

Initially, the active areas, including the gate and channel, of the transistor are immersed in the chloroplast isolation buffer solution in a polydimethylsiloxane (PDMS) well as shown in **Figure 1**. The transistor is operated at constant gate potential of $V_{GS} = +0.5$ V and constant source–drain potential of $V_{SD} = -0.4$ V until the channel current I_{SD} is stable. After stabilization, the buffer solution is exchanged with the chloroplast solution. As a control experiment, a transistor without the enzyme but still including the chitosan and nanoparticles is examined and applied to the same chloroplast solution. Therefore, by comparing the current change between control device and the functionalized sensor device, we can extract and quantify the changes in device response due to glucose export from the chloroplasts. In addition, by using a vertical configuration in our setup ensures that there is no interference from precipitated chloroplasts along the active areas of the transistor. All measurements (daytime and nighttime) were performed in darkness to avoid any variation of the current due to light absorption. **Figure 3** displays the typical characteristics of the current response of the OECT sensor when immersed in daytime and nighttime-isolated chloroplasts, in combination with typical response performance of a control device. Chloroplasts in daytime mode do not export any glucose at a measurable concentration as both sensor and control devices have similar response.

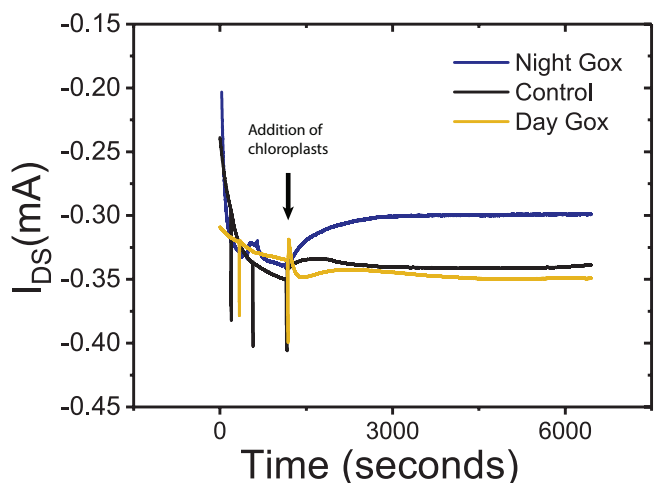


Figure 3. Real-time response of OECTs in fresh extracted chloroplast solutions. Typical current response from: control device (without GOx functionalization) in black, GOx-OECT in daytime chloroplasts solution in yellow, and GOx-OECT in nighttime chloroplasts solution in blue.

On the other hand, chloroplasts in the nighttime mode export glucose as seen from the response of the sensor device where the current decreases with time while the control device shows negligible changes. This observation agrees with the current understanding of plant metabolism.^[25] These results demonstrate that the OECT platform is able to monitor the relevant concentrations of glucose export from active chloroplasts. Based on the calibration curves (Figure 2) we performed a quantitative analysis in order to determine the amount of glucose that is exported from chloroplasts during the nighttime mode.

The characteristics of the exported glucose versus the concentration of intact chloroplasts, for chloroplasts harvested in the nighttime mode, daytime mode, and for the control devices are given in Figure 4. Initially, we observe a fast export of glucose from the nighttime chloroplasts with an increasing trend that lasts for up to 30 min. Then the signal saturates and remains almost constant implying that outflux of glucose from the chloroplasts is smaller than the beginning and that it becomes constant. The absolute glucose concentration in the solution for

the saturation regime is in the range of $80\text{--}500 \times 10^{-6}$ therefore below the saturation regime of the sensor. We monitor the process for up to 60 min, since this is the time period for which we can ensure that the chloroplasts will remain active. During 1 h, we record an average export of $170 \text{ nmol glucose mg}^{-1}$ chloroplast. These values agree well with the ones reported in literature for isolated chloroplasts extracted from spinach while measured with traditional enzymatic assays.^[6,7] Further, with the OECT sensor we are also able to resolve the glucose export dynamics with a resolution of 1 min during the first 10 min. The direct coupling of the chloroplasts with the biosensor allows us to monitor the initial export kinetics at a speed that is not possible with other typical conventional methods, in part due to time lagging that appears from sample preparation.

This reported work is the first example of coupling active plant organelles with a biosensor based on the organic electrochemical transistor. We demonstrate that the OECT sensor can operate in complex media and that it can directly detect the products of the biological unit without any need for additional purification steps or complex sample handling. In addition, the OECT sensor platform is capable to measure the export of glucose in real time, from isolated chloroplasts, with a temporal resolution of 1 min, thus our technology outperforms conventional methods, making it an attractive tool for studying the kinetics of biological processes in general. Further engineering of the device can allow higher temporal resolution with multi-component biochemical sensing.

Experimental Section

OECT Fabrication: A heat-stabilized polyethylene naphthalate (Teonex Q65HA, 125 μm , Peutz Folien GmbH) circular 4 in. substrate was cleaned with acetone and water. Metal films of 2 nm titanium (Ti) and 50 nm gold (Au) were evaporated upon it. Contacts, wiring, channel, and gate(s) are patterned using a Shipley positive resist and photolithography (Karl Suss MA/BM 6 mask aligner), and then wet etched in I_2/KI solution for Au, and $\text{H}_2\text{O}_2/\text{NH}_4\text{Cl}/\text{H}_2\text{O}$ for Ti. After the substrate was stripped with acetone, a PEDOT:PSS (Clevios PH1000) mixture with 5% v/v EG (ethylene glycol) and 0.5% v/v GOPS (3-glycidyloxypropyl) trimethoxysilane) was spin-coated and patterned using a Shipley positive

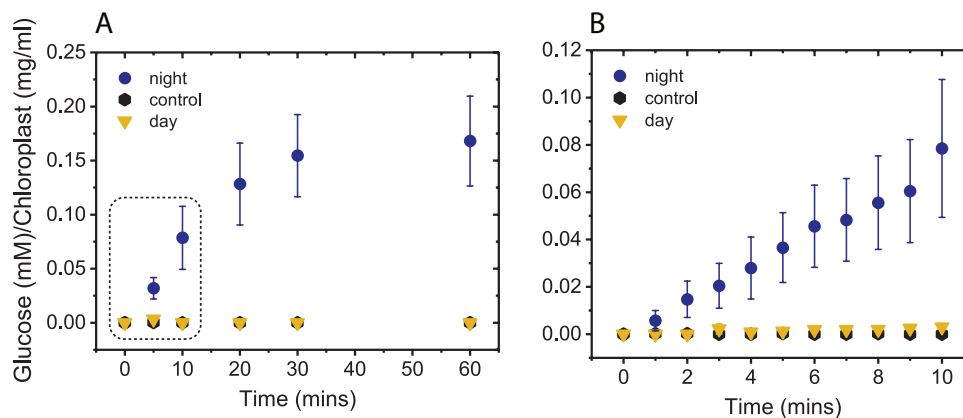


Figure 4. Exported glucose per intact chloroplasts concentration as a function of time. A,B) Quantification of glucose export from 0–60 min with 5 min resolution and 0–10 min with 1 min resolution, from nighttime chloroplasts in blue (average of five independent measurements), daytime chloroplasts in yellow (four independent measurements), and control response in black (eight independent measurements).

resist and CF_4/O_2 reactive ion etch to define the channel and gate. After another resist strip an ion exchange was made by quickly dipping it into a sodium chloride solution to neutralize the PEDOT:PSS acidity. Finally, the substrate was encapsulated and active areas were defined using SU-8 2010 (MicroChem). Chemicals were used as received from Sigma-Aldrich unless stated otherwise.

OECT Biofunctionalization: A $5 \times 10^{-3} \text{ M}$ H_2PtCl_6 in aqueous $50 \times 10^{-3} \text{ M}$ H_2SO_4 solution was used to deposit Pt nanoparticles on the PEDOT:PSS gate through electrochemical deposition (potentiostat, BioLogic SP-200) using the gate as working electrode, and applying a first fixed potential of +0.7 V for 10 s and a second fixed potential of -0.2 V for 15 s. Enzyme immobilization was performed by drop-casting $1.5 \mu\text{L}$ of 0.5 mg mL^{-1} filtered chitosan (Sigma Aldrich) solution in $50 \times 10^{-3} \text{ M}$ CH_3COOH on the gate electrode. After 30 min the electrode was rinsed with deionized water to remove the remaining CH_3COOH . To crosslink the chitosan, $1.5 \mu\text{L}$ of glutaraldehyde 2.5 wt% was deposited on top of the membrane for 5 min. As final step $1.5 \mu\text{L}$ of 6 mg mL^{-1} glucose oxidase (Sigma-Aldrich, 100k Units) in PBS (Thermo Fisher) was drop-casted on top of the chitosan membrane and let dry overnight at 4°C . Then the gate was rinsed and dried gently with a nitrogen stream.

OECT Characterization and Experimental Setup: Standard curves in phosphate buffer saline ($50 \times 10^{-3} \text{ M}$ pH 7.4) and in CIB were performed in a horizontal setup. OECT coupling with active chloroplasts for real-time monitoring experiments and nonactive chloroplasts (extracted chloroplasts from leaves kept in a fridge for several days) and CIB buffer solution 1:1 for standard curves were performed in an inclined setup (see Figure 1) using a PDMS well with a Keithley 2600 series Source Meter. All measurements were carried out at room temperature and real-time measurements were performed in dark. The transistor was operated at constant bias mode with $V_{\text{SD}} = -0.4 \text{ V}$ and $V_{\text{SG}} = +0.5 \text{ V}$. The transistor response was stabilized by exchanging the test solution three times before adding any glucose or the active chloroplasts.

Plant Materials and Growth Conditions: The tobacco (wild-type SR1) plants were grown in long-day (16 h light/8 h dark) photoperiodic conditions under white fluorescent light ($200 \mu\text{mole m}^{-2} \text{ s}^{-1}$) at room temperature with 50–60% relative humidity. 8–10 weeks old tobacco plants were used in experiments. For the experiment of glucose dose–response curve in nonactive chloroplasts solution, the chloroplasts were isolated from commercial spinach leaves that were kept in fridge for many days.

Isolation of Chloroplasts: Chloroplasts were isolated using the modified protocol of the Sigma Chloroplasts Isolation Kit (Sigma-Aldrich, CP-ISO). All isolation steps were performed at $2\text{--}4^\circ\text{C}$. $\approx 30 \text{ g}$ of tobacco leaves were washed with deionized water and the midrib veins were removed and cut into $\approx 2 \text{ cm}^2$ pieces. Then the pieces were homogenized in a blender (Bosch, ErgoMixx) with 180 mL CIB containing bovine serum albumin (BSA) (4 mL mg^{-1} of leaves) with 5 s strokes. After filtration with a $100 \mu\text{m}$ nylon mesh, the chloroplasts suspension was centrifuged at $1000 \times g$ for 7 min. The supernatant was discarded and the remaining green pellet was gently resuspended with 4 mL of $1 \times$ CIB with BSA by pipette to avoid frothing. Then, the suspension was centrifuged at $1000 \times g$ for 3 min and the remaining green pellet was gently resuspended with 0.5 mL of $1 \times$ CIB without BSA by pipette. For the night experiment, the leaves were collected at least 2 h after in the dark while for the day experiments the leaves were collected 6–8 h after the onset of light period. BSA helps to preserve the activity of isolated chloroplasts and refines the separation. In order to evaluate the stability of the isolated chloroplasts, the intactness of freshly isolated chloroplasts left in room temperature over the course of 2 h was measured. The intactness decreased by 4.5% after 30 min, by 5.67% after 60 min, and by 8.29% after 120 min, all values with respect to $t = 0$. Freshly extracted chloroplasts were always used in the experiments.

Measurement of the Concentration and Intactness of Chloroplasts: The total chlorophyll concentration of chloroplasts was measured to estimate the yield of isolated intact chloroplasts according to Porra et al. method.^[31] $10 \mu\text{L}$ of the chloroplast solution was diluted in 5 mL of acetone–deionized (DI) water mixture (80% acetone) and the solution was mixed with vortex. The solution was then centrifuged at $3000 \times g$

for 5 min. The absorbance of the supernatant was measured at 647 and 664 nm using microplate reader (BioTek, Synergy H1). The reference blank was the acetone–DI water mixture (80% acetone). The chlorophyll concentration was calculated using Equation (1)

$$(\text{g L}^{-1}) = [(17.76 \times A_{647}) + (7.34 \times A_{664})] / 2 \quad (1)$$

The intactness of the isolated chloroplasts was measured using a modified ferricyanide photoreduction method.^[29] The percentage of intact chloroplasts in the preparation was assessed by comparing the rate of photoreduction of ferricyanide with or without the osmotic shock of chloroplasts. For each of the following reactions, an amount of chloroplasts that is equivalent to $100 \mu\text{g}$ of chlorophyll was used. To prepare the solution without osmotic shock of chloroplasts (solution A), the chloroplasts were mixed with 4 mL of $1 \times$ CIB. Then $60 \mu\text{L}$ of $100 \times 10^{-3} \text{ M}$ ferricyanide was added. To prepare the solution with osmotic shock of chloroplasts (solution B), the chloroplasts were mixed with 2 mL of DI water. Then incubated for at least 15 s to allow the osmotic shock to take place and then 2 mL of $2 \times$ CIB and $60 \mu\text{L}$ of $100 \times 10^{-3} \text{ M}$ ferricyanide were added. Solution A and B were placed in 96-well plate and absorbance was measured at 410 nm before illumination and after illumination with 46 W white light every 2 min for 8 min. The percent of intact chloroplasts was calculated with Equation (2)

$$\% \text{ intact chloroplasts} = (B - A) / B \times 100 \quad (2)$$

Data Analysis: In order to quantify the glucose concentration, the NR was calculated using Equation (3)

$$\text{NR} = -\frac{I_n - I_0}{I_0} \quad (3)$$

where I_n is the current at the n th concentration for the standard curve or the current at any given point at the sensing experiment and I_0 is the current at the baseline. The amount of glucose exported by chloroplasts during nighttime and daytime was determined using the chloroplast solution dose–response curve, fitted with a sigmoid function $y = ax / (b + x)$, where a and b are constants. The amount of glucose from the current was normalized by the amount of intact chloroplasts with Equation (4)

$$\text{Glucose exp} (\text{Mg}^{-1} \text{L}^{-1}) = \frac{\text{Glucose (M)}}{\text{Intact chloroplasts} (\text{g L}^{-1})} \quad (4)$$

where Glucose exp is the amount of glucose exported from chloroplast, glucose (M) is the amount of glucose obtained from the dose–response curve, and Intact chloroplast (g L^{-1}) is the concentration of chloroplasts multiplied by the intactness.

Supporting Information

Supporting Information is available from the Wiley Online Library or from the author.

Acknowledgements

C.D., J.W.L., and P.J. contributed equally to this work. The authors wish to thank Åsa Strand, Tamara Hernández-Verdeja, and Totte Niittylä from Umeå Plant Science Center, Benoit Piro from Paris-Diderot University and Xenofon Strakosas from Linköping University for fruitful discussions. Funding was provided by the Knut and Alice Wallenberg Foundation, Linköping University and industry through the Wallenberg Wood Science Center, the Swedish Foundation for Strategic Research (SSF), Vetenskapsrådet (VR), Önnestjerna Foundation, VINNOVA and the Swedish Government Strategic Research Area in Materials Science on

Functional Materials at Linköping University (Faculty Grant SFO-Mat-LiU No. 2009-00971). Additional funding was provided by the European Union's Horizon 2020 research and innovation programme under Grant Agreement No. 800926 (FET-OPEN-HyPhOE) to E.S. and G.D. and a Marie Skłodowska Curie Individual Fellowship (MSCA-IFEF-ST, Trans-Plant, 702641) to E.S. GM was also supported by a grant from the Swedish MSCA Seal of Excellence program.

Conflict of Interest

The authors declare no conflict of interest.

Keywords

chloroplasts, glucose sensing, organic electrochemical transistor, photosynthesis, real-time monitoring

Received: March 27, 2019

Revised: May 9, 2019

Published online: June 11, 2019

- [1] J. Soll, E. Schleiff, *Nat. Rev. Mol. Cell Biol.* **2004**, *5*, 198.
- [2] J. Smirnova, A. R. Fernie, M. Steup, *Starch Metab. Struct.* **2015**, *239*.
- [3] A. Graf, A. Schlereth, M. Stitt, A. M. Smith, *Proc. Natl. Acad. Sci. USA* **2010**, *107*, 9458.
- [4] F. Rolland, E. Baena-Gonzalez, J. Sheen, *Annu. Rev. Plant Biol.* **2006**, *57*, 675.
- [5] G. Ritte, K. Raschke, G. Ritte, *New Phytol.* **2003**, 195.
- [6] J. C. Servaites, D. R. Geiger, *J. Exp. Bot.* **2002**, *53*, 1581.
- [7] S. E. Weise, A. P. M. Weber, T. D. Sharkey, *Planta* **2004**, *218*, 474.
- [8] O. Fiehn, J. Kopka, P. Dörmann, T. Altmann, R. N. Trethewey, L. Willmitzer, *Nat. Biotechnol.* **2000**, *18*, 1157.
- [9] M. Stitt, H. W. Heldt, *Plant Physiol.* **1981**, *68*, 755.
- [10] B. D. Nilsson, M. Chen, T. Kugler, T. Remonen, M. Armgarth, M. Berggren, *Adv. Mater.* **2002**, *14*, 51.
- [11] X. Strakosas, M. Bongo, R. M. Owens, *J. Appl. Polym. Sci.* **2015**, *132*, 1.
- [12] J. Rivnay, S. Inal, A. Salleo, R. M. Owens, M. Berggren, G. G. Malliaras, *Nat. Rev. Mater.* **2018**, *3*, 17086.
- [13] G. D. Spyropoulos, J. N. Gelinas, D. Khodagholy, *Sci. Adv.* **2019**, *5*, eaau7378.
- [14] E. Stavrinidou, R. Gabrielsson, E. Gomez, X. Crispin, O. Nilsson, D. T. Simon, M. Berggren, *Sci. Adv.* **2015**, *1*, e1501136.
- [15] F. Mariani, I. Gualandi, M. Tessarolo, B. Fraboni, E. Scavetta, *ACS Appl. Mater. Interfaces* **2018**, *10*, 22474.
- [16] H. Tang, P. Lin, H. L. W. Chan, F. Yan, *Biosens. Bioelectron.* **2011**, *26*, 4559.
- [17] M. Di Lauro, C. Diacci, F. Biscarini, C. A. Bortolotti, V. Beni, M. Berto, D. T. Simon, L. Theuer, M. Berggren, *Flexible Printed Electron.* **2018**, *3*, 024001.
- [18] M. Sessolo, J. Rivnay, E. Bandiello, G. G. Malliaras, H. J. Bolink, *Adv. Mater.* **2014**, 4803.
- [19] L. Kergoat, B. Piro, D. T. Simon, M. C. Pham, V. Noël, M. Berggren, *Adv. Mater.* **2014**, *26*, 5658.
- [20] A. M. Pappa, V. F. Curto, M. Braendlein, X. Strakosas, M. J. Donahue, M. Focchi, G. G. Malliaras, R. M. Owens, *Adv. Healthcare Mater.* **2016**, *5*, 2295.
- [21] A. Aliane, G. Marchand, V. F. Curto, R. Coppard, R. M. Owens, X. Strakosas, G. G. Malliaras, P. Mailley, G. Scheiblin, *MRS Commun.* **2015**, *5*, 507.
- [22] D. J. Macaya, M. Nikolou, S. Takamatsu, J. T. Mabeck, R. M. Owens, G. G. Malliaras, *Sens. Actuators, B* **2007**, *123*, 374.
- [23] X. Strakosas, M. Huerta, M. J. Donahue, A. Hama, A. M. Pappa, M. Ferro, M. Ramuz, J. Rivnay, R. M. Owens, *J. Appl. Polym. Sci.* **2017**, *134*, 1.
- [24] V. F. Curto, B. Marchiori, A. Hama, A. M. Pappa, M. P. Ferro, M. Braendlein, J. Rivnay, M. Focchi, G. G. Malliaras, M. Ramuz, R. M. Owens, *Microsyst. Nanoeng.* **2017**, *3*, 1.
- [25] M. Stitt, S. C. Zeeman, *Curr. Opin. Plant Biol.* **2012**, *15*, 282.
- [26] H. Tang, F. Yan, P. Lin, J. Xu, H. L. W. Chan, *Adv. Funct. Mater.* **2011**, *21*, 2264.
- [27] B. Krajewska, *Enzyme Microb. Technol.* **2004**, *35*, 126.
- [28] E. Stavrinidou, P. Leleux, H. Rajaona, D. Khodagholy, J. Rivnay, M. Lindau, S. Sanaur, G. G. Malliaras, *Adv. Mater.* **2013**, *25*, 4488.
- [29] R. M. C. Lilley, M. P. Fitzgerald, K. G. Rienits, D. A. Walker, *New Phytol.* **1975**, *75*, 1.
- [30] S. P. Robinson, *Photosynth. Res.* **1983**, *4*, 281.
- [31] R. J. Porra, W. A. Thompson, P. E. Kriedemann, *Biochim. Biophys. Acta, Bioenerg.* **1989**, *975*, 384.



Supporting Information

for *Adv. Mater. Technol.*, DOI: 10.1002/admt.201900262

Real-Time Monitoring of Glucose Export from Isolated Chloroplasts Using an Organic Electrochemical Transistor

Chiara Diacci, Jee Woong Lee, Per Janson, Gwennaël Dufil, Gábor Méhes, Magnus Berggren, Daniel T. Simon, and Eleni Stavrinidou**

Supporting Information

Real-Time Monitoring of Glucose Export from Isolated Chloroplasts Using an Organic Electrochemical Transistor

Chiara Diacchi[‡], Jee Woong Lee[‡], Per Janson[‡], Gwennael Dufil, Gábor Méhes, Magnus Berggren, Daniel Simon, Eleni Stavrinidou**

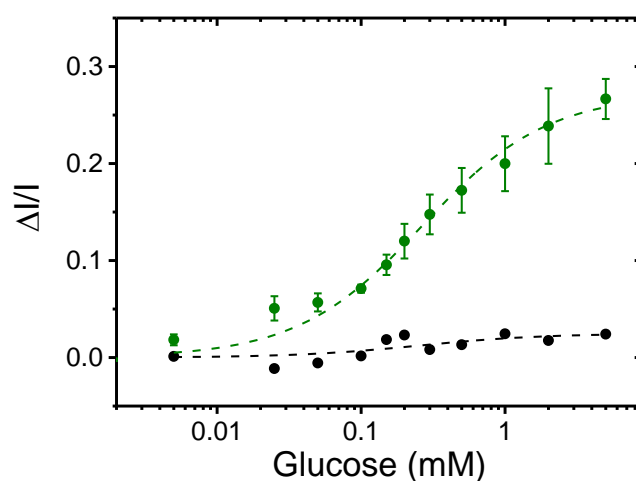


Figure S1: Normalized response of OECTs to increasing glucose concentrations in inactive chloroplasts solution, functionalized with GOx (green) and control device without enzyme (black). Dashed lines are fits to sigmoid function. Error bars represent the standard error from three measurements on three different devices.

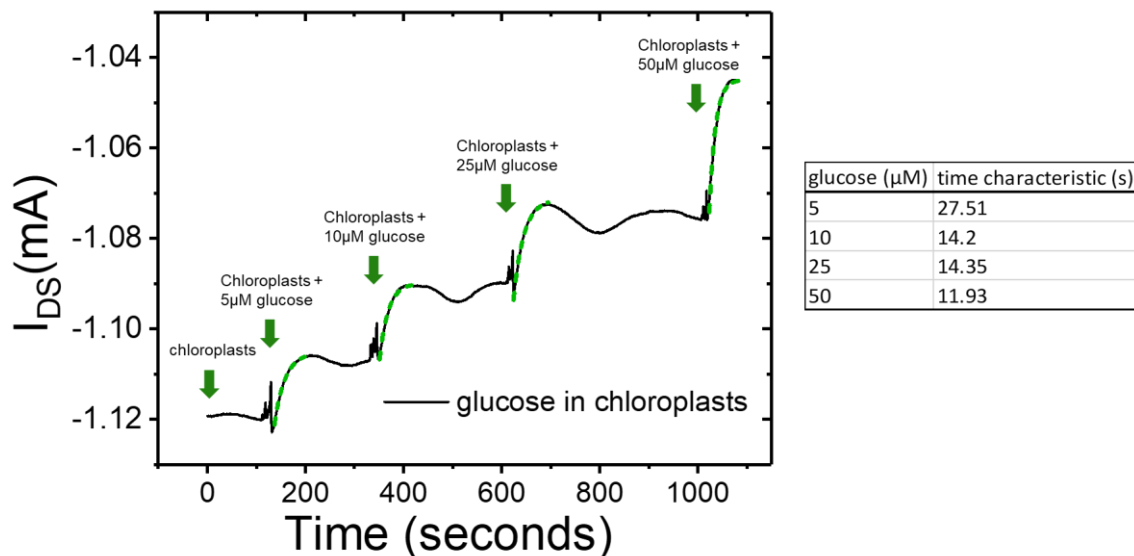


Figure S2: OECT GOx-functionalized device current I_{SD} response to increasing glucose concentrations in inactive chloroplasts solution, ($V_{SD}=-0.4V$ and $V_{SG}=0.5V$). Table shows the time response of the sensor for glucose concentrations from 5 μ M to 50 μ M. Time constants were obtained by fitting the current variations for each concentration with first order exponential growth function (green dashed line).

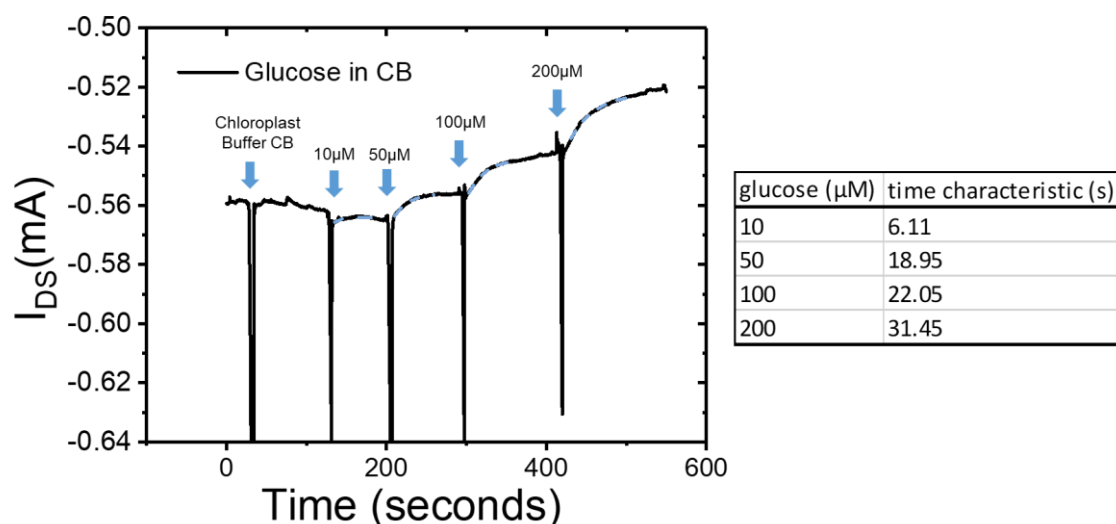


Figure S3: OECT GOx-functionalized device current I_{SD} response to increasing glucose concentrations in Chloroplasts isolation buffer, ($V_{SD}=-0.4V$ and $V_{SG}=0.5V$). Table shows the time response of the sensor for glucose concentrations from 5 μ M to 200 μ M. Time constants were

obtained by fitting the current variations for each concentration with first order exponential growth function (blue dashed line).

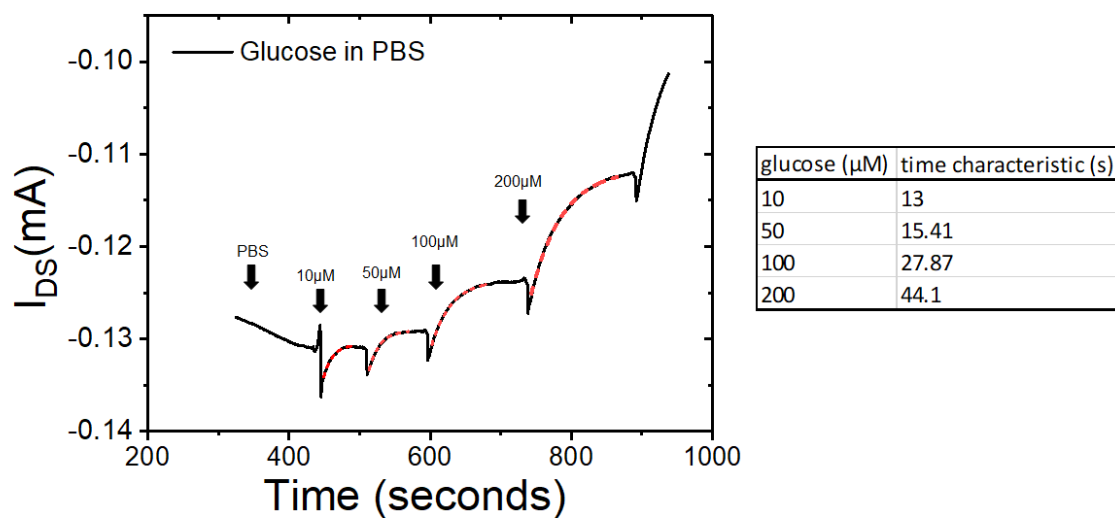


Figure S4: OECT GO_x-functionalized device current I_{SD} response to increasing glucose concentrations in PBS, ($V_{\text{SD}}=-0.4\text{V}$ and $V_{\text{SG}}=0.5\text{V}$). Table shows the time response of the sensor for glucose concentrations from $5\mu\text{M}$ to $200\mu\text{M}$. Time constants were obtained by fitting the current variations for each concentration with first order exponential growth function (red dashed line).

Paper V

Diurnal in vivo xylem sap glucose and sucrose monitoring using implantable organic electrochemical transistor sensors.

Article

Diurnal *in vivo* xylem sap glucose and sucrose monitoring using implantable organic electrochemical transistor sensors

Chiara Diacci,^{1,2} Tayebah Abedi,³ Jee Woong Lee,^{1,4} Erik O. Gabrielsson,¹ Magnus Berggren,^{1,4} Daniel T. Simon,¹ Totte Niittylä,^{3,*} and Eleni Stavrinidou^{1,4,5,*}

SUMMARY

Bioelectronic devices that convert biochemical signals to electronic readout enable biosensing with high spatiotemporal resolution. These technologies have been primarily applied in biomedicine while in plants sensing is mainly based on invasive methods that require tissue sampling, hindering in-vivo detection and having poor spatiotemporal resolution. Here, we developed enzymatic biosensors based on organic electrochemical transistors (OECTs) for in-vivo and real-time monitoring of sugar fluctuations in the vascular tissue of trees. The glucose and sucrose OECT-biosensors were implanted into the vascular tissue of trees and were operated through a low-cost portable unit for 48hr. Our work consists a proof-of-concept study where implantable OECT-biosensors not only allow real-time monitoring of metabolites in plants but also reveal new insights into diurnal sugar homeostasis. We anticipate that this work will contribute to establishing bioelectronic technologies as powerful minimally invasive tools in plant science, agriculture and forestry.

INTRODUCTION

Bioelectronics enable electronic interfacing with the biological world as means for monitoring or stimulating biological processes. The bioelectronics field is highly driven by applications in biomedicine, specifically finding new solutions for diagnosis and therapy (Berggren and Richter-Dahlfors, 2007; Zeglio et al., 2019). Organic electronic devices can be advantageous when applied in the biological milieu since organic electronic materials support sufficient electronic and ionic transport (Paulsen et al., 2020), in a highly coupled manner, and thus enable efficient signal transduction. While the majority of efforts lie within the animal kingdom, applying bioelectronics to other biological organisms has emerged with successful demonstrations of sensing and actuation in bacteria (He et al., 2012; Pitsalidis et al., 2018; Zajdel et al., 2018; Demuru et al., 2019; Di Lauro et al., 2020) and plants (Stavrinidou et al., 2015, 2017; Coppedè et al., 2017; Poxson et al., 2017; Bernacka-Wojcik et al., 2019; Janni et al., 2019; Kim et al., 2019; Vurro et al., 2019; Diacci et al., 2020). Recently, we presented an implantable organic electronic ion pump for *in vivo* delivery of abscisic acid, one of the main hormones involved in plant stress responses (Bernacka-Wojcik et al., 2019), and subsequently the electronic control of physiology in intact plants. Others demonstrated conformable electrodes based on conducting polymers that were directly printed on plant leaves for long term bioimpedance monitoring (Kim et al., 2019). In another work, a yarn-based organic electrochemical transistor (OECT) has been used for electrolyte monitoring in tomato plants in physiological conditions (Coppedè et al., 2017), while in following works, the same concept was used to monitor drought stress (Janni et al., 2019) or changes in vapor pressure deficit (Vurro et al., 2019). Our group coupled an OECT directly with isolated chloroplasts to monitor in real-time the glucose export from the plant organelles with unprecedented time resolution (Diacci et al., 2020). The OECT is a three terminal device where a gate electrode modulates the current, via reduction-oxidation switching of a conducting polymer-based channel (Nilsson et al., 2002; Rivnay et al., 2018). The OECTs operate in aqueous environments and when the gate electrode is functionalized with an enzyme the OECT is converted to an enzymatic biosensor (Tang et al., 2011). When the analyte is present in the solution, an electrochemical reaction takes place at the gate, which becomes amplified through the modulation of the channel current. Signal amplification of the OECTs is important particularly for miniaturized devices where high signal to noise ratio is challenging. Although OECTs have received a lot of attention as amplification biosensors, their application in complex

¹Laboratory of Organic Electronics, Department of Science and Technology, Linköping University, 601 74 Norrköping, Sweden

²Dipartimento di Scienze della Vita, Università di Modena e Reggio Emilia, Via Campi 103, 41125 Modena, Italy

³Umeå Plant Science Centre, Department of Forest Genetics and Plant Physiology, Swedish University of Agricultural Sciences, 90183 Umeå, Sweden

⁴Wallenberg Wood Science Center, Linköping University, 601 74 Norrköping, Sweden

⁵Lead Contact

*Correspondence: totte.niittyla@slu.se (T.N.), eleni.stavrinidou@liu.se (E.S.)
<https://doi.org/10.1016/j.isci.2020.101966>



biological environments has been very limited. So far, most of the enzymatic OECT sensors have been validated in test solutions for the detection of metabolites and neurotransmitters (Shim et al., 2009; Kergoat et al., 2014; Liao et al., 2014; Berto et al., 2018; Pappa et al., 2018). Few demonstrations have been reported where glucose is monitored from natural samples such as sweat (Scheiblin et al., 2015) saliva (Liao et al., 2015; Pappa et al., 2016), or cell media (Curto et al., 2017; Strakosas et al., 2017) and one example focused on epidermal patches for on-body detection (Parlak et al., 2018). Until now, there is no demonstration of an implantable OECT enzymatic sensor for monitoring an analyte directly within the *in vivo* environment.

Sugars are produced by photosynthesis and play a central role in plant growth and development. Several of the primary sugar metabolic pathways, responsible for carbon allocation in plants, are relatively well described. One of the current challenges in the field is to understand how the metabolic pathways of sugar metabolism are regulated, and how changes in sugar flux or concentration are adjusted. In order to address these questions, methods allowing for spatial and temporal real-time quantification of sugar levels are needed. The development of Förster resonance energy transfer (FRET)-based nanosensors for sugars was the first step toward *in vivo* measurements of sugar pools (Deuschle et al., 2006; Chaudhuri et al., 2011). Genetically encoded FRET sensors enable the analysis of steady-state concentration of sugar and dynamic changes in living tissue with high temporal and even subcellular resolution. However, the use of FRET sugar sensors is limited to cells and tissues, which can be monitored using a microscope. Cells buried deep in tissues, as is the case of vascular system, for example, are not accessible. Therefore, sugar analysis in plants, is usually performed by invasive methods that have poor spatial and temporal resolution and lead to disposal of the organism or tissue after sampling. Furthermore, sample analysis requires extraction/processing followed by sugar level determination based on enzymatic assays (Graf et al., 2010), mass spectrometry (Jorge et al., 2016) or high-performance liquid chromatography (Mayrhofer et al., 2004). All of these methods have high accuracy and low detection limit, but do not enable *in vivo* real time sugar level monitoring and therefore impede kinetic studies and analysis of biologically relevant events within the living plant.

In several tree species, including the model tree aspen, sucrose is the predominant form of transported carbon (Rennie and Turgeon, 2009). Sucrose is primarily transported in the phloem to different parts of the plant, but sucrose is also transported within the xylem transpiration stream (Heizmann et al., 2001; Mayrhofer et al., 2004). It was estimated that 9–28% of the carbon delivered to leaves in 3-month-old *Populus* trees over a diurnal cycle was derived from sugars transported in the transpiration stream (Mayrhofer et al., 2004). Several tree species also use the xylem pathway to transport sugars during flowering and bud flush in the spring (Sauter and Ambrosius, 1986). Xylem sap composition is typically analyzed from exudate secreted from a cut stem or leaf petiole. Sometimes, root pressure is sufficient to push out the xylem sap from the cut, but often a pressure chamber is required to squeeze out the sap and there is always a concern that xylem sap may mix with phloem sap or other cell contents at the cut surface. Furthermore, these invasive methods disrupt the transpiration stream, and do not allow monitoring of the sap composition over time. In this work, we overcome the above limitations by developing implantable glucose and sucrose OECT-based sensors that enable *in vivo* real time monitoring in plants (Figure 1). As a demonstration of the proof-of-concept and the kind of biological insights that this technology enables, we observed previously uncharacterized diurnal changes in sucrose levels in the xylem sap of greenhouse-grown hybrid aspen (*Populus tremula x tremuloides*).

RESULTS AND DISCUSSION

OECT-based sugar sensors

The OECT-based glucose and sucrose sensors were fabricated on a 125- μm -thick polyethylene naphthalate (PEN) substrate using standard microfabrication techniques as described in the [Transparent Methods](#) section. Ti/Au is used for source, drain, gate electrodes, and for wiring while the channel is based on the conducting polymer poly(3,4-ethyl-enedioxythiophene):poly(styrenesulfonate) (PEDOT:PSS). The gate electrode is coated with a PEDOT:PSS thin film in order to increase its capacitance for efficient modulation of the channel conductance and is then further functionalized with enzymes and PtNPs. The PtNPs were electrodeposited on the gate while the enzymes were immobilized with the help of a chitosan matrix that is drop-casted onto the gate.

The PEDOT:PSS-based OECT operates in the depletion mode with the channel initially at the high conductance state. When a positive bias is applied at the gate, cations from the electrolyte will penetrate into the channel, compensating the PSS polymer dopants resulting in PEDOT de-doping and a decrease in the

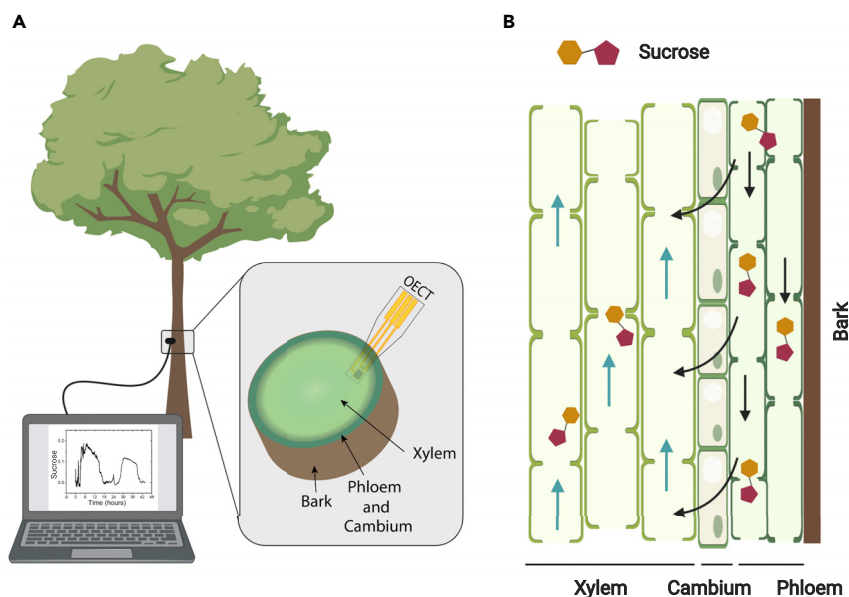


Figure 1. In vivo sugar monitoring in trees with an OECT-based biosensor

(A) Illustration of the experimental setup. In the inset, the OECT biosensor is placed within the tissue of interest, the mature xylem of the tree.

(B) Illustration of the vascular tissue of trees. Phloem is the main tissue responsible for sucrose transport. Sucrose is unloaded from phloem into xylem (black arrow) and then being transported via the transpiration stream (blue arrows).

channel current (Khodagholy et al., 2013). When the analyte is present in the solution an enzymatic reaction will take place at the gate that will result in the generation of H_2O_2 . The H_2O_2 will then be oxidized on the PtNPs on the gate, which is associated with a transfer of electrons that change the effective gate potential and consequently induce a further decrease in the channel current (Bernards et al., 2008) (Figure 2A). Typical transfer curve and transconductance of the OECT are shown in Figure 2B. The transconductance is considered the figure of merit of OECT sensor devices as describes the change in the drain current over the change in gate potential, $g_m = \Delta I_D / \Delta V_G$. Therefore, operation of the device at the high transconductance regime will result in small changes in the gate potential to induce large changes in the channel current. The analytes possible to detect by the enzymatic electrochemical sensors are limited by the availability of enzymes that can take part in redox reactions. Glucose oxidase is an oxido-reductase enzyme that catalyzes the oxidation of β -D-glucose to hydrogen peroxide and D-glucose1,5-lactone. Sucrose on the other hand does not have a corresponding oxidoreductase enzyme. In order to detect sucrose enzymatically, we overcame this limitation by incorporating successfully three enzymes within the chitosan matrix enabling a cascade of reactions to take place in a confined space. First, invertase hydrolyzes sucrose into fructose and α -D-glucose, mutarotase then catalyzes the conversion of α -D-glucose into β -D-glucose and finally β -D-glucose reacts with the glucose oxidase enzyme, Figure 2A.

The performance and sensitivity range of the OECT-based glucose and sucrose sensors were assessed by monitoring the relative change of the channel current in solutions containing increasing concentration of sugars. To achieve high sensitivity, we operated the transistor at voltages across the gate, $V_{GS} = +0.5$ V and channel, $V_{DS} = -0.4$ V (source grounded), where the OECT has high transconductance, and thus exhibiting high amplification of the sensor signal. In order to compare the response of different devices and extract the characteristic calibration curve of the sensor we calculated the normalized drain current response of the device for each analyte concentration ($\Delta I/I = -(I_{[M]} - I_0)/I_0$), where $I_{[M]}$ is the drain current at concentration M and I_0 is the base drain current. In Figure 2C, we show the calibration curves of the sucrose and glucose sensors represented as the mean of the response of 8 and 5 different devices, respectively. We observe that the sensors have similar, close to identical, characteristics with a dynamic range within 100 μ M - 1 mM, as a result of the same concentration of glucose oxidase enzyme in the sucrose and glucose sensor. Furthermore, our biofunctionalization strategy allows us to tune the sensitivity and dynamic response of the sensor by changing the concentrations of the enzymes within the chitosan matrix. As shown in Figure S1, the sensor becomes sensitive to higher concentrations of sucrose when we reduce the

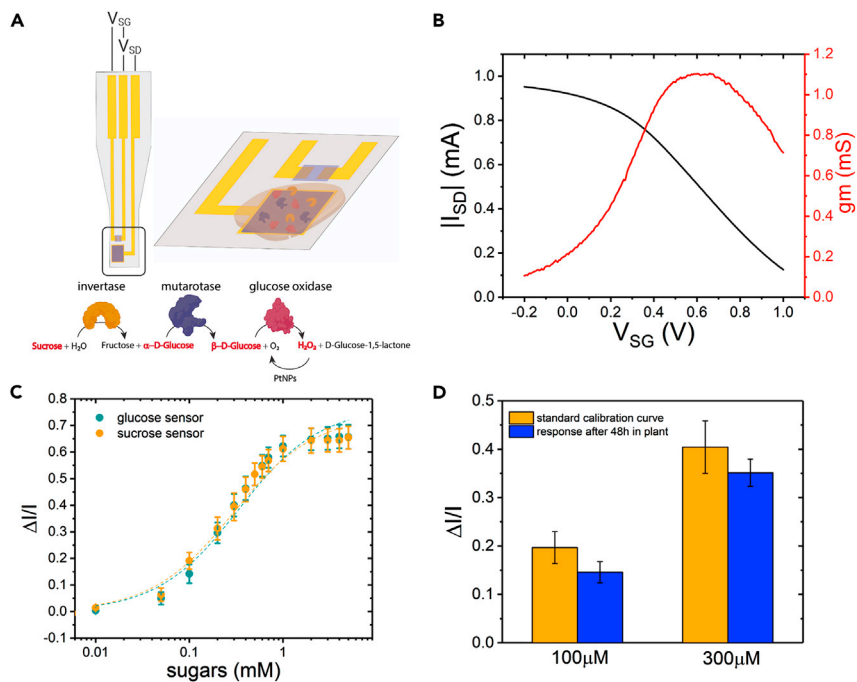


Figure 2. OECT-based sucrose and glucose sensors

(A) Schematic of the OECT-based sucrose sensor. Gate (area = 300 μm × 300 μm) is functionalized with three enzymes in order for sucrose to be converted to H₂O₂ that can then be oxidized at the PtNPs that are on the gate electrode.

(B) Typical transfer curve and transconductance of OECT device after functionalization with PtNPs for V_{SD} = -0.4V and V_{SG} from -0.2V to 1V.

(C) Sucrose sensor (orange) and glucose sensor (cyan) calibration curve in PBS buffer. Dashed lines represent fit to the sigmoidal function. Error bars represent the standard error, n = 8 devices for sucrose sensor and n = 5 devices for glucose sensor.

(D) Sucrose sensor response after 48hr of insertion in the tree for 100 μM and 300 μM sucrose solutions (blue error bars represent the standard error for n = 3). In orange, the sucrose sensor calibration curve is shown for comparison. T test showed no statistical significance (p > 0.05) on the response of the sensors before and after 48hr implantation.

enzymes concentrations. Additionally, we tested the sensitivity of the sucrose sensor to glucose. Indeed, we observe that the sucrose sensor is sensitive to glucose as it is expected, [Figure S2](#). Therefore, for the *in vivo* detection of glucose and sucrose both independent sensors were used simultaneously. Finally, we evaluated the stability of the sensor in the complex biochemical environment of the plant. Sucrose sensor devices (n = 3) were implanted in the bark of hybrid aspen trees for 48hr and after being removed from the tree their response to 100 μM and 300 μM of sucrose test solutions was assessed as shown in [Figure 2D](#). We observe a small decrease in the sensor response in comparison with the standard calibration curve of the sucrose sensors but the difference is not statistically significant.

Device integration and portable measurement setup

Next, we proceed to develop a portable OECT measurement unit set-up based on a low-cost Arduino platform that allow us to perform the sensing experiment in the growth environment of plants. In this case, the measurements were performed inside the greenhouse while these devices can be also operated in growth chambers or even in field conditions ([Figures 3A](#) and [3B](#)). As the platform uses uni-polar analog-to-digital and digital-to-analog converters it was operated using a common drain configuration (i.e. drain was grounded) in order to avoid negative voltages ([Figure 3C](#)). Two identical but separate circuits were used to source gate and source voltages (V_{GD}ⁱⁿ and V_{SD}ⁱⁿ) and simultaneously measure gate and source currents (I_G and I_S).

Each circuit was composed of a voltage output (V_{GD}^{out} or V_{SD}^{out}) connected to one end of a precision resistor (R_G or R_S). The other end of the resistor was connected to a voltage input (V_{GD}ⁱⁿ or V_{SD}ⁱⁿ) and to the gate or source terminals. The drain terminal was connected to the ground of the microcontroller. Externally the gate, source and drain terminals were connected to the OECT using a ZIF connector and a ribbon cable

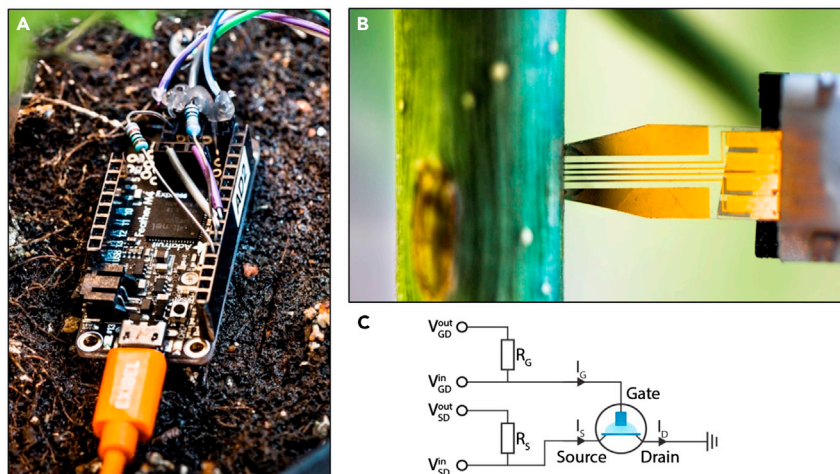


Figure 3. Portable measurement setup

(A) Portable Arduino measurement unit.

(B) OECT connected through ZIF connector and inserted in hybrid aspen tree stem.

(C) Schematic of the Arduino measurement unit circuit. V_{GD} and V_{SD} is related to V_{GS} and V_{DS} through $V_{GD} = V_{GS} - V_{DS}$ and $V_{SD} = -V_{DS}$.

(Figure 3B). Two proportional-integral-derivative (PID) controllers were used to control the voltages applied to the gate and source terminals of the OECT. Upon application of V^{out} , the voltage loss over R reduces the voltage at the gate/source terminal. The PID compensates for this by measuring V^{in} and modulating V^{out} so that V^{in} matches the desired gate/source voltage. The voltage over R , obtained from the difference between V^{out} and V^{in} , was used to calculate I_G and I_S through Ohm's law using the known value of R .

OECT insertion and wounding response

In order to perform meaningful *in vivo* measurements with the OECT sensors it is important to minimize wound responses caused by the sensor insertion. Wounding responses may interfere with the measurements by altering the physiological processes of interest. Therefore, we first evaluated the response to the insertion of the sensor. We used hybrid aspen (*Populus tremula x tremuloides*) as our model system and mature xylem as the tissue of interest. The OECT design was optimized for this specific biological system. The sensors were fabricated on a flexible and thin PEN substrate with a thickness of 125 μm to ensure enough mechanical stability that enables easy insertion while decreasing the footprint to minimize invasiveness. Moreover the device was encapsulated with an SU-8 layer in order to ensure that only the active area of the transistor, gate and channel are exposed to the plant environment. The length of the implanted part of the sensor was chosen to be 3 mm to guarantee that the active sensor site reaches the mature xylem tissue and transpiration stream and the width chosen to be 1 mm. An initial incision with a scalpel was performed to allow sensor insertion to the correct site at 3 mm depth from the epidermis (Figure 4A). This ensured that the sensor gate and channel are located within the mature xylem and are in contact with the transpiration stream. Any local wound response is unlikely to have a substantial effect on the composition of the xylem sap flowing past the sensor, but tissue repair responses may eventually lead to the isolation of the sensor from the transpiration stream. Therefore, wound responses due to the OECT insertion was analyzed over a time course of 1, 2, and 5 days using an optical light microscope. The visual changes in the insertion site were recorded using a camera and analyzed in more detail by preparing 60 μm thick cross sections across the insertion site using a vibratome (Figure 4B). The cross sections were stained with Toluidine Blue O solution to aid the visualization of the cell walls and any tissue level changes. These assays established that a local wound response due to OECT implantation was evident after 48 hr and obvious after 5 days when also a cork tissue formation was observed (Figure 4B). Hence, the following *in vivo* sugar measurements were limited to the first 48 hr following sensor insertion.

Real-time sugar monitoring via implantable OECTs

Sucrose and glucose OECT-based sensors were implanted into the mature xylem of greenhouse grown 8-week-old hybrid aspen trees, and operated at constant gate voltage of $V_{GD} = +0.5$ V and constant

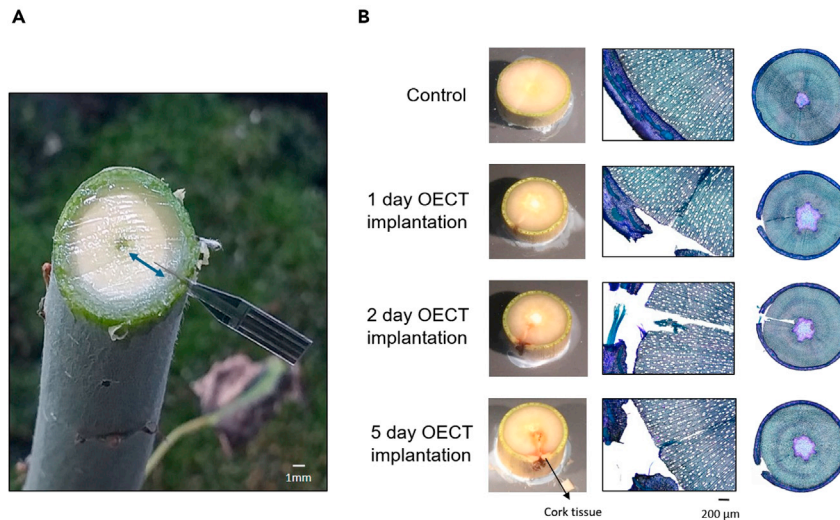


Figure 4. Insertion site and wounding effect

(A) OECT inserted in the hybrid aspen tree stem, showing the active area of the device in the xylem tissue (blue arrow indicates the mature xylem), scale bar 1 mm.

(B) Optical microscopy images of stem cross-sections displaying the OECT wounding effect. Control and hybrid aspen tree response after 1, 2, and 5 days of insertion. Scale bar 200 μm.

source-drain voltage of $V_{DS} = -0.4$ V for 24 hr or 48 hr. Prior to the insertion in the trees, the sensors were treated with oxygen plasma to induce hydrophilicity and to improve the device performance within the xylem tissue (Figure S3). As a control, a device without any included enzyme(s) but with the PtNPs and chitosan matrix was inserted in the same region as the sensor devices. The control device allowed evaluation of any changes in the device response that were not caused from the presence of sugars. Interestingly, the sucrose sensor revealed a variation of the current between day-time and night-time, establishing that sucrose concentration in the xylem sap increases during darkness and decreases at the onset of the light period (Figures 5A and S4). To our knowledge, this is the first time that such diurnal fluctuation in sucrose concentration is observed in xylem sap. At the same time, glucose and control devices did not display any variation between day and night, indicating that glucose homeostasis is not affected by the sucrose changes (Figures 5A and S4). We always observed the same trend in increase of sucrose during the dark period, but the relative magnitude of the changes between different experiments within the same tree or different trees varied. The differences in relative magnitude may be explained by subtle internal and environmental differences, which are known to influence sucrose pools in plants (Farrar et al., 2000). The average change of the normalized response from day-time to night-time for the sucrose sensors is equal to $(I_{\text{high}} - I_{\text{day}}) / I_{\text{day}} = 0.24 \pm 0.1$, $n = 11$), while in the control and glucose sensors there were no significant changes in the current (Figure 5B). We chose to treat our data only qualitatively and not to attempt to quantify the sucrose levels within the xylem due to the uncertainty of the concentration of sucrose in xylem prior insertion of the sensor as will be described below.

In order to compare the OECT findings with conventional methods, we analyzed day and night samples of xylem sap from aspen trees that were collected using the classical stem cutting and sap bleeding method (Alexou and Peuke, 2013). This is a highly invasive method where the tree stem is cut, the phloem is mechanically removed and the xylem sap is collected as it bleeds out from the stem (Figure S5). The collected samples are then analyzed using an enzymatic assay (Stitt et al., 1989). The ex vivo analysis also showed an increase in xylem sap sucrose levels at night (Tables S1 and S2). However, unlike the in vivo measurements with the OECT sensors also glucose levels increased during night (Tables S1 and S2). We suspect that the glucose increase is due to the disruptive nature of the stem cutting and sap bleeding. With this method, pith cells are injured; therefore they are contributing to the collected liquid. Additionally, invertase enzymes, that are known to be induced by wounding (Roitsch and González, 2004), can catalyze sucrose cleavage to glucose and fructose. In support of this hypothesis, fructose levels increased similarly to glucose in the xylem sap collected from the cut stems (Tables S1 and S2). The ex vivo analysis limitations and uncertainties highlight the importance of developing minimally invasive in vivo methods for monitoring

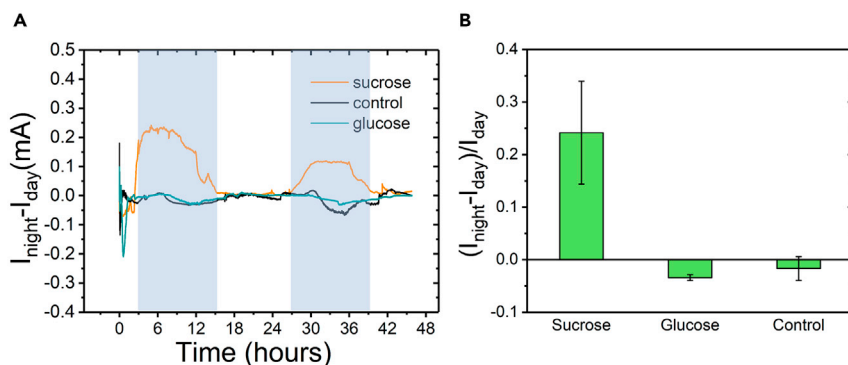


Figure 5. *In vivo*, real-time monitoring of sucrose and glucose in mature xylem of hybrid aspen

(A) Real time response of sucrose sensor (average for four experiments (orange)), glucose sensor (cyan) and control device (black) for 48hr in xylem tissue. Dark areas correspond to night-time and bright areas to day-time.

(B) Averaged normalized response of the sensors devices during night-time. I_{night} and I_{day} values were taken in the middle of the measured time for night and day respectively. Error bars represent the standard errors, sucrose sensors $n = 11$, glucose sensors $n = 3$, control devices $n = 9$.

sugars variations in plants and show how the OECT technology can overcome some of these limitations. Although we could attempt to quantify sucrose concentration changes based on the OECTs sensors response and taking as initial sucrose concentration the daytime value as determined from the *ex vivo* analysis, we avoided to do so considering all the uncertainties involved with the *ex vivo* analysis as described above. This then points out to the need of developing an internal reference system in the OECT that will enable us to treat the data quantitatively as well, something that will be the focus of a future work.

Xylem sap transport of sugars has been reported for several tree species, including birch, willow, sugar maple, and *Populus* (Heizmann et al., 2001; Mayrhofer et al., 2004; Furukawa et al., 2011; Mahboubi and Niitylä, 2018). Changes in xylem sap sugar content are often associated with the spring time initiation of growth and flowering in temperate region species, illustrating the importance of the xylem sap sugar transport pathway for the seasonal growth of trees (Furukawa et al., 2011). Our experiments were conducted under controlled greenhouse conditions in fast-growing young aspen trees, which are not mobilizing long-term stores of carbon. The diurnal fluctuation in xylem sap sucrose levels that we observe with the OECT sensors is therefore likely to be associated with diurnal physiological and metabolic processes such as diurnal growth rate variation and starch degradation at night.

Diurnal xylem processes in trees have been observed for developing wood cell wall biosynthesis in young hybrid aspen trees (Mahboubi et al., 2015), and turgor pressure-driven diurnal changes in the stem diameter in *Cryptomeria japonica* (Hosoo et al., 2003). In the latter case, the stem diameter increased during the night and decreased during the day likely due to diurnal changes in water transpiration. Night time transpiration occurs in trees albeit at a lower level compared to day time (Daley and Phillips, 2006). However, since the OECT measurements showed that xylem sap glucose levels did not change, the sucrose change may be related to sucrose transport and/or storage rather than to sucrose cleavage, or a reduction in the xylem sap transport rate. We hypothesize that the diurnal changes in the xylem sap sucrose may be relevant for carbon allocation and as a diurnal cue at whole tree level. This example illustrates that the OECT sensor technology can provide new insights to carbon allocation and sugar metabolism in trees that cannot be obtained using classic xylem sap sampling methods.

Conclusions

In this work, we developed implantable OECT-based enzymatic biosensors that can operate in the complex *in vivo* environment for 48hr and in real-time monitor sugar variations in the vascular tissue of trees. We extended the range of analytes that can be detected enzymatically with an OECT by developing a bio-functionalization strategy that allows multiple enzymes to be immobilized in the same device and catalyze a chain reaction. Furthermore, we designed a cheap Arduino-based source-measure unit that allows the operation of the device in the growth environment of plants and showcase its potential for application in field conditions. One of the main limitations of our technology is that we can make only qualitative

observations as quantification is hindered by the unknown initial concentration of the analyte in the *in vivo* environment. Nevertheless, relative changes in biology are very important, and we report for the first time that sucrose in mature xylem shows a diurnal dependence indicating that sucrose transport in the xylem is correlated to metabolic or physiological processes. The principle of OECT technology can be applied to assess many metabolites, as well as, the effect of developmental and environmental cues, or abiotic and biotic stresses on the metabolites levels. The sensors are an example of non-invasive dynamic monitoring technology, which will contribute to a better understanding of tree growth dynamics. The technology may also find applications in related areas such as the study of xylem sap feeding insect behavior. Since the operation of the sensors does not depend on genetic modification, they can be readily applied in agriculture and forestry without ethical or societal restrictions. Although OECT technology development is highly driven by biomedical applications, our work demonstrates the usefulness and applicability of bioelectronic technologies in plants for elucidating fundamental questions that currently cannot be answered with the conventional methods and tools.

Limitations of the study

In this work, we reported OECT enzymatic biosensors for *in vivo*, real-time monitoring of sucrose and glucose variations in the xylem vascular tissue of hybrid aspen trees. Currently, our technology can be used only for qualitative observations as quantification is hindered by the unknown initial concentration of the analyte in the *in vivo* environment. Although relative changes in biology are important, quantifying the concentration of sugars will provide additional insight on the sugars transport. Furthermore, the wounding assay revealed that the plant is creating cork tissue after five days of implantation at the insertion point of the sensor which could result in isolating the sensors from the xylem and therefore limiting the duration of *in vivo* monitoring. Future work will focus on engineering further the sensor design to first enable quantitative *in vivo* sensing and secondly to minimizing cork tissue formation for extending the duration of real-time monitoring to several days.

Resource availability

Lead contact

Further information and requests for resources and materials should be directed to and will be fulfilled by the lead contact, Dr. Eleni Stavrinidou (eleni.stavrinidou@liu.se)

Materials availability

This study did not generate new unique reagents.

Data and code availability

Source data for the figures published in this the paper are available per request.

METHODS

All methods can be found in the accompanying [Transparent Methods supplemental file](#).

SUPPLEMENTAL INFORMATION

Supplemental Information can be found online at <https://doi.org/10.1016/j.isci.2020.101966>.

ACKNOWLEDGMENTS

The authors wish to thank Benoit Piro from Paris-Diderot University, Xenofon Strakosas and Per Jansson from Linköping University for fruitful discussions for the sensors design. Special thanks to Thor Balkhed, Linköping University for the photographs of [Figures 3A](#) and [3B](#). Funding was provided by the European Union's Horizon 2020 research and innovation program under grant agreement No 800926 (FET-OPEN-HyPhOE), the Swedish Foundation for Strategic Research (SSF), the Knut and Alice Wallenberg Foundation, the Wallenberg Wood Science Center, Vetenskapsrådet (VR), and the Swedish Government Strategic Research Area in Materials Science on Functional Materials at Linköping University (Faculty Grant SFO-Mat-LiU No. 2009-00971). This work was also supported by the Umeå Plant Science Center, Berzelii Centre for Forest Biotechnology funded by VINNOVA. Additional funding was provided by a Marie Skłodowska Curie Individual Fellowship (MSCA-IFEF-ST, Trans-Plant, 702641) to ES and by an ERC-Advanced Grant to MB. Figures were created with BioRender.com.

AUTHOR CONTRIBUTIONS

E.S. and T.N. conceived and designed the project, C.D. fabricated and characterized the OECT-sensors and performed all in vivo experiments with the help of T.A. and J.L., T.A. performed the wounding assay and the ex vivo xylem sap collection and analysis, C.D. and T.A. analyzed data; E.G. developed the portable measurement platform; C.D., T.A., E.G., T.N. and E.S. wrote the initial draft and final manuscript with input from all the authors; E.S. and T.N. supervised the project.

DECLARATION OF INTERESTS

The authors declare no competing interests.

Received: September 21, 2020

Revised: December 4, 2020

Accepted: December 15, 2020

Published: January 22, 2021

REFERENCES

- Alexou, M., and Peuke, A.D. (2013). Chapter 13 methods for xylem sap collection. *Plant Mineral. Nutrients* 953, 195–207.
- Berggren, M., and Richter-Dahlfors, A. (2007). Organic bioelectronics. *Adv. Mater.* 19, 3201–3213.
- Bernacka-Wojcik, I., Huerta, M., Tybrandt, K., Karady, M., Mulla, M.Y., Poxson, D.J., Gabriellson, E.O., Ljung, K., Simon, D.T., Berggren, M., and Stavriniidou, E. (2019). Implantable organic electronic ion pump enables ABA hormone delivery for control of stomata in an intact tobacco plant. *Small* 15, 1–9.
- Bernards, D.A., Macaya, D.J., Nikolou, M., DeFranco, J.A., Takamatsu, S., and Malliaras, G.G. (2008). Enzymatic sensing with organic electrochemical transistors. *J. Mater. Chem.* 18, 116–120.
- Berto, M., Diacci, C., Theuer, L., Di Lauro, M., Simon, D.T., Berggren, M., Biscarini, F., Beni, V., and Bortolotti, C.A. (2018). Label free urea biosensor based on organic electrochemical transistors. *Flexible and Printed Electronics*, 3 (IOP Publishing), p. 24001.
- Chaudhuri, B., Hörmann, F., and Frommer, W.B. (2011). Dynamic imaging of glucose flux impedance using FRET sensors in wild-type Arabidopsis plants. *J. Exp. Bot.* 62, 2411–2417.
- Coppede, N., Janni, M., Bettelli, M., Maida, C.L., Gentile, F., Villani, M., Ruotolo, R., Iannotta, S., Marmiroli, N., Marmiroli, M., and Zappettini, A. (2017). An in vivo biosensing, biomimetic electrochemical transistor with applications in plant science and precision farming. *Sci. Rep.* 7, 1–9.
- Curto, V.F., Marchiori, B., Hama, A., Pappa, A.-M., Ferro, M.P., Braendlein, M., Rivnay, J., Flocchi, M., Malliaras, G.G., Ramuz, M., and Owens, R.M. (2017). Organic transistor platform with integrated microfluidics for in-line multiparametric in vitro cell monitoring. *Microsyst. Nanoeng.* 3, 1–12.
- Daley, M.J., and Phillips, N.G. (2006). Interspecific variation in nighttime transpiration and stomatal conductance in a mixed New England deciduous forest. *Tree Physiol.* 26, 411–419.
- Demuru, S. et al. (2019) 'Flexible Organic Electrochemical Transistor with Functionalized Inkjet-Printed Gold Gate for Bacteria Sensing', 2019 20th International Conference on Solid-State Sensors, Actuators and Microsystems and Eurosensors XXXIII, TRANSDUCERS 2019 and EUROSENSORS XXXIII. IEEE, 1(June), pp. 2519–2522. not available in PubMed, Crossref
- Deuschle, K., Chaudhuri, B., Okumoto, S., Lager, I., Lalonde, S., and Frommer, W.B. (2006). Rapid metabolism of glucose detected with FRET glucose nanosensors in epidermal cells and intact roots of Arabidopsis RNA-silencing mutants. *Plant Cell* 18, 2314–2325.
- Di Lauro, M., la Gatta, S., Bortolotti, C.A., Beni, V., Parkula, V., Drakopoulou, S., Giordani, M., Berto, M., Milano, F., Cramer, T., et al. (2020). A bacterial photosynthetic enzymatic unit modulating organic transistors with light. *Adv. Electron. Mater.* 6, 1–5.
- Diacci, C., Lee, J.W., Janson, P., Dufil, G., Mehes, G., Berggren, M., Simon, D.T., and Stavriniidou, E. (2020). Real-time monitoring of glucose export from isolated chloroplasts using an organic electrochemical transistor. *Adv. Mater. Tech.* 5, 1–6, 1900262.
- Farrar, J., Pollock, C., and Gallagher, J. (2000). Sucrose and the integration of metabolism in vascular plants. *Plant Sci.* 154, 1–11.
- Furukawa, J., Abe, Y., Mizuno, H., Matsuki, K., Sagawa, K., Kojima, M., Sakakibara, H., Iwai, H., and Satoh, S. (2011). Seasonal fluctuation of organic and inorganic components in xylem sap of *Populus nigra*. *Plant Root* 5, 56–62.
- Graf, A., Schlereth, A., Stitt, M., and Smith, A.M. (2010). Circadian control of carbohydrate availability for growth in Arabidopsis plants at night. *Proc. Natl. Acad. Sci. U S A* 107, 9458–9463.
- He, R.-X., Zhang, M., Tan, F., Leung, P.H.M., Zhao, X.-Z., Chan, H.L.W., Yang, M., and Yan, F. (2012). Detection of bacteria with organic electrochemical transistors. *J. Mater. Chem.* 22, 22072–22076.
- Heizmann, U., Kreuzwieser, J., Schnitzler, J.-P., Brüggemann, N., and Rennenberg, H. (2001). Assimilate transport in the xylem sap of pedunculate oak (*Quercus robur*) saplings. *Plant Biol.* 3, 132–138.
- Hosoo, Y., Yoshida, M., Imai, T., and Okuyama, T. (2003). Diurnal differences in the innermost surface of the S2 layer in differentiating tracheids of *Cryptomeria japonica* corresponding to a light-dark cycle. *Holzforschung* 57, 567–573.
- Janni, M., Coppede, N., Bettelli, M., Briglia, N., Petrozza, A., Summerer, S., Vurro, F., Danzi, D., Cellini, F., Marmiroli, N., et al. (2019). In vivo phenotyping for the early detection of drought stress in tomato. *Plant Phenomics* 2019, 1–10.
- Jorge, T.F., Mata, A.T., and António, C. (2016). Mass spectrometry as a quantitative tool in plant metabolomics. *Philos. Trans. A. Math. Phys. Eng. Sci.* 374, 20150370, Philosophical Transactions of the Royal Society A: Mathematical, Physical and Engineering Sciences.
- Kergoat, L., Piro, B., Simon, D.T., Pham, M.C., Noël, V., and Berggren, M. (2014). Detection of glutamate and acetylcholine with organic electrochemical transistors based on conducting polymer/platinum nanoparticle composites. *Adv. Mater. Weinheim* 26, 5658–5664.
- Khodagholy, D., Rivnay, J., Sessolo, M., Gurfinkel, M., Leleux, P., Jimison, L.H., Stavriniidou, E., Herve, T., Sanaur, S., Owens, R.M., and Malliaras, G.G. (2013). High transconductance organic electrochemical transistors. *Nat. Commun.* 4, 1–6.
- Kim, J.J., Allison, L.K., and Andrew, T.L. (2019). Vapor-printed polymer electrodes for long-term, on-demand health monitoring. *Sci. Adv.* 5, eaaw0463.
- Liao, C., Zhang, M., Niu, L., Zheng, Z., and Yan, F. (2014). Organic electrochemical transistors with graphene-modified gate electrodes for highly sensitive and selective dopamine sensors. *J. Mater. Chem. B* 2, 191–200.
- Liao, C., Mak, C., Zhang, M., Chan, H.L., and Yan, F. (2015). Flexible organic electrochemical transistors for highly selective enzyme biosensors and used for saliva testing. *Adv. Mater. Weinheim* 27, 676–681.
- Mahboubi, A., Linden, P., Hedenström, M., Moritz, T., and Niittylä, T. (2015). ¹³C tracking

after 13CO₂ supply revealed diurnal patterns of wood formation in aspen. *Plant Physiol.* **168**, 478–489.

Mahboubi, A., and Niittylä, T. (2018). Sucrose transport and carbon fluxes during wood formation. *Physiol. Plant* **164**, 67–81.

Mayrhofer, S., Heizmann, U., Magel, E., Eiblmeier, M., Müller, A., Renneberg, H., Hampp, R., Schnitzler, J.P., and Kreuzwieser, J. (2004). Carbon balance in leaves of young poplar trees. *Plant Biol. (Stuttg)* **6**, 730–739.

Nilsson, D., Chen, M., Kugler, T., Remonen, T., Armgarth, M., and Berggren, M. (2002). Bi-stable and dynamic current modulation in electrochemical organic transistors. *Adv. Mater.* **14**, 51–54.

Pappa, A.M., Curto, V.F., Braendlein, M., Strakosas, X., Donahue, M.J., Flocchi, M., Malliaras, G.G., and Owens, R.M. (2016). Organic transistor arrays integrated with finger-powered microfluidics for multianalyte saliva testing. *Adv. Healthc. Mater.* **5**, 2295–2302.

Pappa, A.M., Ohayon, D., Giovannitti, A., Maria, I.P., Savva, A., Uguz, I., Rivnay, J., McCulloch, I., Owens, R.M., and Inal, S. (2018). Direct metabolite detection with an n-type accumulation mode organic electrochemical transistor. *Sci. Adv.* **4**, 1–8.

Parlak, O., Keene, S.T., Marais, A., Curto, V.F., and Salleo, A. (2018). Molecularly selective nanoporous membrane-based wearable organic electrochemical device for noninvasive cortisol sensing. *Sci. Adv.* **4**, eaar2904.

Paulsen, B.D., Tybrandt, K., Stavriniidou, E., and Rivnay, J. (2020). Organic mixed ionic–electronic conductors. *Nat. Mater.* **19**, 13–26.

Pitsalidis, C., Pappa, A.M., Porel, M., Artim, C.M., Faria, G.C., Duong, D.D., Alabi, C.A., Daniel, S.,

Salleo, A., and Owens, R.M. (2018). Biomimetic electronic devices for measuring bacterial membrane disruption. *Adv. Mater.* **30**, 1–8.

Poxson, D.J., Karady, M., Gabrielson, R., Alkattan, A.Y., Gustavsson, A., Doyle, S.M., Robert, S., Ljung, K., Grebe, M., Simon, D.T., and Berggren, M. (2017). Regulating plant physiology with organic electronics. *Proc. Natl. Acad. Sci. U S A* **114**, 4597–4602.

Rennie, E.A., and Turgeon, R. (2009). A comprehensive picture of phloem loading strategies. *Proc. Natl. Acad. Sci. U S A* **106**, 14162–14167.

Rivnay, J., Inal, S., Salleo, A., Owens, R.M., Berggren, M., and Malliaras, G.G. (2018). Organic electrochemical transistors. *Nat. Rev. Mater.* **3**, 1–14, 17086.

Roitsch, T., and González, M.C. (2004). Function and regulation of plant invertases: sweet sensations. *Trends Plant Sci.* **9**, 606–613.

Sauter, J.J., and Ambrosius, T. (1986). Changes in the partitioning of carbohydrates in the wood during bud break in *betula pendula* roth. *J. Plant Physiol.* **124**, 31–43.

Scheiblin, G., Aliane, A., Strakosas, X., Curto, V.F., Coppard, R., Marchand, G., Owens, R.M., Mailley, P., and Malliaras, G.G. (2015). Screen-printed organic electrochemical transistors for metabolite sensing. *MRS Commun.* **5**, 507–511.

Shim, N.Y., Bernards, D.A., Macaya, D.J., Defranco, J.A., Nikolou, M., Owens, R.M., and Malliaras, G.G. (2009). All-plastic electrochemical transistor for glucose sensing using a ferrocene mediator. *Sensors (Basel)* **9**, 9896–9902.

Stavriniidou, E., Gabrielson, R., Gomez, E., Crispin, X., Nilsson, O., Simon, D.T., and Berggren, M. (2015). Electronic plants. *Sci. Adv.* **1**, e1501136.

Stavriniidou, E., Gabrielson, R., Nilsson, K.P., Singh, S.K., Franco-Gonzalez, J.F., Volkov, A.V., Jonsson, M.P., Grimoldi, A., Elgländ, M., Zozoulenko, I.V., et al. (2017). In vivo polymerization and manufacturing of wires and supercapacitors in plants. *Proc. Natl. Acad. Sci. U S A* **114**, 2807–2812.

Stitt, M., Lilley, R.Mc., Gerhardt, R., Heldt, H.W., et al. (1989). [32] Metabolite levels in specific cells and subcellular compartments of plant leaves. In *Biomembranes Part U: Cellular and Subcellular Transport: Eukaryotic (Nonepithelial) Cells* (Academic Press), pp. 518–552.

Strakosas, X., Huerta, M., Donahue, M.J., Hama, A., Pappa, A.M., Ferro, M., Ramuz, M., Rivnay, J., and Owens, R.M. (2017). Catalytically enhanced organic transistors for in vitro toxicology monitoring through hydrogel entrapment of enzymes. *J. Appl. Polym. Sci.* **134**, 1–7.

Tang, H., Yan, F., Lin, P., Xu, J., and Chan, H.L.W. (2011). Highly sensitive glucose biosensors based on organic electrochemical transistors using platinum gate electrodes modified with enzyme and nanomaterials. *Adv. Funct. Mater.* **21**, 2264–2272.

Vurro, F., Janni, M., Coppede, N., Gentile, F., Manfredi, R., Bettelli, M., and Zappettini, A. (2019). Development of an in vivo sensor to monitor the effects of vapour pressure deficit (VPD) changes to improve water productivity in agriculture. *Sensors (Switzerland)* **19**, 4667.

Zajdel, T.J., Baruch, M., Méhes, G., Stavriniidou, E., Berggren, M., Maharbiz, M.M., Simon, D.T., and Ajo-Franklin, C.M. (2018). PEDOT:PSS-based multilayer bacterial-composite films for bioelectronics. *Sci. Rep.* **8**, 1–12.

Zeglio, E., Rutz, A.L., Winkler, T.E., Malliaras, G.G., and Herland, A. (2019). Conjugated polymers for assessing and controlling biological functions. *Adv. Mater.* **31**, e1806712.

iScience, Volume 24

Supplemental Information

Diurnal *in vivo* xylem sap glucose and sucrose monitoring using implantable organic electrochemical transistor sensors

Chiara Diacci, Tayebah Abedi, Jee Woong Lee, Erik O. Gabrielsson, Magnus Berggren, Daniel T. Simon, Totte Niittylä, and Eleni Stavrinidou

Supplemental Information

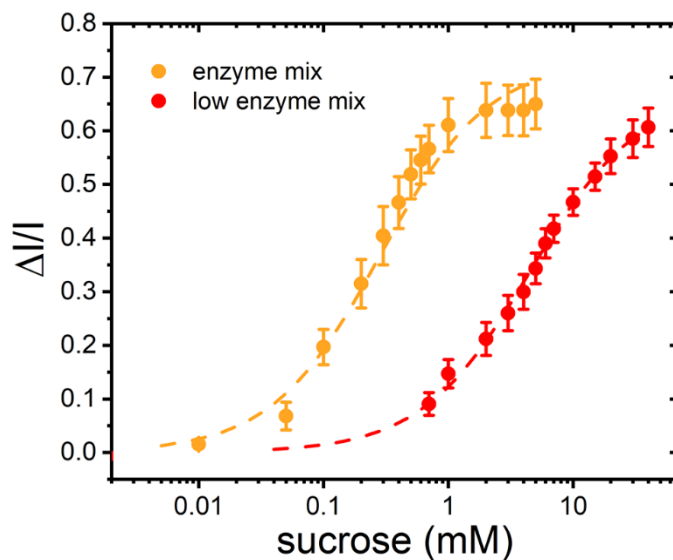


Figure S1: Calibration curves of sucrose sensors with different dynamic range in PBS buffer (Related to Figure 2). Normalized response of sucrose sensors optimized for sucrose detection from 10 μ M to 1mM (orange) and from 1mM to 40mM (red). Dashed lines represent the sigmoid fit function. Error bars represent the standard error, n=8 for orange curve and n=5 for red curve.

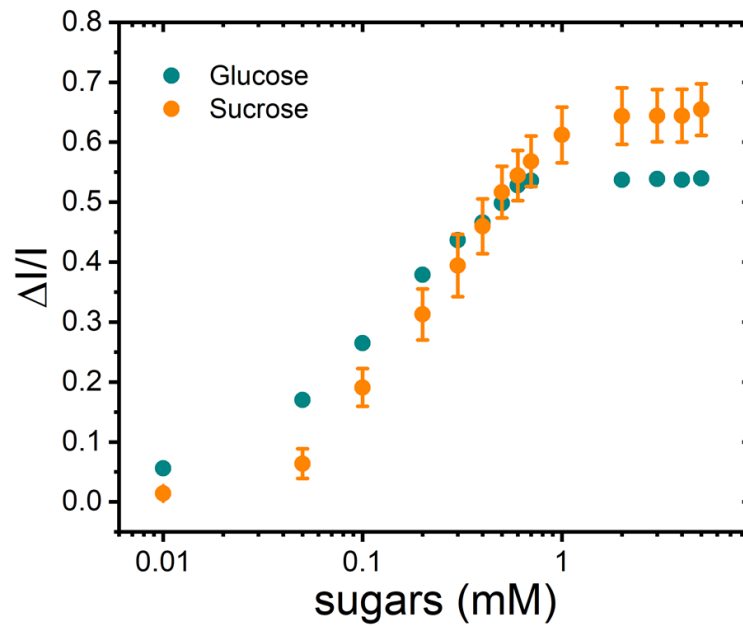


Figure S2: Calibration curves of sucrose sensor for sucrose (orange) and glucose (cyan) solutions (Related to Figure 2). Device responses are the same for glucose solution and sucrose solution due to the presence of same amount of glucose oxidase.

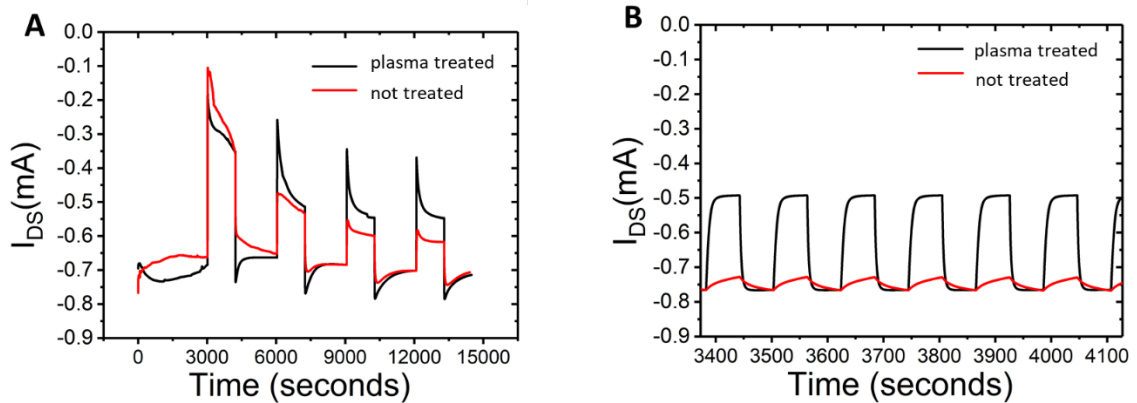


Figure S3: OECT sucrose sensors drain current I_{DS} response in the xylem tissue and effect of hydrophilicity (Related to Figure 5). (A) A pulse gate voltage was applied ($V_{GS} = (0V, +0.5V)$, $V_{SD} = -0.4 V$) right after insertion in the xylem tissue in device that was treated with oxygen plasma (black) and non-treated device (red). (B) Same characterization as in (a) performed after 24h from the insertion time. The non-treated device shows poor modulation.

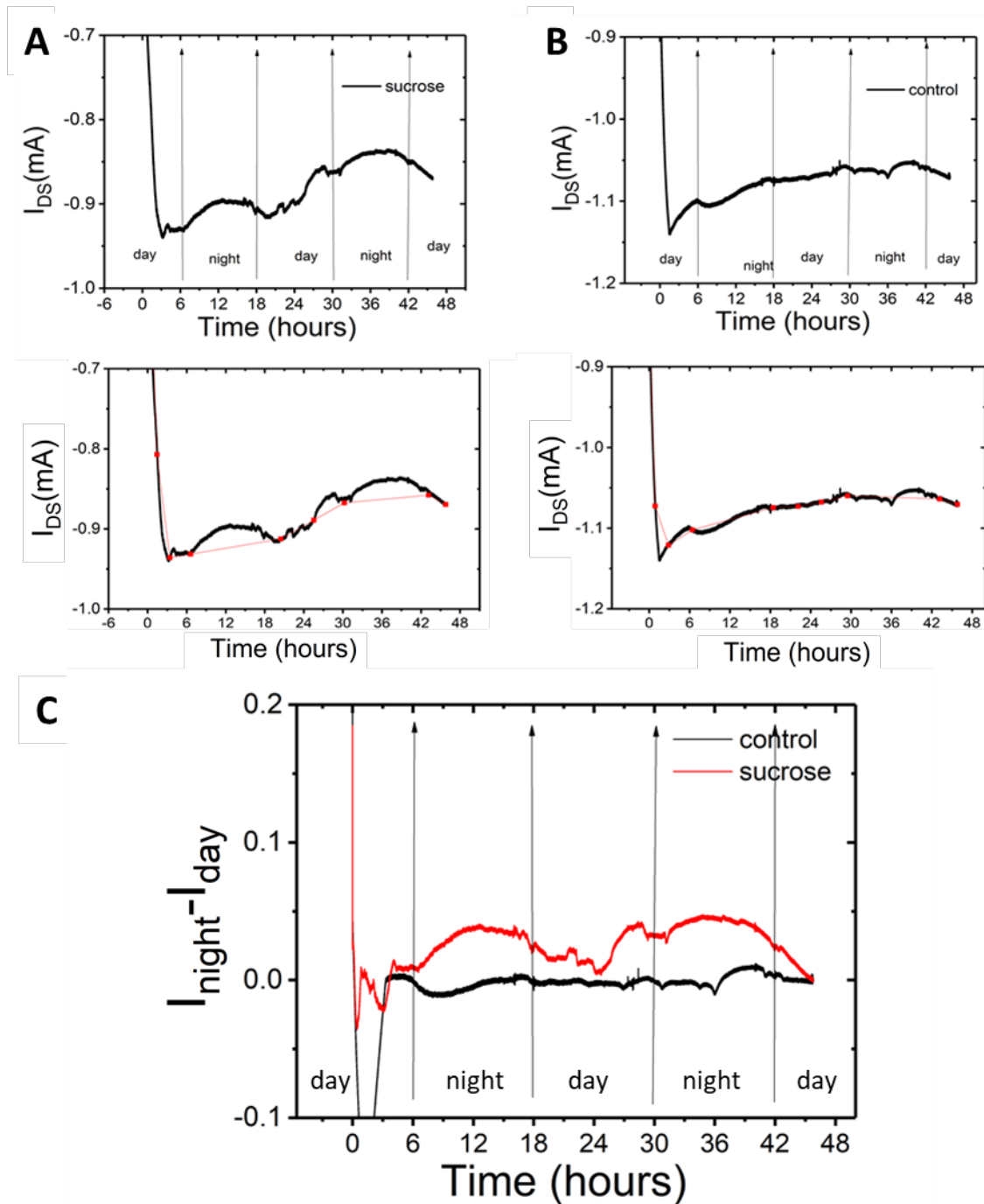


Figure S4: Baseline correction for in-vivo sensing measurements (Related to Figure 5). The drain current of sucrose sensor (A) and control device (B) was recorded for 48 hours in the xylem tissue. The baseline for both measurements was defined as the drain current values during day-time, I_{day} . (C) Corrected current temporal response ($I_{night} - I_{day}$) for 48 hours for sucrose sensor and control device.

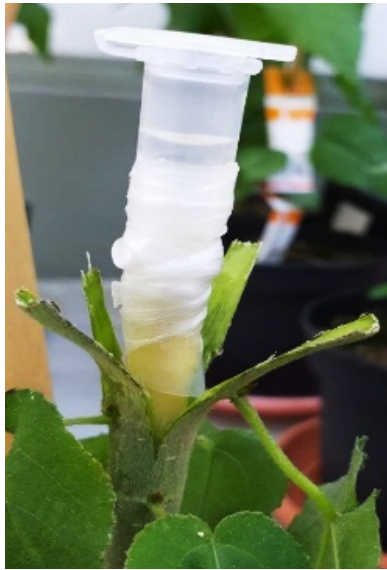


Figure S5: Xylem sap root pressure exudate collection from aspen stem (Related to Figure 5).

Table S1: Soluble sugar concentrations during day as determined from ex-vivo xylem sap analysis (Related to Figure 5)

| Day | mM Glucose ± SD | mM Fructose ±SD | mM Sucrose ± SD |
|----------------|------------------------|------------------------|------------------------|
| Sample 1 | 0.30± 0.01 | 0.34± 0.0 | 0.43± 0.01 |
| Sample 2 | 0.05± 0.01 | 0.06± 0.0 | 0.02± 0.01 |
| Sample 3 | 0.1± 0.01 | 0.1± 0.0 | 0.16± 0.0 |
| Sample 4 | 0.16± 0.01 | 0.21± 0.0 | 0.34± 0.0 |
| Sample 5 | 0.22± 0.01 | 0.25± 0.0 | 0.27± 0.0 |
| Average | 0.17±0.1 | 0.19±0.11 | 0.24 ± 0.16 |

Table S2: Soluble sugar concentrations during night as determined from ex-vivo xylem sap analysis (Related to Figure 5)

| Night | mM Glucose ± SD | mM Fructose ±SD | mM Sucrose ± SD |
|----------------|------------------------|------------------------|------------------------|
| Sample 1 | 3,91± 0,02 | 2,92± 0,03 | 3,86± 0,05 |
| Sample 2 | 2,95± 0,04 | 2,01± 0,05 | 5,79± 0,25 |
| Sample 3 | 2,76± 0,04 | 2,3± 0,03 | 3,54± 0,09 |
| Sample 4 | 2,66± 0,01 | 1,93± 0,01 | 2,66± 0,08 |
| Sample 5 | 1,63± 0,02 | 1,35± 0,01 | 3,18± 0,25 |
| Average | 2.78± 0.81 | 2.1±0.57 | 3.81±1.20 |

Transparent Methods

Device fabrication

For the device fabrication a polyethylene naphthalate foil (Teonex Q65HA, 125 μm , Peutz Folien GMBH) was cut in a circular 4" substrate. The substrate was cleaned with water and acetone, then vacuum backed for 90 s at 120°C. Metal films of 2nm titanium (Ti) and 50 nm gold (Au) were evaporated onto the clean surface. Photolithography (Karl Suss MA/BM 6 mask aligner) and a Shipley 1805 positive resist were used to pattern contacts, wiring, channel and gate. The substrate was then wet etched in I_2/KI solution for Au, and $\text{H}_2\text{O}_2/\text{NH}_4\text{Cl}/\text{H}_2\text{O}$ for Ti. The remaining resist was stripped with acetone. A PEDOT:PSS (Clevios PH1000) mixture with 5% v/v EG (ethylene glycol) and 1% v/v GOPS (3-Glycidyloxypropyl)trimethoxysilane) and dodecylbenzenesulfonic acid (50 μl drop per 5 ml) was spin-coated and patterned using a Shipley 1813 positive resist, then dry etched with CF_4/O_2 reactive ions, in order to create channels and gates. The remaining resist was stripped again with acetone. In the end, the substrate was encapsulated with SU-8 2010 (MicroChem) and openings on the active areas are defined by wet etching with developer mr-Dev 600 (Microresist Technology). Chemicals were used as received from Sigma-Aldrich unless stated otherwise.

Device functionalization

Pt nanoparticles were deposited onto the PEDOT:PSS gate electrode using a solution of 5 mM H_2PtCl_6 in aqueous 50 mM H_2SO_4 , through electrochemical deposition (potentiostat, BioLogic SP-200). Deposition was performed using gate as working electrode and applying a first fixed potential of +0.7 V for 10 seconds and a second fixed potential of -0.2 V for 15 seconds. Two different enzyme mixtures were prepared to functionalize respectively sucrose and glucose sensor. The sucrose sensor mixture was prepared by adding 3 mg/ml Glucose oxidase, 5mg/ml Invertase and 2.5% v/v of Mutarotase Suspension (Wako) in in Phosphate Buffer Saline (PBS,

Thermo Fisher). The glucose sensor mixture was prepared with 3mg/ml Glucose Oxidase only. Enzyme solutions were mixed with a solution of filtered chitosan 5 mg/ml in 50 mM CH₃COOH in a proportion 1:2 and 2,5% v/v of glutaraldehyde 2.5 wt% (Sigma Aldrich). Immobilization was performed by drop-casting 1.5 µl of enzyme/chitosan mixture on the gate electrode. After 30 minutes, the electrode was rinsed with deionized water to remove the remaining CH₃COOH. Chemicals were used as received from Sigma-Aldrich unless stated otherwise.

Arduino measurement units

Each unit was built using an Adafruit Feather M4 Express microcontroller (Adafruit Industries). Each OECT channel (gate and source) circuit used one analog-digital converter (ADC), one digital-analog converter (DAC), and one precision resistor (1 kOhm for source and 1 MOhm for gate). The ADCs and DACs were configured for 12-bit operation, and the sampling times for the ADCs optimized for the expected gate/source impedances (60 µs for source, 340 µs for gate). Two PIDs running on the microcontroller regulated the channel voltages (measured at the corresponding input using the ADCs) to match the setpoints by changing the corresponding output voltage (using the DACs). The PIDs iterated at about 1700 Hz, and for each iteration the resistor voltages, calculated as the difference between channel output and input voltages, were inserted into a digital 10Hz low-pass filters. Measurements were produced at 10 Hz, by transferring the mean resistor voltages over the measurement period by serial communication through a USB cable. A LabView interface was used to send commands and collect data from the three Arduino units, and to convert the resistor voltages to gate and drain currents using Ohm's law and Kirchhoff's current law.

Devices characterization and experimental set-up

Sucrose and glucose dose-curve responses were performed in Phosphate Buffer Saline (50 mM pH 7.4) with a Keithley 2600 series Source Meter. All measurements were carried out at room temperature and devices were operated at constant bias mode with $V_{DS} = -0.4$ V and the $V_{GS} = +0.5$ V. Devices designated for in vivo measurements were treated with oxygen plasma (Zepto W6) at 50W for 2 minutes, in order to increase surface wettability. In vivo measurements were performed with Arduino units, in the greenhouse environment for period of 24 or 48 hours in four different trees. Devices were connected to the Arduino system through ZIF connectors and inserted subsequently a 3-4 mm scalpel incision into the tree stem. A drop of sodium alginate gel (2% in PBS) was added at the epidermis exactly at the insertion site to prevent drying of the tissue. When the gel dried it formed a seal ensuring that the insertion site was no longer exposed to air.

Plant material and growing conditions

Hybrid aspens (*Populus tremula x tremuloides*) were grown in the greenhouse in a commercial soil/sand/fertilizer mixture (Yrkes Plantjord; Weibulls Horto, <http://www.weibullshorto.se>) at 20/15 °C (light/dark) with a 18 h light/6 h dark photoperiod and 60% relative humidity. Trees were watered every other day and they were fertilized using approximately 150 ml 1% Rika-S (N/P/K 7:1:5; Weibulls Horto) once a week after planting. 4 hybrid aspen trees (*populus tremula x tremuloide*), 8 weeks old, were then cultivated in day-neutral photoperiodic condition (12 hour light/12 hour dark) under white fluorescent light (250 $\mu\text{mole m}^{-2} \text{s}^{-1}$) at room temperature with 50-60 % relative humidity. In the sensing experiments 8-16 weeks old trees were used.

Optical microscopy images

For the stem tissue analysis after sensor insertion, cross sections were prepared from OECT insertion sites located at 3mm depth from the surface of the stem as well as control trees without sensor insertion. Then the effect of was followed for 1, 2 and 5 days. A total of 12 trees were assessed, three for each time course and three for control. For each stem five stem cross-sections at 60 μm thickness were prepared using a vibratome apparatus (Leica VT 1000S). The stem sections were then stained in 0.02% (W/V) Toluidine Blue O solution. Samples were observed under a Leica DMI8 inverted optical microscope.

Data analysis

Sucrose and glucose calibration curves (Fig.2C) were calculated by normalizing the drain current I using the equation (1):

$$\Delta I/I = \frac{I_{[M]} - I_0}{I_{[M]}} \quad (1)$$

Where $I_{[M]}$ is the drain current (I_D) at the $[M]$ concentration for sucrose and glucose and I_0 is the drain current at the baseline. The calibration curves were fitted with a sigmoid function $y = ax/(b + x)$, where a and b are constants.

The in vivo measurements (Figure 5) recorded for 24 and 48 hours were corrected for a baseline obtained using the drain current during day-time with equation (2):

$$I_{corrected} = I_{night} - I_{day} \quad (2)$$

Where I_{night} is the current for night-time and I_{day} is the current for day-time as described in the SI (Fig. S4). The sucrose sensor trace in Fig.5A is the average of four different experiments. Normalized average variations, Fig.5B $(I_{night} - I_{day})/I_{day}$ for sucrose (n=11), glucose (n=3) and control devices (n=9) were calculated considering current values at the halftime of the measurement for day-time and night-time. For each experiment we always used a new device. For the experiments with a duration of 24 hours we get one set of data for day/night cycle. For the experiments with duration of 48hours we get 2 set of data of day/night cycle from the same device. The bar chart corresponds to the average of the normalized signal $(I_{night} - I_{day})/I_{day}$ both for the 24hours duration experiments and 48hour duration experiments.

Ex-vivo xylem sap collection and analysis

For collecting xylem sap, root pressure exudate method was used (Alexou *et al.*, 2013). Plants were cut at the bottom of trees about 10 cm from soil surface and then 1–2 cm of the bark below the cut site was removed. Then root pressure sap was collected in individual plant at midday and midnight for 1 hour (Figure S5 and Tables S1, S2).

Soluble sugars; Glucose (Glc), fructose (Fru) and sucrose (Suc), in xylem sap were assayed enzymatically (Stitt *et al.*, 1989). Briefly, 50 μ l of diluted xylem sap was boiled for 10 min and then was used for soluble sugar measurement. Glc, Fru and Suc contents were sequentially quantified in each sample by enzyme-based spectrophotometric assay of NADP⁺ reduction at 340 nm.

Alexou, M. and Peuke, A. D. (2013) 'chapter 13 Methods for Xylem Sap Collection', *Plant Mineral Nutrients*, 953(July), pp. 195–207.

Stitt, M. *et al.* (1989) '[³²P] Metabolite levels in specific cells and subcellular compartments of plant leaves', in *Biomembranes Part U: Cellular and Subcellular Transport: Eukaryotic (Nonepithelial) Cells*. Academic Press, pp. 518–552.